

E.S.R. STUDIES OF  
TCNQ COMPLEX SALTS

by

GLYNNIS ANNE OWENS, B.Sc.

Thesis submitted to the University of Nottingham  
for the degree of  
Doctor of Philosophy  
October 1978.

## ACKNOWLEDGEMENTS

The past three years at the University of Nottingham have been enjoyable and most rewarding, and I would like to express my gratitude to the numerous people who have made it so.

Firstly, I would like to thank Professor D.D.Eley, F.R.S., O.B.E. for the interest he has shown in this work, and to Dr.M.R.Willis for his continued guidance and encouragement. Also in the academic field, thanks are due to various members of the semiconductor group with whom I have had valuable discussions.

I would also like to take this opportunity of thanking the technical staff of the Chemistry Department, particularly Mr.W.E.Porter, Mr.R.Parsons and Mr.N.D.Brown, and also Mr.J.L.Dennis of the Physics Department.

Thanks are also due to my colleagues, to Mr.T.J.Spencer for careful typing of this manuscript, and the Science Research Council for financial support.

I would like to thank my fiancé, Derek, for his patience and understanding and, finally, I wish to express my sincere and deep gratitude to my parents for their support, encouragement and enthusiasm throughout my education. To them I dedicate this thesis.

To Mum and Dad

## CONTENTS

		<u>Page</u>
<u>CHAPTER 1</u>	INTRODUCTION	
1.1	The concept of conduction.	1
1.2	Studies of the organic solid state.	2
1.3	Superconductivity.	4
1.4	The TCNQ molecule.	7
1.5	TCNQ salts.	9
1.6	Structural factors influencing the physical properties.	12
1.7	Reported progress in the search for a superconductor.	16
1.8	The role played by electron spin resonance in the study of TCNQ complex salts.	22
<u>CHAPTER 2</u>	MAGNETIC PROPERTIES	
	Forward	26
2.1	Magnetic properties of matter.	26
2.2	Diamagnetism.	28
2 2.3	Paramagnetism.	31
2.3.1	The Curie law.	31
2.3.2	Van Vleck paramagnetism and Pauli paramagnetism.	34
2.3.3	Ferromagnetism, antiferromagnetism and ferrimagnetism.	36
2.4	Electron spin resonance.	39
2.4.1	Magnetic properties of the electron.	40
2.4.2	Interaction with a magnetic field.	41
2.4.3	The resonance condition.	43

	<u>Page</u>	
2.4.4	Relaxation processes.	46
2.4.5	Lineshapes and linewidths.	48
2.4.6	Fine structure.	51
2.4.7	Nuclear hyperfine structure.	52
2.4.8	Exchange interactions.	53
2.4.9	Convention of the spin Hamiltonian.	54
2.5	Magnetic properties of TCNQ complex salts.	55
2.5.1	Triplet excitons.	56
2.5.2	E.s.r. spectral characteristics associated with triplet excitons in TCNQ complex salts.	63
<u>CHAPTER 3</u>	EXPERIMENTAL	
3.1	Sample preparation.	71
3.2	Electron spin resonance studies.	74
3.2.1	Equipment.	74
	(i) The spectrometer.	74
	(ii) The cooling unit.	77
	(iii) High temperature equipment.	79
	(iv) The analog integrator.	79
	(v) Sample holders.	81
3.2.2	Calibration experiments.	82
	(i) Microwave power attenuators.	82
	(ii) 100KHz receiver attenuators.	83
	(iii) Thermocouple calibration.	85
	(iv) Sweep rate calibration.	85

3.2.2	(v)	Purity of DPPH.	87
	(vi)	Oscilloscope measurements.	89
3.2.3		Electron spin resonance measurements on TCNQ complex salts.	91
	(i)	g factor measurements.	91
	(ii)	Molar susceptibility measurements.	95
	(iii)	Temperature dependence of the signal intensities.	96
	(iv)	Dipolar interaction study.	98
	(v)	Lineshape study.	99
	(vi)	Spin-lattice relaxation time study.	100
	(vii)	Estimate of Curie spins.	103

CHAPTER 4 RESULTS AND DISCUSSION OF E.S.R. STUDIES OF TCNQ COMPLEX SALTS AVAILABLE AS SINGLE CRYSTALS.

4.1		DCBP(TCNQ) <sub>3</sub> .	105
4.2		DMPA(TCNQ) <sub>4</sub> (I).	132
4.3		DPB(TCNQ) <sub>4</sub> .	143
4.4		TPT(TCNQ) <sub>4</sub> .	151

CHAPTER 5 RESULTS AND DISCUSSION OF E.S.R. STUDIES OF TCNQ COMPLEX SALTS AVAILABLE ONLY IN POLYCRYSTALLINE FORM.

5.1		DMPA(TCNQ) <sub>4</sub> (II).	162
5.2		DPPE(TCNQ) <sub>5</sub> .	170
5.3		DBPE(TCNQ) <sub>5</sub> .	174
5.4		DHPE(TCNQ) <sub>5</sub> .	177

CHAPTER 6 CONCLUDING REMARKS.

182

REFERENCES.

APPENDICES.

## ABSTRACT

The technique of electron spin resonance was used to study the magnetic properties of a number of complex salts of 7,7',8,8'-tetracyanoquinodimethane (TCNQ) in order to obtain a more complete understanding of the electronic states in these materials.

All but one of the cations used in the preparation of these compounds were divalent and their TCNQ complex salts exhibit magnetic behaviour characteristic of thermally accessible triplet excitons. Three of these compounds, 1,2-di(N-p-cyanobenzyl-4-pyridinium)ethylene (DCBP)-(TCNQ)<sub>3</sub>, 1,2-di(N-methyl-4-pyridinium)ethane (DMPA)-(TCNQ)<sub>4</sub> (I), and 1,4-di(N-pyridinium)butane (DPB)-(TCNQ)<sub>4</sub>, were available as single crystals and could be studied in detail. Four of these, however, were only available in polycrystalline form and these were DMPA(TCNQ)<sub>4</sub> (II) and 1,2-di(N-alkyl-4-pyridinium)ethylene (DRPE)-(TCNQ)<sub>5</sub>, in which R equals n-propyl (P), n-butyl (B), and cyclohexyl (H). The existence of two phases (I and II) of DMPA(TCNQ)<sub>4</sub>, first indicated by the electrical data, was supported by the different magnetic behaviour observed in this work.

The absolute magnitudes of the signal intensity for DPPE(TCNQ)<sub>5</sub>, DHPE(TCNQ)<sub>5</sub> and DMPA(TCNQ)<sub>4</sub> (II) were found to be well described by an approximate solution to the Heisenberg Hamiltonian, which indicates an exciton

band is present in these compounds. The absence of dipolar splitting and the high d.c. conductivity supports this interpretation.

However,  $\text{DMPA}(\text{TCNQ})_4$  (I),  $\text{DPB}(\text{TCNQ})_4$ ,  $\text{DBPE}(\text{TCNQ})_5$  and  $\text{DCBP}(\text{TCNQ})_3$  gave results indicative of localised triplet excitons. The latter compound exhibits dipolar splitting, and information concerning the exciton dynamics could be obtained. These results were consistent with the conductivity data and, where available, the crystal structure determinations.

The complex salt  $\text{TPT}(\text{TCNQ})_4$  was available in single crystal form and contained the only trivalent cation studied in this work. The temperature independent signal intensity indicated that triplet excitons were not present, and this behaviour was typical of Pauli paramagnetism. This observation was consistent with the semi-metallic d.c. conductivity observed and was explained in terms of the high degree of disorder present, as indicated by the crystal structure determination.

CHAPTER 1

INTRODUCTION

"All that glisters may not be gold,  
but at least it contains free electrons."

John Desmond Bernal

1901 - 1971

## 1.1 THE CONCEPT OF CONDUCTION

Scientists throughout the centuries have observed chemical changes and phenomena associated with the electron, and explanations ranged from demons and spirits to the relatively recent 'phlogiston hypothesis'. It was not until about 1800 that the flow of heat through a substance was attributed to motion of particles, and the particle itself was discovered in 1897 by J.J.Thompson. This elementary particle, the electron, is responsible for the conduction of heat, the conduction of electricity, and chemical reactions, all of which provide man with the conveniences and comforts of modern life.

The motion of the electron through a substance is dependent on the nature of the substance and how readily the electrons can be detached from their atoms. Consequently, materials can be classified in terms of their electrical conductivity and named metals (good conductors), semiconductors (intermediate conductors), and insulators (poor conductors). This can be understood with reference to Figure 1.1, which shows the bands of energy levels which are allowed to electrons in a solid. These energy bands originate from the discrete energy levels associated with the isolated atoms comprising the solid and consist of a large number of closely spaced levels. In a metal (Figure 1.1(a)) band B is only partly filled and electrons close to the surface can

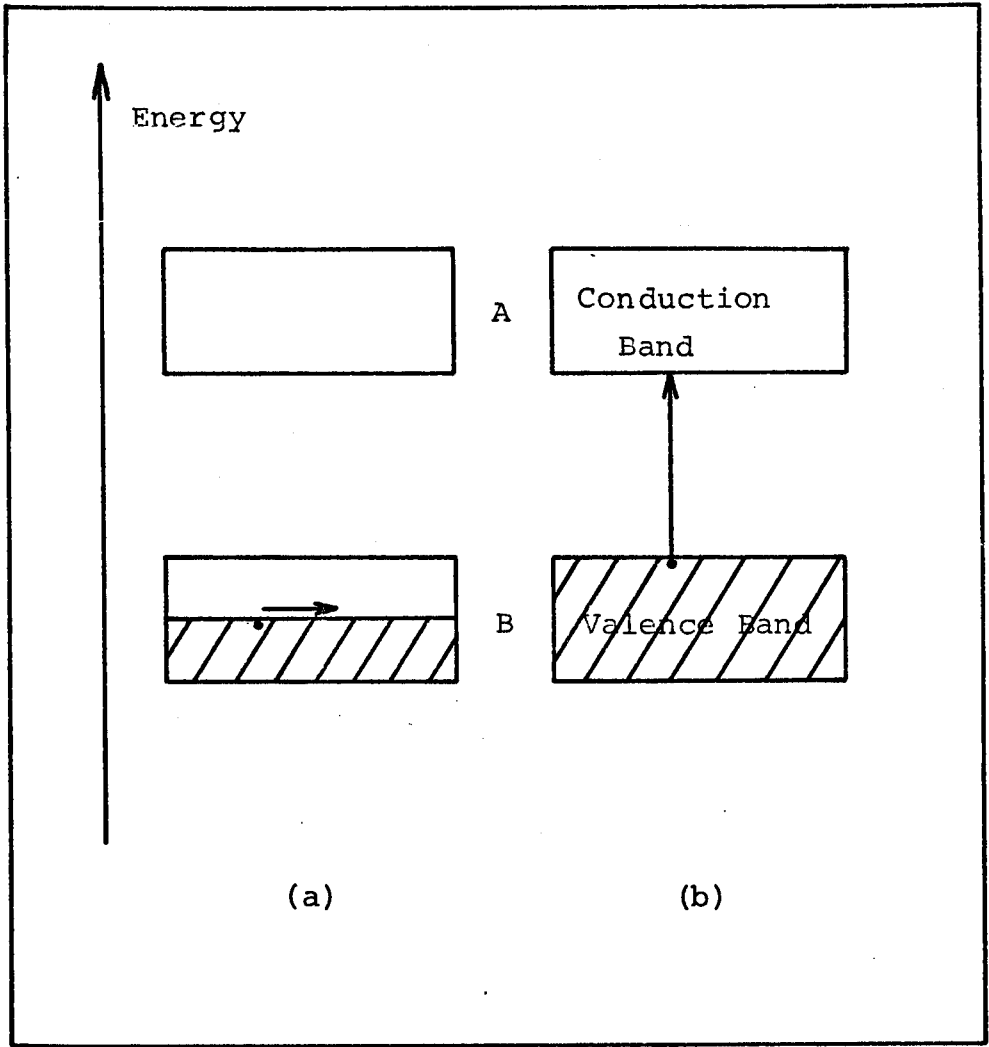


Figure 1.1

Schematic Diagram for electrical conduction in

(a) a metal, and (b) a semiconductor.

move freely through the material. In a semiconductor (Figure 1.1(b)) band B is completely filled and electrical conduction can only occur by exciting the electrons across the energy gap into band A. This is achieved by thermal energy in the case of electrical conduction, and by electromagnetic radiation in photoconduction. Figure 1.1(b) can also be used to represent insulators, only in this case the energy gap is greater.

All three classes of materials have their uses in industry today, particularly semiconductors which are extensively used in solid state electronic devices. The emphasis on semiconductors is based on the fact that their electrical conductivity and other properties can be changed, not only by the addition of small amounts of other materials, but by external stimuli such as temperature change, electric field, and incident radiation.

## 1.2 STUDIES OF THE ORGANIC SOLID STATE

Most of the early work on semiconductors was carried out on the inorganic elements silicon and germanium and, although these are widely used in industry, there has been a growing need for materials with better mechanical properties. Organic compounds were an obvious choice as the considerable flexibility of organic chemistry enables the design and synthesis of molecules with specific physical and chemical properties.

The first step in this field was made by Pochettino<sup>1</sup> in 1906 with the observation of photoconduction in anthracene. This was followed, however, by very few investigations, and it was not until the Second World War that further interest in the organic solid state was aroused. This was initiated by Szent-Györgyi<sup>2</sup> who suggested that many biochemical problems might be solved if discussed in terms of electron transport in living matter. It was this impetus that opened the organic semiconductor field, not only with biological macromolecules but also simpler molecules and molecular complexes.

Semiconductivity was subsequently observed in wool plus 8% absorbed water<sup>3,4</sup> and later photoconductive effects were reported<sup>5</sup> in gelatine to which various dyes had been added. Further significant work followed with the observation of intrinsic semiconduction in the biologically significant organic dye, phthalocyanine<sup>6,7</sup>, and polynuclear hydrocarbons and quinones were also shown to exhibit semiconducting behaviour<sup>8</sup>.

Although research into biological macromolecules has continued and expanded, interest has developed in bimolecular organic systems also. This diversification was a result of the observation of high d.c. electrical conductivities in certain bimolecular organic solids<sup>9</sup>.

These materials became known as charge transfer (CT) complexes and were formed from potential electron donor and potential electron acceptor molecules. The complex formed exhibited a spectral band not associated with either of the individual components, but was in fact due to the transfer of an electron from the donor to the acceptor molecule, hence the name of charge transfer. Frequently this results in paramagnetic compounds and many of these CT complexes have been found<sup>10</sup> to contain unpaired electrons in the solid state using the technique of electron spin resonance.

These CT complexes had wide ranging properties depending on the donor and acceptor strengths of the component molecules. Although complexes of weak donors and weak acceptors were usually poor conductors, whereas strong donors and acceptors exhibited higher conductivities, it became apparent that charge transfer alone did not determine the electrical conductivity of these complexes. Scientists have since been trying to understand the thermal, transport, magnetic and optical properties of organic solids in terms of the various interactions between the constituent molecules in the solid state.

### 1.3 SUPERCONDUCTIVITY

The phenomenon of superconductivity was

discovered by the Dutch physicist Heike Kammerlingh Onnes in 1911, and is associated with the total disappearance of electrical resistance in a material. The transition from a normal to a superconducting state was treated from a thermodynamic viewpoint and, from 1929 to 1950, the developments in the theory of superconductivity consisted of refinements to this treatment. It was not until 1957 that superconductivity was explained in terms of microscopic solid state phenomena by Bardeen, Cooper and Schrieffer <sup>11</sup>.

According to the BCS theory, there are two major conditions that must be met for superconductivity to occur. Firstly, there must be an attractive interaction between pairs of electrons which is strong enough to overcome the normal Coulomb repulsion between them. Moreover, this attractive interaction must be sufficiently strong for bound pairs to result. Secondly, all these bound pairs of electrons must be in identically the same quantum mechanical state in order to remain bound.

Many inorganic materials and alloys are known to exhibit superconducting behaviour but this state exists only in a particular range of temperature. The temperature at which the transition from a superconducting state to an ordinary metallic state occurs is known as the

critical temperature,  $T_c$ , the highest value being about 21K, and corresponds to the breaking up of all bound pairs.

The technological potential of superconductors is virtually limitless, but the low temperatures involved makes most of the proposed applications not economically feasible. Therefore, the production of new superconductors with large values of  $T_c$  is of tremendous technological importance. However, theoretical calculations predicted that a value of 40K for  $T_c$  is unlikely to be exceeded by any inorganic metal or alloy, thereby destroying the dream of a high temperature superconductor. This is where the organic solid state once again provoked interest.

Little<sup>12</sup> proposed in 1964 that an organic compound of appropriate structure could theoretically be a high temperature superconductor. Figure 1.2 shows the model organic polymer used by Little to explain the mechanism. He proposed a slight variation of the BCS theory by suggesting that an electron moving along the spine of this model polymer would induce a dipole in the highly polarisable molecules of the side chain. This induced charge would then attract a second electron, resulting in the formation of a pair of electrons (Cooper pair) having an attractive interaction between

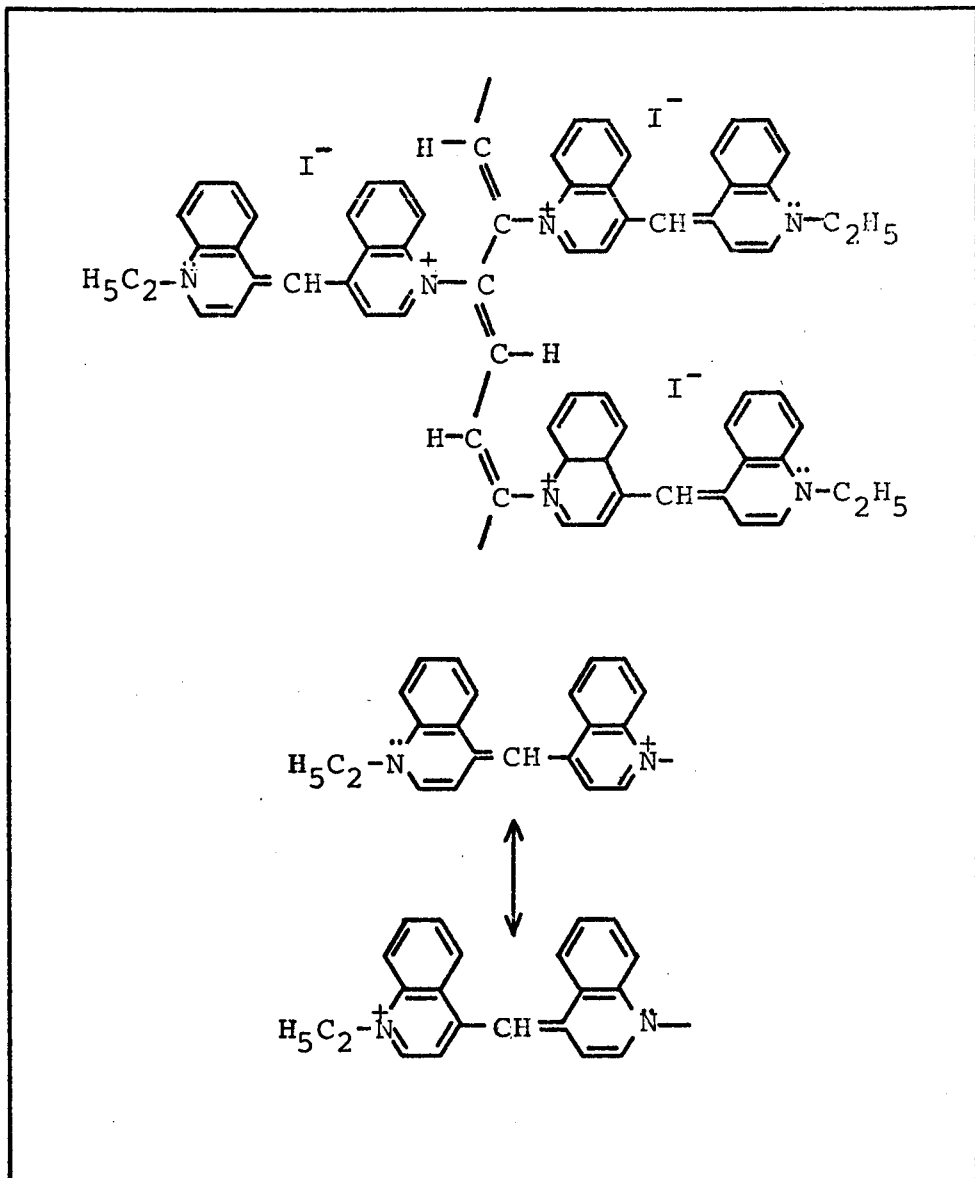


Figure 1.2

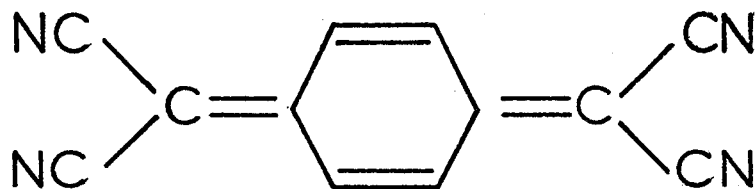
Little's model organic superconductor and the canonical forms of the side group.

them. This mechanism differs from the BCS theory in that an electronically polarisable entity is used instead of the polarisable ionic lattice. Therefore, the very small electronic mass, instead of the larger ionic mass, appears in the theoretical calculation of  $T_c$ , resulting in a value at least an order of magnitude above that possible for a conventional metal or alloy.

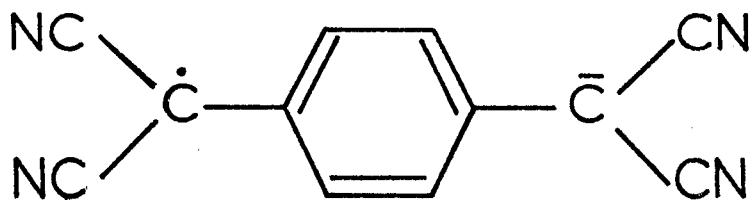
Little's theory is very hypothetical and has been the subject of much criticism<sup>13-15</sup>, but the technological and academic importance of his proposal has stimulated interest in attempting to synthesise molecular systems similar to the model polymer.

#### 1.4 THE TCNQ MOLECULE

The organic molecule 7,7',8,8'-tetracyanoquinodimethane (TCNQ), and the compounds associated with it, have been under intensive investigations since it was first synthesised in 1960 by the company E.I. du Pont de Nemours and Co. in the U.S.A.<sup>16</sup>. The TCNQ molecule is a closed-shell almost planar quinoid molecule (Figure 1.3 (a)) having four highly electron-withdrawing cyanide groups located at the terminal methylene carbon atoms. These characteristics account for its very large electron affinity and associated behaviour of taking one electron when in contact with virtually any electron donor to form the open-shell  $\text{TCNQ}^-$  monoanion radical (Figure 1.3 (b)),



(a)



(b)

Figure 1.3

(a) Neutral TCNQ molecule.

(b) TCNQ anion radical.

whose molecular geometry is slightly different from that of the neutral molecule.

The single unpaired electron on  $\text{TCNQ}^-$  occupies the lowest energy empty  $\pi$ -level and is expected to reside, mainly localised, on the terminal dicyano methylene carbon groups in order to take advantage of the strong electron affinity of the cyanides. Confirmation of the electronic structure has been provided by the small hyperfine coupling of the ring protons in solution studies<sup>17</sup>, by analysis of the X-ray bond lengths associated with the anion radical<sup>18,19</sup>, and by a theoretical study<sup>20</sup>.

Many aromatic organic molecules, other than TCNQ, are known to be good electron acceptors, for example, quinones and substituted quinones, and combine readily with good electron donors to form paramagnetic CT complexes. However, TCNQ complexes have received the most interest, there being two main reasons for this. Firstly, the majority of the compounds exhibit semiconducting behaviour and are, therefore, significant as pointed out in section 1.2. Secondly, the complexes are similar in structure, being essentially one-dimensional, to the model system proposed by Little for the organic high temperature superconductor.

## 1.5 TCNQ SALTS

The first stable salts of TCNQ (frequently also called complexes) were prepared by Melby et al<sup>16,21</sup> and these compounds may be represented by the general formula  $D^+(TCNQ)^-$ , where D is the cation which frequently contains no unpaired electrons. The most commonly used cations are aromatic molecules generally containing nitrogen atoms. However, TCNQ forms complexes with various alkali and transition metals as well as with organic bases.

The compounds having the above general formula are known as simple salts, each TCNQ existing in the form of an anion radical, but neutral TCNQ molecules may also take part, in which case the compounds are called complex salts. The stoichiometry is 1:1 in the simple salts, but is often found as 2:3, 1:2, or even 1:4 in the complex salts, the latter therefore having the general formula of  $D^{n+}(TCNQ)_n^-(TCNQ)_x^0$ , where n is the valency of the cation and x is the number of neutral TCNQ molecules.

Both the simple and the complex salts of TCNQ exhibit interesting electrical<sup>21,22</sup> and magnetic<sup>23,24</sup> properties unusual for organic systems. The number of TCNQ complexes synthesised is well into the hundreds, but they can all be grouped into three classes<sup>22</sup>, each specified by the similarity of physical properties. The range of room temperature electrical conductivities varies

from  $10^{-9}$  to  $10^3$  ohm<sup>-1</sup> cm<sup>-1</sup> and it is this property which forms the basis of the segregation into classes.

The most highly conducting group of complexes, where the cation is normally derived from a planar heterocyclic base, shows near metallic properties having a high conductivity of  $10^1$  to  $10^3$  ohm<sup>-1</sup> cm<sup>-1</sup> which increases with decreasing temperature. This class of complexes also usually exhibits temperature-independent paramagnetic susceptibility, normally associated with Pauli paramagnetism, which is characteristic of a degenerate electron gas such as occurs in metals.

The conductivity of the so-called intermediate-conductivity complexes is smaller by several orders of magnitude and decreases with decreasing temperature. Their paramagnetic susceptibility also decreases as the temperature is lowered, thereby indicating the existence of a gap in the magnetic excitation spectrum.

The third and final class incorporates the low-conductivity complexes which are practically insulators and mostly diamagnetic at room temperature, consequently provoking little interest.

Although there are examples of both types in all the three classes, it is generally found that the complex

salts exhibit higher conductivities than the simple salts. The proposed explanation<sup>25</sup> for this considers the problem in terms of the coulomb repulsion between the electrons. For the simple salt, the conduction mechanism involves the removal of an odd electron from TCNQ<sup>-</sup>, leaving a neutral molecule, and is added to another TCNQ<sup>-</sup> to give a doubly negative molecule. For a complex salt, transport of an electron can occur without putting two electrons on the same TCNQ site, as there are neutral TCNQ molecules available. The fact that two electrons do not reside on the same molecule in the complex salts has also been confirmed<sup>23</sup> by comparison of electron spin resonance data.

In the attempt to understand the conduction mechanisms involved and to synthesise more highly-conducting compounds, polymeric salts of TCNQ have also been studied<sup>26-28</sup>. However, these polymers were found to be poorer conductors than the monomers from which they were derived, and the electrical properties varied according to the polymer crystallinity, this behaviour having been observed previously on compounds other than TCNQ salts<sup>29,30</sup>.

It is apparent that chemists and physicists have been faced with the tremendous challenge of how to explain and interpret the wide range of physical properties exhibited by TCNQ complexes, which remain

unprecedented in the field of the organic solid state. Many attempts have been made<sup>24,25,31,32</sup>, with the goal of Little's superconductor providing the motivation, but even today a fully comprehensive understanding of this family of salts is yet to be achieved.

#### 1.6 STRUCTURAL FACTORS INFLUENCING THE PHYSICAL PROPERTIES

The wide range in physical properties of TCNQ complexes is not surprising when one considers the variety of crystal structures adopted. The early X-ray crystal structure determinations<sup>33,34</sup> elucidated one of the reasons for the high conductivity observed with some of the TCNQ complexes, although there are undoubtedly other important factors involved. It was discovered that a characteristic feature of the complexes is the presence of columns of the TCNQ molecules arranged with their molecular planes almost parallel to each other. These stacks are separated in one direction through the crystal by planes of the cations (Figure 1.4). This mode of packing provides a facile conduction pathway for the unpaired  $\pi$ -electrons in one direction, along the stack, and this is reflected in the electrical conductivities.

Large anisotropies of the physical properties have been observed in these materials which allows a certain correlation of conductivity to be made with structure. This has in fact been used by Dahm et al<sup>35</sup> to

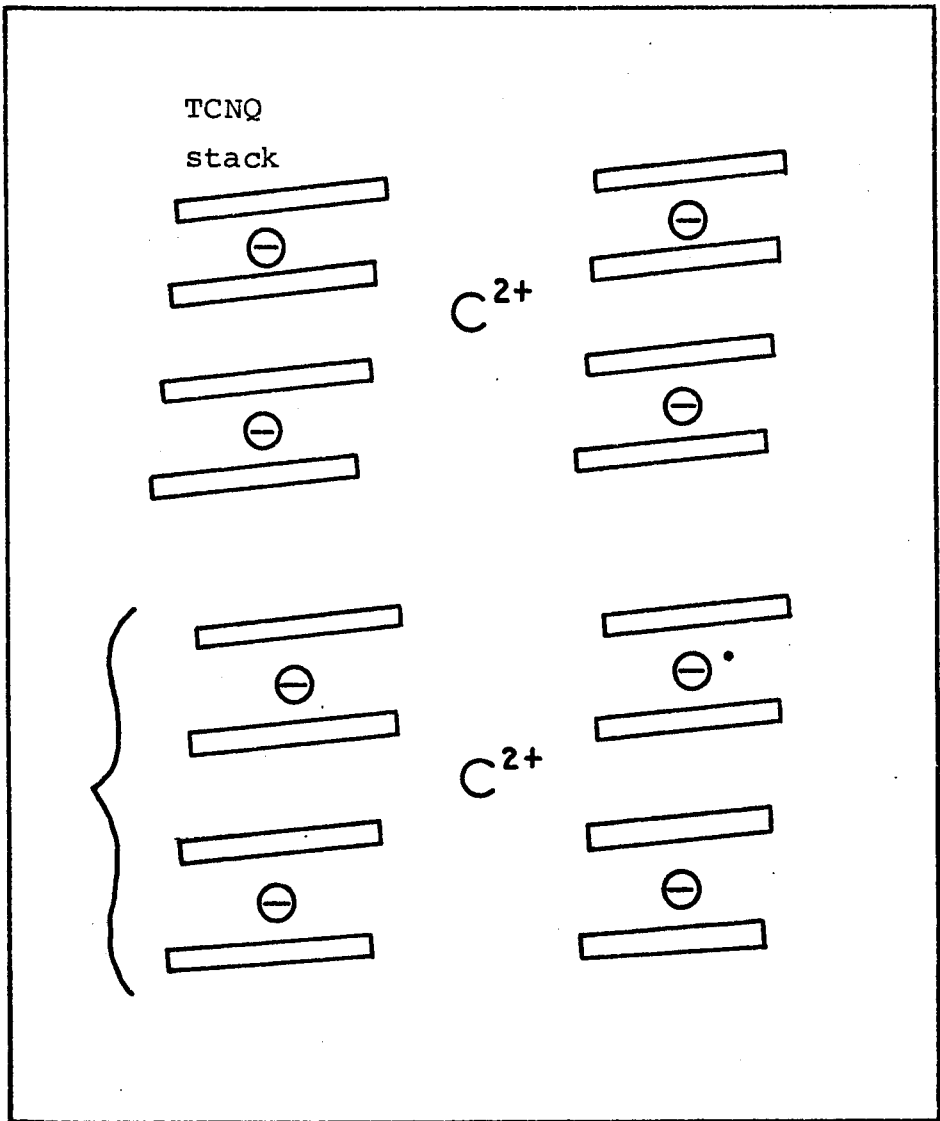


Figure 1.4

Schematic representation of the crystal structure of a typical TCNQ complex salt. The bracket indicates a group of 4 TCNQ molecules within the stack.

form the basis of a classification of the TCNQ complexes. If the compound possesses mixed stacks of alternating donors and acceptors, these stacks are described as 'heterosoric' (eg. ADAD....). If in the mixed stacks there are isolated pairs (diads), threes (triads) or fours (tetrads) of TCNQ molecules, they are described as 'non-soric' (eg. ADDADDA....). However, if the compound possesses separate stacks of cations and TCNQ molecules, each stack only containing molecules of one type, then they are known as 'homosoric'.

Another property characterising the stacks is the nature of the  $\pi$ -orbital overlap between component TCNQ molecules. Using an extended Hückel approach, it has been shown<sup>19,36</sup> that a minimum intermolecular pairing energy between charged TCNQ dimers in a stack occurs when they are overlapped with the ring of one over the external double bond of the other. This is specified as the 'ideal' overlap (Figure 1.5(a)) and maximises  $\pi$ -orbital interaction whilst minimising Van der Waals repulsion. However, this ideal overlap is only present in some TCNQ complexes and, together with the stacking behaviour, bears some relation to the conductivity.

An ideal lattice for high electrical conductivity is, therefore, one in which the stacking arrangement is homosoric, there is ideal overlap between the adjacent

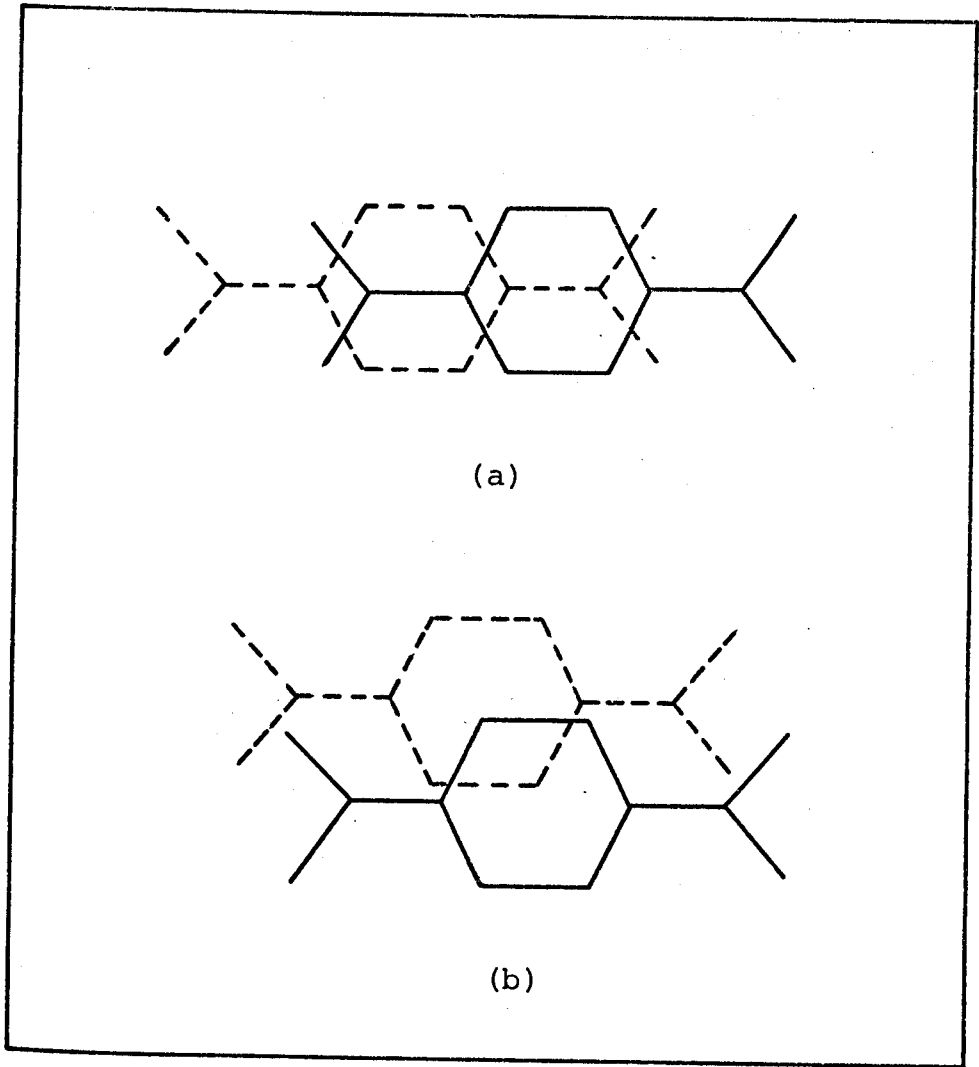


Figure 1.5.

(a) 'Ideal' overlap.

(b) A variation of the overlap.

TCNQ molecules, and also there is a regular interplanar molecular separation of approximately 0.32nm. This mode of packing ensures maximum overlapping of the wave functions of adjacent molecules at minimum Van der Waals repulsion. Moreover, delocalisation of the electrons occurs rendering all the TCNQ's equivalent along the stack.

In the intermediate-conductivity class, the molecules forming the stack are not equivalent, and also differ in the mode of overlap as well as in the interplanar spacings. This causes the column to be divided into repeating units of 2,3 or 4 TCNQ molecules (Figure 1.4), each group being separated by a larger spacing than the spacings between molecules within the group. Furthermore, the overlap is also usually different within the stack (Figure 1.5(b)), and tends to restrict the unpaired electrons to a particular group of TCNQ molecules. The existence of these charged 'supermolecules' within the linear one-dimensional stack has been confirmed by electron spin resonance studies<sup>23</sup>, thereby supporting the X-ray crystallography data.

Although it is accepted that the physical properties of these salts is indeed directly related to the structure, the question still remains as to why such a variety of structures occurs. There have been many attempts to explain this in terms of one variable, assumed

to be the most important parameter. It has been proposed<sup>37</sup> that differences in the distortions of the molecular stacks result from variations in the degree of charge transfer from donor to acceptor, which in turn is partly determined by the ionisation potential of the donor and the strength of the ionic bonding in these materials. The importance of the donor molecules has also been discussed in terms of their symmetry<sup>38,39</sup> and polarisability<sup>25,40</sup>.

By incorporating into the lattice easily polarisable molecular cations of the appropriate size and geometry, a reduction of the effective coulomb repulsion between the electrons on the TCNQ stack results<sup>41</sup>. This is closely related to Little's indirect electron-electron interaction via polarisable side-chains, and so makes possible the achievement of more highly-conducting behaviour. Organic molecules, being large in size, make possible a significant reduction of the coulomb repulsion and give rise to highly-conducting complexes, whereas salts with metal cations generally have low to intermediate conductivities.

The similarities between the proposed criteria for conduction in the TCNQ salts and Little's model polymer, that is, the one-dimensional conduction pathway and the role played by polarisation, show why these salts have been studied so extensively. Furthermore, one of the

criticisms against Little's theory is the high activation energy for conduction exhibited by polyene chains<sup>42</sup>, whereas Little's theoretical calculations require a small activation energy. This objection cannot be applied to TCNQ salts as they have, in general, activation energies an order of magnitude smaller than for polyene chains.

The situation is extremely complex, with a wide variety of properties and an even wider variety of possible explanations and effects to be considered. For example, Thomas<sup>43</sup>, suggested that superconductivity is most probably rendered unattainable in these systems by the presence of structural imperfections, which affect the continuity of the conducting spine and the configuration of the polarisable environment. However, the results obtained with TCNQ salts are encouraging and progress is being made, even though a superconducting compound within this family of salts has not yet been found.

#### 1.7 REPORTED PROGRESS IN THE SEARCH FOR A SUPERCONDUCTOR

Since Little's theory in 1964, systems similar to his model polymer have been under intense investigation, and three of these systems are particularly suitable:

- (a) TCNQ complexes
- (b) Square planar complexes of transition metals
- (c) Polymeric strands of  $(SN)_x$

Group (a) has had particular emphasis for reasons outlined in the preceding sections.

The first salts of TCNQ found to exhibit metallic conductivity were N-methyl-phenazinium(NMP)-TCNQ, quinolinium(Qn)-(TCNQ)<sub>2</sub> and acridinium(Ac)-(TCNQ)<sub>2</sub>. However, these salts all undergo a metal to semiconductor transition at 200K<sup>44</sup>, 223K<sup>45</sup> and 150K<sup>46</sup> respectively. All these cations (Figure 1.6) are large aromatic hydrocarbons containing a nitrogen atom, therefore fulfilling the criterion of high polarisability. Also, the linear stacking behaviour is uniform above the transition temperature, with the cations surrounding the chains in a sense reminiscent of Little's polymer. Although not superconducting, these salts were a step in the right direction.

The first indication that an organic superconductor might indeed be within reach came with the preparation of tetrathiofulvalinium(TTF)-TCNQ<sup>47</sup>. TTF is a highly polarisable donor (Figure 1.6) and forms a highly conducting solid with TCNQ, having a unique structure<sup>48</sup> markedly different from the other salts. The structure shows that the molecules of both species are stacked vertically in separate columns, therefore either stack could provide a facile conduction pathway. The two radical ions have similar sizes and undergo reversible

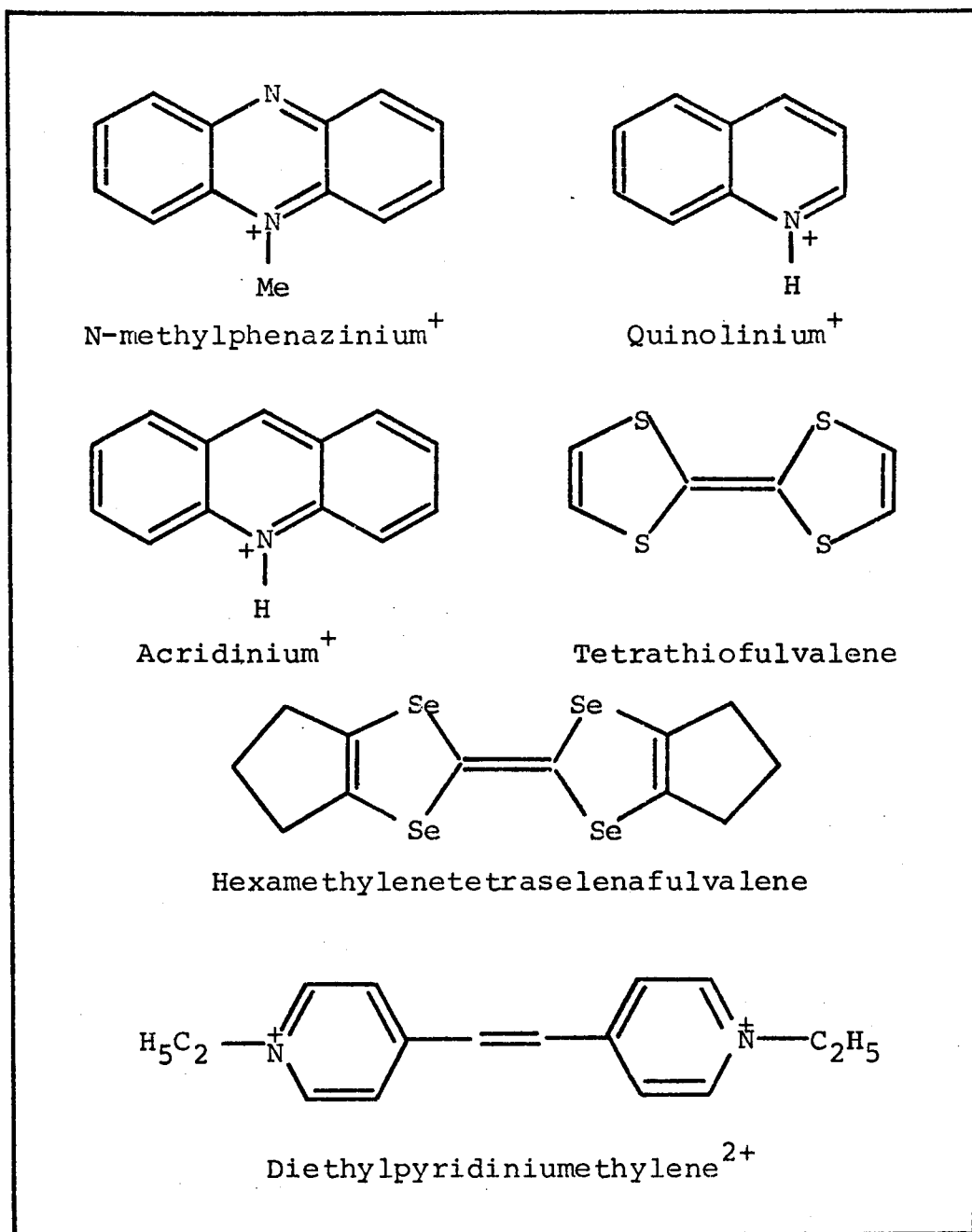


Figure 1.6

Structures of the cations in some of the metallic TCNQ complexes.

electron transfer at similar potentials<sup>49</sup>. These factors are important in enabling it to assume a structure so favourable to electrical conduction, yet here lies an example of the complexity of these systems, as the salt tetramethyl-phenylenediamine (TMPD)-TCNQ also contains radical ions of very similar redox potential and size, but it forms a heteroseric semiconductor.

The electrical<sup>47,50</sup> and magnetic<sup>51</sup> properties of TTF-TCNQ have been extensively investigated. A large number of crystals have been studied giving a conductivity of between 200 and 2000  $\text{ohm}^{-1} \text{cm}^{-1}$  along the direction of stacking, with a metal to semiconductor transition at 60K. However, in a small number of perfectly formed crystals (3 out of 70), it was observed<sup>50</sup> that the conductivity showed a sharp peak just before the onset of this transition, with a value nearly 500 times that at room temperature.

This high conductivity peak has been postulated<sup>50</sup> as being due to superconducting fluctuations at 60K, but the validity of this observation has been criticised on the basis of microwave conductivity experiments<sup>52</sup> which show no such anomaly, and on the possibility of misalignment of electrical contacts which has been shown<sup>53</sup> to induce similar high conductivity peaks in TTF-TCNQ.

In all the TCNQ salts mentioned so far, the metallic state is unstable and lattice distortions result in the occurrence of insulating behaviour at low temperatures. This transition was predicted by Peierls<sup>54</sup> and was proposed to occur in one-dimensional metals in order to lower the kinetic energy of the electrons in the partially filled conduction band. However, several complexes have been found to exhibit metallic conductivity throughout the available temperature region. The first reported organic material having a stable metallic state was hexamethylene-tetraselenafulvalenium (HMTSF)-TCNQ<sup>55</sup>, the compound having a room temperature conductivity ranging from 1390 to 2178  $\text{ohm}^{-1} \text{cm}^{-1}$  and remaining metallic down to 1.1K. The structure of the cation is shown in Figure 1.6.

Progress has also been made in this department with the discovery of diethylpyridiniumethylene (DEPE)-(TCNQ)<sub>4</sub>, the first complex salt to show a monotonic increase in conductivity on cooling from room temperature to 30mK<sup>56</sup>. The structure of this cation is also shown in Figure 1.6.

Since these findings, work has been focused on understanding the unusual properties of TTF-TCNQ and to explore the effects of chemical modifications in both the donor and acceptor molecules. The TTF donor has been

replaced with a similar molecule tetraselenafulvalene (TSeF) but the metallic state of the TCNQ salt was not stable throughout the entire temperature range studied<sup>57</sup>. The effect of changing the symmetry of the TTF donor has also been examined<sup>58</sup> using the asymmetric donor trimethylene-tetrathiofulvalene (t-TTF), but this was found to have a detrimental effect on the physical properties. Similarly, studies of the TCNQ salt of tetramethyl-tetraselenafulvalene (TMTSF), the tetramethyl analog of HMTSF, have been undertaken<sup>59</sup> in an attempt to understand the factors influencing the stability of the metallic state. Tetrathiotetracene (TTT), unlike the other donors mentioned, is not a derivative of TTF, but the complex (TTT)(TCNQ)<sub>2</sub> also undergoes a metal to semiconductor transition<sup>60</sup>. However, the electrical and magnetic properties of (TTT)<sub>2</sub>I<sub>3</sub> proved more interesting with a recently reported<sup>61</sup> stable metallic state down to 3.3K, but a variety of suggestions followed<sup>62-64</sup> proposing different interpretations of the observed behaviour. An immense number of variations have in fact been investigated, the donors being mostly based on the prototype TTF.

In a similar way, effort has also been directed towards different acceptor molecules, for example, the bis-dithiolene(BDT) metal complexes<sup>65</sup>. The close analogy between these complexes and TCNQ has been noted<sup>66</sup> and they also form donor-acceptor compounds with organic molecules.

Tetracyanonaphthoquinodimethane (TNAP) is a larger molecule than TCNQ with lower symmetry and slightly higher electron affinity, but the complex TTF-TNAP was found not to exhibit a stable metallic state<sup>67</sup>. Similarly, salts of dicyanonaphthoquinone (DCNQ)<sup>68</sup>, tetrachlorodiphenoquinone (TCDQ) and its bromo analog (TBDQ)<sup>69</sup>, and dichlorodicyanobenzoquinone (DDQ)<sup>70</sup> have also been investigated, but the resistances observed were discouragingly high.

All these studies were attempts to understand the important interactions in the organic solid state governing the physical properties. Although conclusive explanations are still being sought, the importance of discovering the cause of stable metallic states in these compounds is clear, for the metallic state is a prerequisite for superconduction.

The search for a superconductor has not been restricted to organic systems and one of the most interesting classes is that of the square planar complexes of transition metals. An example of a one-dimensional metallic conductor is the mixed valence organometallic compound  $K_2Pt(CN)_4Br_{0.3} \cdot 2.3H_2O$ <sup>71</sup>. Here, the linear conducting chains consist of squares carrying the metal atom at the centre and cyanide groups at the corners (Figure 1.7(a)). The spacings between the adjacent metal atoms within the chains can be very short (0.28 to 0.29nm),

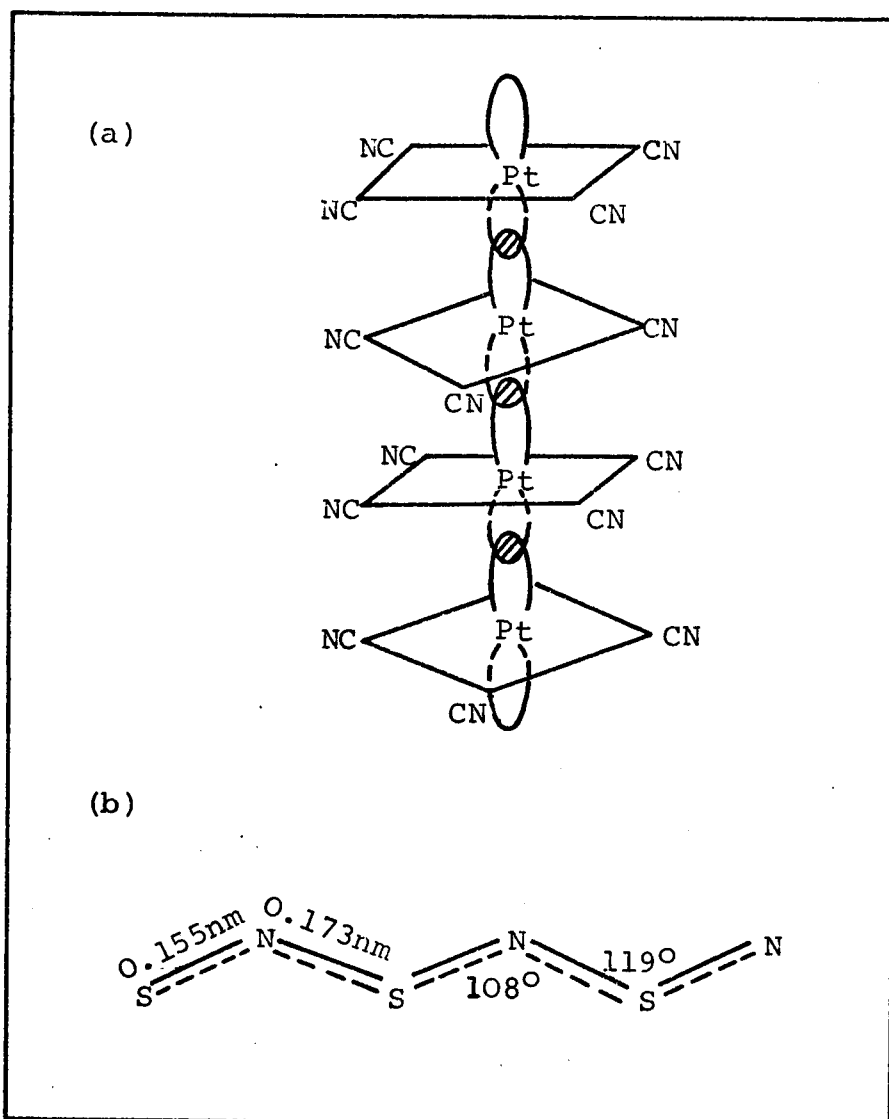


Figure 1.7

(a) Structure of  $\text{K}_2\text{Pt}(\text{CN})_4\text{Br}_{0.3} \cdot 2.3\text{H}_2\text{O}$  showing the overlapping of the  $d_z^2$  electron orbitals.

(b) Structure of the inorganic polymer  $(\text{SN})_x$ .

giving rise to noticeable overlapping of the  $d_z^2$  electron orbitals.

Although Little's hypothesis has yet to be substantiated, the most promising development with regard to this is the polymer polysulphur nitride  $(SN)_x$ , shown in Figure 1.7(b). This is an exception to most polymers in which the extent of the electron delocalisation within the chain is very small. This polymer has been known since 1910<sup>72</sup> but its significance has only recently been discovered<sup>73</sup>. Crystals of this inorganic polymer exhibit one-dimensional metallic conductivity over a temperature range extending from 300K to below 1K, with a weak maximum at 33K when measurements are performed along the chain axis. However, at 0.26K the polymer becomes superconducting and provides encouragement in the search for a high temperature superconductor.

#### 1.8 THE ROLE PLAYED BY ELECTRON SPIN RESONANCE IN THE STUDY OF TCNQ COMPLEX SALTS

Since the discovery of electron spin resonance (e.s.r.) by Zavoisky<sup>74</sup> in 1945, this technique has been an invaluable tool for the chemist, physicist and materials scientist interested in the properties of solids on an atomic scale. Biologists have also shown considerable interest in e.s.r. in a variety of plant and animal tissues and natural products.

The e.s.r. absorption of a free radical was first observed<sup>75</sup> in 1947 using the compound  $(C_6H_5)_5C_5$ . This observation paved the way for the use of e.s.r. in the investigations of solid CT complexes, which consist of free radical ions for a strong donor and strong acceptor. Early work was primarily concerned with establishing whether the observed paramagnetism of such solids was an intrinsic property of the solid or arose from impurities, and whether or not there was a connection between the solid's paramagnetism and its electrical conductivity.

Bijl, Kainer and Rose-Innes<sup>10</sup> were the first to consider the temperature dependences of the e.s.r. signal intensities of solid CT complexes, the compounds they studied being a series of complexes based on quinones and p-phenylenediamines. In all cases, strict conformity to a Curie Law dependence was observed, indicative of doublet state species. Subsequent to this study, an exponential e.s.r. intensity temperature dependence was reported<sup>76</sup> to be displayed by the perylene-iodine complex. This indicated that, in this case, the paramagnetism arose from species residing in higher multiplicities.

Similar results to the above have been obtained with TCNQ salts although, as previously mentioned, a wide variety of magnetic excitations is exhibited<sup>77</sup>. The most commonly found magnetic behaviour in TCNQ complexes is the existence

of a strong antiferromagnetic exchange interaction along the stacks and the absence of appreciable interaction between stacks. This results in pairwise spin correlation with a singlet ground state and a thermally-accessible excited triplet state. The extent of this interaction is dependent on the same structural parameters on which the conductivity depends. Therefore, e.s.r. studies on these complexes are invaluable in aiding in the interpretation of the electrical data.

The advantages of e.s.r. over static susceptibility measurements are listed below and outline the reasons why this particular technique is so applicable to the study of this family of organic solids:

(a) E.s.r. is a highly sensitive technique, allowing both single crystals and uncompactd powders to be studied. This is important as many TCNQ complexes are not readily prepared in crystal form.

(b) The wide variety of crystal structures exhibited by TCNQ complexes results in different spin interactions, therefore small variations in crystal structure can be investigated by paramagnetic susceptibility measurements.

(c) The one-dimensional linear arrays of TCNQ molecules separated by planes of cations result in large anisotropies, which are very difficult to interpret from static susceptibility measurements.

(d) The number of paramagnetic sites is readily established, not requiring knowledge of the diamagnetic correction, which could introduce errors if not known precisely.

(e) E.s.r. absorption lines may show a hyperfine splitting by nuclei in the solid, therefore leading to information about the localisation of the unpaired electron.

There is a co-ordinated effort in this department to achieve an understanding of the physical properties of TCNQ complex salts in the solid state. The investigations include a.c. and d.c. conductivity, Seebeck effect, crystal structure and magnetic properties. The aim of the work presented in this thesis is to investigate, interpret and correlate the e.s.r. data, obtained using crystalline and polycrystalline forms of TCNQ complex salts, with structural and electrical data in order to provide theoretical models consistent with the physical properties.

CHAPTER 2

MAGNETIC PROPERTIES

"The electron is not as simple as it looks."

Sir William Lawrence Bragg

1890 - 1971

## FORWARD

In the preceding chapter, mention was made of the three classes into which TCNQ complexes fall. By far the largest of these is the intermediate-conductivity class and these compounds exhibit the widest range of magnetic properties, which are interpreted in terms of triplet excitons. In this chapter, reference will occasionally be made, for the sake of simplicity, to doublet state species in order to explain fundamental aspects of the theory. However, later in the chapter, a more detailed account of the theory applicable to triplet excitons in TCNQ complex salts will be presented.

### 2.1 MAGNETIC PROPERTIES OF MATTER

All matter is electrical by nature and consequently has associated magnetic properties. The bulk magnetic property of a material is known as its magnetic susceptibility,  $\chi$ , and is defined in equation 2.1:

$$\chi_v = \frac{M}{H} \quad \dots (2.1)$$

where M is the magnetisation per unit volume of a material, and H is the applied magnetic field intensity. This equation gives, therefore, the volume susceptibility of the sample.

In all systems of units this quantity is dimensionless, but the actual value obtained with the c.g.s. system differs from the value obtained using the S.I. system by a factor of  $4\pi$ . In view of the overwhelming amount of

published work in this field using the non-rationalised c.g.s. system, all susceptibility values will be in these units throughout this thesis.

In the c.g.s. system, the volume susceptibility, although dimensionless, is expressed as electromagnetic units (e.m.u.). However, magnetic susceptibility can also be expressed in terms of the sample weight and this can be calculated from equation 2.2 in which  $\rho$  is the density of the sample in  $\text{g cm}^{-3}$ . The gram susceptibility would, therefore, have units of e.m.u.  $\text{cm}^3 \text{g}^{-1}$ .

$$\chi_g = \frac{\chi_v}{\rho} \quad \dots(2.2)$$

Similarly, equation 2.3 gives the molar susceptibility in units of e.m.u.  $\text{cm}^3 \text{mol}^{-1}$ , where M.W. is the molecular weight of the sample.

$$\chi_m = \chi_g \times \text{M.W.} \quad \dots(2.3)$$

The symbol H, used to represent the magnetic field intensity in equation 2.1, is also commonly used to represent the field strength in a sample. This quantity should be strictly denoted by B, defined in equation 2.4.

$$B = H + 4\pi M \quad \dots(2.4)$$

However, the relative difference between H and B is of the order  $10^{-6}$  -  $10^{-7}$  and so the use of H instead of B is of no practical consequence in the absence of strongly magnetic materials. B and H are both expressed in the

same units (gauss) and, in accordance with the majority of the literature, H is used in this thesis to represent the field strength in a sample.

Magnetic susceptibility can have either a negative or a positive value, and materials having such susceptibilities are termed as diamagnetic or paramagnetic respectively (see Figure 2.1). These types of behaviour are very different and each is dealt with in the following two sections.

## 2.2 DIAMAGNETISM

Diamagnetism is associated with the tendency of electrical charges to partially shield the interior of a body from an applied magnetic field. This behaviour results from Lenz's law which states that, when the flux through an electrical circuit is changed, an induced current is set up in such a direction as to oppose the flux change. This induced current persists for as long as the magnetic field is applied in the case of a resistanceless circuit, in a superconductor, or in an electron orbit within an atom. The magnetic field produced by the induced current is opposite to the applied field, this resulting in a negative contribution to the magnetic susceptibility.

By restricting the application of Lenz's law to

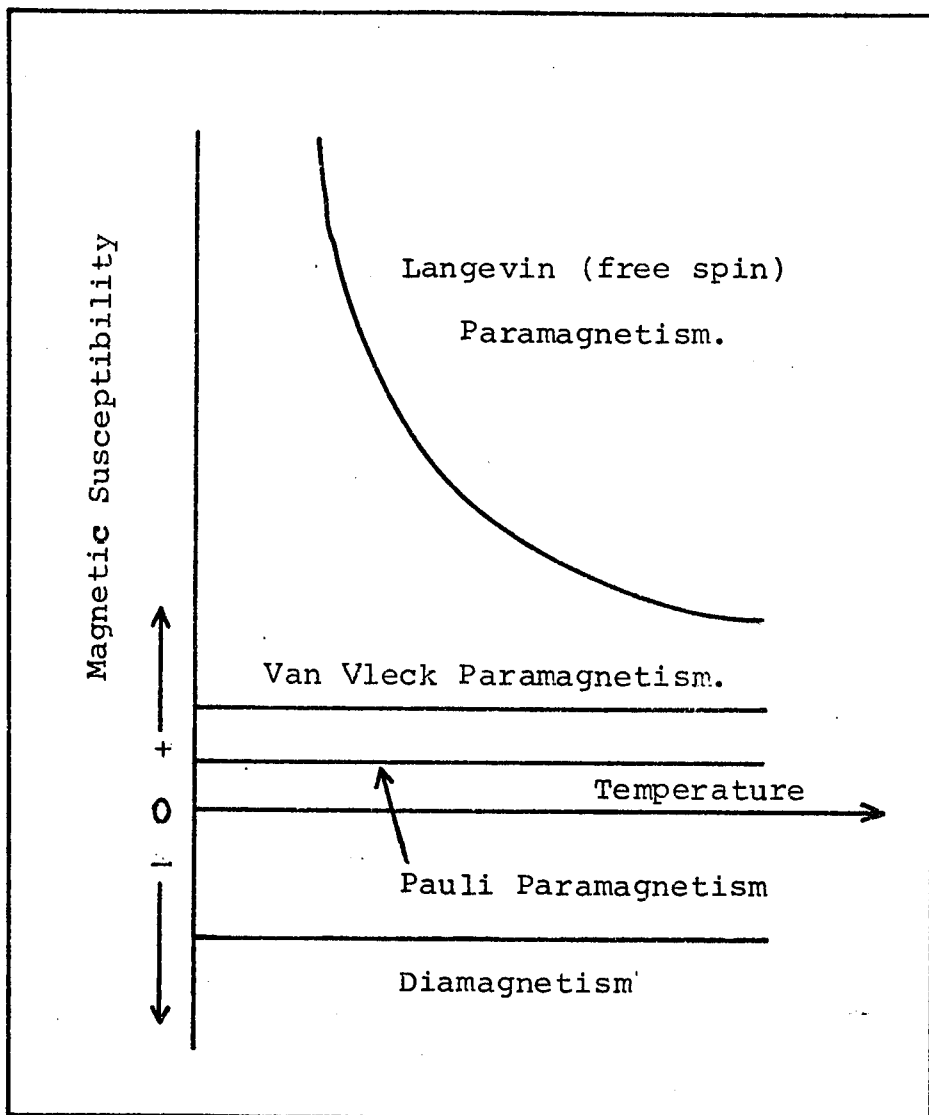


Figure 2.1

Characteristic relative magnitudes of the magnetic susceptibilities of diamagnetic and paramagnetic substances.

monoatomic molecules, the concept of diamagnetism can be treated using the Larmor theorem<sup>78</sup>. Briefly, this states that the motion of electrons around a central nucleus in a magnetic field is the same, to first order, as the motion in the absence of the field, except for a precessional motion superimposed upon the resultant magnetic moment vector. This Larmor precession (Figure 2.2) is in such a direction as to produce a magnetic moment opposite to the direction of the applied field. The angular frequency of precession,  $\omega$ , is called the Larmor frequency and is related to the applied field,  $H$ , by equation 2.5:

$$\omega = \gamma H \quad \dots (2.5)$$

where  $\gamma$  is the magnetogyric ratio of the electron, that is, the ratio of the magnetic moment to the angular momentum. It is important to note that the precession frequency does not depend on the angle of inclination,  $\theta$ .

Quantum-mechanical and classical (Langevin) treatments of this behaviour both result in equation 2.6 for the diamagnetic susceptibility per unit volume.

$$\chi = \frac{-NZe^2 \overline{r^2}}{6mc^2} \quad \dots (2.6)$$

In this expression,  $Z$  is the number of electrons per atom,  $N$  is the number of atoms per unit volume,  $e$  and  $m$  are the electronic charge and mass respectively,  $c$  is the velocity of light, and  $\overline{r^2}$  is the mean square distance of the electrons from the nucleus.

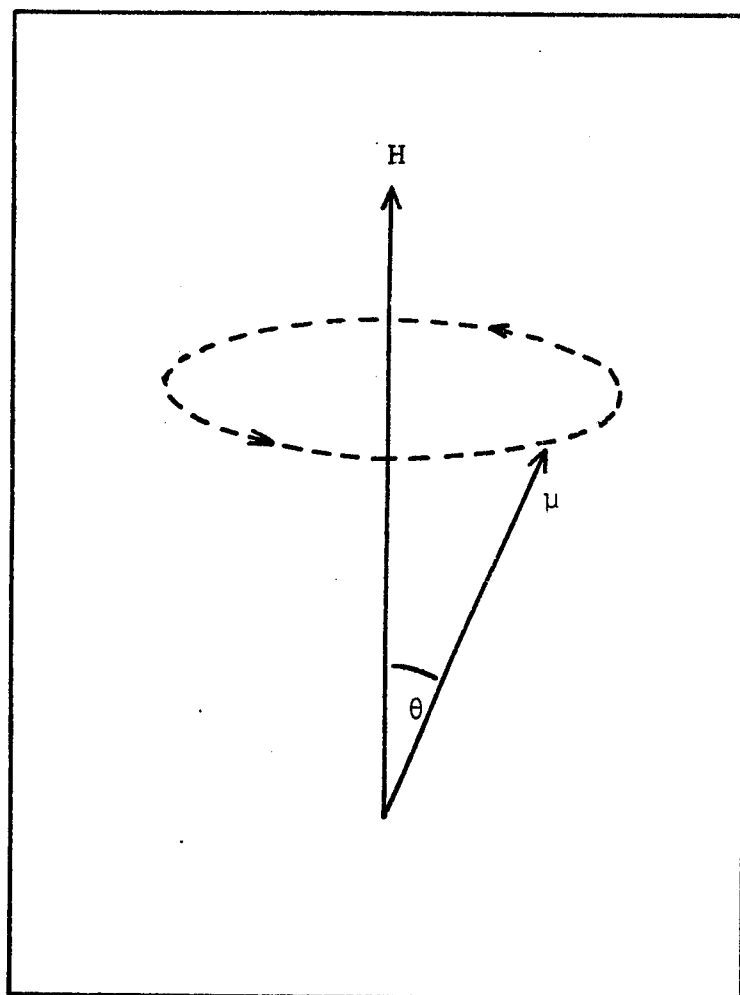


Figure 2.2

Precessional motion of the magnetic dipole,  $\mu$ , of an electron about the direction of the applied magnetic field,  $H$ .

$\theta$  is the angle between the axis of the dipole and the field direction.

It can be seen from equation 2.6 that the problem of calculating the diamagnetic susceptibility is reduced to the evaluation of  $\overline{r^2}$ , which amounts to the determination of the electron charge distribution within the atom. Also, since the value of  $\overline{r^2}$  is practically unaltered by temperature, the susceptibility of a diamagnetic substance is temperature independent to a good approximation.

The derivation of the Larmor theorem assumes that the field direction is an axis of symmetry of the system and, therefore, equation 2.6 only applies to atoms and mononuclear ions. In most molecular systems this condition is not satisfied, and the treatment of this situation results in the addition of an extra term in the equation for the susceptibility. This second term is known as Van Vleck paramagnetism and will be discussed in section 2.3.2.

The work of Pascal<sup>79</sup> is generally accepted as having paved the way in the study of the diamagnetism of compounds and is still widely used as a basis for the calculation of diamagnetic corrections. However, more sophisticated equipment and a deeper theoretical knowledge have resulted in additive formulae which allow for more accurate estimations<sup>80</sup>. Evaluation of the diamagnetic susceptibility of organic molecules is complicated by the

fact that the law of additivity must be supplemented with structural contributions, and by the frequently strong anisotropy of ring molecules. This is one reason why the study of magnetic properties of organic anion radical salts is best accomplished using e.s.r., which requires no knowledge of the diamagnetic correction.

### 2.3 PARAMAGNETISM

Electronic paramagnetism (positive contribution to  $\chi$ ) is found in:

(a) Atoms, molecules, and lattice defects possessing an odd number of electrons, as here the total spin of the system cannot be zero.

(b) Free atoms and ions with a partly filled inner shell.

(c) A few compounds with an even number of electrons, but in which two or more are unpaired, for example, molecular oxygen, and excited triplet states.

(d) Metals.

Paramagnetism can be wide ranging in both its magnitude and temperature dependence, and can be classified into three groups, each of which will be individually discussed in the following sections.

#### 2.3.1 The Curie Law

The most commonly found paramagnetic behaviour is where the susceptibility is inversely proportional to

temperature and is associated with the existence of permanent magnetic dipoles within the sample. The electrons in a system are known to be spinning about their own axes and, having mass, they possess angular momentum. It is by virtue of this fact that an electron has associated with it a magnetic dipole, the magnitude of which is usually discussed in terms of its magnetic moment,  $\underline{\mu}$  (the underlining denotes a vector quantity). This magnetic moment is related to the angular momentum by equation 2.7.

$$\underline{\mu} = -g \times \beta \times \text{Angular Momentum} \quad \dots(2.7)$$

The symbol  $\beta$  represents the Bohr magneton which is defined as  $eh/4\pi mc$ , where  $h$  is Planck's constant and  $e$ ,  $m$  and  $c$  represent the same quantities as defined in equation 2.6. The introduction of  $\beta$  into the equation arises from the quantum-mechanical result that angular momentum is quantised and can only take values which are integral multiples of  $h/2\pi$ . The quantity  $g$  is a dimensionless constant called the spectroscopic splitting factor and is used in the equation to allow for the various ratios of spin and orbital momenta (having the quantum numbers  $\underline{s}$  and  $\underline{l}$  respectively for a single electron) which make up the total angular momentum. If the electron only possesses orbital angular momentum,  $g$  is equal to 1 whereas, for an electron possessing only spin angular momentum, quantum-mechanics shows  $g$  to be equal to 2.00232.

For systems with more than one electron, angular momenta are combined vectorially to give a resultant, designated by quantum number  $\underline{J}$ . The usual procedure for doing this is known as Russell-Saunders coupling, which involves obtaining the vector sums  $\underline{L}$  and  $\underline{S}$ , of  $\underline{l}$  and  $\underline{s}$  respectively for all the electrons, the vector sum of  $\underline{L}$  and  $\underline{S}$  then giving  $\underline{J}$ .

For a free atom or ion, the spectroscopic splitting factor can then be calculated from the Landé equation given by equation 2.8.

$$g = 1 + \frac{J(J+1)+S(S+1)-L(L+1)}{2J(J+1)} \quad \dots (2.8)$$

However, this has different values for an atom or ion in a crystal because the part of the magnetic moment arising from the orbital motion of the electrons is modified by the crystalline electric field. In some cases, where this field removes the orbital degeneracies, the orbital moment is greatly reduced (quenched) and  $g$  may then be very close to that of a free electron. Consequently, the  $g$  value cannot then be calculated and becomes an experimental parameter.

In a paramagnetic sample the individual dipoles align themselves along the direction of an applied magnetic field, so that the material possesses a resultant magnetisation. However, the tendency towards parallel orientation of the dipoles is opposed by thermal motion

within the lattice and this results in an inverse relationship between the susceptibility and temperature. This type of behaviour is governed by the Curie law, the classical derivation of which was given by Langevin using Boltzmann's statistics. The quantum-mechanical treatment<sup>81</sup> involves the occupancy of all the possible  $\underline{J}$  states, with population differences following the Boltzmann distribution as before, and results in equation 2.9 for the volume susceptibility.

$$\chi_v = \frac{Ng^2\beta^2 \underline{J}(\underline{J}+1)}{3kT} = \frac{C}{T} \quad \dots (2.9)$$

In the above expression,  $k$  represents the Boltzmann constant,  $T$  is the absolute temperature,  $C$  is the Curie constant, and the remaining symbols have been previously defined.

### 2.3.2 Van Vleck Paramagnetism and Pauli Paramagnetism

In section 2.2 the concept of diamagnetism was discussed and understood in terms of a non-magnetic ground state. However, as previously mentioned, if the field direction is not an axis of symmetry of the molecular system, the susceptibility expression contains an extra term which is paramagnetic. This results from the mixing of the non-magnetic ground state with an excited state having a permanent magnetic dipole. This contribution, called Van Vleck paramagnetism, is quite small in magnitude and is independent of temperature. Whether the material is diamagnetic or paramagnetic depends on which of these two terms in the susceptibility expression is the

greater.

Pauli paramagnetism is also temperature independent and quite small in magnitude. It is the type of magnetic behaviour exhibited by metals and arises from the conduction electrons, which might be expected to follow Curie law behaviour. However, the observed magnitude and temperature dependence of the paramagnetism differs from that expected from classical free electron theory. The correction of the theory to account for the paramagnetic behaviour of metals was made by Pauli<sup>82</sup> by application of the Fermi-Dirac distribution function.

In order to observe Curie-type behaviour, the dipoles within a material must align themselves along the direction of the applied magnetic field, and the net magnetisation results from the greater probability of parallel alignment to that of antiparallel alignment. Most conduction electrons, however, have zero probability of turning over when a field is applied because most electrons are spin-paired in orbitals. This results from the band structure of metals which require that all electronic states up to the Fermi level are doubly occupied at absolute zero. Therefore, at this temperature, there are no unpaired electrons to contribute to the susceptibility but, as the temperature is increased, the electrons within a range  $kT$  of the top of the Fermi

distribution are unpaired and have a chance to turn over in the field. This small percentage of the total number of electrons is the reason for the very small paramagnetic susceptibility observed, which is given by equation 2.10:

$$\chi_v = \frac{3N\beta^2}{2E_F} \quad \dots (2.10)$$

where  $E_F$  represents the Fermi energy.

In the derivation<sup>81</sup> of the above equation, the spatial motion of the electrons was assumed to be not affected by the magnetic field. However, the wavefunctions are indeed modified by the magnetic field and Landau<sup>83</sup> has shown that, for free electrons, this causes a diamagnetic effect equal to one third of the paramagnetic contribution. Therefore, the resulting expression for the paramagnetism of metals is given by equation 2.11.

$$\chi_v = \frac{N\beta^2}{E_F} \quad \dots (2.11)$$

This can also be of the form given in equation 2.12 where  $\chi_m$  is the molar susceptibility and  $N_F$  is the density of states at the Fermi level<sup>84</sup>.

$$\chi_m = 64 \times 10^{-6} \times N_F \quad \dots (2.12)$$

### 2.3.3 Ferromagnetism, Antiferromagnetism and Ferrimagnetism

Ferromagnetism, antiferromagnetism and ferrimagnetism are three groups of magnetic behaviour which are known collectively as co-operative phenomena. | A ferro-

magnet is a material having a magnetic moment even in zero applied magnetic field, which indicates that the electron spins and their dipoles are arranged in a regular manner. This orientation must be due to some internal interaction tending to line up the magnetic moments parallel to each other. Weiss<sup>85</sup> was the first to postulate an internal magnetic field, as well as being referred to as the Weiss field. The orienting effect of this field is opposed by thermal agitation and, at elevated temperatures, the spin order is destroyed. Consequently, the spontaneous magnetic moment is only present in a certain temperature range, and the temperature above which this magnetisation vanishes is known as the Curie temperature,  $T_c$ . Below  $T_c$ , the material exhibits ordered ferromagnetic behaviour and, above  $T_c$ , a disordered paramagnetic phase results which follows a temperature dependence governed by the Curie-Weiss law, given in equation 2.13.

$$\chi_v = \frac{C}{(T-T_c)} \quad \dots (2.13)$$

This expression describes fairly well the observed susceptibility variation in the paramagnetic region.

However, detailed calculations predict a slightly different behaviour at temperatures close to  $T_c$ , in general agreement with experimental data, and the resulting expression is given in equation 2.14.

$$\chi_v = \frac{C}{(T-\theta)} \quad \dots (2.14)$$

The symbol  $\theta$  has a value which is appreciably greater than the actual transition temperature,  $T_c$ .

In an antiferromagnet, a similar ordering is present, only in this case the spins are arranged equally upon two sublattices. The dipoles upon each sublattice are antiparallel to those on the other. As there are an equal number of dipoles on each sublattice, there results a zero net moment in the temperature region where ordering is present. However, once again thermal energy destroys the order and the point at which this occurs is known as the Néel temperature,  $T_N$ . The magnetic behaviour of an antiferromagnetic also follows the Curie-Weiss law but with a slight modification, shown in equation 2.15.

$$\chi_v = \frac{C}{(T+\theta)} \quad \dots(2.15)$$

All the symbols in the above equation have been previously defined.

The term ferrimagnetic was originally used to describe an important class of magnetic oxides known as ferrites. This magnetic behaviour is very similar to the two types already discussed, ordering of the spins again being present. As in the antiferromagnetic case, a two sublattice model is applicable but the spins are not arranged equally between each sublattice. Instead, there is an excess of spins having a particular orientation.

This results in a spontaneous magnetisation below  $T_c$ , when the ordering is present.

Although all three types of behaviour are very similar, the magnitudes of their interactions with a magnetic field are considerably different. For a ferromagnetic material, the interaction is very strong, whereas the antiferromagnet exhibits a negligible interaction, and a ferrimagnetic material is intermediate between the two.

#### 2.4 ELECTRON SPIN RESONANCE

It is a fundamental postulate of the quantum theory that electrons possess angular momentum in integral multiples of a basic unit. Consequently, the associated magnetic moment must also be quantised, corresponding to a finite number of possible orientations with respect to an external magnetic field. Each orientation represents a discrete energy level and transitions between them may be induced, under appropriate conditions, by interaction with electromagnetic radiation. For a single unpaired electron in a doublet state, there are only two possible orientations, with the axis of the magnetic dipole approximately parallel or antiparallel to the direction of the external magnetic field. By absorbing energy from the electromagnetic radiation, the spin of the electron can be reversed. It is this phenomenon which forms the basis of the electron spin resonance method of studying para-

magnetic materials. In order to explain this technique more fully, it is necessary to examine the way in which the magnetic properties of the electron follow from its orbital and spin motion, and how the resulting dipole interacts with a magnetic field. These concepts will be outlined in the next two sections and will be followed by a discussion of the conditions necessary for energy absorption to occur.

#### 2.4.1 Magnetic Properties of the Electron

In atoms and molecules, electrons move around the nuclei in orbitals, and it is the motion of the electron which produces a magnetic dipole moment. The phenomenon of orbital angular momentum was used by Bohr<sup>86</sup> to predict the position and number of lines observed in the hydrogen atomic absorption spectra. However, it was found that Bohr's theory did not explain the absorption spectra of the more complicated atoms, and did not predict the doublets observed in the spectra of alkali metals. This indicated that the description of the energy levels in terms of orbital angular momenta alone was inadequate. Uhlenbeck and Goudsmit<sup>87</sup> postulated the existence of an additional angular momentum term associated with the rotation of the electron about its own axis. Evidence in support of electron spin followed when Pauli<sup>88</sup>, at approximately the same time as Darwin<sup>89</sup>, produced a wave equation for the electron which incorporated this concept. Further evidence also became available when Dirac<sup>90</sup> showed that

the solution of the Schrödinger equation resulted in spin momentum, after allowance had been made for a relativistic correction.

Like orbital momentum, spin momentum is also quantised and this was demonstrated most effectively by the Stern-Gerlach experiments<sup>91,92</sup>. A beam of alkali metal atoms was passed through a strong inhomogeneous magnetic field which provided a deflecting force, the direction of the deflection depending on the orientation of the dipole. If only two quantised spin states are possible, the atoms should emerge in two narrow beams rather than in a diffuse band, and this is exactly the behaviour observed.

The magnitude of the magnetic moment associated with the spinning electron has approximately twice the value of the moment associated with its orbital momentum, and it is the combination of both these momenta which determine the resultant magnetic moment,  $\mu$ , as described in section 2.3.1. The practical significance of the relations between orbital and spin angular momenta and the associated magnetic moments may be illustrated by considering their interaction with a magnetic field.

#### 2.4.2 Interaction of a Dipole with a Magnetic Field

The energy of a magnetic dipole of moment  $\mu$  in

a field  $H$  is given by equation 2.16.

$$E = - \mu H \cos\theta = - \underline{\mu} \cdot \underline{H} \quad \dots (2.16)$$

where  $\theta$  is the angle between the axis of the dipole and the field direction (see Figure 2.2). Therefore, different orientations of the electronic magnetic moment vector correspond to different energies. However, quantisation restricts the number of possible orientations. For an atom with total angular momentum  $\underline{J}$ , there are  $(2J+1)$  possible orientations, designated by a magnetic quantum number with the values  $M_J = J, J-1, J-2, \dots, -J$ . This quantum number is the component of the total angular momentum in the direction of the applied field, and only these values have physical significance.

If the magnetic moment is derived from spin angular momentum only, i.e.  $\underline{L} = 0$ ,  $M_J$  may be replaced by  $M_S$ . The constant component of the magnetic moment in the field direction is then given by equation 2.17:

$$\underline{\mu}_S = -g\beta M_S \quad \dots (2.17)$$

where  $g$  is the spectroscopic splitting factor and  $M_S = S, S-1, \dots, -S$ . The symbol  $S$  denotes the total spin angular momentum and, for a system containing  $n$  electrons, can take the values  $n/2, (n/2)-1, \dots, -n/2$ . The corresponding energy levels for the atom are, therefore, given by equation 2.18.

$$E = g\beta M_S H \quad \dots (2.18)$$

Similarly, if the atom has a magnetic moment derived from orbital angular momentum only, i.e.  $\underline{S} = 0$ , the allowed energy levels in the presence of a magnetic field are given by equation 2.18 in which  $g$  equals one and  $M_S$  is replaced by  $M_L$ .

#### 2.4.3 The Resonance Condition

In the absence of a magnetic field, the energy levels discussed in the last subsection are degenerate. However, the application of a magnetic field removes this degeneracy and this phenomenon is known as the Zeeman effect. The splitting of the energy levels allows transitions to occur between them, if the required energy is available. In order to explain the conditions which govern these transitions, the simple case of a free spin will be discussed, that is, a single electron having no orbital angular momentum.

The spinning motion of the electron can be clockwise or anticlockwise and results, therefore, in only two spin states, which are degenerate in the absence of a magnetic field. The magnitude of the spin angular momentum for a single electron is  $\frac{1}{2}h/2\pi$ , where  $h/2\pi$  is the basic unit postulated by Bohr. Consequently, an electron is commonly referred to as having a spin of  $\frac{1}{2}$ . The spin state resulting from anticlockwise rotation is denoted as the  $\beta$  or 'spin-down' state and corresponds to the situation

in which the dipole moment is parallel to the magnetic field. Clockwise rotation results in an antiparallel alignment of the dipole moment with the field and is referred to as the 'spin-up' or  $\alpha$  state. Consequently, the moments associated with the two spin states are in opposite directions. These components of the spin angular momentum for a single electron are often denoted by the quantum number  $m_s$ , which is equal to  $+\frac{1}{2}$  for the  $\alpha$  state and  $-\frac{1}{2}$  for the  $\beta$  state.

Substituting these two values into equation 2.18 yields equations 2.19 and 2.20 which give the energies,  $E_{m_s}$ , of the two spin states in a magnetic field.

$$E_{+\frac{1}{2}} = \frac{g\beta H}{2} \quad \dots (2.19)$$

$$E_{-\frac{1}{2}} = \frac{-g\beta H}{2} \quad \dots (2.20)$$

The energy difference,  $\Delta E$ , between these two Zeeman levels is, therefore, given by equation 2.21.

$$\Delta E = g\beta H \quad \dots (2.21)$$

It can be seen from this equation that the difference between the energy levels can be varied by changing the magnitude of the magnetic field  $H$  and, if  $g$  is constant, the divergence of the levels will be linear with field (Figure 2.3).

Transitions between the Zeeman levels can be induced by the introduction of electromagnetic radiation

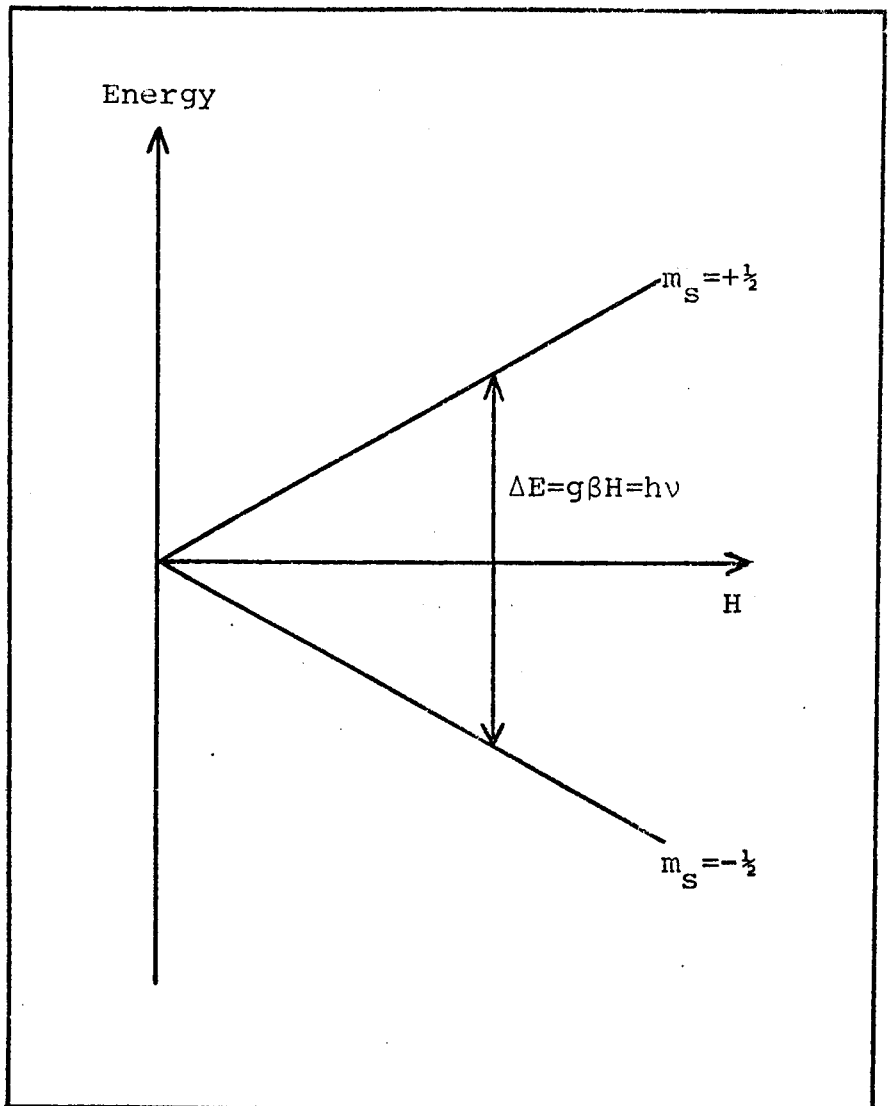


Figure 2.3

Zeeman energy levels for a single unpaired electron as a function of the magnetic field, H.

of frequency  $\nu$  such that the quantum of energy equals the separation of the levels. The resonance condition is, therefore, given by equation 2.22.

$$h\nu = g\beta H \quad \dots(2.22)$$

The interaction which causes the transitions is between the precessing magnetic dipole of the electron and the oscillating magnetic field accompanying the electromagnetic radiation. Consider the application of a field,  $H_1$ , perpendicular to  $H$ . The dipole,  $\mu$ , will experience an additional torque,  $\mu H_1 \cos\theta$ , tending to cause precession about  $H_1$  (Figure 2.4). At this point it is important to note that the oscillating magnetic field can be regarded as the combination of two magnetic vectors rotating with the same frequency but in opposite directions. One of these vectors will be rotating in the same direction as the precessing dipole and, if this component is rotating about  $H$  with the same frequency as the dipole, a change in  $\theta$  will result. Since a change in  $\theta$  corresponds to a change in energy of the system, and there are only two allowed energy states for a single electron, the induced transition corresponds to the dipoles being 'flipped' from the parallel to the antiparallel state. In general, where there are more than two possible energy levels, the selection rule for such transitions is  $\Delta M_J = \pm 1$ .

In the case discussed above for the single

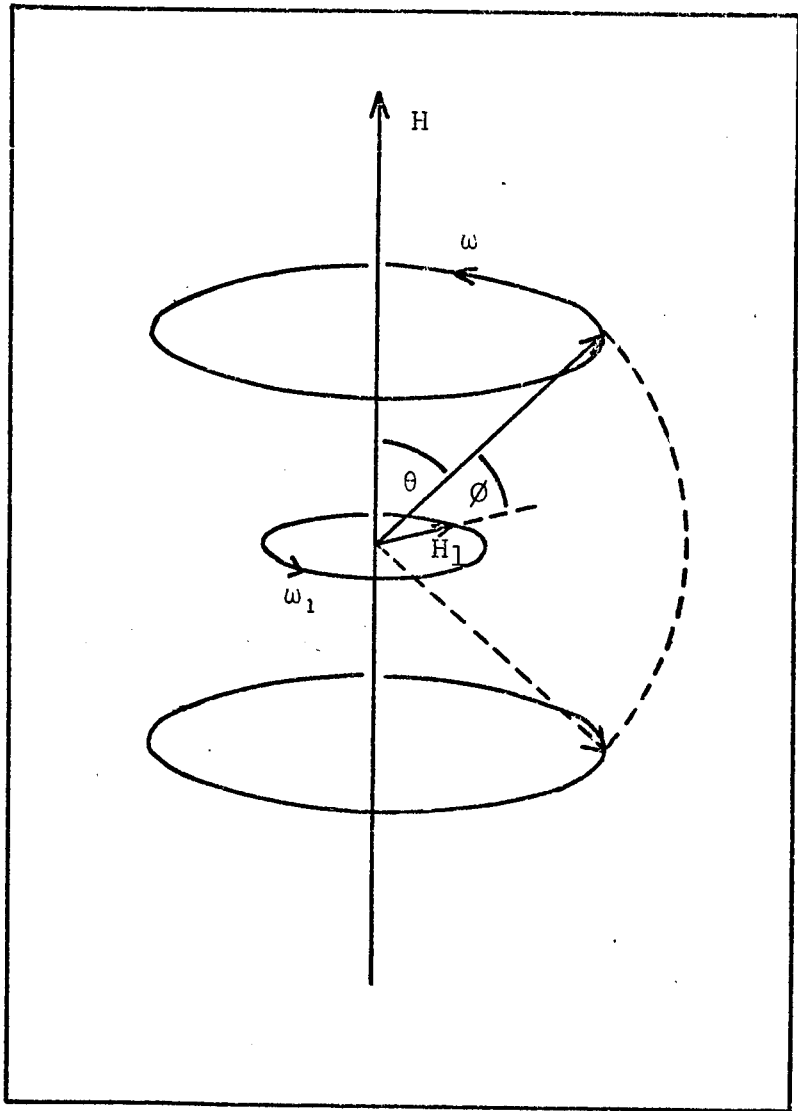


Figure 2.4

Precession of a magnetic dipole under the influence of a static magnetic field,  $H$ , and a rotating magnetic field,  $H_1$ .

unpaired electron, energy is absorbed by the sample, but induced emission can also occur with equal probability corresponding to the reverse process. If the system remains in thermal equilibrium, more spins are in the parallel state because of its lower energy, so that there is a net absorption of power from the electromagnetic radiation. The number of spins in the sample under study can be determined by the power absorbed and it is the detection of this absorption that forms the basis of e.s.r. spectroscopy.

So far in this section, the fundamental principles of e.s.r. have been outlined using the simplest case of a free electron. Detailed accounts involving more complicated examples can be found in references 93 and 94 and other standard texts on this subject.

Having established the conditions under which resonance absorption occurs, it is now necessary to investigate the various other interactions involved in order to interpret the spectra obtained using the technique of e.s.r.

#### 2.4.4 Relaxation Processes

It has been established that resonance absorption occurs because the population of the ground state and the upper state are not equal. However, if this were the only

process taking place, clearly the populations would rapidly be equalised and absorption would cease. Since the system must return eventually to the original Boltzmann distribution when the cause of the disturbance is removed, there must be a mechanism acting to restore the equilibrium. Such a mechanism is called a relaxation process, this concept first being introduced into magnetic resonance by Bloch<sup>95</sup>. Although originally formulated to describe the dynamic magnetic behaviour of nuclear spins, his theoretical treatment also applies in principle to electron spins, and the resulting Bloch equations form the basis of the study of relaxation.

One of the ways in which an electron in the upper state can lose its absorbed energy and return to the lower state is by spin-lattice relaxation. This implies a coupling between the species with the unpaired electrons (spin system) and the surrounding molecules known as the lattice. It is this interaction which provides the dominant relaxation process in e.s.r., and is characterised by a relaxation time  $T_1$ , which is the time for the spin system to lose  $1/e$ th of its excess energy.

Another relaxation process is one whereby a spin can communicate its energy to another spin. Although such interactions are not energy dissipating and, therefore, do not contribute directly in returning the spin system to

equilibrium, the spin-lattice transition may become enhanced if the spin-spin process brings the excess energy to a position for a favourable transition. The spin-spin or transverse relaxation time,  $T_2$ , is the time taken for this energy transfer between spins to take place and is often much more rapid than spin-lattice relaxation. Consequently, it is usually considered that spin-spin relaxation is the mechanism which keeps the spin system in internal equilibrium and that this system as a whole then relaxes to the lattice.

For the population difference to be maintained and resonant absorption to continue, it is essential that the dissipation of the excess energy is rapid, that is, the relaxation times must be short. Slow relaxation times can cause the populations of the upper and lower spin states to approach equally so that the rate of absorption of energy diminishes. This is known as saturation and is always avoided experimentally by ensuring that the energy from the microwave field is supplied to the spin system less rapidly than it can be transferred to the lattice.

#### 2.4.5 Lineshapes and Linewidths

It is now possible to comment on the width and the shape of the resonance absorption line. Lineshapes are determined by the types of interactions between the spin-system and its environment while the widths depend on

the strength of the interaction and the relaxation time.

It might be expected that all spins would absorb energy at one particular value of the magnetic field  $H$ . However, the existence of relaxation processes results in a broadening of the absorption line. Any mechanism which reduces the lifetime of the spin state causes a corresponding uncertainty in the energy content according to the Heisenberg uncertainty principle. This means that the energy absorption from the constant frequency oscillating field occurs over a range of magnetic field, resulting in an absorption line of finite width, which is inversely related to the relaxation time. Weak interactions between the spin system and its environment lead to long relaxation times and narrow lines, whereas short relaxation times and wide lines result from strong interactions.

In a simple homogeneous system, where relaxation is controlled by spin-lattice interactions and the energy absorbed from the radiation field is distributed so that the spin system maintains thermal equilibrium throughout the resonance process, the Bloch equations predict the lineshape should be Lorentzian (Figure 2.5(a)).

In an inhomogeneous spin system, the individual electrons find themselves in differing local magnetic fields. If the spin-spin interaction is slow compared

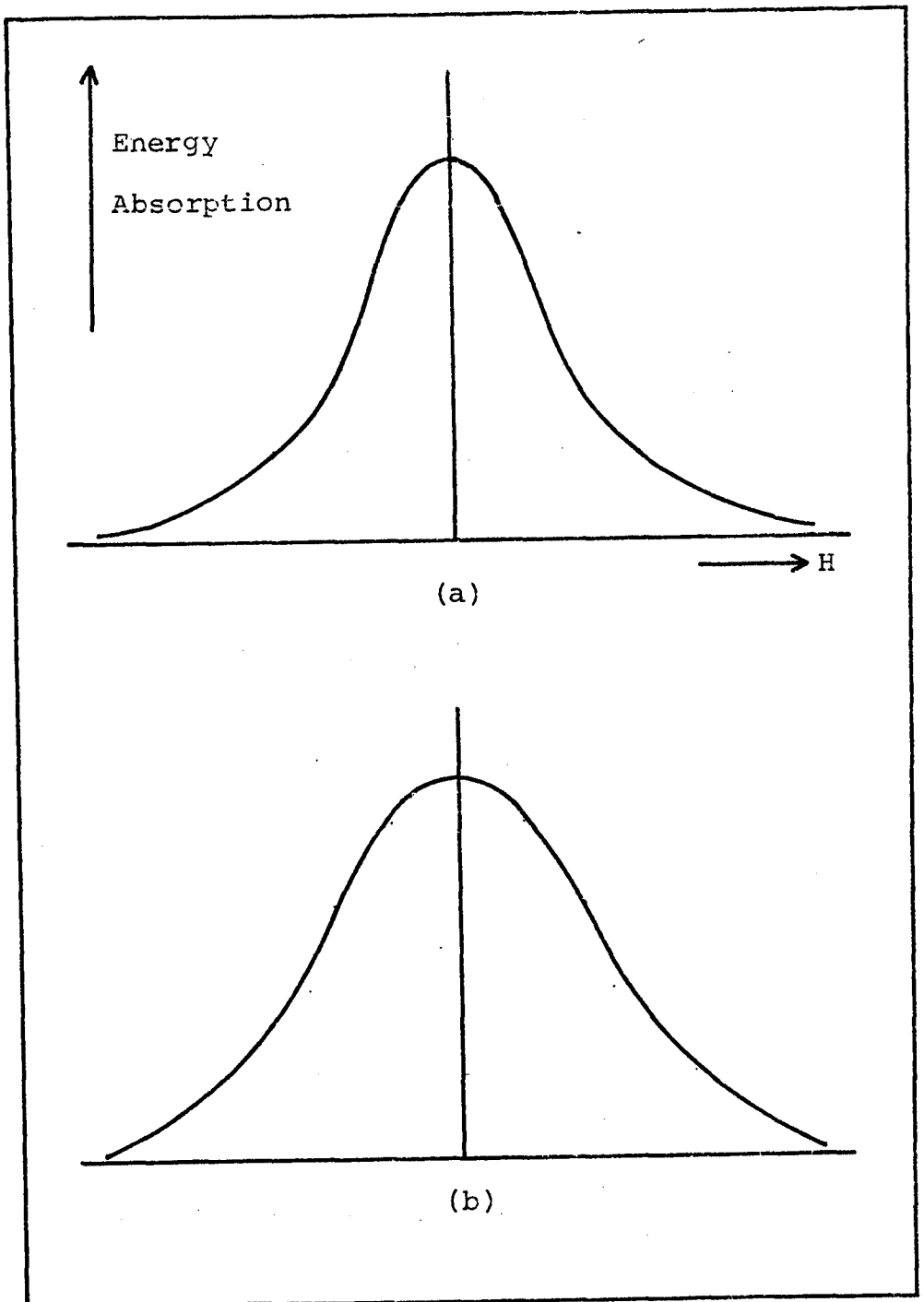


Figure 2.5

E.s.r. absorption curves

(a) Lorentzian lineshape.

(b) Gaussian lineshape.

with the relaxation to the lattice, the spin system will not reach thermal equilibrium and the absorption curve will have a Gaussian shape (Figure 2.5 (b)).

Therefore, the actual shape of the absorption curve is determined by the dominating relaxation process. However, the energy levels in spin systems can be broadened in various other ways, thereby adding to the linewidth. These sources of line broadening can be categorised<sup>96</sup> as homogeneous or inhomogeneous and are given below:

Homogeneous:

- (a) Dipole-dipole interaction between like spins.
- (b) Spin-lattice relaxation.
- (c) Interaction of spins with the radiation field.
- (d) Motion of the unpaired spins in the microwave field.
- (e) Diffusion of the spin system excitation through the paramagnetic sample.
- (f) Motionally narrowed fluctuations in the local field.

Inhomogeneous:

- (a) Hyperfine interactions.
- (b) Anisotropy of the splitting of the spin levels.
- (c) Dipolar interactions between spins with different Larmor frequencies.
- (d) Inhomogeneities in the applied magnetic field.

The spin system as a whole remains in thermal equilibrium throughout spin resonance only if the line broadening effects are homogeneous, and Lorentzian lineshapes result. In the case of inhomogeneous broadening, different groups of spins experience differing local fields which may arise from any of the points listed above in this category, and result in a Gaussian shape.

#### 2.4.6 Fine Structure

In section 2.4.2, mention was made of the number of allowed energy levels for an atom in an applied magnetic field. For an atom having a total spin  $S$ , there are  $(2S+1)$  levels and the situation for  $S=\frac{1}{2}$  has been previously discussed. However, many situations occur for which  $S>\frac{1}{2}$  and more than two magnetic levels result. In the presence of crystalline electrostatic fields, the degeneracy of these energy levels may be removed even in the absence of an external field, this phenomenon being known as zero-field splitting. Such a situation is illustrated for the case of  $S=\frac{3}{2}$  in Figure 2.6. Transitions occur, governed by the selection rule  $\Delta M=\pm 1$ , between the energy levels but the observed lines are situated at different field values. The multiple spectral lines are called fine structure and their relative positions will depend on the orientations of the crystal in the magnetic field. This is because the crystalline fields are essentially anisotropic in nature, being governed by the symmetry of the crystal.

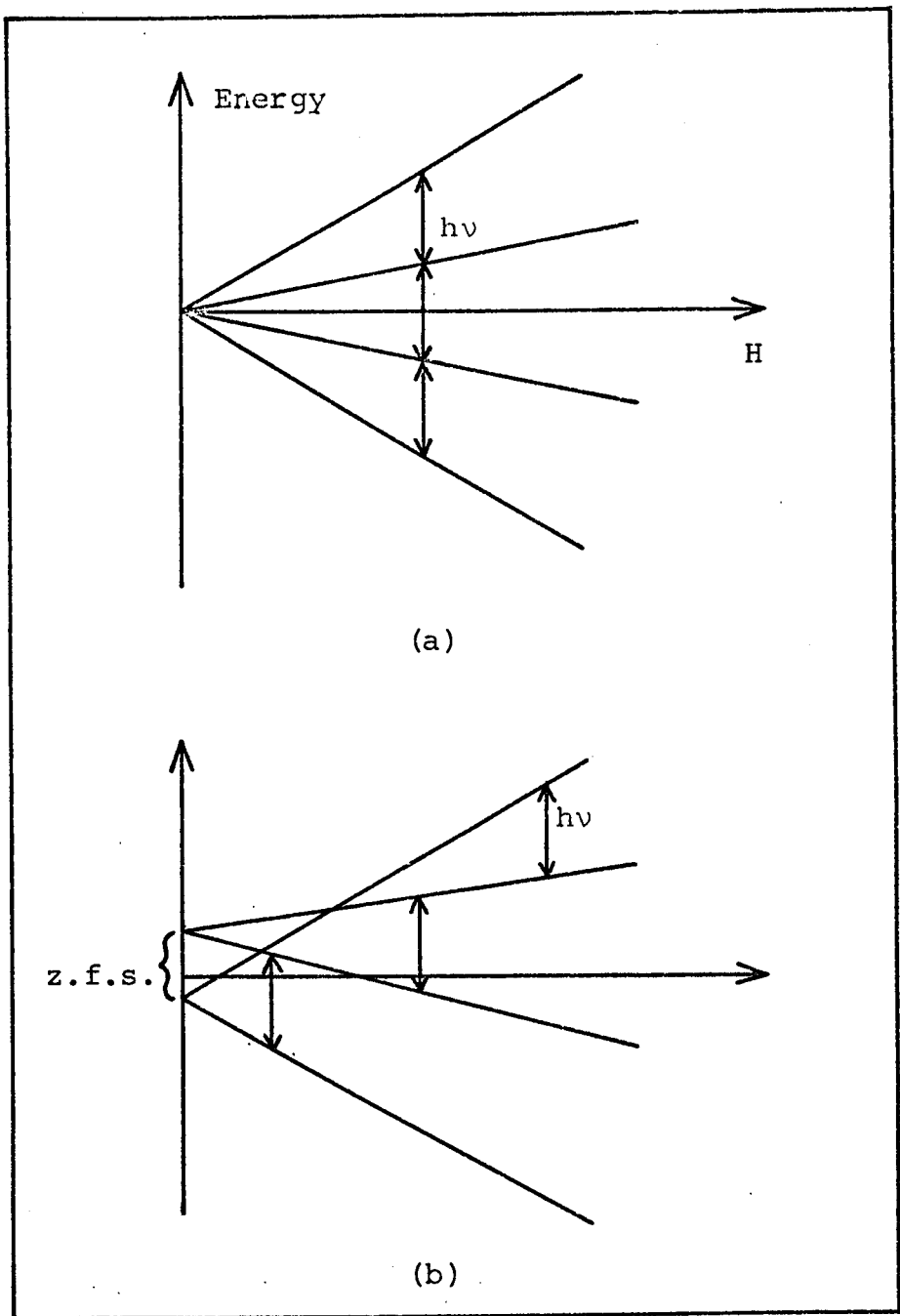


Figure 2.6

Energy levels for a system with spin  $S=3/2$  as a function of the magnetic field,  $H$ .

(a) With no zero-field splitting, giving only one absorption.

(b) With zero-field splitting, giving three absorption peaks.

The specific case of this effect for a triplet state species, having  $S=1$ , involves the magnetic dipolar interaction between two electrons, and will be discussed in more detail in section 2.5, which deals with the theoretical models applicable to TCNQ complex salts.

#### 2.4.7 Nuclear Hyperfine Structure

If the nucleus of the paramagnetic atom also possesses a resultant angular momentum and hence a magnetic moment, this will interact with the magnetic field. Nuclear spin is, of course, also quantised and there are  $(2I+1)$  possible orientations of the nuclear magnetic moment vector with respect to the field. The symbol  $I$  is the nuclear spin value and  $M_I$  is the nuclear magnetic quantum number. The interaction of the nucleus with the field is very much smaller than that of the electron. Consequently, the interaction of the unpaired electrons, having  $(2S+1)$  allowed energy levels, with such a nucleus causes each electronic energy level to be subdivided into  $(2I+1)$  components. Figure 2.7 illustrates this for the simplest case of an atom with  $S=\frac{1}{2}$ ,  $I=\frac{1}{2}$  and  $L=0$ . In this diagram, the allowed transitions are shown and correspond to the selection rule  $\Delta M_S = \pm 1$ ,  $\Delta M_I = 0$ . As in the case of zero-field splitting, multiple spectral lines are observed and this additional splitting due to magnetic nuclei is known as hyperfine structure.

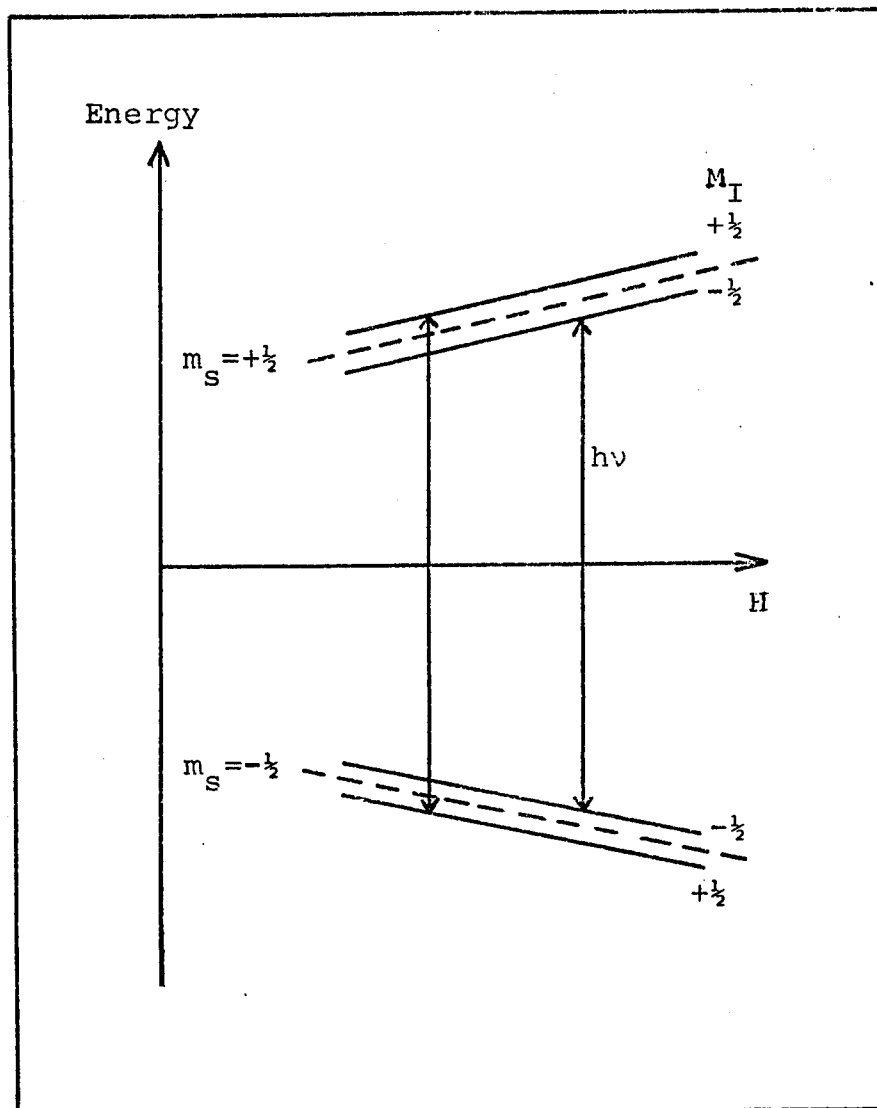


Figure 2.7

Energy levels and hyperfine splitting for a system with  $S = \frac{1}{2}$ ,  $I = \frac{1}{2}$ ,  $L = 0$ , as a function of magnetic field,  $H$ .

#### 2.4.8 Exchange Interactions

When paramagnetic atoms are brought close together, the orbitals of the unpaired electrons overlap and this gives rise to the quantum-mechanical concept of exchange. This treatment takes into account the impossibility of identifying the electrons in this situation with particular atoms. The energy of this interaction, for atoms  $i$  and  $j$  bearing spins  $S_i$  and  $S_j$ , contains the term given in equation 2.24.

$$U = -2J \underline{S}_i \cdot \underline{S}_j \quad \dots (2.24)$$

In the above expression,  $J$  is the exchange integral for the atoms  $i$  and  $j$  and is related to the overlap of the charge distributions.

The charge distribution of a system of two spins depends on whether the spins are parallel or antiparallel, for the Pauli principle excludes two electrons of the same spin from being at the same place at the same time. Therefore, the electrostatic energy of a system will depend on the relative orientation of the spins. The difference in energy is called the exchange energy and has an exchange frequency associated with it.

The importance of exchange lies in its effect on lineshape and linewidth. A strong indication of the presence of exchange interactions is the change from a

Gaussian to a Lorentzian lineshape. However, although strong exchange will narrow the e.s.r. line, it will not shift the Larmor absorption frequency<sup>97</sup>.

A further effect of strong exchange in crystals is the collapse of any nuclear hyperfine interactions. The initial effect is to broaden the hyperfine lines, and may even cause them to coalesce to give a single Lorentzian line, in which case the hyperfine splittings have been effectively reduced to zero.

#### 2.4.9 Convention of the Spin Hamiltonian

It is apparent that there are many interactions and effects to be considered when interpreting the absorption spectra in e.s.r. The usual approach to the theoretical problems of this sort is to express the interactions affecting the electronic energy levels in terms of Hamiltonian operators, each one representing the effect of a particular interaction. The sum of these gives the total Hamiltonian which describes the electronic interactions contributing to the total energy of the atom.

Calculations with the total Hamiltonian are very difficult, therefore a simplified accounting of the most likely interactions is performed with a spin Hamiltonian, originally developed by Abragam and Pryce<sup>98</sup>. The permitted energy levels of the spin system in a magnetic

field can be obtained from this spin Hamiltonian, represented by  $\mathcal{H}$ , using the following operator equation:

$$\mathcal{H} \psi = E_0 \psi \quad \dots (2.23)$$

where  $E_0$  represents the eigenvalues corresponding to the permitted energy levels, and  $\psi$  represents the wave functions of the effective spin states.

The magnitudes of the various terms in this Hamiltonian are measured by such parameters as the  $g$  factor, the zero-field splittings, and the hyperfine structure constants, all of which are experimentally observable.

## 2.5 MAGNETIC PROPERTIES OF TCNQ COMPLEX SALTS

The intermediate-conductivity class of TCNQ complexes is by far the largest group and has wide ranging magnetic properties. The low and high-conductivity classes, however, have magnetic properties which are usually readily interpreted and not so wide ranging. In general, the complexes exhibiting very low d.c. conductivities have been found to be essentially diamagnetic<sup>24</sup> and to have only very small e.s.r. signals, the behaviour of which approximately obeys the Curie law<sup>99</sup>. The complexes designated as metallic, however, have generally been observed to display Pauli paramagnetism<sup>24</sup>, with a Curie law contribution superimposed upon this, which is normally attributed to the presence of defects in the lattice<sup>100</sup>.

The work presented in this thesis has been entirely devoted to TCNQ complex salts in the intermediate-conductivity class, that is, compounds containing formally neutral TCNQ molecules in addition to the anion radicals, and which exhibit semiconducting behaviour. Therefore, the following discussion will be concerned with the observed magnetic properties and proposed interpretations for the complex salts which fall into this group.

### 2.5.1 Triplet Excitons

Mulliken's treatment<sup>101</sup> of CT complexes considered the ground state to be non-ionic in character. However, it was proposed<sup>10</sup> that a predominantly ionic ground state could be achieved using component molecules of very different electron affinities. Furthermore, it was suggested that the free radicals obtained in this situation could interact in the solid state to produce magnetic states of higher multiplicities than the simple doublet state of a single unpaired electron.

An exchange interaction between electron pairs was considered which gives rise to a ground singlet state and a thermally accessible triplet as the first excited state. The semiconducting TCNQ complex salts represent such a case and the resulting excitations have become known as triplet excitons, the size of which is approximately a unit cell along the chain. Since the ground state is the

singlet and the triplet state is higher in energy, the interaction is said to be antiferromagnetic and the energy gap between the two states is given by  $J$ . At absolute zero, the triplet state will not be populated but, as the temperature is raised, thermal energy excites the electrons into this excited state.

The singlet state is the energy level occupied by two electrons of opposite spin, therefore giving an effective spin of  $S=0$  and no e.s.r. absorption. The triplet state, however, consists of three degenerate energy levels and triplet excitons have magnetic properties characteristic of an effective spin of  $S=1$ . In the presence of an applied magnetic field, the degeneracy is removed and e.s.r. transitions can occur between these three Zeeman levels. The observed paramagnetism will, therefore, increase as the temperature is increased and the triplet state becomes more populated. The temperature dependence of the intensity  $I$  of the e.s.r. absorption, for the case of a ground singlet state and a thermally accessible triplet state, was found<sup>10</sup> to be that given in equation 2.25:

$$I/T \propto (\exp(J/kT) + 3)^{-1} \quad \dots (2.25)$$

where  $J$  is the energy difference between the singlet and triplet states, and  $k$  and  $T$  are as defined for equation 2.9.

The above expression was found to be a very good explanation of the activated paramagnetism exhibited by the

earliest semiconducting TCNQ complex salts investigated<sup>23,102</sup>. This provided evidence that the unpaired electrons associated with the stacked TCNQ molecules were indeed correlated, for a Curie law temperature dependence is expected for electrons having no such interaction.

The early investigations showed that TCNQ complex salts had very interesting magnetic properties, and were the start of intensive studies of the temperature dependence of the magnetic susceptibilities of these compounds. It was in such a study that equation 2.26 was introduced by Kepler<sup>24</sup>.

$$\chi = \frac{2Ng^2\beta^2}{kT} (3 + \exp(J/kT))^{-1} \quad \dots (2.26)$$

All the symbols in the above expression have been previously defined. However, if the susceptibility is a molar value, then N is Avogadro's number. This expression adequately described the behaviour of some of the semiconducting complex salts but was found not to agree with the observed magnitudes of the susceptibilities for others. Consequently, a temperature dependent value of J was introduced to account for the discrepancies, and this stimulated interest in more theoretical treatments of triplet excitons.

As previously mentioned, TCNQ complex salts have characteristic one-dimensional arrangements of the TCNQ

molecules with groups of 2, 3 or 4 molecules within the stacks. Therefore, the interaction between neighbouring unpaired electrons is of an alternating nature along the stacks. Consequently, the interaction behaviour of the spin system can be represented by the one-dimensional Heisenberg Hamiltonian, shown in equation 2.27.

$$\mathcal{H} = \sum_{i=1}^{\frac{1}{2}N} J (S_{2i} \cdot S_{2i+1} + \gamma S_{2i} \cdot S_{2i-1}) \quad \dots (2.27)$$

This Hamiltonian was the starting point of the early theoretical investigations of triplet excitons in TCNQ complex salts and numerous papers have appeared on the subject<sup>103-114</sup>.

The above expression represents the interaction of a pair of spins, denoted by  $2i$  and  $2i+1$ , which compose the  $i^{\text{th}}$  site and are coupled through the exchange integral  $J$ . There are  $N$  molecules, therefore resulting in  $N/2$  sites. Each spin of the  $i^{\text{th}}$  site interacts to a lesser extent with a spin from a neighbouring site with the exchange integral  $J\gamma$ , where  $\gamma$  is effectively an alternation parameter. This parameter describes the degree of non-uniformity of the exchange coupling between sites along the chain, and can have values between 0 and 1. The intrasite exchange integral  $J$  is expected to be larger than the intersite exchange integral  $J\gamma$  just from their distance dependence. This is represented schematically in Figure 2.8.

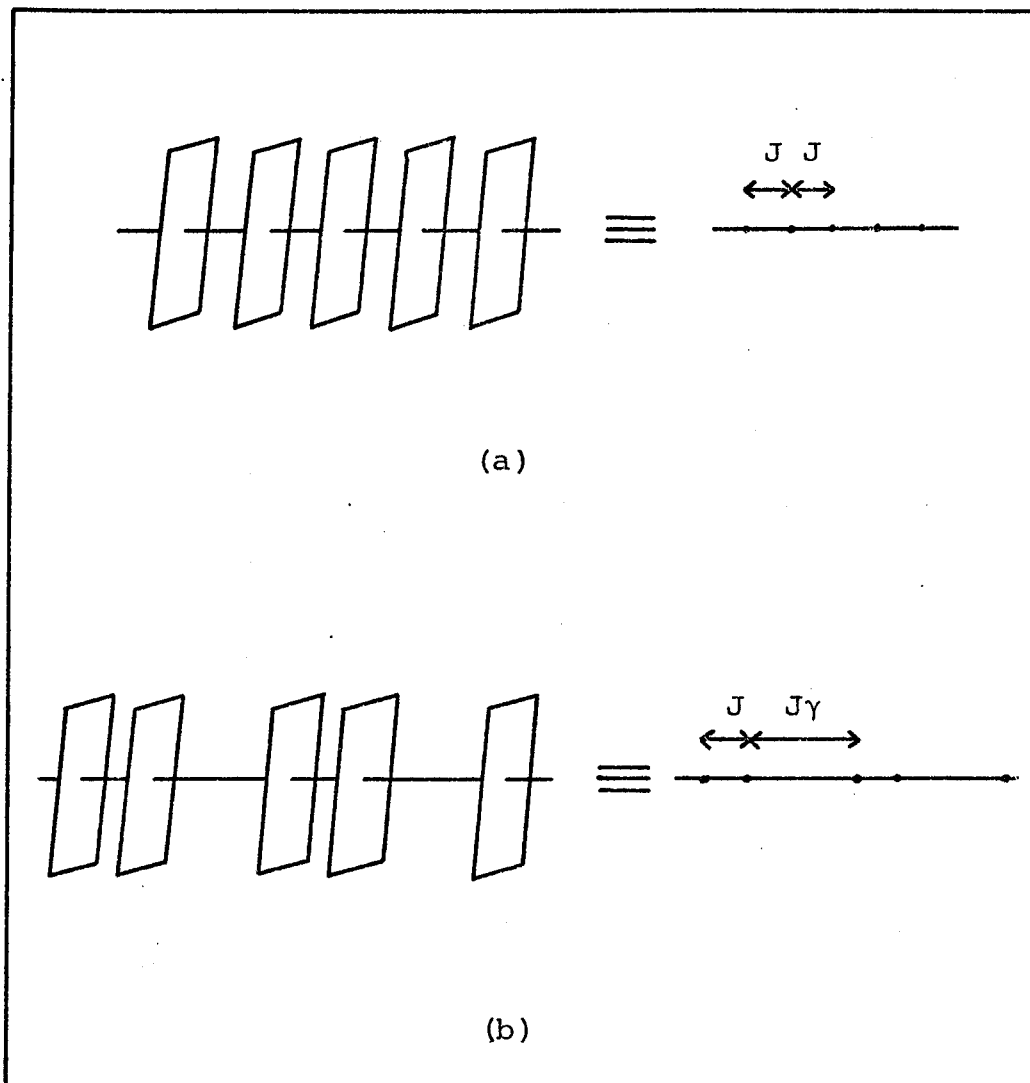


Figure 2.8

Schematic representation of (a) a regular and (b) an alternating one-dimensional array of exchange-coupled TCNQ molecules.

When an exciton is localised on one repeat unit within the stack and there is no interaction with the neighbouring site,  $\gamma$  equals zero and the solution to equation 2.27 yields equation 2.26. Therefore, this represents the limiting case of strong alternation and equation 2.26 is representative of localised triplet excitons. In the opposite extreme limit, where  $\gamma=1$ , the low lying excitations are spin waves with no gap in their energy spectrum and their properties have been worked out extensively<sup>111-113</sup>. However, values of  $\gamma$  between these two limits are less well understood, and in all the various treatments of this problem approximations have had to be employed to obtain solutions to the Hamiltonian. Lynden-Bell and McConnell<sup>104</sup> described the region where  $0 < \gamma < 1$  in terms of non-interacting mobile triplet excitons to account for various features of the e.s.r. spectra of TCNQ complex salts. Soos<sup>107</sup> attempted to solve the problem for all values of  $\gamma$  and his solution is in good agreement with experiment for  $\gamma < 1$ , but failed to agree with exact results known in the limit  $\gamma=1$ . Similarly, Duffy and Barr<sup>114</sup> tried to perform exact numerical calculations for the solution of equation 2.27 but again the work failed to explain the magnetic behaviour of the system in the limit  $\gamma=1$ .

One of the more promising treatments involves the application of narrow band theory to the electronic states of the TCNQ stack. Vegter<sup>115</sup> and Hibma<sup>116</sup> proposed that

the exciton states result from the interaction between an electron and a hole, which constitute the first excited state of the system. Such an exciton can be described<sup>117</sup> as being strongly bound (a Frenkel exciton, corresponding to  $\gamma=0$ ) or weakly bound (a Wannier exciton, corresponding to  $\gamma=1$ ), and band theory allows for all intermediate cases between these extremes. Although this treatment adequately explained the observations on a number of compounds studied<sup>116</sup>, it did not, however, reproduce equation 2.26, the limiting solution of equation 2.27.

The most promising treatment recently developed was first presented by Etemad<sup>118</sup> and this approach was based upon the theoretical studies of Bulaevskii<sup>113</sup>.

Etemad's treatment resulted in equation 2.28 which is the susceptibility expression for an infinite chain of spins with variable degrees of alternation.

$$\chi = \frac{2Ng^2\beta^2 a(\gamma)}{kT} \exp(-J\Delta(\gamma)/kT) \dots (2.28)$$

The term  $J\Delta(\gamma)$  represents the effective singlet-triplet energy gap. The only symbols not previously defined are  $a(\gamma)$  and  $\Delta(\gamma)$ , and these are tabulated values in Etemad's work that are dependent upon  $\gamma$  and the temperature range under investigation. In the limit of strong alternation,  $a(\gamma)$  and  $\Delta(\gamma)$  are both unity and, therefore, equation 2.28 is identical to the expression to which equation 2.26 reduces, once the inequality given in equation 2.29 is applied.

$$\exp (J/kT) \gg 3 \quad \dots (2.29)$$

It can be seen from equation 2.28 that a plot of  $\ln \chi T$  against  $1/T$  will have a slope of  $-J\Delta(\gamma)$ , and the intercept  $K$  on the natural logarithm axis is given by equation 2.30.

$$K = \ln \frac{(2Ng^2\beta^2 a(\gamma))}{k} \quad \dots (2.30)$$

From a knowledge of the intercept,  $a(\gamma)$  can be found and, from this, a value for  $\gamma$ ,  $\Delta(\gamma)$ ,  $J$  and  $W$ , the exciton bandwidth, which is also a tabulated function of  $\gamma$ . For  $\gamma=0$ , there is zero bandwidth and all the triplet excited states are degenerate, in contrast to the finite exciton bandwidth for  $\gamma \neq 0$ .

Although equation 2.28 is only strictly valid in the region  $0.035 < T/J < 0.25$ , and the whole approach is only applicable to situations where  $\gamma < \frac{1}{2}$ , this treatment has proved to be a valuable asset in the interpretation of the magnetic properties of semiconducting TCNQ complex salts. The importance of such an approach, which includes values of  $\gamma$  differing from zero, is that it allows for triplet exciton motion, which is essential for the explanation of the e.s.r. absorption spectra exhibited by these compounds. Consequently, this treatment will be used in this thesis to interpret the results obtained.

2.5.2 E.s.r. Spectral Characteristics Associated with Triplet Excitons in TCNQ Complex Salts.

While more accurate solutions of the spin Hamiltonian may lead to a better understanding of various details, the significant result remains the identification of the excited states as mobile triplet excitons. One of the consequences of this migration is that the hyperfine structure is not observed experimentally even at low temperatures and for all values of  $\gamma$ . Theoretical studies<sup>104,107</sup> reconciled this observation with the averaging of the nuclear hyperfine splittings to zero due to rapid propagation of the excitons along the linear chains. As the exciton moves from molecular entity to molecular entity, the nuclear spin state experienced by the triplet electrons is changing rapidly with time, and this places a lower limit on the 'jumping' rate of the exciton corresponding to the hyperfine frequencies involved. The observed effect on the e.s.r. spectrum of such a mobile triplet species is schematically shown in Figure 2.9.

Spectra of the type shown in Figure 2.9 (b) were first observed by Chestnut and Phillips<sup>23</sup> in a number of anion radical salts based on TCNQ. The two absorption lines are typical of species having an effective spin value of  $S=1$  and arise from the phenomenon of zero-field splitting, previously described in section 2.4.6. In this case, the degeneracy of the three energy levels comprising

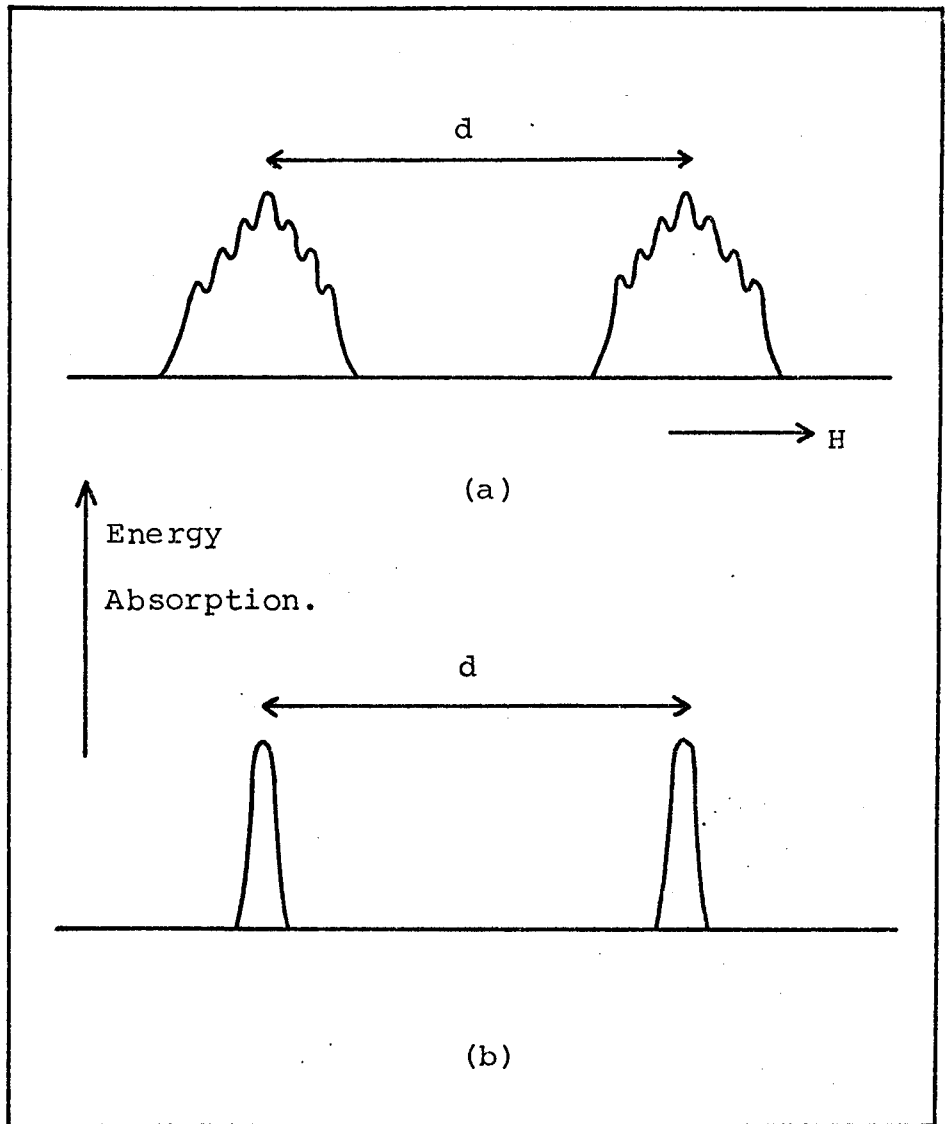


Figure 2.9

Schematic representation of the high-field e.s.r. spectrum of:

(a) a triplet exciton, confined on a single repeat unit, showing hyperfine structure.

(b) a highly mobile triplet exciton showing no hyperfine structure.

the triplet state is removed by the dipolar interaction of the two electrons. Therefore, on application of a magnetic field, the energy levels diverge, as shown in Figure 2.10, giving rise to two resonance absorption lines corresponding to transitions governed by the high-field selection rule of  $\Delta M = \pm 1$ . These transitions occur at widely different fields according to the orientation of the field, and this anisotropy is a direct result of the dipolar coupling of the two electrons.

A second consequence of this interaction is that the dipolar coupling may become comparable with the Zeeman energy,  $g\beta H$ , and it is no longer possible to assume that the two spin angular momentum vectors are independently quantised in the external field. This results in a breakdown of the usual selection rule and there is a small finite probability of observing the transition corresponding to  $\Delta M = \pm 2$ , which occurs at approximately half the field value appropriate to the  $\Delta M = \pm 1$  transitions. This probability increases if the microwave field is applied parallel to the external field, instead of perpendicular to it, as is normal in e.s.r. experiments.

A complete theoretical treatment<sup>119</sup> of dipolar interaction between two electrons resulted in equation 2.31, which is a two-electron Hamiltonian representing the magnetic interactions between the two spins and the field.

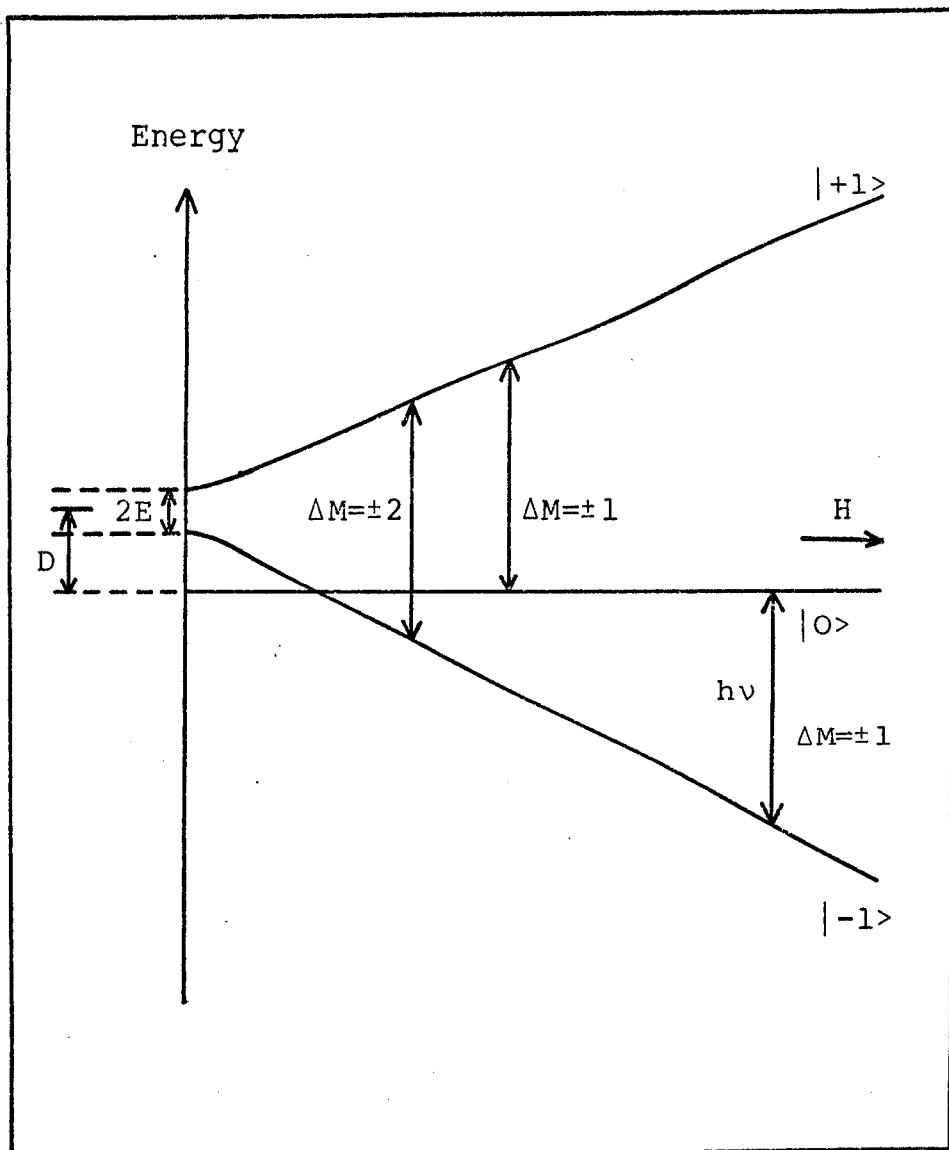


Figure 2.10

Energy levels and e.s.r. transitions as a function of magnetic field for an oriented triplet state molecule.

$$\mathcal{H} = \beta \underline{H} \cdot \underline{g} \cdot \underline{S} + 4\beta^2 \frac{\underline{S}_1 \cdot \underline{S}_2}{r^3} - \frac{3(\underline{r} \cdot \underline{S}_1)(\underline{r} \cdot \underline{S}_2)}{r^5} \dots (2.31)$$

In this expression, the subscripts 1 and 2 refer to the two electrons,  $r$  is their separation and  $S$  is the overall spin. In this treatment, spin-orbit coupling is neglected, and the zero-field energy levels, the spin wave functions of which are represented by equations 2.32 to 2.34, are evaluated by appropriate integrations over spatial coordinates.

$$|+1\rangle = \alpha\alpha \dots (2.32)$$

$$|0\rangle = (1/\sqrt{2})(\alpha\beta + \beta\alpha) \dots (2.33)$$

$$|-1\rangle = \beta\beta \dots (2.34)$$

The magnetic (dipolar) interaction between the two electrons can be expressed in terms of the zero-field splitting parameters  $D$  and  $E$ , and gives rise to the more familiar form of equation 2.31, given in equation 2.35.

$$\mathcal{H} = \beta \underline{H} \cdot \underline{g} \cdot \underline{S} + DS_z^2 + E(S_x^2 - S_y^2) \dots (2.35)$$

$S_x$ ,  $S_y$  and  $S_z$  are the quantised spin values in the directions  $x$ ,  $y$  and  $z$  respectively, and the above equation is only valid in the principal axes coordinate frame of the dipolar interaction. For an arbitrary orientation, the laboratory coordinate system will not coincide with the principal axes coordinate system. However, the two systems can be related through the Eulerian angles  $\phi$ ,  $\theta$  and  $\psi$ <sup>78</sup>, defined in terms of successive counterclockwise rotations about the axes  $z$ ,

$\eta$  and  $z'$  respectively (Figure 2.11). In the e.s.r. experiment, only  $\varnothing$  is varied as a crystal is rotated about an axis perpendicular to the static magnetic field, and the angular variation of the observed doublet separation,  $d$ , is given by equation 2.36<sup>23</sup>.

$$d = C_1 \cos^2 \varnothing + C_2 + C_3 \cos \varnothing \sin \varnothing \quad \dots (2.36)$$

The values of  $C_1$ ,  $C_2$  and  $C_3$  are related to the zero-field splitting parameters and are given by equations 2.37 to 2.39.

$$C_1 = 3D \sin^2 \theta - 3E \cos 2\psi (1 + \cos^2 \theta) \quad \dots (2.37)$$

$$C_2 = -D + 3E \cos 2\psi \quad \dots (2.38)$$

$$C_3 = 6E \sin 2\psi \cos \theta \quad \dots (2.39)$$

A similar functional relation is found<sup>23</sup> for the  $g$  factor of the  $\Delta M = \pm 1$  transitions and is given in equation 2.40.

$$g = K_1 \cos^2 \varnothing + K_2 + K_3 \cos \varnothing \sin \varnothing \quad \dots (2.40)$$

Here,  $g$  is defined as the mean resonant field of the observed doublet and  $K_1$ ,  $K_2$  and  $K_3$  are expressed in equations 2.41 to 2.43.

$$K_1 = (g_y - g_x) (\cos^2 \theta \cos^2 \psi - \sin^2 \psi) + (g_z - g_x) \sin^2 \theta \quad \dots (2.41)$$

$$K_2 = g_x + (g_y - g_x) \sin^2 \psi \quad \dots (2.42)$$

$$K_3 = (g_x - g_y) \sin 2\psi \cos \theta \quad \dots (2.43)$$

The anisotropy of the  $g$  factor can, therefore, be expressed in terms of the values  $g_x$ ,  $g_y$  and  $g_z$  along the three principal magnetic axes.

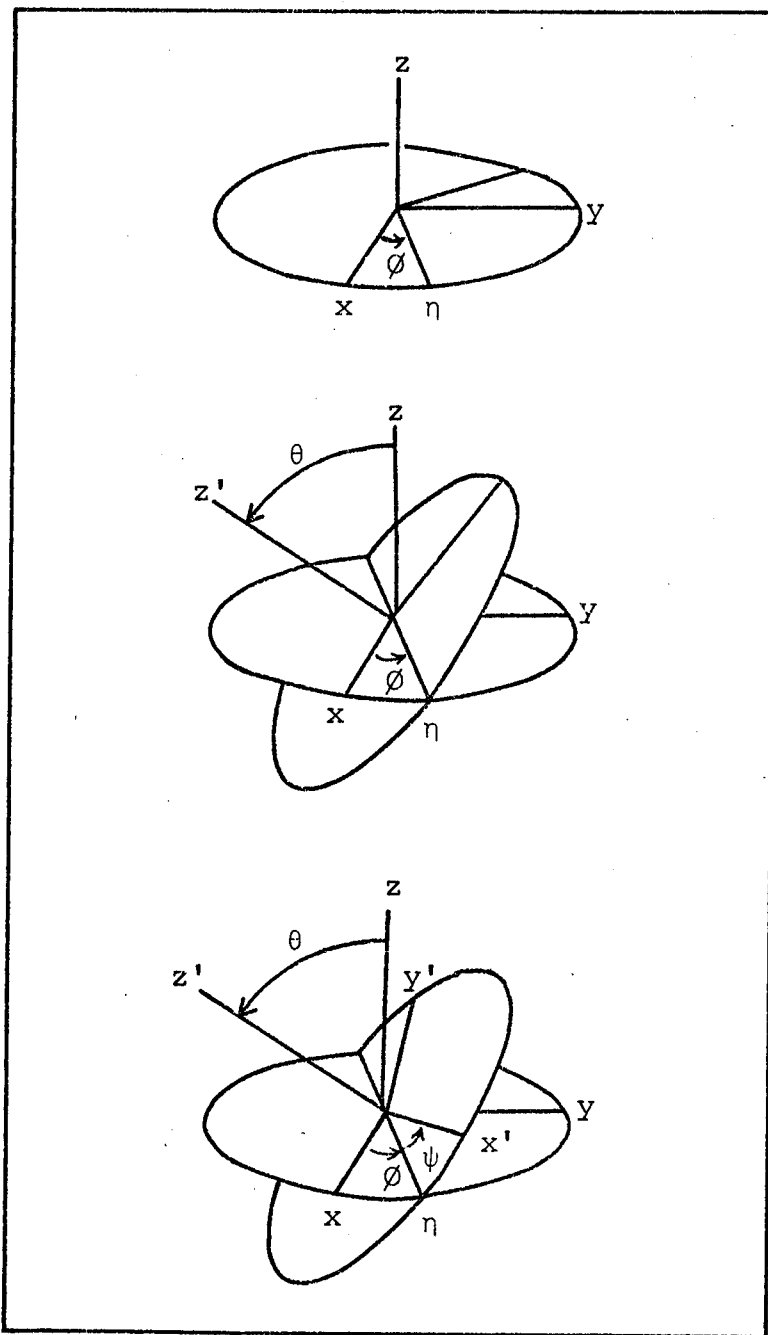


Figure 2.11

The successive counterclockwise rotations about  $z$ ,  $\eta$  and  $z'$  defining the Eulerian angles  $\phi$ ,  $\theta$  and  $\psi$ .

$x$ ,  $y$  and  $z$  are the axes of the laboratory co-ordinate system.

$x'$ ,  $y'$  and  $z'$  are the principal magnetic axes of the TCNQ molecule.

The extent of the dipolar interaction is very dependent on the distance between the electrons constituting the triplet state. Indeed, various TCNQ complex salts have been studied<sup>23,33,120,121</sup> which display this splitting to varying degrees. Not only does this represent the average separations of the two electrons, but also reflects the extent of localisation or delocalisation of the triplet exciton. For the more delocalised excitons, having values of  $\gamma$  somewhat greater than zero, dipolar splitting would not be expected to be observed because the increased separation of the electrons would result in a splitting smaller in magnitude than the exciton's natural linewidth. This has in fact been verified experimentally<sup>27</sup> and the observation of dipolar splitting is, therefore, associated with localised triplet excitons, having values of  $\gamma$  close to zero.

Triplet exciton spectra of the type illustrated in Figure 2.9 (b) are only observed at temperatures low enough for small thermal concentrations of excitons because, just as the motion of the exciton removes hyperfine structure, it also removes the fine structure as the temperature is increased. The separation of the two absorption lines decreases and the linewidth of each signal broadens. Then, with further increase in temperature, the two lines coalesce to form a single absorption line which narrows to a limiting value. This effect on the e.s.r.

derivative spectrum is shown in Figure 2.12 and is characteristic of an exchange interaction, which is assumed to be a spin-exchange of the triplet excitons resulting from exciton-exciton collisions.

Jones and Chestnut<sup>122</sup> studied this behaviour in detail and their theoretical interpretation is widely accepted. For an understanding of the spectral features arising from this phenomenon, it is necessary to consider two distinct temperature regions : the 'slow' exchange and the 'fast' exchange region. The former is the region in which the doublet spectrum is observed, whereas the latter corresponds to the presence of only one absorption line. The observed effects in the 'slow' exchange region are represented by equations 2.44 and 2,45, whilst equation 2.46 corresponds to the region of 'fast' exchange.

$$2\nu^2 = (d_0^2 - d^2) \quad \dots (2.44)$$

$d_0 \gg \sqrt{2}\nu :$

$$\nu = \sqrt{3} (\Delta H - \Delta H_0) \quad \dots (2.45)$$

$$d_0 \ll \sqrt{2}\nu : \quad \nu = \frac{d_0^2}{2\sqrt{3}} (\Delta H - \Delta H_0)^{-1} \quad \dots (2.46)$$

In the above equation,  $d$  and  $d_0$  represent the separation of the doublet in gauss, in the presence and absence of exchange respectively,  $\Delta H$  and  $\Delta H_0$  are the linewidths in gauss with and without exchange,  $\nu$  is the frequency of the exchange process. The linewidths, referred to above, are measured

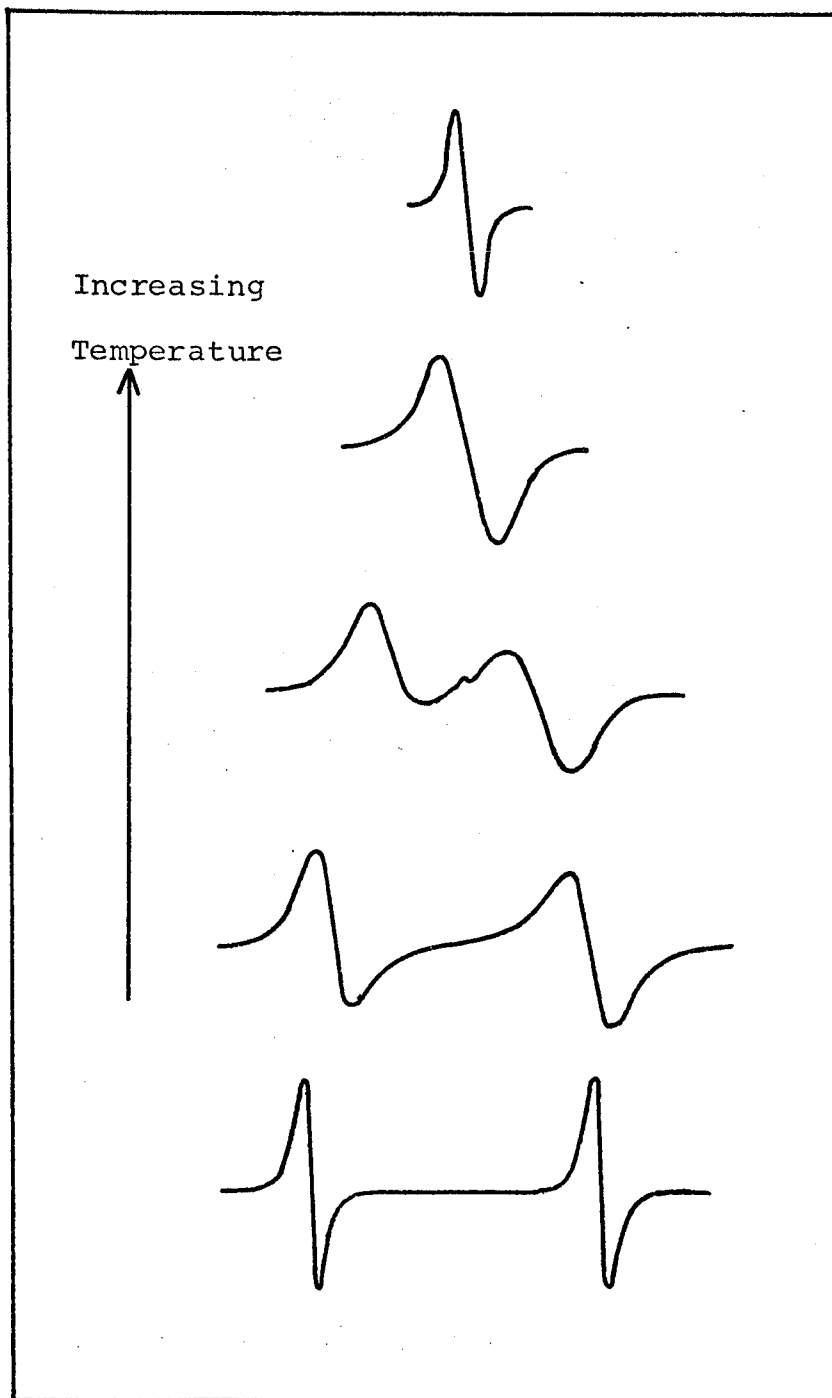


Figure 2.12

Effect of exchange interaction with increasing temperature on the two-line e.s.r. derivative spectrum arising from zero-field splitting for a species with  $S=1$ .

from points of extreme slope of the derivative of the absorption curve, which is the normal manner in which the spectra are recorded in e.s.r. experiments.

The approximations given in equations 2.44 to 2.46 follow an experimental temperature dependence given by equation 2.47:

$$v = v_0 \exp(-\Delta E_e/kT) \quad \dots (2.47)$$

where  $v_0$  is a pre-exponential factor, and  $\Delta E_e$  is the activation energy for exchange. The exchange frequency is also proportional to the exciton concentration and this relationship is shown in equation 2.48.

$$v \propto (\exp(J/kT) + 3)^{-1} \approx \exp(-J/kT) \quad \dots (2.48)$$

From these last two equations, it might be expected that an equality would exist between  $\Delta E_e$  and  $J$ . However, generally  $\Delta E_e$  is substantially larger than  $J$ <sup>122,123</sup>, which indicates that there must be some other activated process contributing to the activation energy for exchange. This difference can be justified<sup>77</sup> by considering an activation energy for migration of the triplet exciton,  $\Delta E_m$ , and equation 2.49 can be derived.

$$\Delta E_e = J + \Delta E_m \quad \dots (2.49)$$

The treatment outlined in this section adequately explains most of the experimental observations arising from the effects of exchange on the spectra of TCNQ

complex salts and will, therefore, be used in this thesis when interpreting the results obtained from single crystal studies.

CHAPTER 3

EXPERIMENTAL

"There is no higher or lower knowledge, but  
one only, flowing out of experimentation."

Leonardo da Vinci

1452 - 1519

### 3.1 SAMPLE PREPARATION

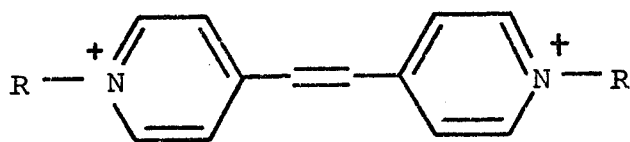
All the compounds studied in this work were complex salts of TCNQ and were prepared by various members of this department. The general procedure is basically the same for all the compounds and detailed experimental accounts typical of the procedure used have been presented elsewhere<sup>125,126</sup>. However, a brief description of the general method of preparation will be outlined in this section.

TCNQ was obtained from Eastman-Kodak Ltd. and used without further purification, as were the precursors of the cations used in this work. The basic structures of these cations are presented in Figure 3.1, together with the abbreviations to be used for them in this thesis, the correct nomenclature being given in Table 3.1.

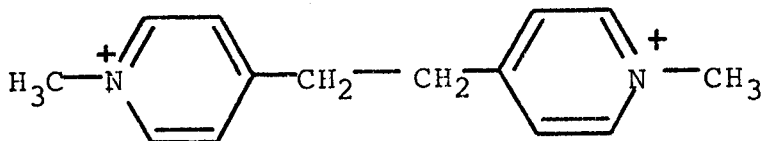
Table 3.1

Nomenclature and Abbreviations for the Cations  
in Figure 3.1.

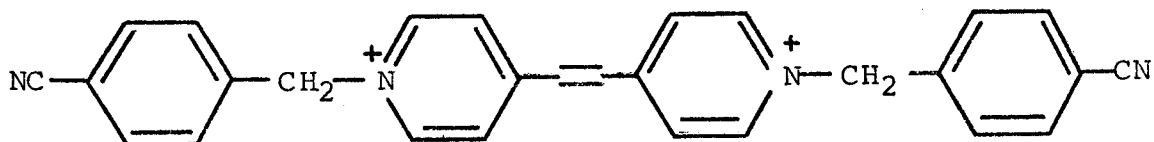
Abbreviation	Nomenclature
DRPE	1,2-di (N-Alkyl-4-Pyridinium)Ethylene.
DMPA	1,2-di (N-Methyl-4-Pyridinium)Ethane.
DCBP	1,2-di (N-p-CyanoBenzyl-4-Pyridinium)Ethylene.
DPB	1,4-di (N-Pyridinium)Butane.
TPT	2,4,6-tri (N-Methyl-2-Pyridinium)Triazine.



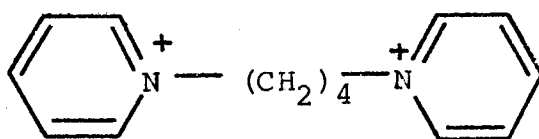
DRPE



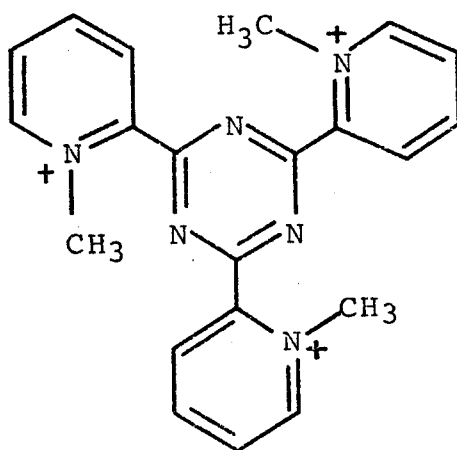
DMPA



DCPB



DPB



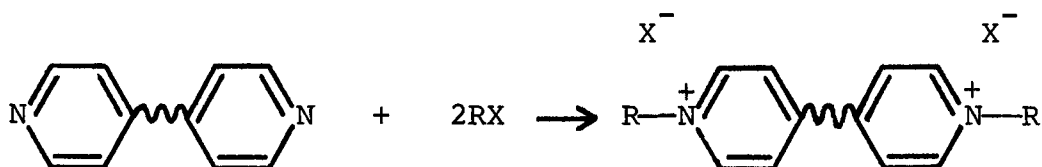
TPT

Figure 3.1

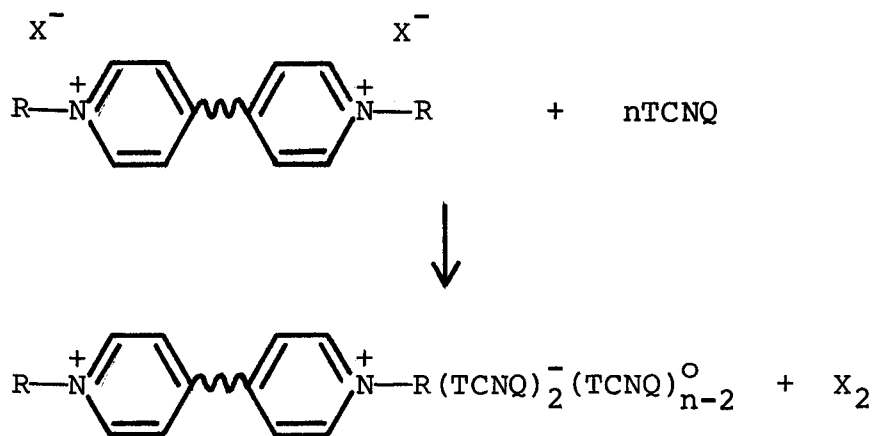
Cations used in the preparation of TCNQ complex salts studied in this work.

R = n-propyl(P), n-butyl(B), cyclohexyl(H).

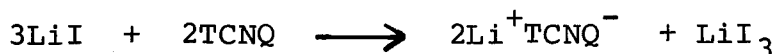
All the cations, except DPB, were prepared from their precursors by a one-step quaternisation procedure of the pyridine rings, using an alkyl halide RX:



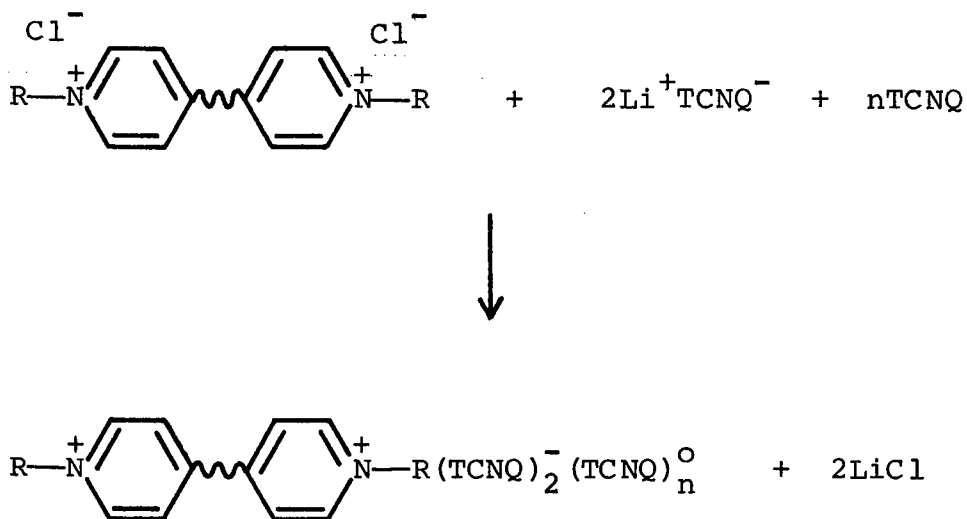
A hot solution of the cation in water was then added to a hot acetonitrile solution of TCNQ, the actual amounts used depending on the stoichiometry of the desired product.



If X=Cl, the above step involves the intermediate  $\text{Li}^+\text{TCNQ}^-$ , which is produced by the direct action of TCNQ on lithium iodide in acetonitrile:



The addition of  $\text{Li}^+\text{TCNQ}^-$  is required as TCNQ itself will not discharge the chloride ion. The reaction in this case is as follows:



After refluxing, the hot solution was allowed to cool slowly and the almost black product could then be filtered off and washed with toluene followed by ether to remove any unreacted TCNQ. The crystal size of the product and its stoichiometry depends on the amount of solvent used and the relative amounts of each reactant. In some cases, crystals were obtained quite readily, whereas in other cases only small microcrystals could be obtained. The exact conditions required for obtaining the complex salts in the desired form have yet to be fully determined.

Analysis of the products involved a spectroscopic technique<sup>124,126</sup> whereby the stoichiometry of the complex salt could be determined by its ultraviolet spectrum. TCNQ<sup>-</sup> in acetonitrile absorbs at 395nm and 842nm, whereas TCNQ<sup>0</sup> absorbs only at 395nm. From the peak height ratio at these two wavelengths, obtained from a solution of the

complex in acetonitrile, the relative amounts of  $\text{TCNQ}^-$  to  $\text{TCNQ}^0$  were obtained.

Microanalytical data were also used to confirm the stoichiometry obtained using the spectroscopic analysis. In the case of single crystals, X-ray crystallographic data complemented the above techniques.

### 3.2 ELECTRON SPIN RESONANCE STUDIES

#### 3.2.1 Equipment

##### (i) The Spectrometer

The spectrometer used throughout this work was a Decca X3 operating in the X-band with a klystron generating a constant frequency of 9270 MHz. The microwave radiation was kept at this fixed frequency by an automatic frequency control (AFC) locked to a crystal oscillator, and the resonance condition was satisfied by varying the magnetic field.

The spectrometer (illustrated in Figure 3.2) a microwave reflection system, and the reflection cavity operated in the  $\text{TE}_{102}$  mode. In this system, it is essential that all the input radiation is absorbed by the cavity, at a field value off the point of resonance, and the cavity is then said to be tuned. This occurs when the resonant frequency of the cavity matches that of the klystron, and this is achieved using tuning screws, which

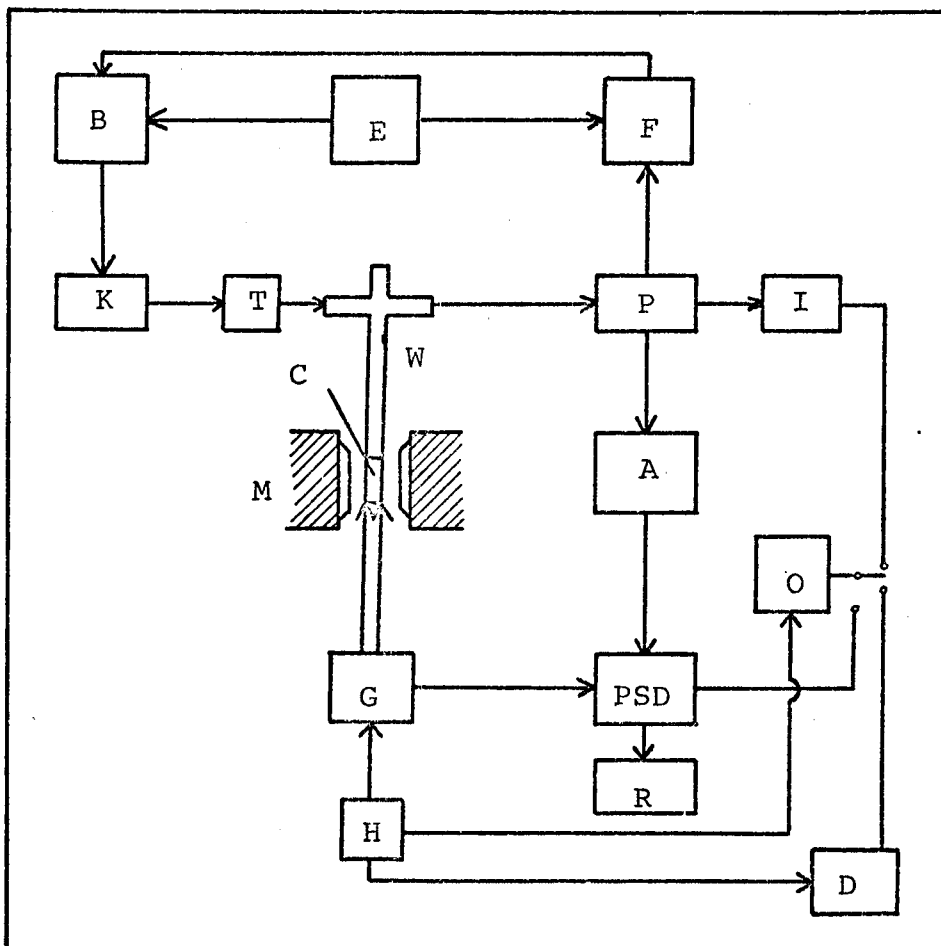


Figure 3.2

Block Diagram of the e.s.r. spectrometer.

A 100KHz amplifier.

I Audio amplifier.

B Klystron power supply.

K Klystron.

C Cavity.

M Magnet.

D Audio PSD.

O Oscilloscope.

E Automatic frequency control (AFC) signal generator.

P Pre-amp.

PSD 100KHz phase sensitive detector.

F AFC discriminator.

R Recorder.

G 100KHz generator.

T Attenuator.

H Audio sweep generator.

W Waveguide.

effectively distort the cavity dimensions to change its resonant frequency. When resonance occurs, power is absorbed by the sample and the cavity becomes detuned. Consequently, power proportional to that absorbed by the sample is reflected back to the detector, a semiconducting crystal diode rectifier, which converts microwave power into direct current.

The spectrometer also operated phase-sensitive detection (PSD), which enables small signals, normally obscured by noise, to be observed. This system requires application to the sample of a 100KHz modulating magnetic field with amplitude,  $H_m$ , much less than the linewidth. This field is supplied by a coil around the cavity and could be varied using calibrated attenuators from 40 to 0.01G. During the traverse of the peak, the output signal is approximately proportional to the slope of the absorption curve (Figure 3.3(a)). After amplification, this 100KHz signal is mixed with a reference signal of the same frequency, of constant amplitude but variable phase, in the phase-sensitive detection circuit to produce a d.c. output signal of the shape shown in Figure 3.3(b). This is the first derivative of the absorption curve and, for this to be a true representation of the absorption, it is essential that the amplitude of the 100KHz modulating field is less than one tenth of the linewidth  $\Delta H$ . Linewidths are usually quoted in terms of the distance from peak to peak

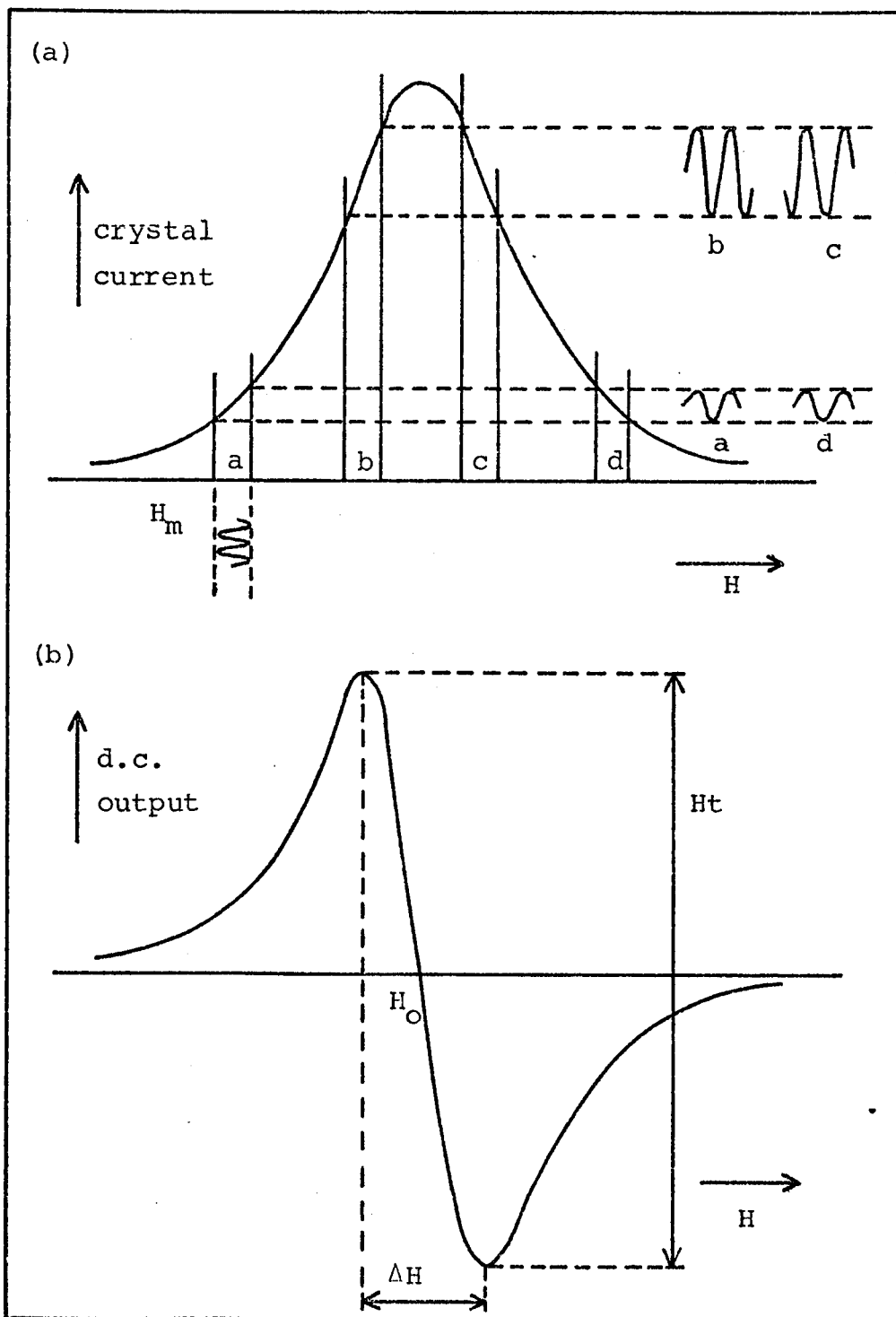


Figure 3.3

(a) Effect of superimposing a 100KHz modulation field ( $H_m \ll H_0$ ) during the traverse of an absorption peak.

(b) The d.c. output after phase-sensitive detection (first derivative curve). This is also typical of the e.s.r. signal obtained with single crystals of TCNQ complex salts.

on the first derivative curve, and this convention has been used in this thesis for all symmetrical signals.

The efficiency of a cavity in storing microwave energy is expressed quantitatively by its Q-factor which can be defined by equation 3.1:

$$Q = \frac{\omega \times \text{energy stored}}{\text{rate of energy loss}} \quad \dots (3.1)$$

where  $\omega$  is the resonant frequency. If energy loss is only caused by dissipation in the walls, this definition gives the unloaded Q-factor but, if energy loss through the coupling holes is included, it measures the loaded Q-factor. In either definition, the higher the Q, the more efficient is the cavity.

The method of measuring the Q was a standard feature of the Decca X3 spectrometer, and differed from the classical Voltage-Standing-Wave Ratio method. The V.S.W.R. method involves measuring the amplitude difference of the input and output standing waves, whereas the Decca method involves measurement of the reflected wave voltage using a high directivity directional coupler. Loss of energy by sample absorption gives rise to a change in the Q value and, therefore, the quality factor is of importance during measurements of signal intensity. In order to take account of the changes in Q with sample, temperature, and sample positioning, all signal intensities observed were

normalised by dividing by the corresponding Q value measured. The relative accuracy of a series of Q measurements was quoted by the manufacturers as 2%, however, the absolute accuracy is regarded as being somewhat less than this.

Another important feature of the basic spectrometer was a Newport Instruments Type P Mark III magnetometer. The magnetic field could be measured with the proton resonance probe fitted in the magnet gap, the proton in a water sample providing the standard. The accuracy of the field measurement for this magnetometer was quoted by the manufacturers as one part in  $10^5$  at 5KG.

There had been one modification to the spectrometer and this had involved the replacement of the integrator circuit, responsible for the control of the magnetic sweep rate, with a solid state circuit. This modification was found to be an improvement with respect to the long rate reproducibility<sup>127</sup>.

The remaining basic features of the spectrometer and its operation are common to many commercial e.s.r. systems, and so no further discussion is presented of these features.

#### (ii) The Cooling Unit

The temperature within the sample cavity of the spectrometer was varied in the temperature range 300 to

4.5K by passing helium gas into the cavity by means of an Oxford Instruments ESR9 continuous flow cryostat. The basic design of this equipment is shown in Figures 3.4 and 3.5.

The temperature could be controlled by controlling the transfer of the coolant gas from the storage vessel by means of a pump which transfers the gas by suction via a flexible syphon. The actual temperature required was maintained by a heating coil situated close to the sample in the cavity, which automatically adjusted the rate of heating to compensate for any changes in helium flow and to balance the heat leaks into the cryostat. This automatic control of the temperature was provided by an Oxford Instruments Precision Temperature Controller used in conjunction with the cryostat, and also provided a digital display of the temperature. With this facility, the temperature could be controlled to  $\pm 0.1\text{K}$  at an accuracy of  $0.1\text{K}$  from room temperature to  $10\text{K}$ , and at a stability of  $\pm 0.5\text{K}$  from  $10$  to  $4.5\text{K}$ .

The sample temperature was measured using the gold-0.03% iron/chromel thermocouple shown in Figure 3.5. The voltage from this thermocouple was converted to the digital display and a calibrated chart was provided with the equipment.

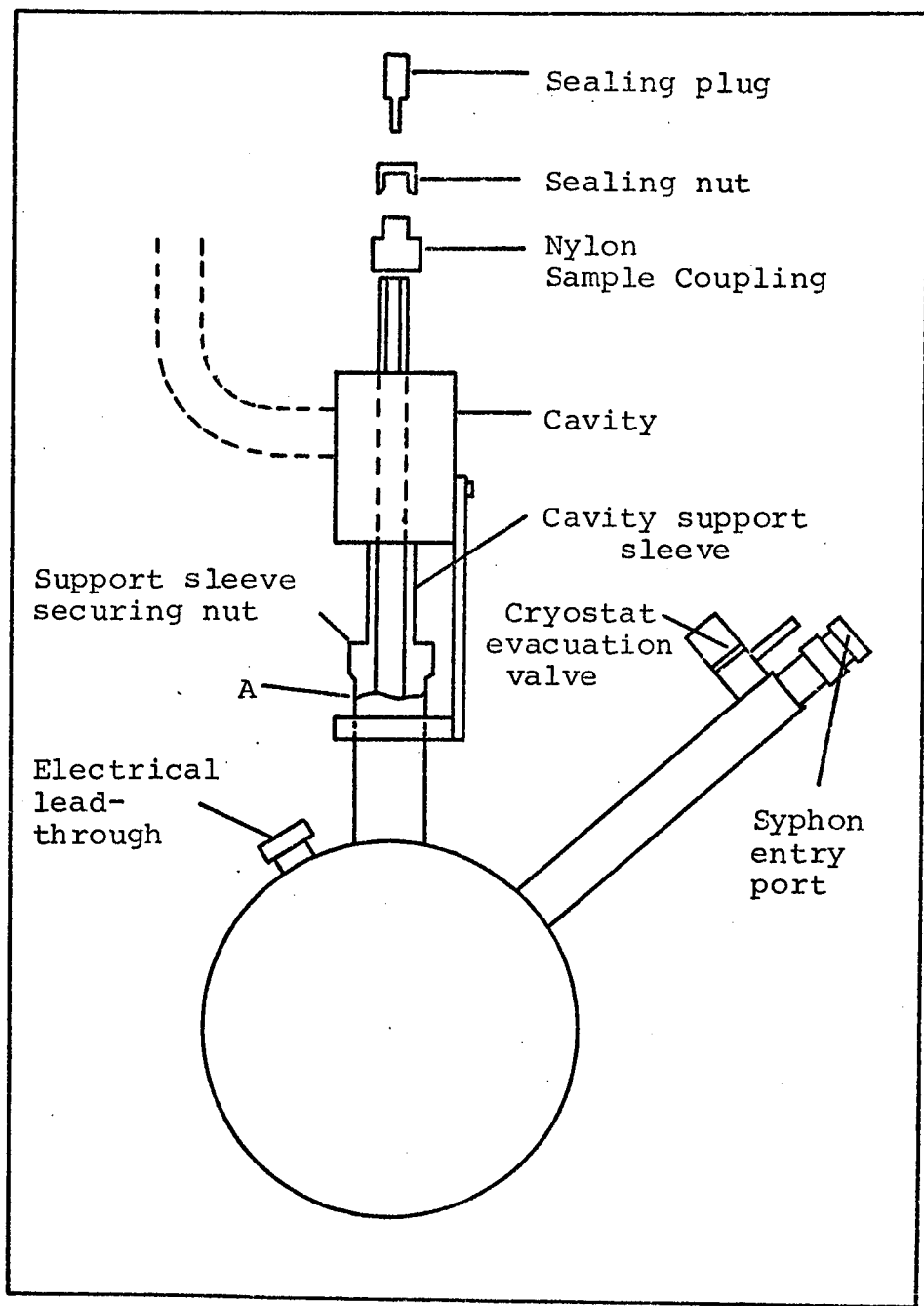


Figure 3.4

The Oxford Instruments E.S.R.9 continuous flow cryostat (partially open view down to the level marked A).

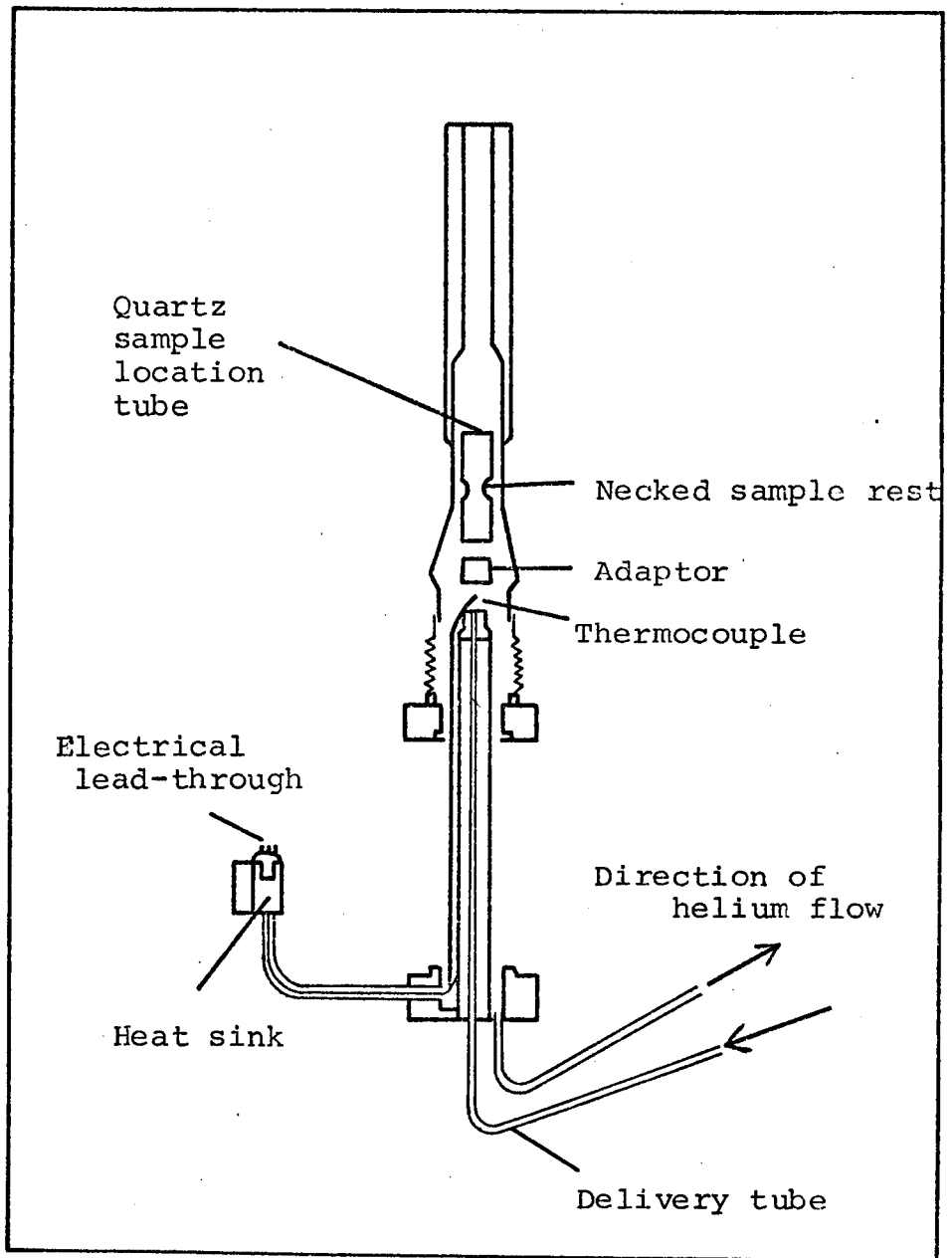


Figure 3.5

Cross-section through the sample region of the Oxford Instruments E.S.R.9 continuous flow cryostat.

Below room temperature, care had to be taken to prevent any condensable materials collecting in the cavity area and so depreciating the Q value. This was prevented by passing nitrogen gas at a small flow rate through the e.s.r.cavity area.

(iii) High Temperature Equipment

Measurements above room temperature, up to 340K, could be performed using the heating coil in the cavity combined with warm air introduced into the cavity by the pump. The flexible syphon was replaced by a rod, of suitable dimensions which fitted into the cryostat, and attaching this rod to a copper coil situated in a furnace. This apparatus enabled warm air to be drawn into the cryostat, and hence the cavity. Although the digital display could not be used above 300K, the temperature could be measured using a voltmeter and the calibration chart provided.

(iv) The Analog Integrator

Estimation of the intensity of a symmetrical e.s.r. signal is straightforward and is described in section 3.2.3(iii). However, for asymmetrical signals, the intensities are not so readily obtained. The well known numerical integration technique<sup>93</sup> involving the measurement of the peak height of the first derivative e.s.r. signal at uniform intervals throughout the spectrum,

is both tedious and time-consuming and the accuracy depends upon the size of the intervals taken. Also, although the accuracy for this technique is quite good for Gaussian lineshapes, it is not so good for Lorentzian lineshapes unless a very wide sampling range is used<sup>128</sup>.

In order to surmount the problem, an analog integrator was used, which was built to the design of Randolph<sup>129</sup>. The integrator was connected to the pen-recorder and had two output channels. The first of these allowed the power absorption curve to be displayed, and the second gave a voltage which was directly proportional to the integrated signal intensity and was also displayed on the recorder. Although this technique did not increase the accuracy of the integration, it did decrease the time consumed in obtaining a measurement of the signal intensity.

Great care had to be taken, however, in using the integrator as any drift in base-line resulted in a completely false integration of the spectrum. Before a spectrum was taken, the two outputs were checked to ensure there was no drift, and again after the spectrum had been displayed to ensure that no drift had occurred as the sweep continued through the spectrum. If any drift had occurred, the output would vary, and intensity values were only taken from those spectra which showed no such drift. In order to obtain a valid spectrum, the phasing

had to be set perfectly and this proved to be one of the benefits of using the integrator. Due to the asymmetry of the signals obtained with polycrystalline samples, the correct shape was not immediately obvious but, with the necessity for setting the phasing perfectly, a true spectral shape was obtained.

(v) Sample Holders

The type of sample holder used depended upon the nature of the sample to be studied. In the case of single crystal samples, a silica glass rod of diameter 4mm was used. The end 8mm of its length was removed on one side leaving a semi-circular portion of radius 2mm which provided a flat platform on which to mount the crystal. The modified end of the glass rod was then annealed to remove as many as possible of the radicals that may have been generated in the grinding process.

Silica glass was used as pyrex glass contains paramagnetic impurities that would give rise to an e.s.r. signal. The silica glass rod, with a small amount of silicone grease on the flat portion, was investigated for the presence of any signal at various temperatures and spectrometer settings. A very small signal was observed below 100K at about the free electron g factor. This signal was so small at most of the commonly used spectrometer settings, that it was unlikely to interfere

with any measurements made on the single crystals of the TCNQ complexes studied. However, the investigations performed enabled the signal to be identified should the need arise.

The crystals were mounted on the rod using silicone grease and the orientation of the crystal with respect to the magnetic field was varied by means of an Oxford Instruments goniometer attached to the top of the cavity. This allowed changes in the orientation of a sample to be made to an accuracy of 6 radians.

In the case of polycrystalline samples, silica glass tubes of diameter 4mm were used. A weighed sample, usually 3-4mg, of the TCNQ complex to be studied was inserted into the tube which was then evacuated to a pressure of  $10^{-3}$  Pa for about twelve hours, before being sealed under vacuum. An empty sealed tube was also investigated at various temperature and spectrometer settings and a very small signal was observed at about the free electron g factor as before.

### 3.2.2 Calibration Experiments

#### (i) Microwave Power Attenuators

The manufacturers had provided a calibration graph of microwave power against microwave attenuation. The powers quoted were for a new Decca klystron, so since

several EMI klystrons were used in this work, the power at a certain attenuation was incorrect. However, although the power levels will be different from klystron to klystron, the ratios of the power levels indicated by the various attenuator settings should be the same.

This was checked by investigating the size of a signal from a crystal of  $\text{DPB}(\text{TCNQ})_4$  as a function of microwave power. In the range of microwave attenuation studied (15 to 40db), the linewidth of the signal remained the same which indicated that the signal was not saturated. A plot of the square root of the microwave power against signal intensity is shown in Figure 3.6 and shows the expected linear relationship.

(ii) 100KHz Receiver Attenuators

When comparing signal intensities from spectra taken using different attenuator settings of the 100KHz receiver, it was vital for an accurate comparison that the attenuator calibration was correct. This was checked by investigating the signal intensity from a crystal of  $\text{DPB}(\text{TCNQ})_4$  at various values of the 100KHz receiver attenuators. Six attenuator settings were studied in the range 13 to 28db and, if they were correctly calibrated, the product of the signal intensities and the voltage ratio appropriate to the attenuator setting should give rise to the same intensity values. The results obtained for the six

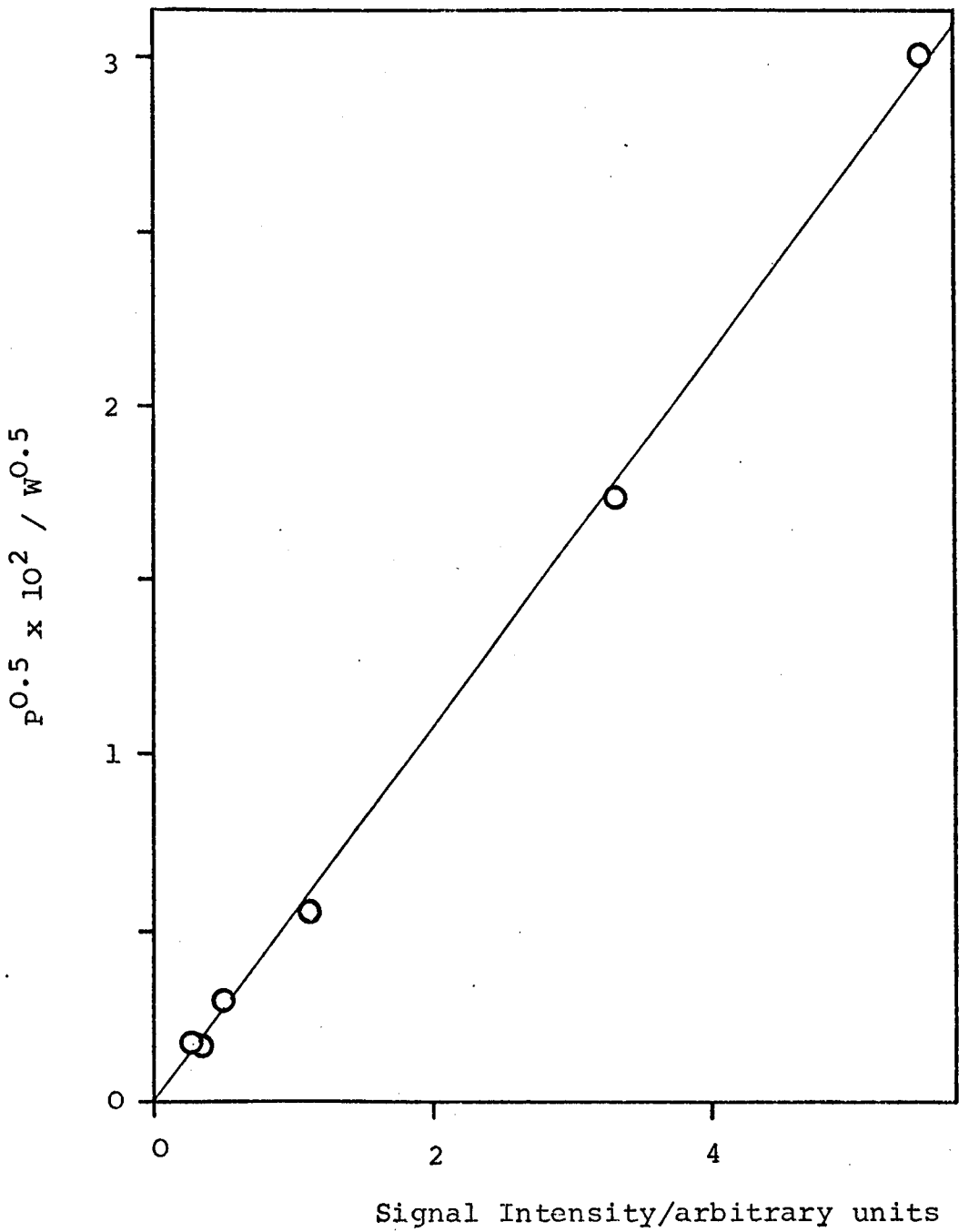


Figure 3.6

Plot of the square root of the microwave power against the signal intensity observed for a crystal of  $\text{DPB}(\text{TCNQ})_4$ .

attenuator settings are shown in Table 3.2.

Table 3.2 Comparison of Signal Intensities obtained with different Attenuator Settings of the 100KHz Receiver.

Attenuation (db)	Signal Intensity (arbitrary units)	Voltage Ratio for Attenuator Setting.	Product of Voltage Ratio and Signal Intensity
13	6,153	4.47	27,502
16	4,649	6.31	29,338
19	3,334	8.91	29,702
22	2,356	12.59	29,668
25	1,719	17.78	30,559
28	1,086	25.12	27,280

The mean value obtained in the last column of Table 3.2 is 29,010 with a standard deviation of 1,318. This is only about 4% of the mean value, which is within the error involved in assessing the signal intensities. Consequently, it was felt that the attenuator calibration was sufficiently correct for the comparisons of signal intensities, taken with different attenuator settings, to be made.

(iii) Thermocouple Calibration

The thermocouple of the ESR9 cryostat was situated very close to the sample, as shown in Figure 3.5. Consequently, the thermal gradient between the two points must have been very small indeed, and any attempt to measure it would result in error larger than the value itself.

However, by supplying voltages corresponding to the output of the gold-0.03% iron/chromel thermocouple (obtained from the manufacturer's calibration chart), the digital display of the Precision Temperature Controller could be checked. The results indicated that the displayed temperature was inaccurate up to 3K at certain temperatures. The thermocouple voltage has a curved dependence upon temperature, and the deviation in the display resulted from this as the electronics of the equipment segmented this curve into three linear portions. However, by checking the display throughout the temperature range 4.5 to 300K and noting the deviation, allowance could be made when taking temperature measurements during this work.

(iv) Sweep Rate Calibration

The sweep rate could be altered in two main ways. Firstly, the actual sweep rate in gauss could be set at either 1% or 10% of the magnetic field level chosen, the maximum field value being 6KG. The field value used

throughout this work was approximately 3300G and, therefore, the sweep ranges used were approximately 33 and 330G.

Secondly, the sweep time could be varied from 10 to 10,000 seconds. Consequently, uncertainties arose in the estimated sweep rate from the errors in both the sweep range and sweep times. Also, the pen-recorder was of the y-t type, and so the response was not directly triggered by the magnetic field.

The sweep times and rate at which the pen-recorder ran was readily checked using a stop-clock, thus leaving only the error in the sweep range unknown. The method used to evaluate this error entailed taking a spectrum of a sample having known spectral parameters. The compound used was p-benzosemiquinone, the spectrum of which consists of a quintet caused by the hyperfine splitting of the ring protons. The separation of the peaks is established and known to be  $6.64\text{MHz}^{130}$ .

The p-benzosemiquinone radicals were generated by mixing equal volumes of approximately 0.1M solutions of hydroquinone and sodium hydroxide in ethanol and water (30:70 by volume). The radicals decomposed quite readily, this being indicated by the solution changing colour from yellow to brown, and so it was necessary to make a fresh mixture for each spectrum taken. A special cell had to

be used for these samples in order to minimise the effects of the high dielectric loss of the water in the microwave region. An aqueous solution silica cell was, therefore, used having a thickness of only 0.1mm but a width of 1cm. This had to be positioned in the cavity so that the intrusion of the sample into the microwave electric field was minimised, so preserving the Q of the cavity. This was achieved by having the cell with its 1cm width parallel to the external magnetic field H, as shown in Figure 3.7.

From the distance observed between the quintet peaks on the resulting spectrum, and knowing the sweep time, pen-recorder speed and the known value of the hyperfine splitting, the sweep range was calculated. This was repeated for both the 1% and 10% sweep range settings.

The sweep times and sweep ranges were known to change slowly as the electronics governing these settings aged. Consequently, it was found necessary to repeat this calibration every six months throughout the course of this work and the estimated accuracy in the sweep rate after each calibration was approximately 2%.

(v) Purity of DPPH

When making spin measurements, it was necessary to have a standard with a known number of spins per mole.

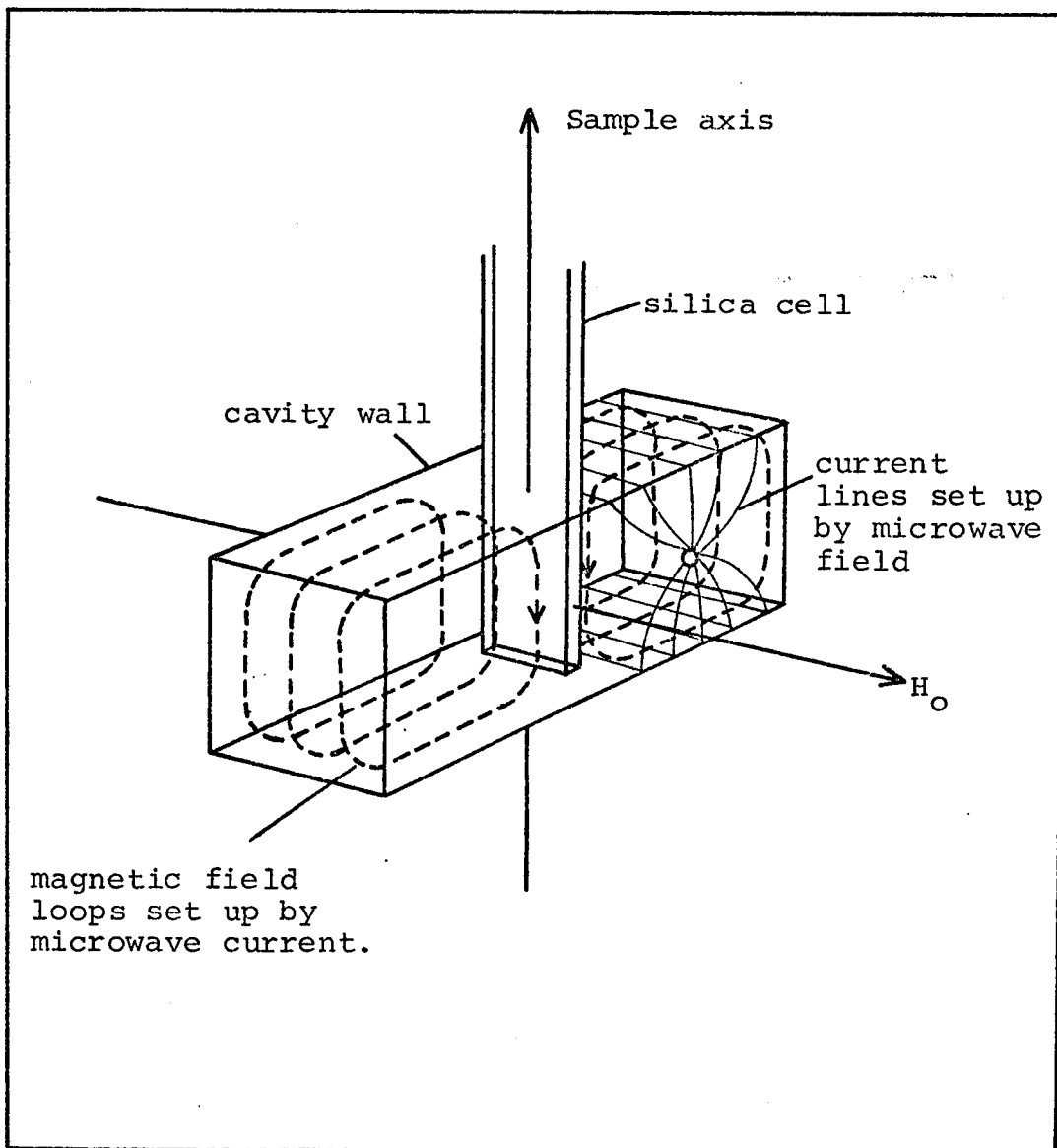


Figure 3.7

The resonant cavity, showing the positioning of the silica solution cell.

Only some of the electric field lines are shown for clarity. There is another set in front of the silica cell in the diagram.

The standard used throughout this work was 1,1-diphenyl-2-picrylhydrazyl (DPPH), which has a g value of 2.0036 and a linewidth comparable to those of TCNQ complex salts. DPPH was obtained from Koch-Light Laboratories Ltd., who quoted the free radical concentration as 85 to 88% of the theoretical maximum value. The melting point of the DPPH was given as 410 to 412K which indicated that the compound was in the crystallographic form designated as DPPH II by Duffy and Strandburg<sup>131</sup>.

The DPPH had been recrystallised from chloroform by the suppliers, and some of the solvent would most certainly have remained in the solid as DPPH is known to form a complex with chloroform<sup>132</sup>. This is probably the reason for the comparatively poor purity quoted, and also could explain the slight asymmetry observed in the spectrum of DPPH<sup>133,134</sup>. The magnetic susceptibility of this material agreed very well with that of a sample of DPPH recrystallised from chloroform previously studied<sup>135</sup>, and was found to be  $1.123 \times 10^{-3}$  e.m.u.  $\text{cm}^3 \text{mol}^{-1}$  at 295K for both materials.

The purity of the DPPH used in this work was estimated by a spectroscopic technique. Standard solutions ( $<10^{-3}$ M) of the DPPH in chloroform were prepared and their extinction coefficients at 529nm taken. Now, with a knowledge of the literature value of the extinction

coefficient<sup>136</sup>, it was possible to calculate the actual amount of DPPH present in the standard solutions used and hence the percentage purity of the DPPH. The purity was found to be 79%, and this value was used to assess the number of radicals in each of the standard DPPH samples used in this work.

The spin concentration of DPPH samples decreases with time<sup>137</sup> and, consequently, the standard samples were degassed and the silica tubes sealed under vacuum, as previously described in section 3.2.1(v). By evacuating the samples in this way and also keeping them in the dark, the decrease in spin concentration could be reduced to 1-2% per year<sup>138</sup>.

#### (vi) Oscilloscope Measurements

Most TCNQ complex salts studied show an increased signal intensity at low temperatures which obeys a Curie temperature dependence, and this tends to dominate the signal observed<sup>116</sup>. This Curie signal is due to unpaired electrons in the doublet state which are thought to result from defects in the lattice<sup>100</sup>, for example irregularities in the stoichiometry of the complex.

In order to obtain an order of magnitude estimate of the number of these species, a technique was employed which involved comparison of the signal under

study with signals from DPPH samples. The spectra of the TCNQ complex salts were displayed on the oscilloscope screen and, providing the signal shape was symmetrical, the intensity could be calculated quite readily by taking measurements from the screen. With a knowledge of the  $Q$  of the cavity at the particular temperature, and taking a series of measurements at different temperatures, a plot of the normalised intensity against the absolute temperature could be obtained. The slope of such plots depended upon the number of spins giving rise to the signal and also upon the spectrometer settings used. In order to determine how the slope depended on the settings, samples of DPPH were used. Measurements of the spectra displayed on the screen were taken at various temperatures and using the same settings as before for the TCNQ complex salts. The normalised intensities were, therefore, found and an example of the resulting plots is shown in Figure 3.8. Knowing the number of spins in the DPPH sample, a correction factor could be calculated to allow for the spectrometer settings.

The number of spins in a DPPH sample was obtained in the following way. The molar susceptibility behaviour of DPPH II, in the temperature range studied, is given by equation 3.2<sup>131,135</sup>.

$$\chi_m = \frac{N C}{(T-24)} \dots (3.2)$$

In this case,  $N$  is 97% of Avogadro's number,  $T$  and  $C$  have

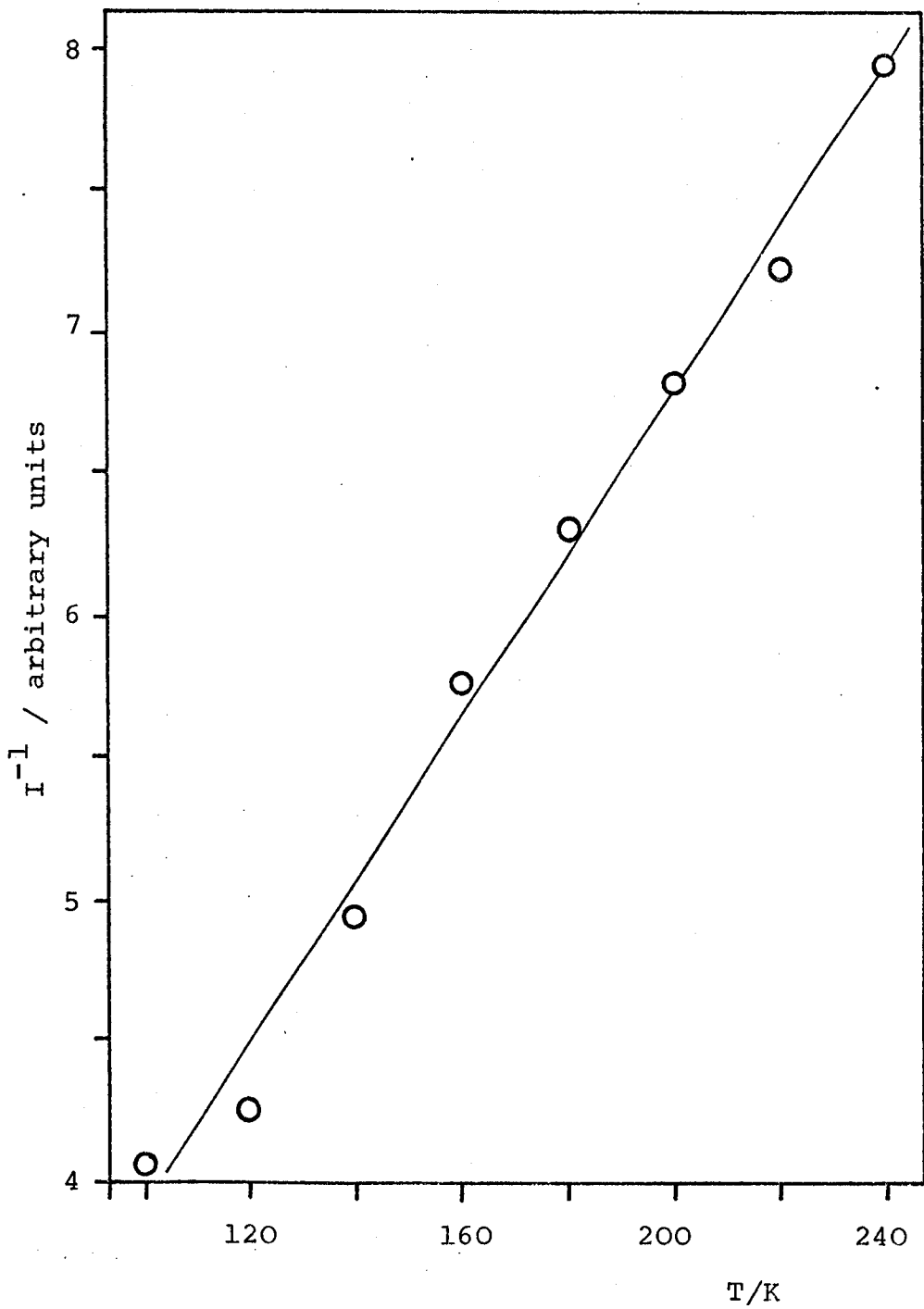


Figure 3.8

Plot of the reciprocal of the normalised intensity against temperature for a DPPH sample.

been previously defined in section 2.3.1 of Chapter 2, and  $\underline{J}$  is equal to  $\frac{1}{2}$ . Consequently, the calculation of the number of spins giving rise to the Curie law signal in a TCNQ complex salt assumes there is no orbital contribution to the angular momentum. However, since the signals observed were close to the free electron g value, this is considered to be a justified assumption.

This calibration also involves another assumption that the lineshape of the signals from the TCNQ complex salts was the same as that of DPPH. This is involved because the signal intensities for the TCNQ complex salts and DPPH were calculated using equation 3.3, which will be given in section 3.2.3(iii). Comparisons of intensities obtained using this equation require this assumption to be made. However, any error incurred due to different lineshapes would have been smaller than the overall error involved in this technique.

### 3.2.3 Electron Spin Resonance Measurements on TCNQ Complex Salts.

#### (i) g Factor Measurement

The actual position of the spectrum in relation to the magnetic field is of value in ascertaining the nature of the species giving rise to the signal, and this is measured in terms of the g factor. The principal magnetic axes within a crystal can also be located from a

knowledge of the  $g$  values. For these two reasons, this study was undertaken on all single crystals used and on most of the polycrystalline samples.

The magnetometer probe was set so that the proton resonance was locked to 3300G. The point at which the sweep passed through this field value was marked on the pen-recorder, and the sweep was allowed to continue until the signal had been drawn. The distance from the 3300G marker to the point where the first derivative of the absorption curve cuts the base-line (see Figure 3.3(b)) was then converted to a field separation using the calibrated sweep rates. The exact point of resonance could be calculated and, subsequently, the  $g$  factor at that orientation, using equation 2.22.

The error involved in this estimation resulted from the magnetometer ( $\pm 0.33\text{G}$  at 3300G), the sweep rate ( $\pm 0.15\text{G}$  in sweeping 6G), and the klystron frequency ( $\pm 0.1\text{MHz}$  at 9270MHz using the cavity locking system). This gave an error of  $\pm 0.0003$  for  $g$  factors in the resonance region of 3306G.

The  $g$  factors were calculated at  $10^\circ$  intervals from  $0$  to  $180^\circ$  by rotating the crystal around the sample axis using the goniometer. By rotating through the remaining  $180^\circ$  the same angular variation would be

observed<sup>23</sup> and, therefore, results only from the first 180° rotation were taken. The principal magnetic axes within a crystal were readily located by observing the maximum and minimum g factors obtained and noting the particular orientation to which they corresponded.

Certain TCNQ complexes cannot be prepared in the form of single crystals and, therefore, the investigation of these compounds was carried out using polycrystalline samples. Although it was once believed that randomly oriented triplet state molecules could not give rise to a meaningful signal as the absorption would be smeared over a wide field range, in fact it has been shown<sup>139</sup> that useful information can be deduced from the spectra. The less anisotropic  $\Delta M = \pm 2$  transition was observed initially<sup>140</sup>, and it was subsequently found that the peaks due to the  $\Delta M = \pm 1$  transitions could also be detected<sup>141</sup>. However, single crystal measurements usually give less ambiguous results and so polycrystalline samples were only used where single crystals could not be obtained.

In the case of polycrystalline samples, the peaks observed have been shown<sup>121,141</sup> to be located at exactly the positions at which resonance would occur if single crystals of the material were oriented with their principal magnetic axes co-linear with the axes of the laboratory coordinate system. The spectral shape observed for

polycrystalline samples is shown in Figure 3.9, and the method of determining the  $g$  factors is the same as that outlined above, with the distances measured to the points corresponding to  $g_{\parallel}$  and  $g_{\perp}$  as shown in the diagram. However, these points were only a true indication of the  $g$  factors if contributions from all possible orientations of the microcrystals were contained in the spectrum. This was checked by rotating the sample and observing whether the spectral shape changed with change of orientation.

Spectra with the type of shape shown in Figure 3.9 have been previously reported for single crystals<sup>142</sup> and polycrystalline samples<sup>143,144</sup> of CT complexes, and also for a number of TCNQ complexes<sup>27</sup>. The dependence of the splitting upon the spectrometer frequency has been investigated<sup>144</sup> in order to discover the source of such a signal. This study showed that the structure observed in such a spectrum was caused by differences in  $g$  factor resulting from  $g$  factor anisotropy rather than the existence of two species with different  $g$  factors. Another likely cause of such structure could be dipolar interaction. However, splittings from this phenomenon are of the order of 300MHz for TCNQ complexes<sup>23,33,118,127</sup>, whereas the splitting observed with this spectral shape are in the region of 3MHz. Also, a crystal structure determination of a TCNQ complex salt<sup>145</sup> showed that all the potential exciton sites were equivalent and, therefore, the structure

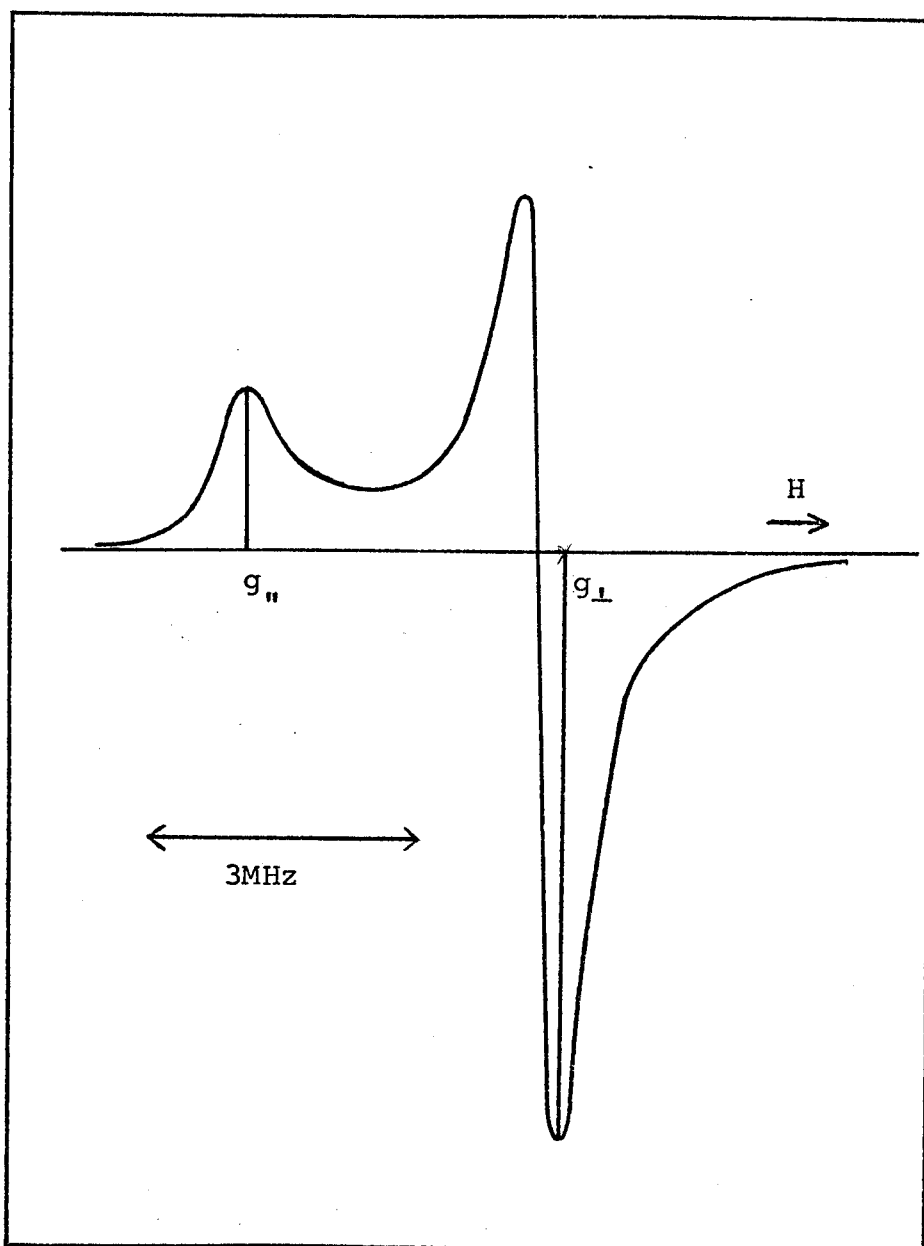


Figure 3.9

Typical e.s.r. signal obtained with polycrystalline samples of TCNQ complex salts.

could not be due to the presence of two species with different  $g$  factors.

Theoretical interpretations<sup>146,147</sup> of the lineshape shown in Figure 3.9 have shown the structure to arise from an axially symmetrical  $g$  factor. Two of the  $g$  factors are equal ( $g_{\perp}$ ) and correspond to the high field peak of the spectrum, and the unique  $g$  factor ( $g_{\parallel}$ ) corresponds to the low field peak. Consequently, it is possible to obtain the principal values of the  $g$  factors from a polycrystalline sample.

(ii) Molar Susceptibility Measurements

Before any measurements were taken which involved a true intensity value and, therefore, a true representation of the spectrum, all the spectra were checked to ensure that the sample was not saturated. This was accomplished by displaying the spectrum on the oscilloscope and observing the effect produced by increasing the microwave power. Also, every precaution was taken to eliminate any modulation broadening, and the amplitude of the 100KHz modulating field was not allowed to increase to a value above one tenth of the signal linewidth.

The molar susceptibilities of both single crystals and polycrystalline samples were obtained by comparison of the signal intensities with standard DPPH

samples, using the same spectrometer settings. This involved knowledge of the weights of the DPPH samples and the samples under study, the number of spins in the DPPH samples, and the molecular weights. The accuracy of the molar susceptibilities estimated using this method was not very good, being of the order of about 20%, and resulted from the error in the small weights of the samples, the uncertainty in the consistency of sample positioning, and the errors involved in the integration of the signals and the assessment of the cavity Q. Although larger samples would have been more desirable, more than 3-4mg of the TCNQ complex salts led to serious depreciation of the Q of the cavity and, therefore, could not be used.

From a knowledge of the exchange integral, J, obtained as described in the next subsection, the theoretically expected molar susceptibility value for a localised triplet exciton could be calculated using equation 2.26. This value could then be compared with the experimentally observed value to assess the localisation of the electrons giving rise to the signal.

(iii) Temperature Dependence of the Signal Intensities

Single crystals were oriented at room temperature with one of the principal magnetic axes parallel to the external magnetic field, as outlined in section 3.2.3(i).

The temperature dependence of the signal intensities was then investigated at this orientation in the temperature region 300 to 4.5K. Absolute susceptibility measurements were only taken at room temperature, and so the results obtained in this study were of the relative intensities with temperature. From these results, using the treatment described in section 2.5.1, semilog plots were obtained of the relative intensity multiplied by temperature against reciprocal temperature, the slope of which gives the value of the exchange integral.

Three crystals were studied in this way for each TCNQ complex salt under investigation. Each principal magnetic axis in turn was the rotation axis and results were obtained with each axis in turn being oriented parallel with the magnetic field, as shown in Figure 3.10. Normally, the three rotation axes chosen corresponded approximately to the three external axes of the crystal, which are also illustrated in Figure 3.10.

The spectrum observed from a single crystal was of the symmetrical form shown in Figure 3.3(b), and the parameters of interest in this intensity study are the linewidth ( $\Delta H$ ) and the peak to peak height ( $H_t$ ). Using the measured values, the intensity  $I$  of the signal was calculated using equation 3.3.

$$I = (\Delta H)^2 \times H_t \quad \dots (3.3)$$

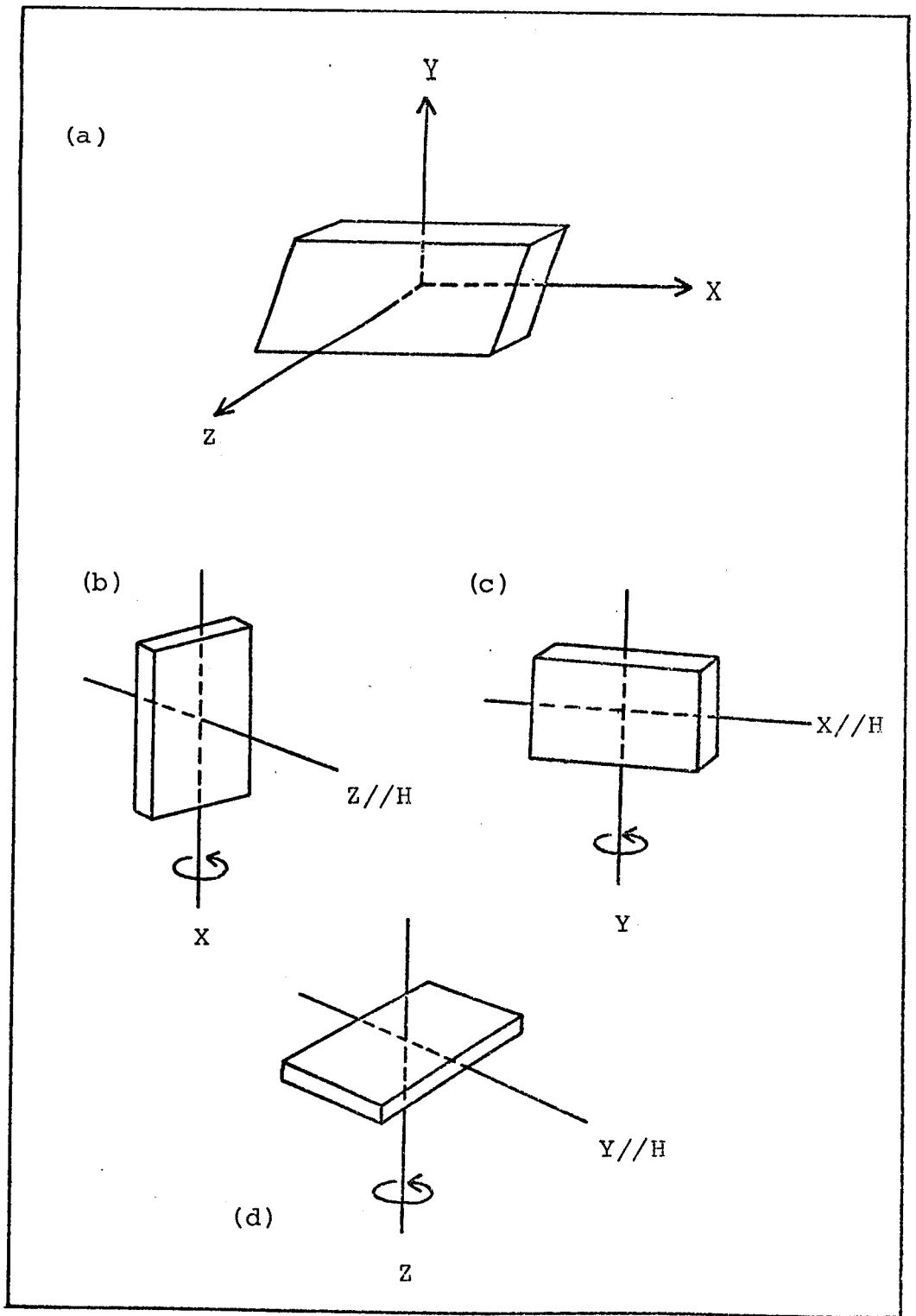


Figure 3.10

- (a) Diagram of a typical crystal of a TCNQ complex salt illustrating the labelling of the external axes.
- (b)(c)(d) The three different mountings of a crystal with each axis in turn being the rotation axis.

In the case of polycrystalline samples, although less information can be gained, the exchange integral can be estimated from the spectra by obtaining the signal intensities using the analog integrator. Two uncompact polycrystalline samples of each TCNQ complex salt were studied in this way to ensure reproducibility of the results.

(iv) Dipolar Interaction Study

At room temperature, the signal from a single crystal of a TCNQ complex salt consists of one single symmetrical peak. However, with some compounds, the linewidth of this signal is seen to increase with decreasing temperature, ultimately splitting into two peaks which then progressively move further apart and their linewidths decrease with further decrease in temperature. The two peaks arise from dipolar interaction between two electrons, previously described in section 2.5.2, and their behaviour with increasing temperature is due to an exchange interaction, also described in Chapter 2.

The narrowing of the two peaks and their separation remain constant below a certain temperature, which depends on the extent of the dipolar interaction, and at this temperature the angular variation of both the  $g$  factor and the peak separation was monitored. The separation,  $d$ , is measured from the cross-over points at the base-line of the two signals, since these points

correspond to the position of maximum intensity in the absorption spectrum. The results were then fitted to the theoretical equations using the University's ICL 1906A computer to obtain the best estimates of the parameters D and E. The programme used was a standard Fortran curve-fitting procedure (denoted by EO4 GAF in the computer) and could also be adapted for use in the g factor study.

The temperature dependence of the peak separation and the linewidths of the fine structure peaks and the resulting single peak are well described by the treatment resulting in equations 2.44 to 2.47. From these equations, it is possible to calculate the frequency of spin exchange,  $\nu$ , from the observed linewidth and peak separation data. The activation energy for exchange,  $\Delta E_e$ , was also obtained from the slope of a semilog plot of the frequency against reciprocal temperature, using equation 2.47. This in turn led to an estimate of the activation energy for exciton migration,  $\Delta E_m$ , using equation 2.49.

(v) Lineshape Study

The lineshape of the spectrum contains information about the environment of the species giving rise to the e.s.r. signal and the extent of its delocalisation. However, although a great deal of information cannot be obtained from the lineshape on its own, it can provide valuable confirmation regarding the

interpretation of other results obtained. Consequently, a simple analysis<sup>137</sup> was performed on the spectra observed in order to ascertain the lineshape. This involved investigating each half of the derivative signal separately, thereby obtaining a measure of the rate at which the signal increases to or decreases from the points corresponding to the maximum or minimum slope of the power absorption curve in relation to the magnetic field. The results could then be compared with the behaviour of standard Gaussian and Lorentzian lineshapes.

(vi) Spin-Lattice Relaxation Time Study

Whereas lineshapes are determined by the types of interactions between the spin system and its environment, the linewidths depend on the strength of the interaction and the relaxation time. Consequently, relaxation times can be obtained from a study performed on the linewidths of the spectra. This study was undertaken for two reasons. Firstly, to confirm and aid in the interpretation of other results obtained and, secondly, to investigate the cause of observed linewidth behaviour not readily explained.

Techniques for determining relaxation times fall into two categories, direct and indirect. In direct methods, the spin system is disturbed from equilibrium by an abrupt power input, and the system is observed during the return

to equilibrium. Indirect methods involve measurements of parameters that are functions of the relaxation times, and the choice of method depends on the complexity of the lineshapes being studied and the complexity of apparatus.

The method employed in this work was that of saturation-broadening and was chosen because the extra apparatus required was available and the lineshapes of all the TCNQ complex salts studied were Lorentzian, a necessary criterion in the theory behind this method.

For Lorentzian lineshapes, it has been shown<sup>148</sup> that the linewidth and the peak height of the derivative of the absorption curve depend upon microwave power in the following way, given in equation 3.4.

$$(\Delta H)^2 = \frac{4}{3} \left[ (1 + H_1^2 T_1 T_2^* \gamma^2) / \gamma^2 (T_2^*)^2 \right] \dots (3.4)$$

$\Delta H$  is the linewidth of the derivative absorption curve,  $H_1$  is the microwave magnetic field strength,  $\gamma$  is the magnetogyric ratio of the electron,  $T_1$  is the spin-lattice relaxation time, and  $T_2^*$  is related to the inverse of the linewidth.

The crystal under study was placed in the cavity at the desired orientation and the linewidths were then obtained as a function of microwave power at different temperatures. The linewidths increased as the microwave power was increased beyond the point at which the signal

became saturated. From these results, a plot of  $(\Delta H)^2$  against  $H_1^2$  was obtained for each temperature studied, which yielded a straight line with a slope equal to  $4T_1/3T_2^*$  and an intercept of  $4/3\gamma^2(T_2^*)^2$ . Furthermore, the calculated values of  $T_1$  and  $T_2^*$  were plotted as a function of inverse temperature in order to observe the variation of these parameters in the temperature range studied.

The microwave magnetic field strength,  $H_1$ , was determined for each temperature and power level used by measuring the incident power using a Marconi Type 6460 powermetre, and making use of the relation<sup>148</sup> given in equation 3.5.

$$H_1^2 = (8Q/vV_c) \left[ 1 + (c/2a)^2 \right]^{-1} (1 \pm |\Gamma_{OE}|) P \quad \dots (3.5)$$

In this expression,  $v$  is the resonant frequency,  $c$  and  $a$  are the length and breadth respectively of the cavity,  $Q$  is the loaded  $Q$  value with the sample present,  $V_c$  is the volume of the cavity,  $P$  is the incident power in mW, and the term  $(1 \pm |\Gamma_{OE}|)$  reduces to unity as the reflection coefficient  $\Gamma_{OE}$  is so small it becomes negligible.

For the cavity used in this work, equation 3.5 reduces to equation 3.6.

$$H_1^2 = (4.90 \times 10^{-7}) PQ \quad \dots (3.6)$$

The  $Q$  measurements were the most inaccurate, having an error of approximately  $\pm 10\%$ , and as such set the limit of accuracy

of the spin-lattice relaxation time measurements.

(vii) Estimate of Curie Spins

The number of spins displaying a Curie law behaviour at low temperatures, usually below 30K, was estimated by comparison with standard DPPH samples, as outlined in section 3.2.2(vi). This study could only be performed on polycrystalline samples for two reasons. In order to obtain a spectrum large enough for such an investigation, at least 2-3mg of the TCNQ complex salts were needed. Also, the single crystals, being of a more regular stoichiometry and greater perfection and, therefore, containing less of the species giving rise to the Curie signal, did not exhibit this behaviour until very low temperatures indeed, and the extremely narrow temperature range available made such a study impossible.

In the case of the polycrystalline samples, the spectrum shape shown in Figure 3.9 usually collapsed at these low temperatures to give a single symmetrical signal, which is essential for this study. However, with some of the samples studied, the spectrum did not lose its axially-symmetric shape and, therefore, an estimate of the number of Curie spins using this technique could not be obtained.

In these cases, and also for single crystals, an estimate could be obtained from the semilog plots obtained

in the investigation described in section 3.2.3(iii). These plots gave a straight line in the temperature region where depopulation of the triplet state was occurring. However, at low temperatures, the plots showed a curvature which was caused by a contribution to the intensity by the Curie Species. At even lower temperatures, where the signal from this species dominates, the product of the intensity with temperature remains constant. Therefore, by extrapolating this curvature to its limiting value, and with a knowledge of the room temperature molar susceptibility, it was possible to estimate the number of spins per mole obeying the Curie law. This was considered to be a valid estimate, as the results obtained in this way agreed very well with results obtained for the same samples using the oscilloscope technique, whenever the latter could be employed.

CHAPTER 4

RESULTS AND DISCUSSION OF E.S.R. STUDIES  
OF TCNQ COMPLEX SALTS AVAILABLE AS  
SINGLE CRYSTALS.

"Science is built up with facts, as a house is with stones. But a collection of facts is no more a science than a heap of stones is a house."

Jules Henri Poincaré

1854 - 1912

#### 4.1 DCBP(TCNQ)<sub>3</sub>

The cation 1,2-di(N-p-cyanobenzyl-4-pyridinium)-ethane (DCBP) is divalent and, consequently, this TCNQ complex salt has one neutral and two negatively charged TCNQ molecules. DCBP(TCNQ)<sub>3</sub> crystallised readily from solution forming crystals of the shape shown in Figure 3.10(a). Therefore it was possible to distinguish three distinct external axes for each crystal, each axis being labelled as the x, y or z axis, as is shown in Figure 3.10(a).

An X-ray crystallographic structure analysis of this compound has been performed in this department, and the projection along the a-axis is illustrated in Figure 4.1. The crystallographic axes a, b and c correspond approximately to the external axes x, y and z respectively. The smallest dimension of the crystal (z-axis) is approximately parallel to the perpendicular to the molecular plane of each TCNQ molecule. The longest crystal dimension (x-axis) is almost parallel to the long molecular axis of each TCNQ molecule and, therefore, the intermediate of the crystal (y-axis) is approximately parallel to the short molecular axis of each TCNQ molecule.

As can be seen from Figure 4.1, the cations not only separate each TCNQ stack, but also separate the triads within each stack. The p-cyanobenzyl end groups protrude into the stack, as if taking the place of a fourth TCNQ

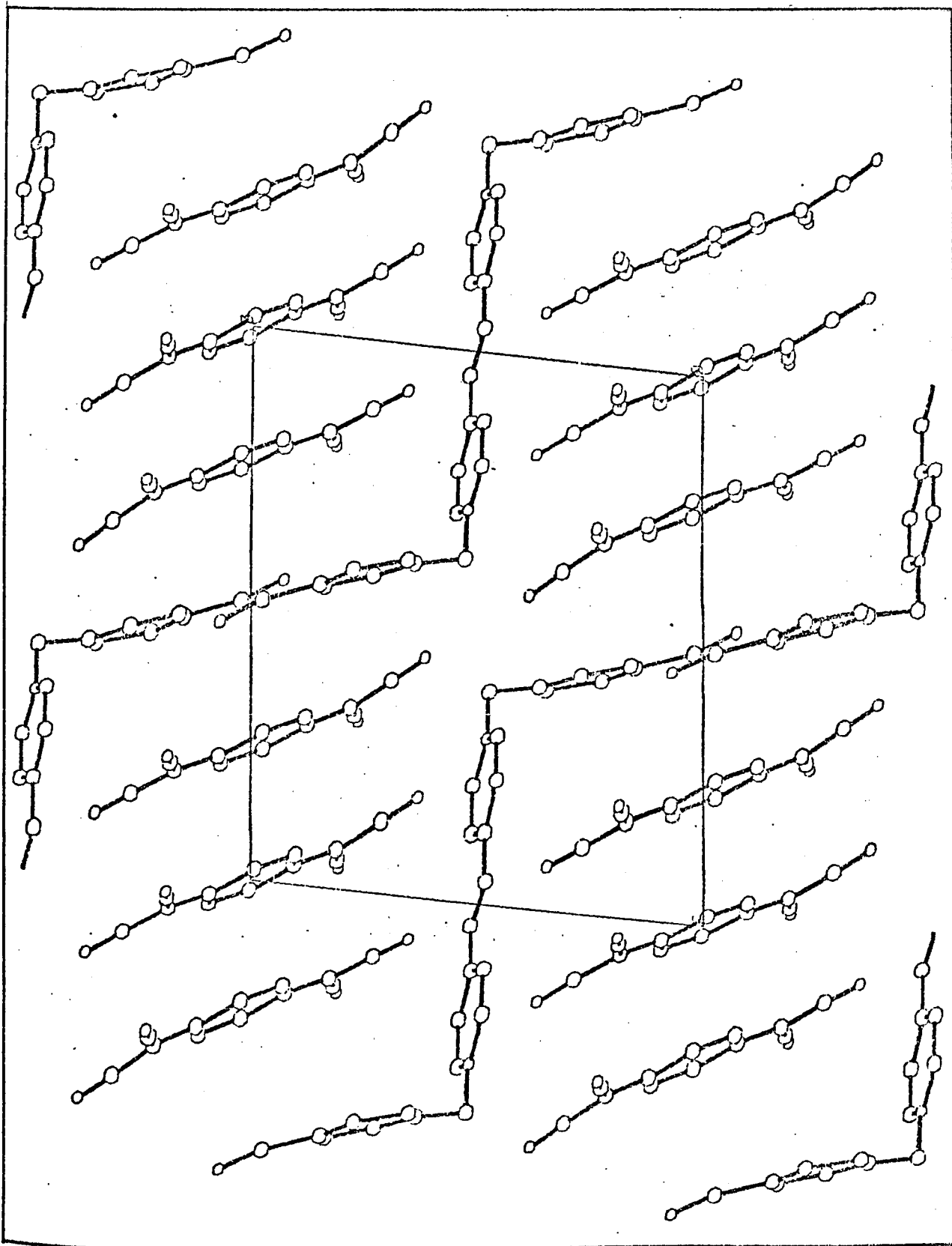


Figure 4.1

DCBP(TCNQ)<sub>3</sub>

Projection of the crystal structure along the a-axis.

molecule, such a tetrad being in actual fact the preferred stoichiometry of TCNQ complex salts having divalent cations. Each triad is isolated from the others, therefore, in directions x and z, but not along y, which is the stack-to-stack direction. This would most probably be expected to result in approximately isotropic conductivities in two directions and a lower conductivity in the direction through the planes of cations. This is fairly unusual for these compounds, as normally all the three directions have differing conductivities. Preliminary conductivity measurements<sup>149</sup> have indicated that the room temperature d.c. conductivity for DCBP(TCNQ)<sub>3</sub> is approximately  $10^{-5}$  ohm<sup>-1</sup> cm<sup>-1</sup>, which is lower by several orders of magnitude than for the similar complex salt N,N'-dibenzyl-4,4'-bipyridinium(DBBP)-(TCNQ)<sub>4</sub>. From the crystal structure of DBBP(TCNQ)<sub>4</sub><sup>150</sup>, the cation does not protrude into the TCNQ stack and, therefore, it would appear that the intrusion of the long cations in DCBP(TCNQ)<sub>3</sub> is reflected in a significant lowering of the conductivity along the stacking direction, which is normally the most conductive axis. In order to investigate how this unusual structure might affect the magnetic properties, e.s.r. studies of this complex salt were undertaken.

Three crystals of DCBP(TCNQ)<sub>3</sub> were studied, each axis in turn being the rotation axis, as described in section 3.2.3(iii) of the previous chapter. Crystal 1 was

mounted with the x-axis as the axis of rotation and, consequently, the plane under study as the crystal was rotated relative to the magnetic field contained the y- and z-axes. Similarly, crystals 2 and 3 were mounted with the z- and y-axes as the rotation axes, and the xy and xz planes respectively were investigated as the crystal was rotated.

During a preliminary investigation of crystal 1, it was found that a single symmetrical e.s.r. signal was observed at room temperature. However, on lowering the temperature, the spectrum changed in the manner shown in Figure 4.2. This is indicative of exchange interaction which results in the collapse of fine structure caused by dipolar interaction between two electrons, these two phenomena having been previously discussed in section 2.5.2 and illustrated in Figure 2.12. This behaviour has been observed in many TCNQ complex salts<sup>23,33,120,121,151,152</sup>, and is associated with the presence of localised triplet excitons. The observation of this behaviour is, therefore, not altogether surprising in DCBP(TCNQ)<sub>3</sub> with regard to the low conductivity observed with this compound and the segregation of the triads, which might be expected to cause the triplet exciton to be restricted on one such group of TCNQ molecules. Furthermore, with only three TCNQ molecules in each group within the stack, the two electrons constituting the triplet species must have a

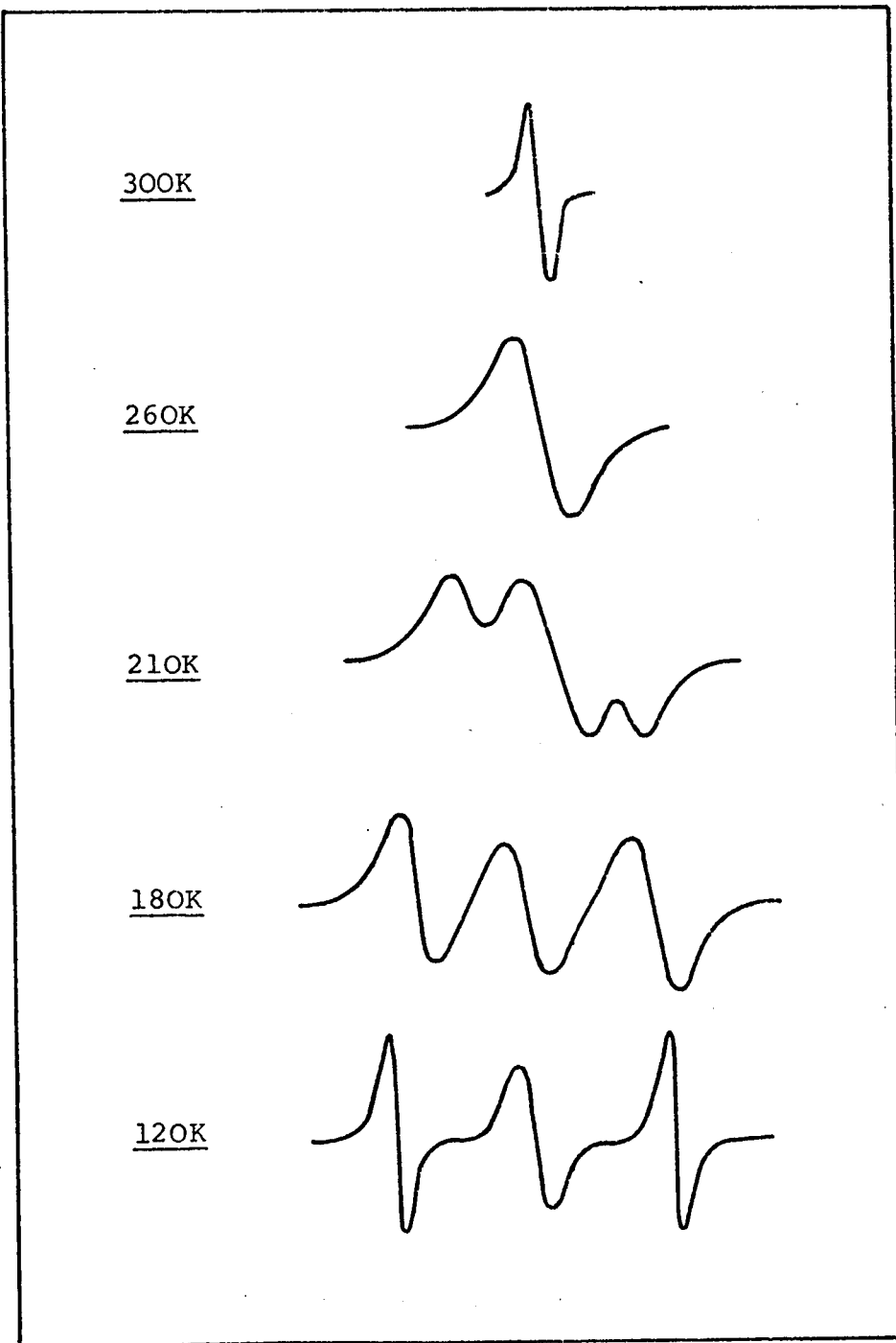


Figure 4.2

DCBP (TCNQ)<sub>3</sub>

Effect of exchange interaction with increasing temperature on the spectrum of a single crystal.

fairly small separation. The observation of measurable dipolar splittings, therefore, confirms the close proximity of the two electrons, as the extent of the dipolar interaction is very dependent on the average distance between them.

Figure 4.2 differs from Figure 2.12 in that there is a central signal in addition to the two outer lines which constitute the fine structure expected from a localised triplet exciton. The type of spectrum shown in Figure 4.2 has also been observed previously with many TCNQ complex salts and the proposed interpretation of this central signal will be discussed with the temperature dependence of the signal intensities presented later in this section.

The dipolar splitting of the two outer peaks remained at a constant value below 120K and, consequently, the angular variations of this splitting and the g factor were monitored at this temperature. The experimental results are shown in Figure 4.3 to 4.8, which also show the results obtained from the computerised least-squares curve-fitting procedure for obtaining  $D$ ,  $E$ ,  $g_x$ ,  $g_y$ ,  $g_z$ ,  $\theta$  and  $\psi$ . The values obtained for all these parameters which give the best fit to the experimental data are presented in Tables 4.1 and 4.2.

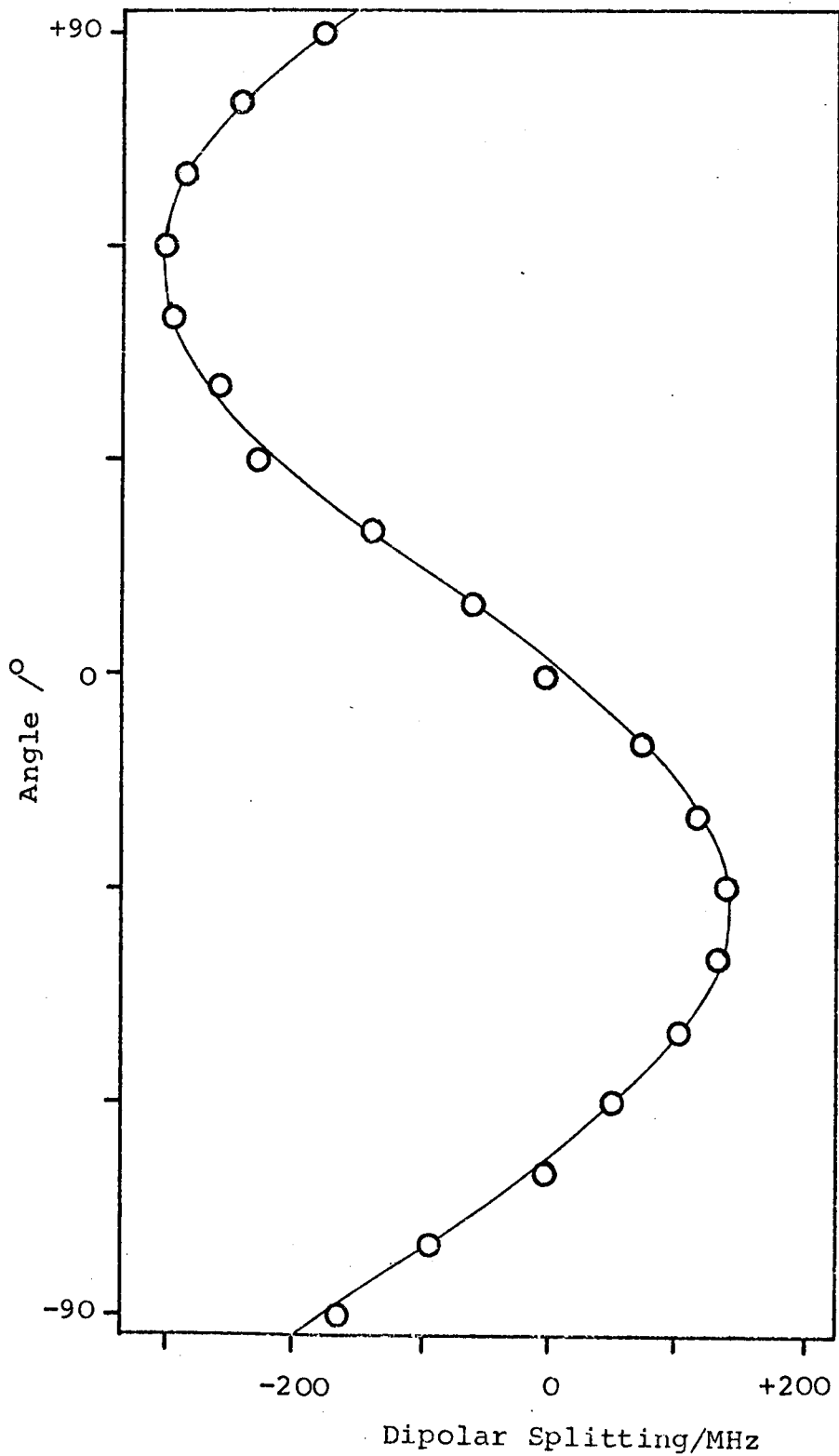


Figure 4.3

DCBP(TCNQ)<sub>3</sub>

Angular variation of dipolar splitting at 120K for crystal 1.

Approximate orientations: H//y-axis at  $-33^\circ$   
H//z-axis at  $+57^\circ$

———— Computer simulation.

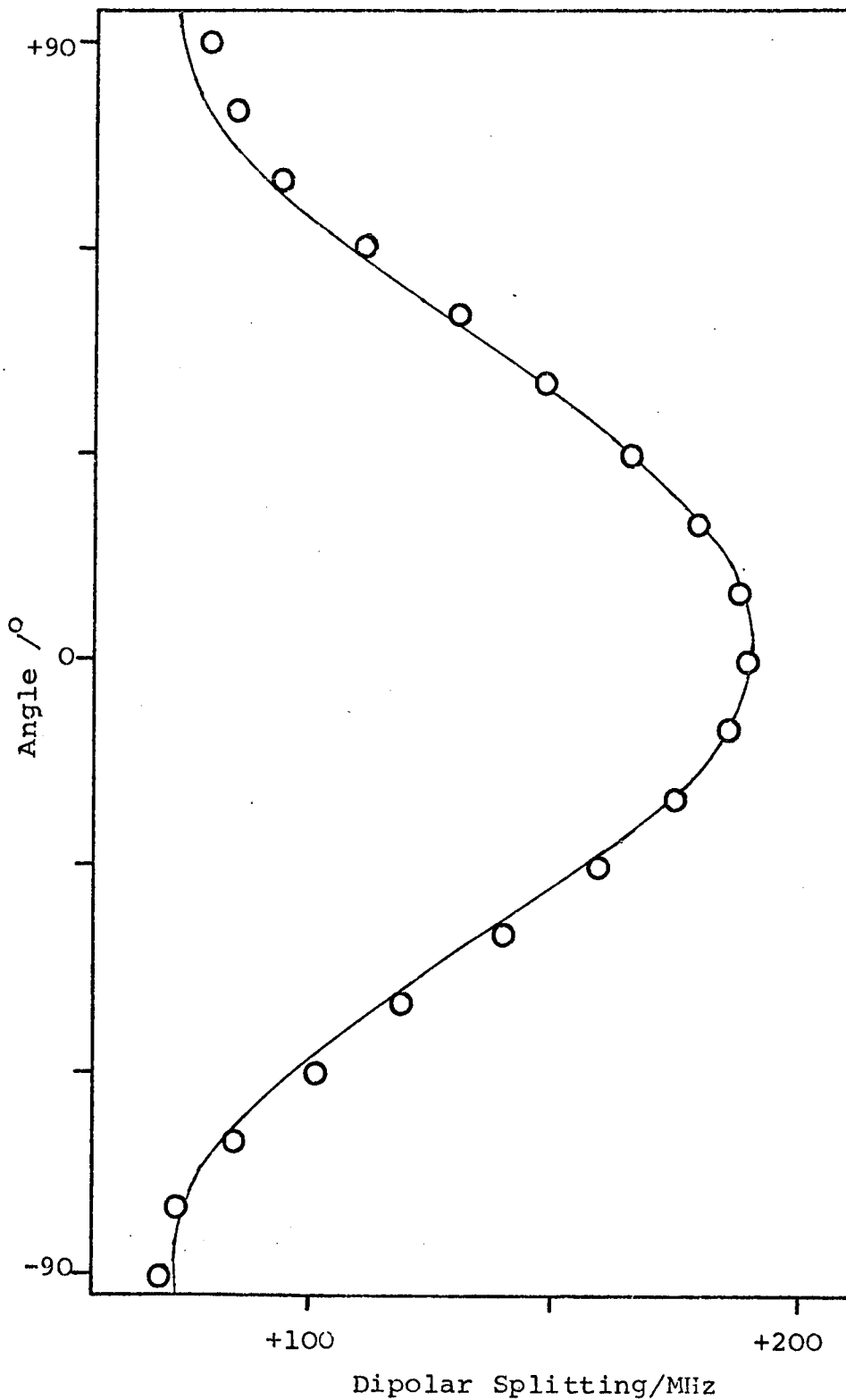


Figure 4.4

DCBP(TCNQ)<sub>3</sub>

Angular variation of dipolar splitting at 120K for crystal 2.

Approximate orientations : H//y-axis at  $-87^\circ$ .

H//x-axis at  $+3^\circ$ .

———— Computer simulation.

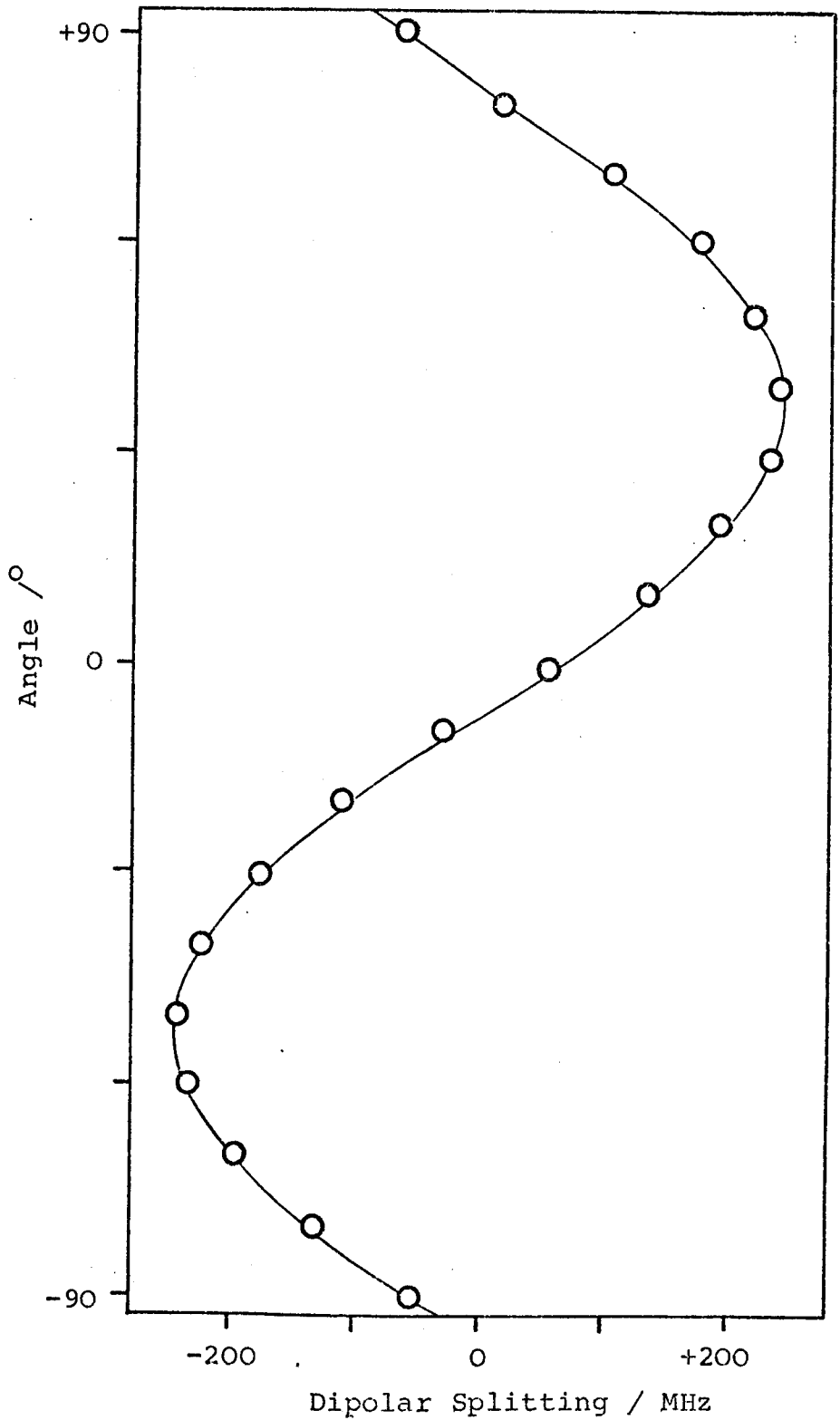


Figure 4.5

DCBP(TCNQ)<sub>3</sub>

Angular variation of dipolar splitting at 120K for crystal 3.

Approximate orientations: H//x-axis at +37°.

H//z-axis at -53°.

— Computer simulation.

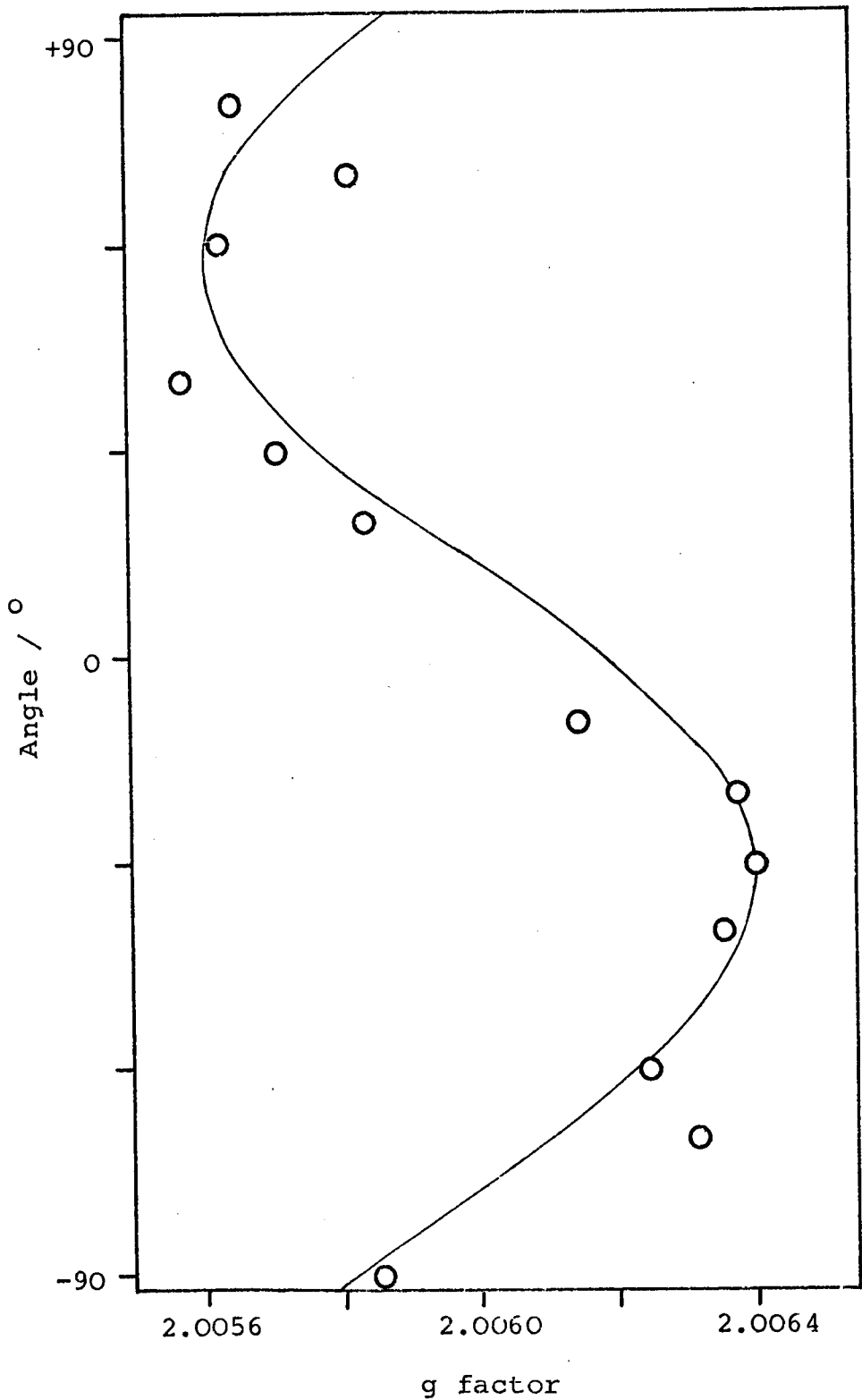


Figure 4.6

DCBP(TCNQ)<sub>3</sub>

Angular variation of g factor at 120K for crystal 1.

Approximate orientations as for Figure 4.3.

— Computer simulation.

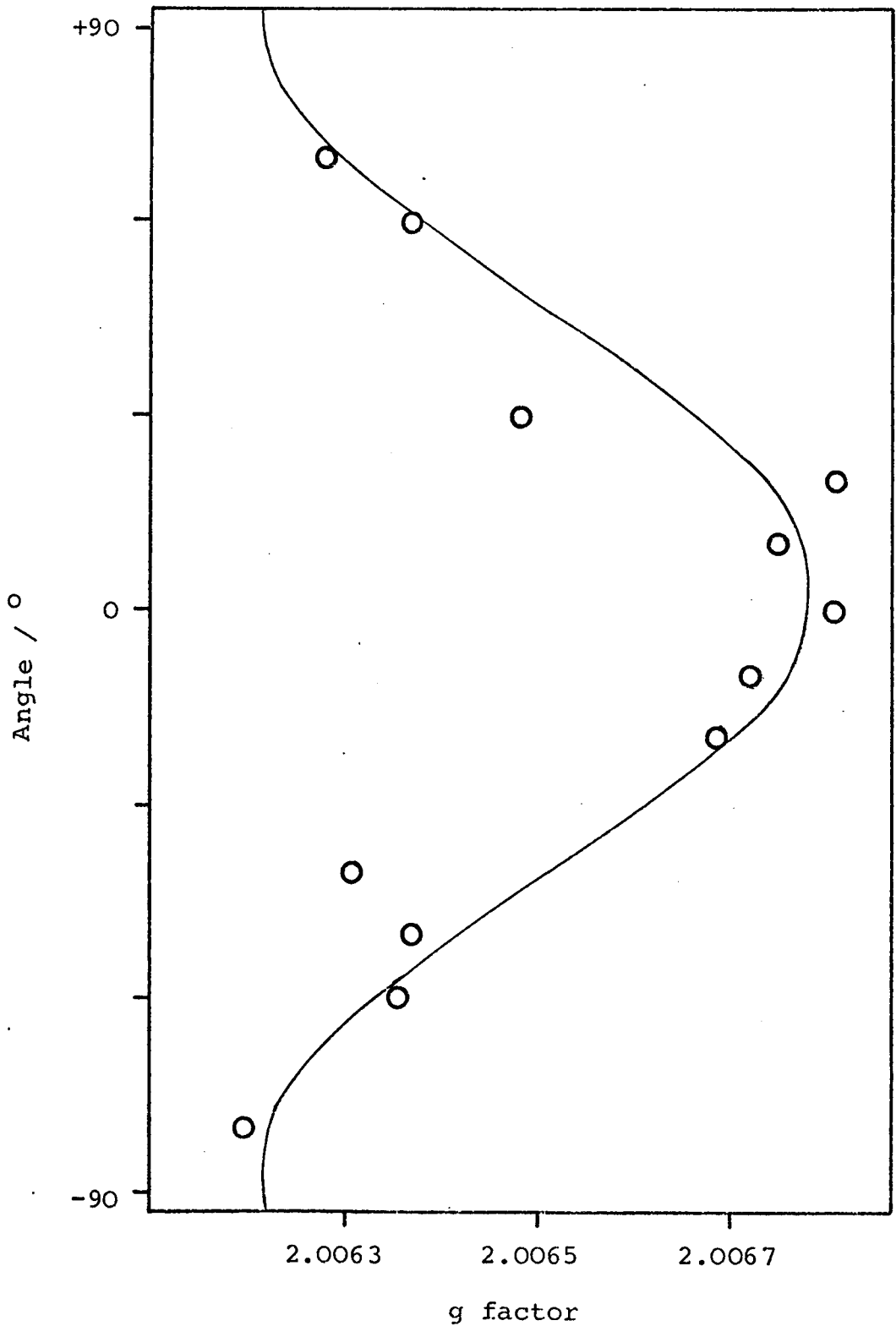


Figure 4.7

DCBP(TCNQ)<sub>3</sub>

Angular variation of g factor at 120K for crystal 2.

Approximate orientations as for Figure 4.4.

— Computer simulation.

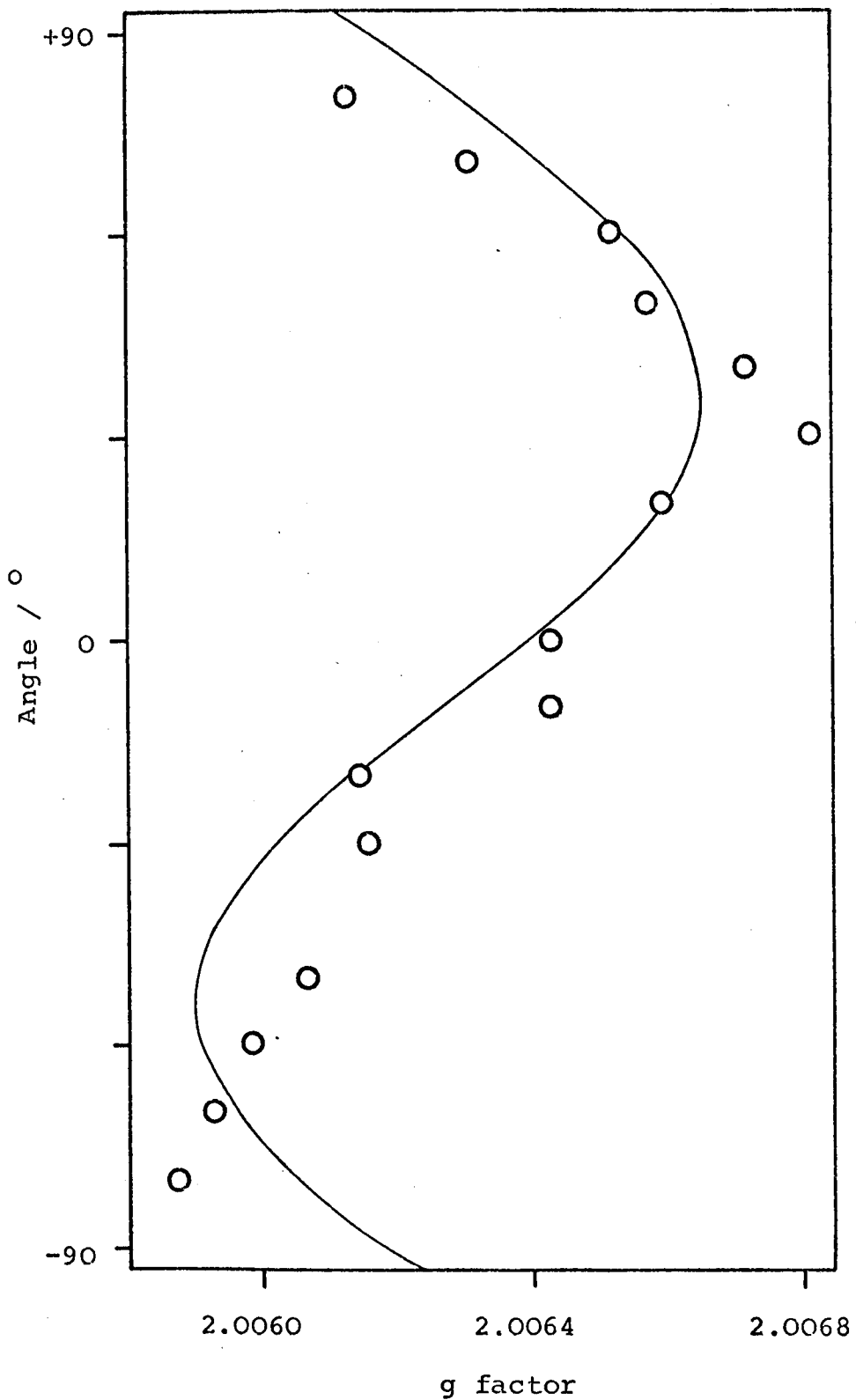


Figure 4.8.  
 DCBP(TCNQ)<sub>3</sub>  
 Angular variation of g factor at 120K  
 for crystal 3.  
 Approximate orientations as for Figure 4.5.  
 — Computer simulation.

Table 4.1 Results of the Dipolar Splitting Study for DCBP(TCNQ)<sub>3</sub>.

Crystal	D (MHz)	E (MHz)	$\theta$ ( $^{\circ}$ )	$\psi$ ( $^{\circ}$ )	Standard Deviation (MHz)
1	-153.15	19.09	0.03	0.02	1.77
2	-131.83	19.57	0.00	0.02	0.66
3	-121.80	39.20	84.97	0.00	1.44

Table 4.2 Results of the g Factor Study for DCBP(TCNQ)<sub>3</sub>.

Crystal	$g_x$	$g_y$	$g_z$	Standard Deviation.
1	2.0065	2.0064	2.0056	0.0002
2	2.0068	2.0062	2.0058	0.0001
3	2.0067	2.0061	2.0059	0.0001

In order for the programme to run successfully, the values of the variable parameters had to be assessed from the experimental points and used as input data. The computer would then calculate the parameters which gave the best fit to the experimental points according to equations 2.36 to 2.43, which are the theoretical equations governing these angular variations. The standard deviations given in the two tables are a measure of the difference

between the calculated and experimental values of the variable parameters. The standard deviation in Table 4.1 is less than the  $\pm 2\%$  error estimated in section 3.2.2(iv) for measurement of the splittings. Similarly, in Table 4.2 the standard deviation is seen to be less than the error involved in the g factor measurement, estimated in section 3.2.3(i).

The signs of D and E values given in Table 4.1 are those given by the computer and show that these two parameters must be opposite in sign for a fit to the experimental data. However, it is not possible to definitely assign D and E as positive or negative, as this can only be done from low temperature measurements<sup>153</sup>. Therefore, the average values obtained in this work for the zero-field splitting parameters of DCBP(TCNQ)<sub>3</sub> are  $\pm(136\pm 18)$ MHz for D and  $\pm(26\pm 13)$ MHz for E.

The dimensionality of these complex salts has been shown<sup>23,51,154</sup> to be reflected by the g factor variation in single crystals. These studies have shown that the g tensor most closely associated with the stacking direction is closer to the free electron value of 2.00232 than those associated with the other two directions. It can be seen from the values of the g factors in Table 4.2 that there is not a great deal of anisotropy of the g factor in this complex salt. The

average values obtained for  $g_x$ ,  $g_y$  and  $g_z$  are 2.0067, 2.0062 and 2.0058 respectively with an experimental error of  $\pm 0.0003$ . The stacking direction (z-axis) has the smallest principal value of the g tensor, that is, the g factor closest to the free electron value. However, the differences between the three g values are not well outside the error involved, and this small degree of anisotropy relates well with the crystal structure analysis. Therefore, the g factor measurements and comparison of the d.c. conductivity with  $\text{DBBP}(\text{TCNQ})_4$  both suggest that the degree of one-dimensionality in this compound has been reduced by the intrusion of the end groups of the cations into the TCNQ stack.

Chestnut and Phillips<sup>23</sup> have compared D and E values obtained with various TCNQ complexes with the parameters observed for naphthalene, in which the triplet state is confined to a single molecule, and also with ethylene. From these comparisons, it became clear that the greater D is with respect to E, the greater is the two-dimensional extent of the molecular plane. Also, the magnitudes of D and E reflect the average spacial distribution of the correlated spins of the exciton. Therefore, as the spins remain near each other so that they interact more strongly, the D and E values increase. The results obtained for  $\text{DCBP}(\text{TCNQ})_3$ , from similar comparisons, agree well with this interpretation, as the

relatively small values of D and E indicate the triplet exciton does not reside on a single molecule, but is delocalised over several TCNQ molecules, which allows the effective distance of separation of the electrons to be comparatively large.

The crystal structure analysis indicated that the two unpaired electrons constituting the triplet exciton are mainly residing on the two outer TCNQ's of the triad at a distance 0.644nm apart, the intermolecular spacing being 0.322nm. The most recent approximate treatment of the variation of D and E with this average separation<sup>121</sup>, assuming the size of the triplet exciton is a unit cell along the stack, shows that the D and E values for DCBP(TCNQ)<sub>3</sub> indicate an average separation of 0.583nm, which is consistent with the charge distribution obtained in the crystal structure analysis. It is interesting to note that, because of the small singlet-triplet energy gap of the majority of TCNQ complex salts, the information obtained at room temperature from crystallography data will largely reflect the electron distribution in the triplet state.

The results obtained<sup>127</sup> for DBBP(TCNQ)<sub>4</sub> give D as  $\pm 202$ MHz and E as  $\pm 36$ MHz, and the distance calculated between the two electrons agrees well with the crystal structure analysis, which indicates that the electrons are localised mainly on the two central TCNQ molecules in the tetrad. The small D and E values obtained for

DCBP (TCNQ)<sub>3</sub> in this work are consistent with these results as they are of the correct order of magnitude expected for the electrons being localised on the outer TCNQ molecules of a triad. Furthermore, as previously mentioned in section 2.5.1, Frenkel spin excitons are strongly correlated electrons which move as a pair, whereas Wannier spin excitons are not strongly correlated and the electrons move independently of each other. Therefore, the observation of measurable dipolar splittings in this complex salt provides evidence for Frenkel triplet excitons localised on the triad, which indicates a value close to zero for the alternation parameter,  $\gamma$ .

Flandrois and Chasseau<sup>155</sup> have examined most of the known crystal structures of TCNQ complexes and have determined a correlation between the zero-field splitting parameters with the degree of charge density, calculated from the bond lengths of the TCNQ molecules, and the separation of the molecules on which the two electrons reside. This treatment has been applied in this work and the results are shown for this and other reported TCNQ complex salts in Figure 4.9. The calculation of the charge density,  $\rho$ , for DCBP (TCNQ)<sub>3</sub> used the TCNQ bond lengths obtained from the crystallography data and a value of 0.644nm for the separation,  $d$ , between the two TCNQ molecules. It can be seen from Figure 4.9 that the results

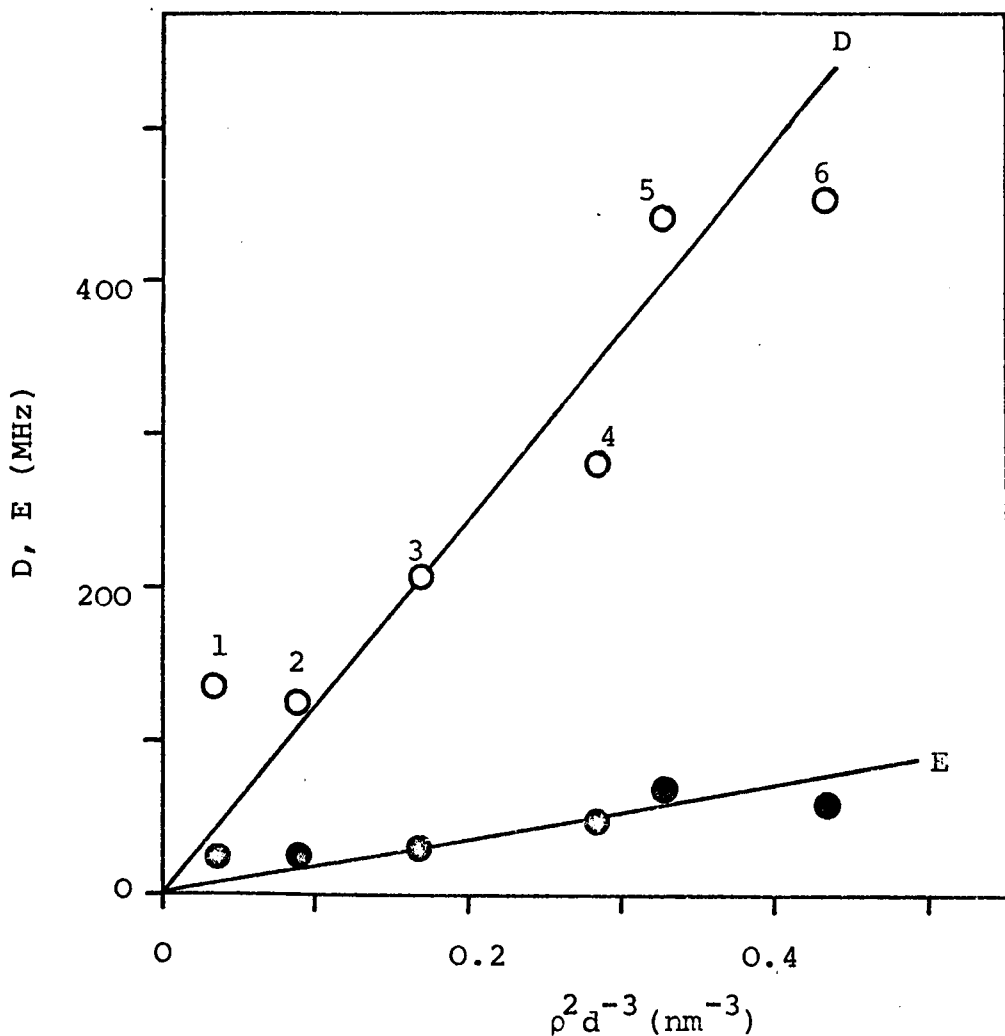


Figure 4.9.

Correlation between the parameters D and E and the charge,  $\rho$ , carried by two TCNQ molecules separated by a distance,  $d$ .

1. DCBP(TCNQ)<sub>3</sub>
2. Triethylammonium(TEA)-(TCNQ)<sub>2</sub><sup>156</sup>.
3. Di-(N-pyridinium-methyl)benzene(TCNQ)<sub>4</sub><sup>155</sup>.
4. Cs<sub>2</sub>(TCNQ)<sub>3</sub><sup>33</sup>.
5. Trimethylbenzimidazolium(TCNQ)<sub>2</sub><sup>121</sup>.
6. Morpholinium(TCNQ)<sub>2</sub><sup>120</sup>.

for the compound under study are in reasonable agreement with results of other complexes.

The collapse of the fine structure observed and the subsequent narrowing of the resulting single e.s.r. peak were investigated from 300 to 120K. As discussed in section 2.5.2, the exchange phenomenon resulting in this behaviour is well described by equations 2.44 and 2.46, and the values of the exchange frequency,  $\nu$ , obtained from these equations can be plotted in the form of  $\log \nu$  against  $1/T$ . Figure 4.10 illustrates a typical example of such a plot for DCBP(TCNQ)<sub>3</sub> and it can be seen that, although results obtained using equations 2.45 and 2.46 agree, there is a discrepancy between these results and those calculated from equation 2.44. Results similar to these, also showing such an anomaly, have been previously reported<sup>120,122,151,157</sup> for other TCNQ complex salts. The linearity of the plots indicates that the exchange interaction is activated and, using equation 2.47, the activation energy for exchange,  $\Delta E_e$ , can be obtained from the slopes. The average value of  $\Delta E_e$  for the three crystals studied in this work, using equations 2.45 and 2.46, is  $13.5 \pm 2.0 \text{ kJ mol}^{-1}$ , whilst the value using equation 2.44 is only  $2.5 \pm 1.1 \text{ kJ mol}^{-1}$ .

The persistent occurrence of this anomaly with respect to the doublet separation data has so far defied

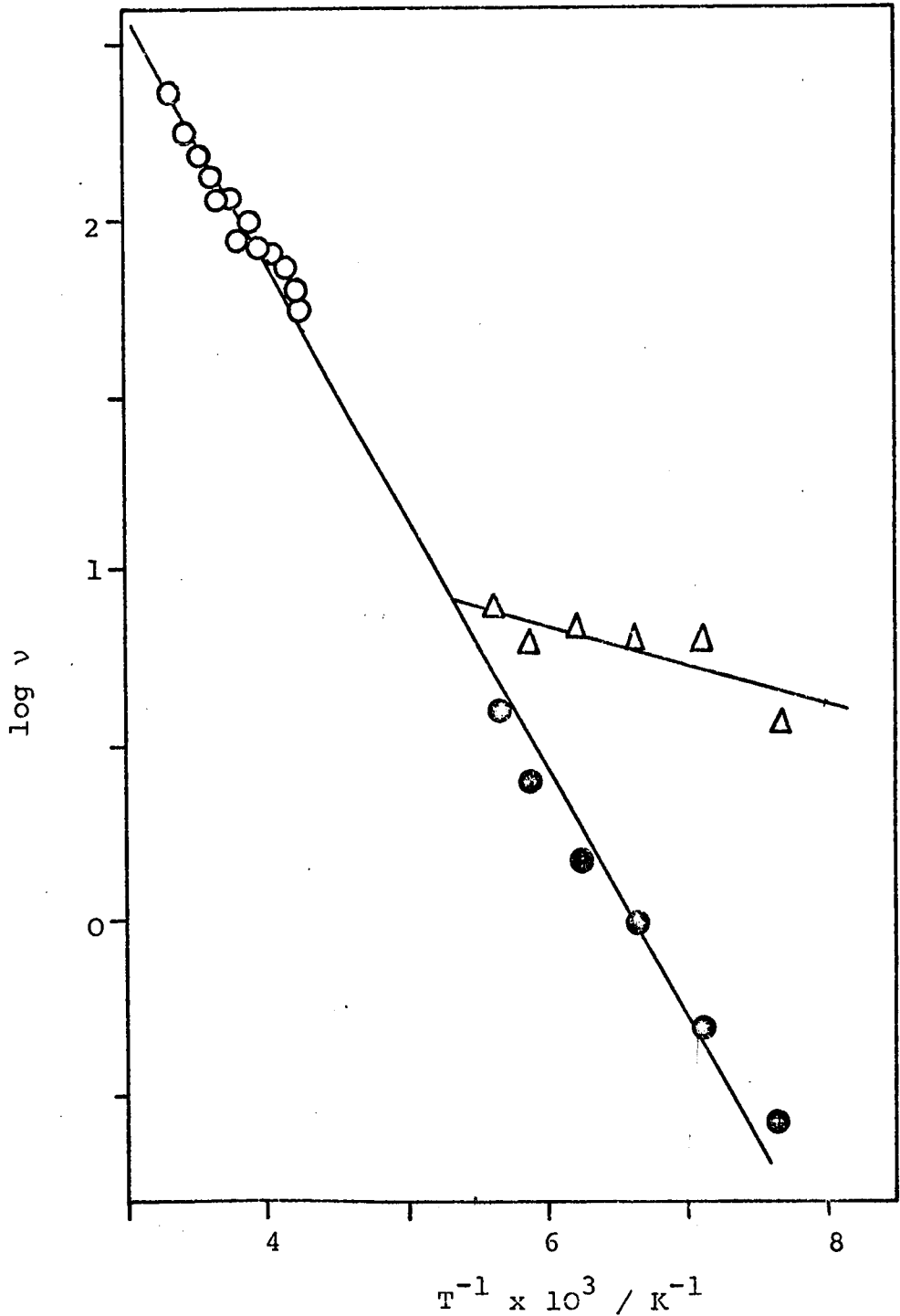


Figure 4.10

DCBP(TCNQ)<sub>3</sub>.

Semilog plot of the frequency (in MHz) of exciton spin exchange interaction against reciprocal temperature for crystal 2.

H is approximately parallel to the y-axis.

Frequencies calculated from:  $\Delta$  Equation 2.44

$\bullet$  Equation 2.45

$\circ$  Equation 2.46

explanation although several proposals have been made. Lynden-Bell and McConnell<sup>104</sup> postulated a temperature dependent  $d_0$  value arising from the existence of broad exciton bands having a bandwidth of the order of  $kT$ . However, the observations made on complex salts displaying measurable dipolar splittings strongly indicate that the effective exciton bandwidth must be very small, because the motion of the exciton is diffusional rather than wavelike<sup>116</sup>. Therefore, this would not be expected to be the case in the localised DCBP(TCNQ)<sub>3</sub>. The most reasonable explanation<sup>158</sup> of the temperature dependence of the dipolar splittings considers the exciton as a result of correlation between an electron and a hole, and proposes that the mean distance between them increases with temperature. This might be caused by expansion of the lattice, which would be expected to result in a temperature dependent value for the singlet-triplet energy gap,  $J$ . Kepler<sup>24</sup> originally discussed such a possibility but also pointed out that any change in the value of  $J$  could only be detected from absolute susceptibility measurements over the temperature range under consideration. As the determination of this quantity is not sufficiently accurate using e.s.r., the proposal could not be investigated for this compound. However, it is generally considered that the activation energies for exchange calculated from the linewidth data are more likely to be correct, as values obtained from the line separation data have been found to be less than  $J$  in this and other works<sup>122,151</sup>. Explanation of the behaviour resulting from

exchange interactions relies on the presence of the triplet excitons, therefore an activation energy for exchange less than the energy required to form a triplet exciton is difficult to perceive. Furthermore, calculations from spin-lattice relaxation measurements<sup>159</sup> have supported the values of  $\Delta E_e$  obtained from the linewidth approximations of equations 2.45 and 2.46.

Although early considerations<sup>23</sup>, which only considered the line separation data, obtained an equivalence of  $J$  and  $\Delta E_e$ , it only led to confusion as the authors concluded that the temperature dependence of the exchange arose simply from the temperature dependence of triplet state population. This led to inconsistencies between experimental results and the theory of exciton-exciton interactions as they neglected the possibility of exciton migration which is essential for the explanation of many of the features of the e.s.r. spectra obtained with TCNQ complex salts. This contribution to the value of  $\Delta E_e$  has been previously mentioned in section 2.5.2 and resulted in equation 2.49. The average value for the activation energy for exciton migration, obtained from this equation, is  $5.6 \pm 2.1 \text{ kJ mol}^{-1}$ , using the average value of  $\Delta E_e$  obtained from the linewidth approximations. This value of  $\Delta E_m$  is further evidence for localised triplet excitons in DCBP (TCNQ)<sub>3</sub> as it indicates an activated hopping process as the mechanism for exciton migration,

The analysis of the observed exchange phenomenon for DCBP(TCNQ)<sub>3</sub> outlined above is in agreement with published results for other TCNQ complex salts, and yields values of the exchange parameters consistent with localised triplet excitons, whose activated motion results in exciton-exciton collisions causing an averaging of the dipolar interaction. These conclusions are supported by lineshape analyses performed on the spectra obtained in both the 'slow' and 'fast' exchange regions, and are presented in Figures 4.11 and 4.12. As mentioned in section 2.4.8, a Lorentzian lineshape is a strong indication of the presence of exchange interactions, and the lineshapes obtained for DCBP(TCNQ)<sub>3</sub> provide confirmation that the observed signals are indeed arising from migrating species. Calculation of the exciton lineshapes, based on the theory of motional narrowing<sup>160</sup>, has been given by Soos<sup>107</sup>. The theory predicts Lorentzian lines for localised diffusional excitons in agreement with experiment<sup>161,162</sup>, and also gives correct residual hyperfine linewidths from the calculated jumping rate. The fact that the anisotropic hyperfine interactions do contribute to the linewidths at low exciton densities has been confirmed by their angular dependence in high magnetic field and by deuterium substitution<sup>162</sup>. This contribution to the linewidth is unresolved even in localised excitons which, although at high temperatures move by a thermally activated process, still move by a non-activated process at low temperatures

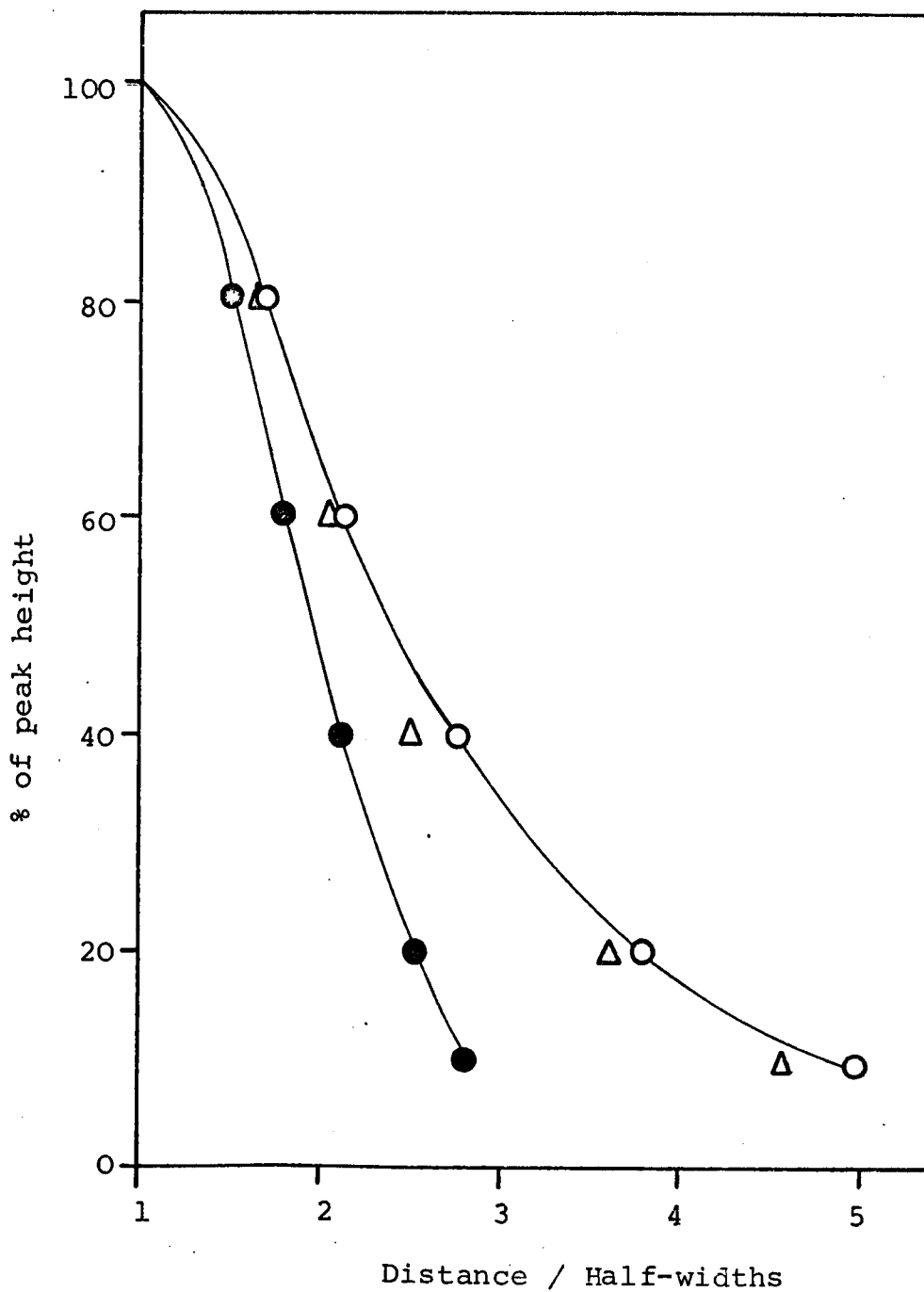


Figure 4.11

DCBP(TCNQ)<sub>3</sub>

Lineshape analysis for crystal 1 at 130K  
('slow' exchange region).

H is approximately parallel to the z-axis.

●—● Gaussian lineshape.

○—○ Lorentzian lineshape

Δ Average shape for crystal

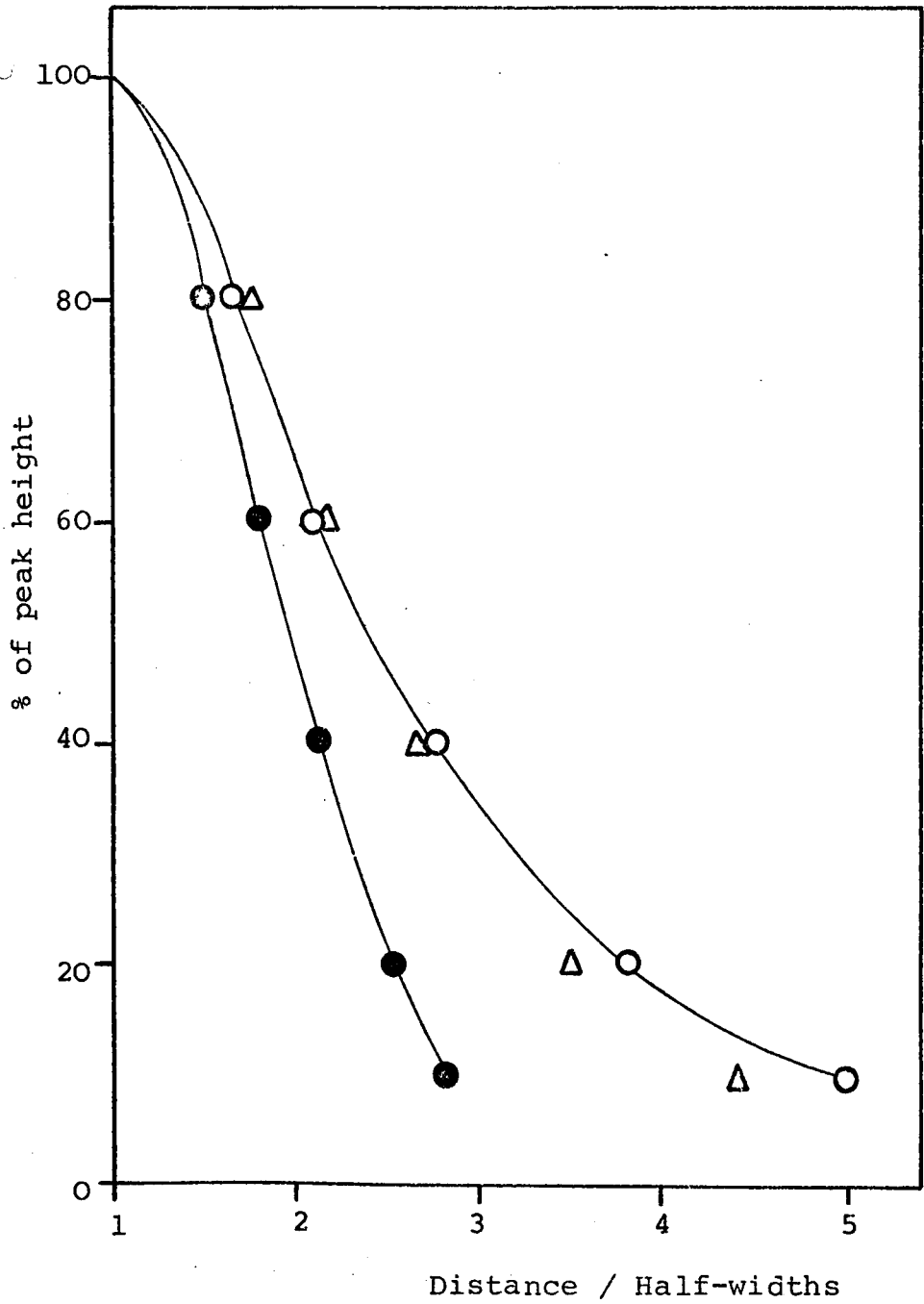


Figure 4.12

DCBP(TCNQ)<sub>3</sub>

Lineshape analysis for crystal 1 at 270K  
('fast' exchange region).

H is approximately parallel to the z-axis.

- Gaussian lineshape
- Lorentzian lineshape
- △ Average shape for crystal.

fast enough to remove hyperfine structure<sup>108</sup>.

The relative intensities of the doublet peaks arising from dipolar interaction were investigated between the temperatures 120 and 95K for all the three crystals in order to obtain the value of the singlet-triplet energy gap. Measurements below 95K were not possible because the doublet peaks had become so small as to be unobservable, whereas measurements above 120K were hindered by the peaks losing their symmetrical shape as the dipolar splitting began to collapse. Similarly, intensity measurements could only be made on the resulting single peak in the narrow temperature range of 300 to 240K.

Figures 4.13 and 4.14 show the typical log IT against  $1/T$  plots obtained in the high temperature and low temperature regions respectively. The average value of the slope for a number of such plots is  $-7.9 \pm 0.7$  kJ mol<sup>-1</sup> and, for a localised triplet exciton having  $\gamma$  close to zero, the slope should be equal to  $-J$  from the temperature dependence given in equation 2.28. This can be confirmed by comparing the molar susceptibility value, obtained at room temperature, with the value predicted by equation 2.28, using the value of  $J$  obtained from the slopes as above. This was found to give a  $\chi_m$  value of  $4.0 \times 10^{-4}$  e.m.u. cm<sup>3</sup> mol<sup>-1</sup>, which is in good agreement with the experimental value of  $(4.3 \pm 0.8) \times 10^{-4}$  e.m.u. cm<sup>3</sup> mol<sup>-1</sup>. Kepler's equation for

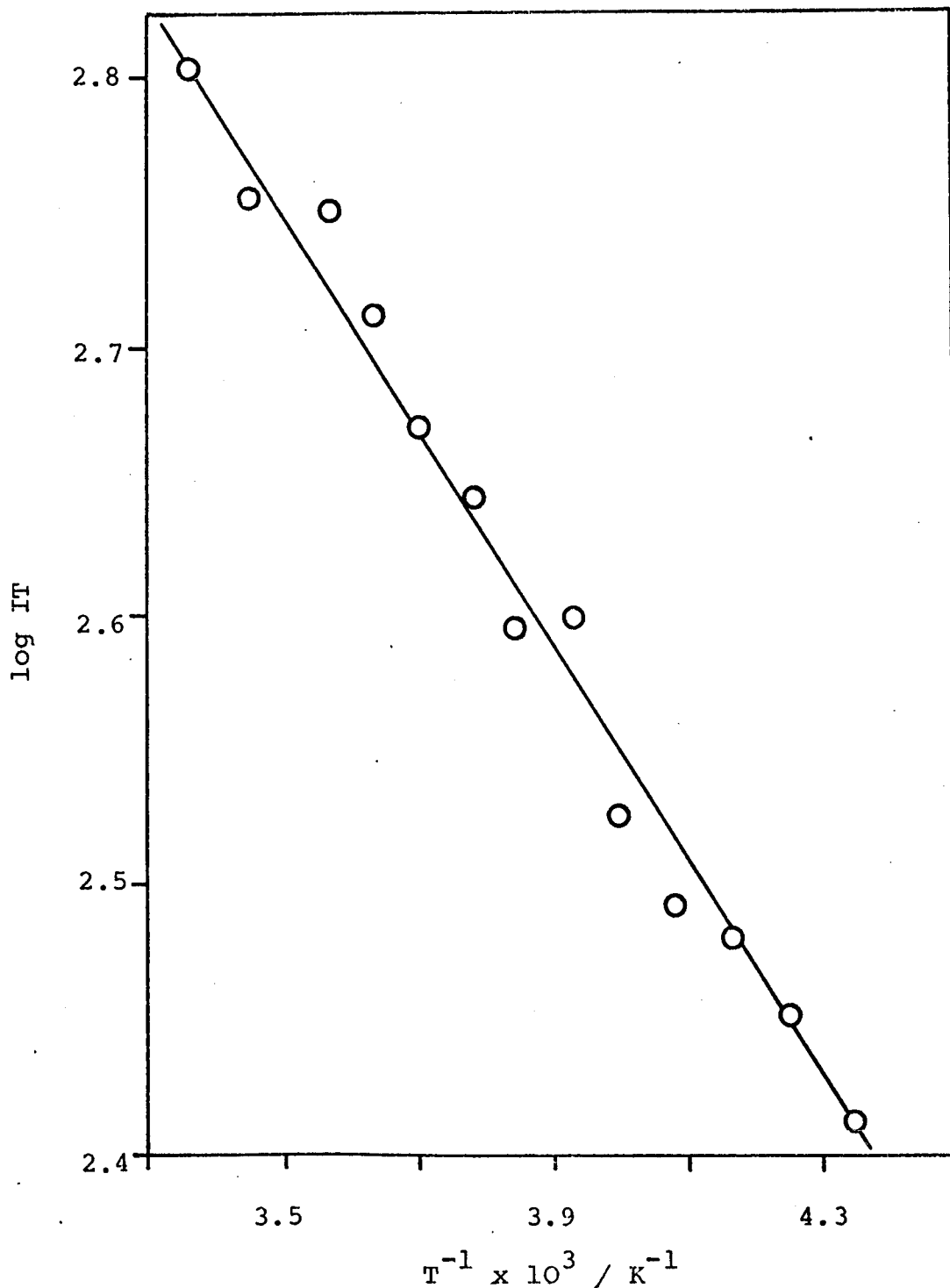


Figure 4.13

DCBP(TCNQ)<sub>3</sub>

Semilog plot of the product of the relative intensity and temperature against reciprocal temperature for crystal 2.

H is approximately parallel to the y-axis.

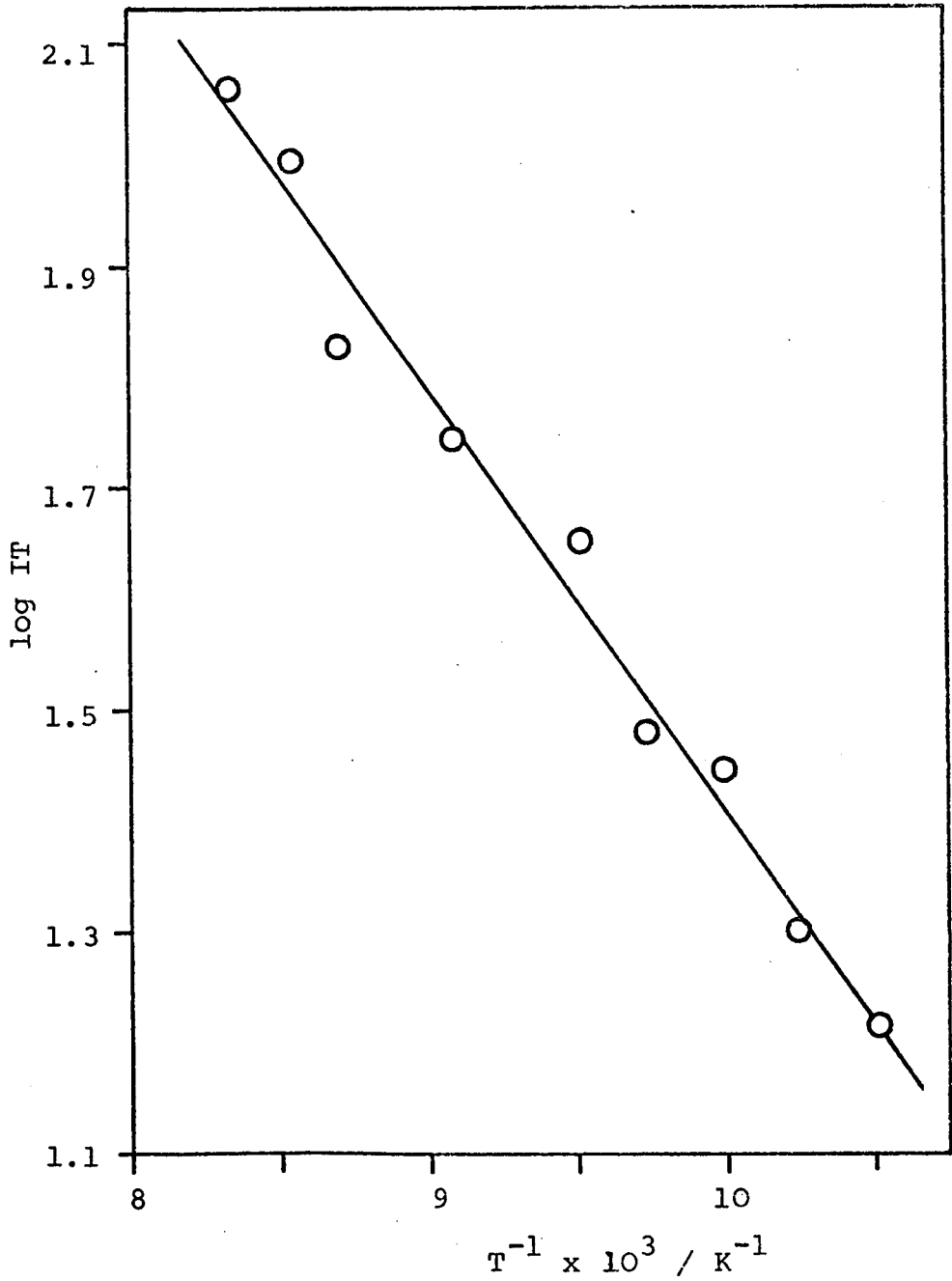


Figure 4.14

DCBP(TCNQ)<sub>3</sub>

Semilog plot of the product of the relative intensity and temperature against reciprocal temperature for crystal 1.

H is approximately parallel to the z-axis.

localised triplet states, given in equation 2.26, yields a theoretical value of  $3.6 \times 10^{-4}$  e.m.u.  $\text{cm}^3 \text{mol}^{-1}$  for this compound. Therefore, comparison of the molar susceptibility values calculated from equations 2.26 and 2.28 with the experimental value indicates the presence of localised triplet excitons in  $\text{DCBP}(\text{TCNQ})_3$ . Although the assessment of the susceptibility is complicated by the presence of the central signal, which will make a contribution to the observed value, the above comparison is considered to be still valid as this contribution is calculated to be very small.

As the temperature was decreased from room temperature, the signal was observed to split into three symmetrical peaks, as illustrated in Figure 4.2. The outer two peaks have been interpreted in terms of the doublet produced as a result of dipolar interaction, and the broader central signal, which had a g factor close to the free electron value, was initially thought to be due to defects in the lattice resulting in isolated monoradical ions. However, the intensity study of this signal, performed below 120K, was not found to follow the expected Curie law behaviour for such doublet state species but followed the behaviour attributed to a ground singlet state with a thermally accessible excited triplet state. Spectra of this type with a central signal have been reported in other TCNQ complexes but, in the majority of cases, the central

signal did follow the expected Curie law temperature dependence<sup>151,157,158,163</sup>. However, there have been reports<sup>23,33,120,121</sup> of central signals displaying triplet behaviour with smaller values of the exchange integral than those of the 'regular' excitons.

A typical log IT against  $1/T$  plot for the central resonance observed in this work is shown in Figure 4.15, and the average value of the slope taken from a number of such plots was found to be  $-2.1 \pm 0.3 \text{ kJ mol}^{-1}$ . The ratio of the intensity of this signal to the intensity of the doublet signal was observed to be of the order of 1% and was approximately the same in all the three crystals studied. This central signal, therefore, appears to be a characteristic property of the system.

As the regular excitons in DCBP(TCNQ)<sub>3</sub> are essentially localised, it is not unreasonable to assume that this new triplet species is also localised. Consequently, the above value obtained from the slopes of the log IT against  $1/T$  plots should be equal to the singlet-triplet energy gap for this species. As the value of J is very dependent on the distance between the electrons constituting the triplet, this new exciton must be larger than the regular one in order to have such a small interaction. Furthermore, for a localised triplet, one might expect to observe dipolar interaction in this exciton also, although such interaction from electrons situated far apart would

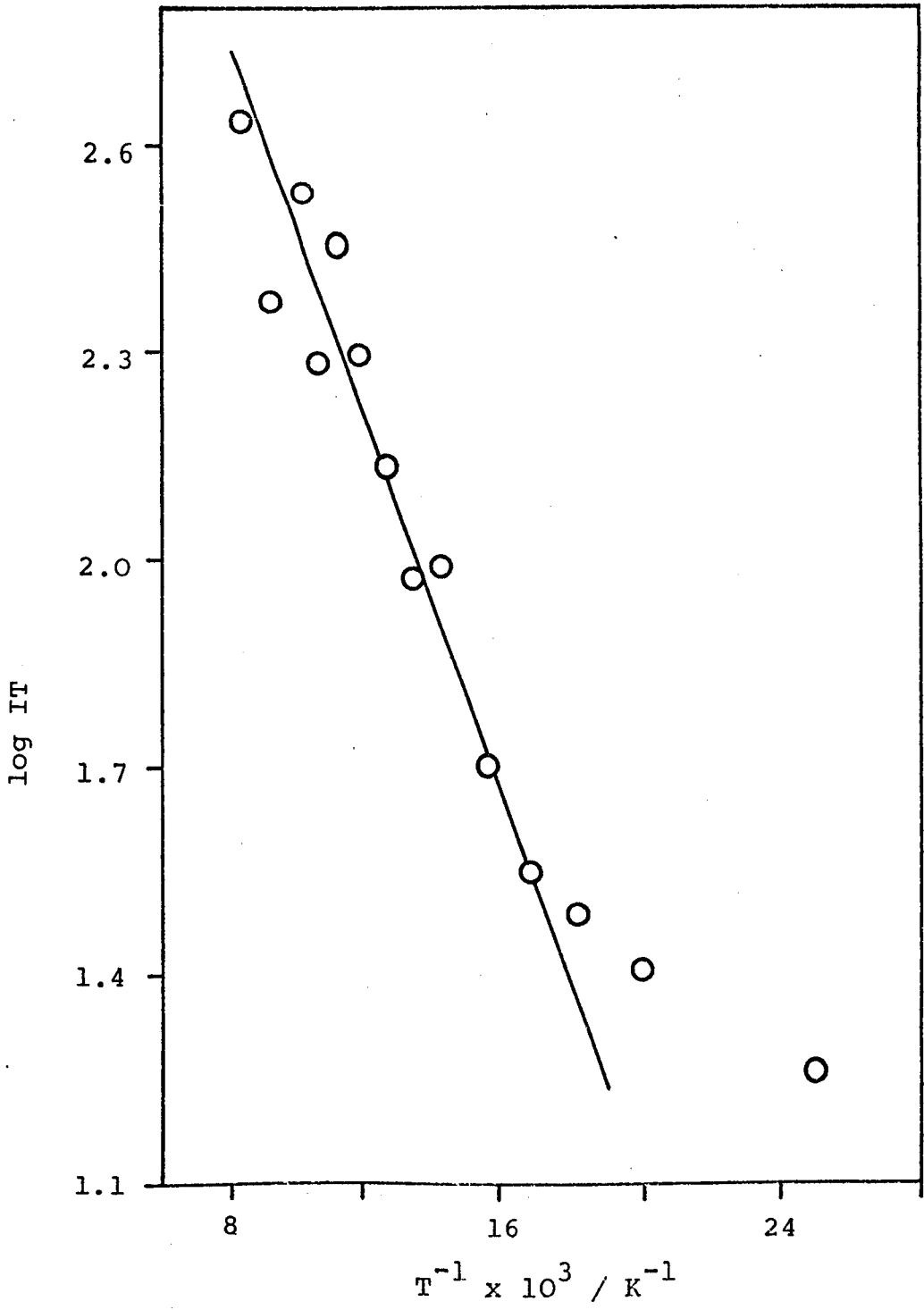


Figure 4.15  
DCBP(TCNQ)<sub>3</sub>  
Semilog plot of the product of the relative intensity and temperature against reciprocal temperature for the central peak for crystal 2. H is approximately parallel to the y-axis.

not give any measurable splitting until low temperatures when the exciton density would be small. Even then, any dipolar splitting might well be smaller than the natural linewidth of the e.s.r. signal and so be undetectable. In fact, at about 30K, the signal observed with crystal 2 did show signs of some splitting, although there was no broadening of the linewidth which usually accompanies the onset of such behaviour. On decreasing the temperature even more, the signal intensity rapidly increased with a Curie law behaviour, thus obscuring any fine structure which may have been observed. Therefore, whether this signal does exhibit dipolar splitting is debatable, although a lineshape analysis (Figure 4.16) showed this signal to have a Lorentzian lineshape, which would be consistent with the presence of exchange interaction associated with a migrating species.

Below 80K the central resonance, which was the only signal observed at this temperature as the doublet peaks were now almost undetectable, appeared to be composed of two lines, a broad line with a superimposed sharp spike at the centre. This type of central signal has been previously observed<sup>120</sup> in other compounds and also showed a similar temperature dependence to that obtained in this work. The spectrum persisted down to approximately 20K, below which a symmetrical signal was observed following Curie law behaviour. In addition, the line began to show

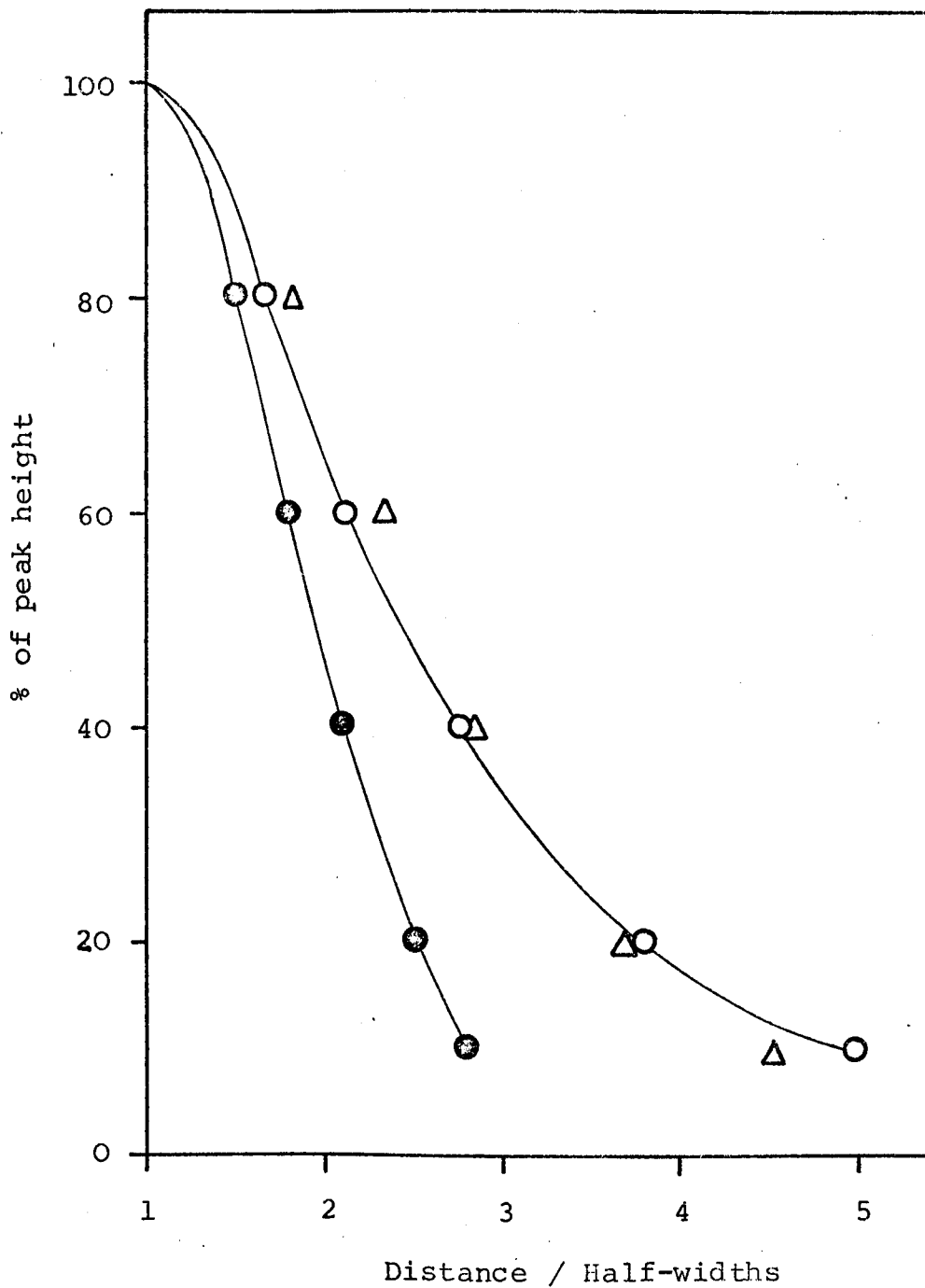


Figure 4.16

DCBP(TCNQ)<sub>3</sub>

Lineshape analysis for central signal at 130K  
for crystal 1.

H is approximately parallel to the z-axis.

●—● Gaussian lineshape

○—○ Lorentzian lineshape

△ Average shape for crystal.

deviations from its regular shape as the temperature was further decreased, and an asymmetrical line resulted. Estimates of the intensity behaviour of this resonance were, therefore, crude in this low temperature region. However, the product of the intensity with temperature appeared to remain nearly constant, shown by the curvature in Figure 4.15, this type of behaviour being that expected for a doublet state species such as a single radical anion of TCNQ existing as an imperfection in the lattice. As previously mentioned, the low temperature Curie signal in TCNQ complexes is widely accepted as arising from such species. Therefore, the problem remains as to the origin of the exponential temperature dependence exhibited at higher temperatures by the central resonance.

The singlet-triplet behaviour of the new exciton could arise from two possible interactions. Firstly, interaction between spins situated on sites which are located on different TCNQ stacks (all of which are equivalent from the crystal structure determination) and, secondly, interaction between unpaired electrons situated on different sites within the same stack. Both these cases would result in triplet excitons having a small interaction from their greater distance separation, which results in a small exchange integral and small dipolar splittings. The first possibility seems unlikely, not only from the fact that TCNQ complex salts are known to have negligible interstack interactions, but also from the angular

dependence of the observed linewidth of this central signal. A typical example is shown in Figure 4.17 and illustrates the same linewidth anisotropy for both the regular exciton and the new exciton, as was the case in all the three crystals studied. It should be noted that the g factors of the signals arising from both species also follow the same angular variation, and this identical orientation behaviour is consistent with the two triplet excitons being located on the same TCNQ stack.

As can be seen from Figure 4.17, the linewidth observed for the new triplet species is larger than that observed for the regular exciton and, in fact, the linewidth of the central signal remained essentially constant with variation of temperature at a given orientation. There is little dispute that the narrow lines observed for the zero-field components of the regular exciton at low concentrations are due to the rapid motion of the exciton. In the case of the central signal, the interpretation is more difficult as the structure of this triplet species is not known in terms of the number of TCNQ molecules over which the two electrons are delocalised. However, it is considered that the greater linewidth could possibly be due to a smaller hopping frequency, although this is only tentatively proposed owing to the lack of available evidence. This would be consistent with a species having such a low energy,

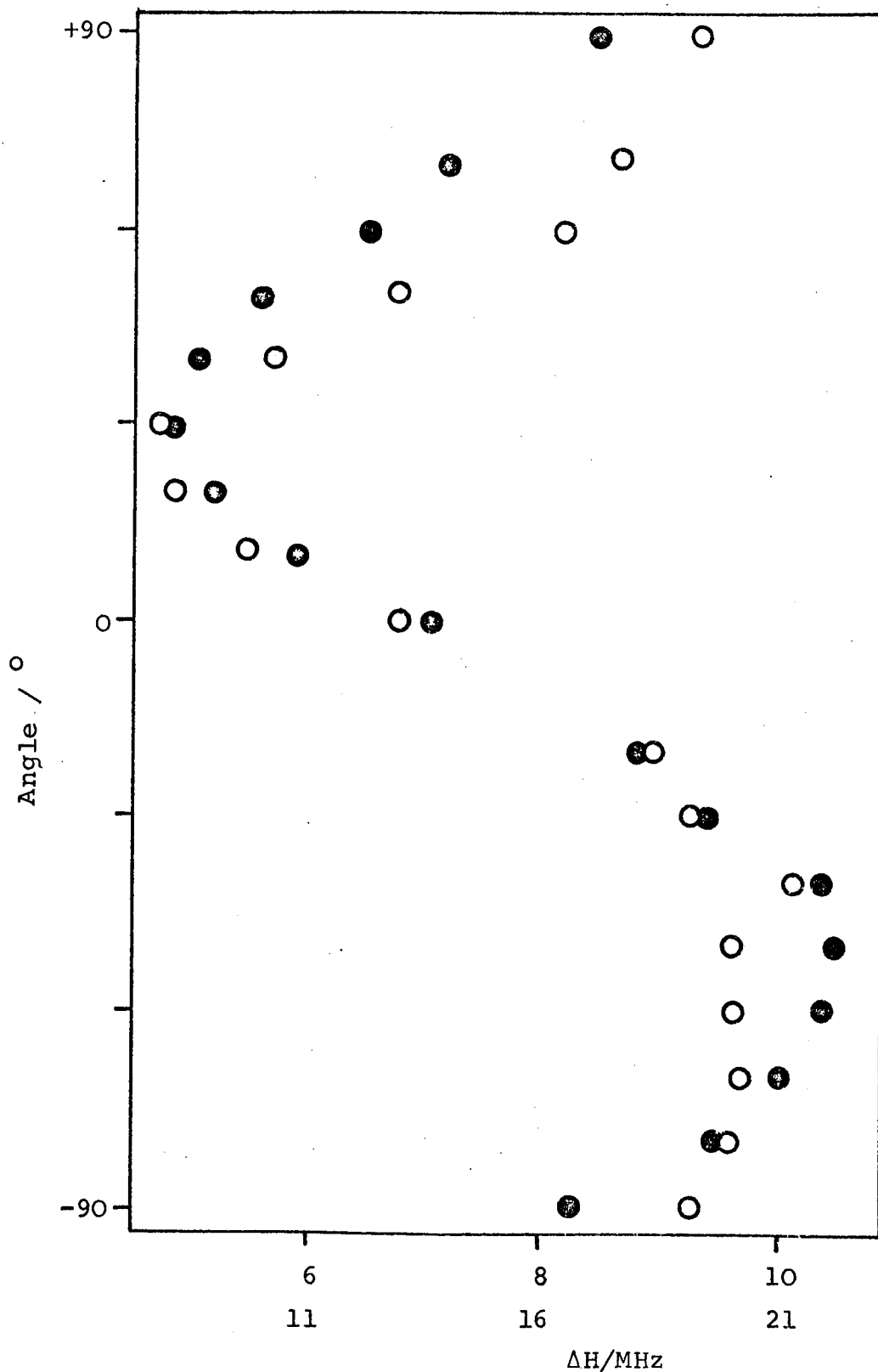


Figure 4.17

DCBP(TCNQ)<sub>3</sub>

Angular variation of linewidths at 120K (for crystal 3).

Approximate orientations as for Figure 4.5.

○ ΔH values for outer doublet peaks (upper linewidth scale).

● ΔH values for central signal (lower linewidth scale).

indicated by the small value of the singlet-triplet energy gap, as this new exciton would require the same energy as the regular exciton in order to exhibit the same degree of motion. In other words, the new triplet exciton is trapped. Hyperfine interactions would, therefore, be expected to make considerable contribution to the linewidth.

Yet another possibility exists which, although seemingly remote, should be mentioned. This is the possible presence of Wannier excitons as a cause of the central resonance. As previously mentioned, these are non-tightly bound electron pairs exhibiting no fine structure splitting and an exponential temperature dependence of the intensity. Such spin excitations are apparently present in certain donor-acceptor CT complexes as, for example, p-phenylenediamine-chloranil (PDC)<sup>142</sup>. In view of the evidence already discussed in terms of a localised species, the origin of this central signal would not seem to be attributable to delocalised Wannier excitons. A treatment of the linewidth with temperature for both types of spin excitations has shown<sup>142</sup> that Frenkel excitons have a greater exchange-narrowed linewidth, which exhibits a different temperature dependence from Wannier excitons. The linewidth of the new exciton in DCBP (TCNQ)<sub>3</sub> remained constant as the temperature was decreased, consistent with the behaviour expected from Wannier excitons. However, the fact that the new exciton has a greater linewidth than the regular exciton is

contradictory to this evidence. It would appear, therefore, that no definite conclusions can be made one way or the other, but the data would seem more consistent with the proposal of localised triplet excitons having a small degree of motion.

The interpretation of the origin of the species giving rise to the central signal is considered to be most probably due to a number of lattice imperfections capable of triplet states with small values of the singlet-triplet energy gap and small zero-field splittings, these species residing on the same TCNQ stack as the regular excitons. The estimation of the percentage of these new species which would give the observed intensity ratio is consistent with such a proposal. The existence of such imperfections is not difficult to visualise in DCBP(TCNQ)<sub>3</sub>, as misalignment of a cation could well result in the situation where the end groups do not protrude into the TCNQ stack. This would allow for the presence of tetrads of TCNQ molecules in the stack, which allows for a greater separation between the two electrons constituting the new triplet and consequently smaller interaction. Such imperfections and broadening by hyperfine interactions, since a localised paramagnetic state is assumed, could well lead to the observed character of the central resonance. However, it must be pointed out that the interpretation of this signal is somewhat speculative as defects in the lattice could

also give rise to doublet species which can be thermally activated into excited states. Such species would exhibit a similar exponential temperature dependence of the signal intensity, consistent with the observed results.

From the extrapolated limit of the curvature obtained at low temperatures from Figure 4.15, and from a knowledge of the room temperature susceptibility, the number of doublet species giving rise to the Curie signal can be estimated. The value obtained for a number of such plots is  $(3.6 \pm 0.8) \times 10^{21}$  spins mol<sup>-1</sup>, which corresponds to a percentage of 0.6, and can be reasonably attributed to the presence of non-interacting monoradical anions possibly originating from sites located at chain ends.

It has been shown<sup>154</sup> that Frenkel and Wannier excitons exhibit strikingly different spin-lattice relaxation rates. Therefore, it was considered that such a study might cast some light on the nature of the species giving rise to the central resonance. Since the e.s.r. lines for both the regular and new excitons were Lorentzian, the spin-lattice relaxation time,  $T_1$ , could be obtained by the method of progressive saturation as described in section 3.2.3(vi). However, unfortunately the maximum microwave power available from the klystron used in this work was not sufficient to saturate the broad central signal and, therefore, the nature of the species

giving rise to this resonance remains speculative. The available power did, however, saturate the outer doublet peaks in the temperature range 120 to 180K, and also the resulting single peak above 260K. The range 180 to 260K was unavailable for study due to the very broad lines observed and the distortion of the signals as the splitting commenced.

Typical examples of the effect of increasing the microwave power on the linewidths of the derivative signals, given by equations 3.4 and 3.6, is shown in Figure 4.18 for two of the temperatures studied. Values of  $T_1$  and  $T_2^*$  obtained from such plots were then plotted against reciprocal temperature and the results are presented in Figure 4.19. The values of  $T_2^*$  reflect the change in the e.s.r. linewidth with temperature, and the values of  $T_1$  appear from the plot to exhibit a minimum at a temperature of approximately 220-230K. This type of behaviour has been previously observed<sup>154,159</sup> in TCNQ complexes and is representative of a Frenkel spin exciton system. These results for DCBP(TCNQ)<sub>3</sub> are, therefore, consistent with the proposal of localised triplet excitons in this complex salt.

The dependence of the minimum in  $T_1$  with spectrometer frequency has been investigated by Jones<sup>159</sup>, and the results showed that the temperature at which it

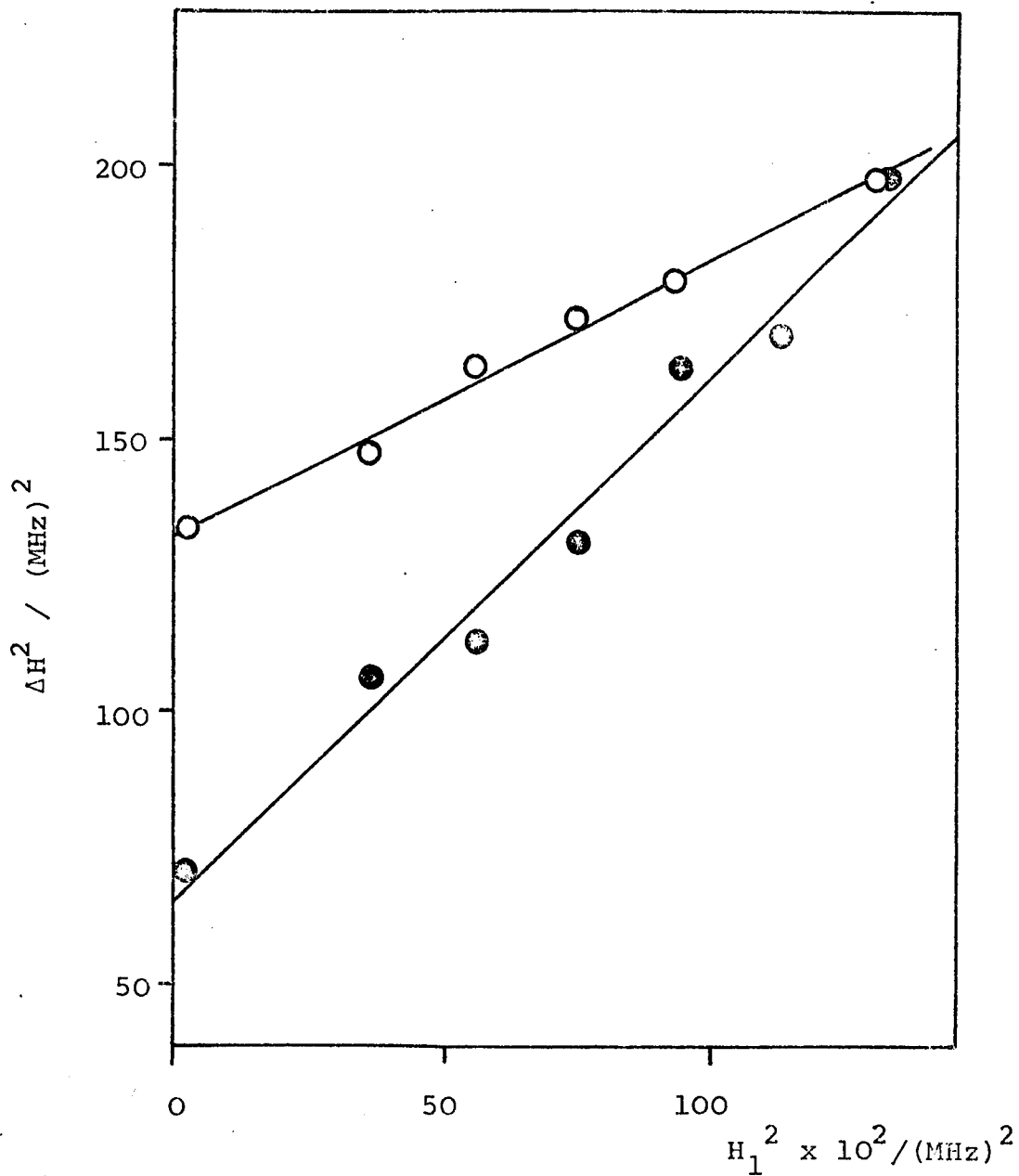


Figure 4.18

DCBP(TCNQ)<sub>3</sub>

Plot of the square of the linewidth against the square of the microwave magnetic field strength for crystal 3 at two temperatures. H is approximately parallel to the z-axis.

○ 150K , ● 120K.

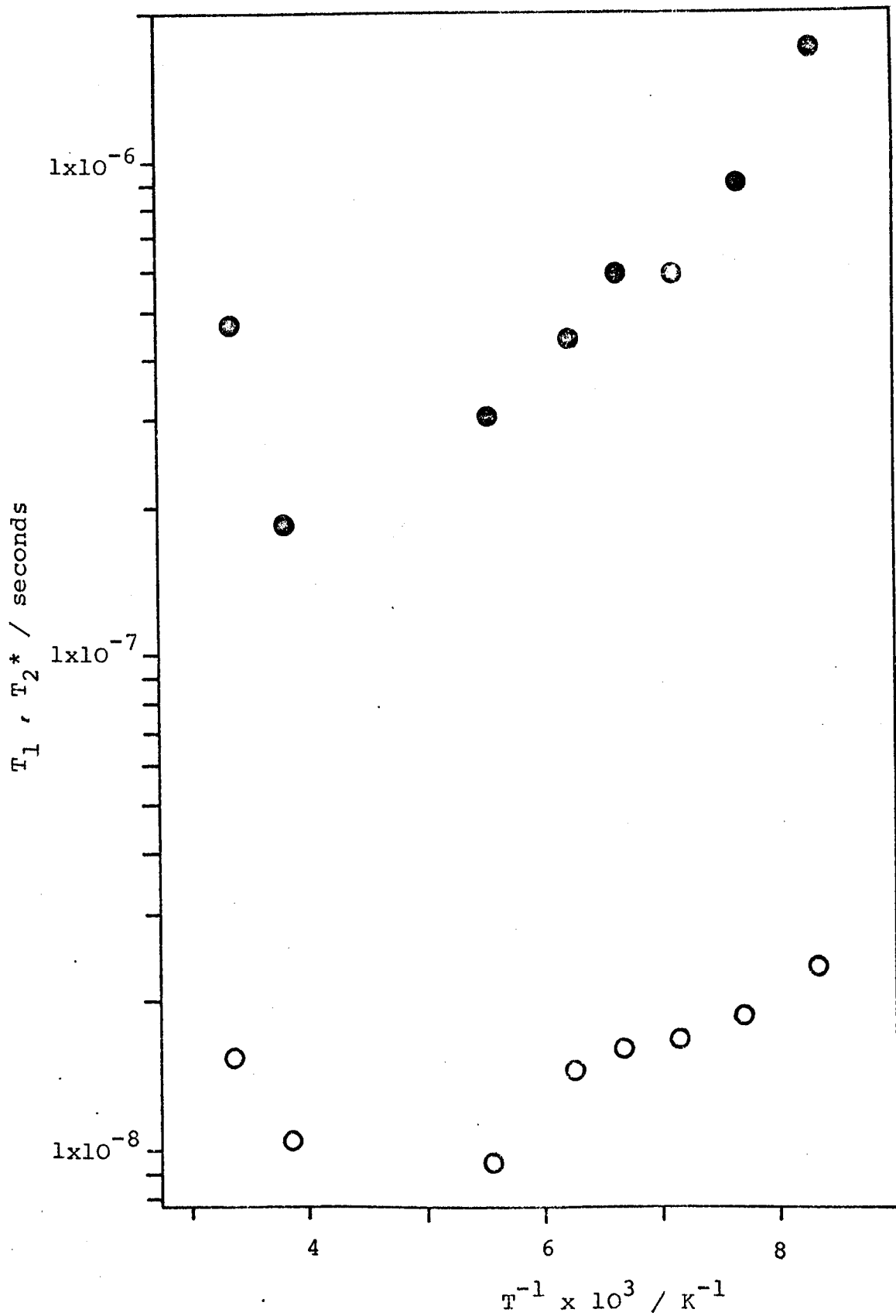


Figure 4.19

DCBP(TCNQ)<sub>3</sub>

Semilog plot of  $T_1$  and  $T_2^*$  against reciprocal temperature for crystal 3.

H is approximately parallel to the z-axis.

●  $T_1$  , ○  $T_2^*$

occurs does in fact depend on the frequency. The most plausible cause for this behaviour and for the observation of such a minimum was considered to be due to spin-spin interactions.

Gorter and Van Vleck<sup>164,165</sup> first suggested that for substances which are characterised by large spin-spin exchange interactions, the dipolar interaction is randomly modulated by exchange interactions in much the same way it is modulated by random motions in liquids. In other words, the exchange interaction in TCNQ complex salts due to exciton-exciton collisions changes the spin states of the colliding triplets and these collisions amount to an averaging of the dipolar interaction.

In order to discuss  $T_1$  for a strongly exchange-coupled system, it is convenient to consider that, in an external magnetic field, the spin system and the lattice may be regarded as three heat reservoirs. These are the Zeeman, exchange and lattice systems, and this model was first proposed by Bloembergen and Wang<sup>166</sup>. Energy absorbed by the Zeeman system from the electromagnetic radiation is eventually transferred to the lattice by a relaxation process involving coupling interactions. Spin-lattice relaxation, in the case of the three-reservoir model, is dominated by the spin-spin interactions characteristic of energy transfer from

the Zeeman system to the exchange system, since direct Zeeman-lattice relaxation is slow and the exchange-lattice relaxation is fast<sup>167</sup>. When circumstances are such that the exchange energy is comparable to, or greater than, the Zeeman energy, the dipolar interaction causes the transfer of energy from the Zeeman system to the exchange system where it is then transferred to the lattice. This can be expressed in terms of the Larmor and exchange frequencies, denoted by  $\nu_z$  and  $\nu_e$  respectively. When  $\nu_e \approx \nu_z$ , the measured  $T_1$  corresponds to the relaxation time associated with energy transfer from the Zeeman system to the exchange system<sup>168</sup>. This is the minimum value of  $T_1$  observed and corresponds to the most efficient relaxation. However, as the temperature is decreased,  $\nu_e$  decreases and the Zeeman-exchange and exchange-lattice couplings become weaker and less important in the relaxation process. This results in direct but less efficient Zeeman-lattice processes and  $T_1$  increases in the region  $\nu_e < \nu_z$  (the region of 'slow' exchange). The resulting minimum in  $T_1$  is a result of induced downward transitions in the spin system when  $\nu_e \approx \nu_z$ . As  $\nu_e$  is increased, by increasing the temperature, to a value above that of the Larmor frequency, it is less effective in inducing downward transitions, therefore  $T_1$  again increases in the region  $\nu_e > \nu_z$  (the region of 'fast' exchange).

The exchange frequency is inversely related to

the correlation time,  $\tau_c$ , which can be expressed as the time a particular orientation of the dipole persists in the magnetic field. If it is assumed that the  $T_1$  dependence upon correlation time is of the same general form as in the case of thermal motion in liquids, equation 4.1 can be applied to the results obtained for DCBP(TCNQ)<sub>3</sub>.

$$\left(\frac{1}{T_1}\right) = k_1 \frac{\gamma^4 \hbar^2}{r^6} S(S+1) \left[ \frac{\tau_c}{(1 + \nu_z^2 \tau_c^2)} \right] \dots (4.1)$$

The only symbols not previously defined are  $\hbar$ ,  $r$  and  $k_1$ .  $\hbar$  is Planck's constant divided by  $2\pi$ ,  $r$  is the minimum distance of closest approach of the colliding species, and  $k_1$  is a collection of constants with a value near unity. It has been found<sup>159</sup> that, as the number of neutral TCNQ molecules is increased in the crystalline lattice relative to the number of TCNQ anions,  $r$  also increases. For example,  $r$  increases from approximately 0.8nm for (TCNQ)<sub>3</sub><sup>2-</sup> to approximately 1.0nm for (TCNQ)<sub>4</sub><sup>2-</sup>. Therefore, for the case of DCBP(TCNQ)<sub>3</sub>, a value of 0.8nm for  $r$  was used in the calculations of  $\tau_c$ .

Equation 4.2 gives the temperature dependence of the correlation times and, from a plot of  $\log \tau_c$  against  $1/T$ , the activation energy,  $\Delta E_e$ , can be obtained from the slope.

$$\tau_c = \tau_c^0 \exp(\Delta E_e/kT) \dots (4.2)$$

Figure 4.20 shows such a plot obtained from the relaxation

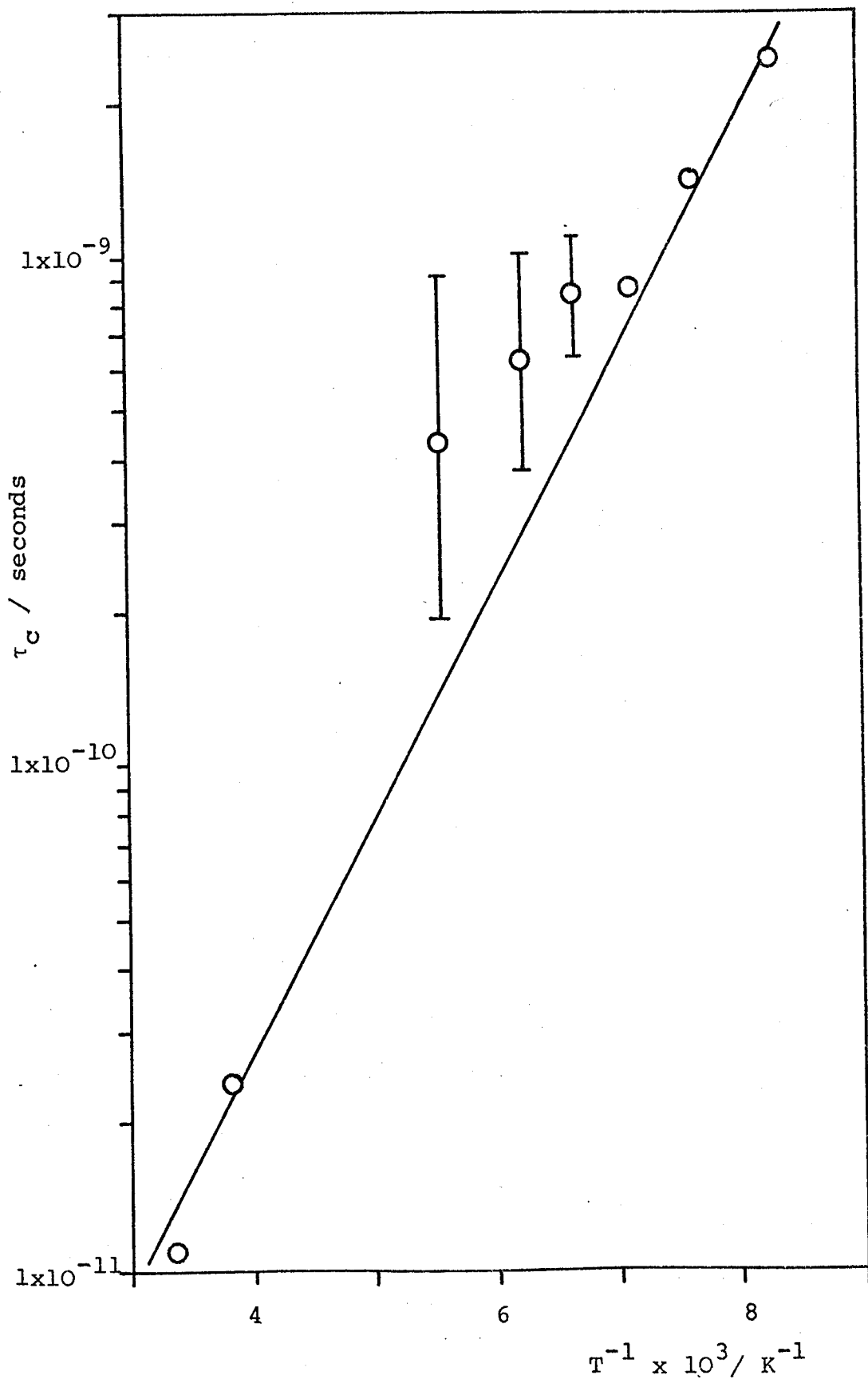


Figure 4.20  
 DCBP(TCNQ)<sub>3</sub>  
 Semilog plot of  $\tau_c$  against reciprocal temperature  
 for crystal 3.  
 H is approximately parallel to the z-axis.

results for DCBP(TCNQ)<sub>3</sub>, and the value of  $\Delta E_e$  from the slope is  $8.6 \pm 2.9 \text{ kJ mol}^{-1}$ . This value is taken from the slope through the points considered to be the most reliable. The results obtained in the temperature region 150-180K were not so good owing to the lack of enough microwave power to broaden the already broad resonance lines sufficiently for accurate measurements to be made. However, it is considered that the value of  $\Delta E_e$  obtained from the relaxation data is in reasonable agreement with the value obtained from the exchange analysis data using the line-width approximations. The inverse of the pre-exponential factor,  $(\tau_c^0)^{-1}$ , is  $3.1 \pm 1.1 \text{ THz}$  and is also closer to the value of the pre-exponential factor  $\nu_0$  from the linewidth approximations than to the value obtained from the line separation approximation, these values being  $0.7 \pm 0.3$  and  $0.001 \pm 0.001 \text{ THz}$  respectively.

In conclusion, the results presented in this section for DCBP(TCNQ)<sub>3</sub> indicate the presence of localised Frenkel excitons, consistent with the low d.c. conductivity exhibited by this compound and the crystal structure determination. No definite conclusions, however, can be proposed for the origin of the species giving rise to the central resonance, although it is felt that a possible explanation would be the existence of lattice imperfections giving rise to larger localised triplet excitons.

#### 4.2 DMPA(TCNQ)<sub>4</sub> (I)

The complex salt DMPA(TCNQ)<sub>4</sub> contains two neutral TCNQ molecules and two TCNQ anion radicals for electrical neutrality with the divalent cation 1,2-di(N-methyl-4-pyridinium)ethane (DMPA). Both single crystals and polycrystalline samples have been prepared in this department and, although found to have the same stoichiometry, they exhibited very different d.c. electrical conductivities<sup>126</sup>. The crystals are semiconducting, having a d.c. conductivity of  $2 \times 10^{-3} \text{ ohm}^{-1} \text{ cm}^{-1}$  along the direction of the TCNQ stack, whereas the polycrystalline form has a much higher conductivity of the order of unity at room temperature. Normally, polycrystalline samples of the same compound have lower conductivities due to the activation energy required to surmount intercrystalline boundaries. Therefore, there appears to be two phases of DMPA(TCNQ)<sub>4</sub> in existence. This situation is not unique in TCNQ complex salts as 1,2-di(N-ethyl-4-pyridinium)-ethylene (DEPE)-(TCNQ)<sub>4</sub> has also been found to exist in two phases, one being semiconducting and the other metallic<sup>169</sup>.

The crystal structure determination and conductivity results for the crystal form of DMPA(TCNQ)<sub>4</sub>, designated as phase I, have been published<sup>170</sup>, and Figure 4.21 shows the projection of the structure along the crystallographic c-axis. The TCNQ molecules are stacked

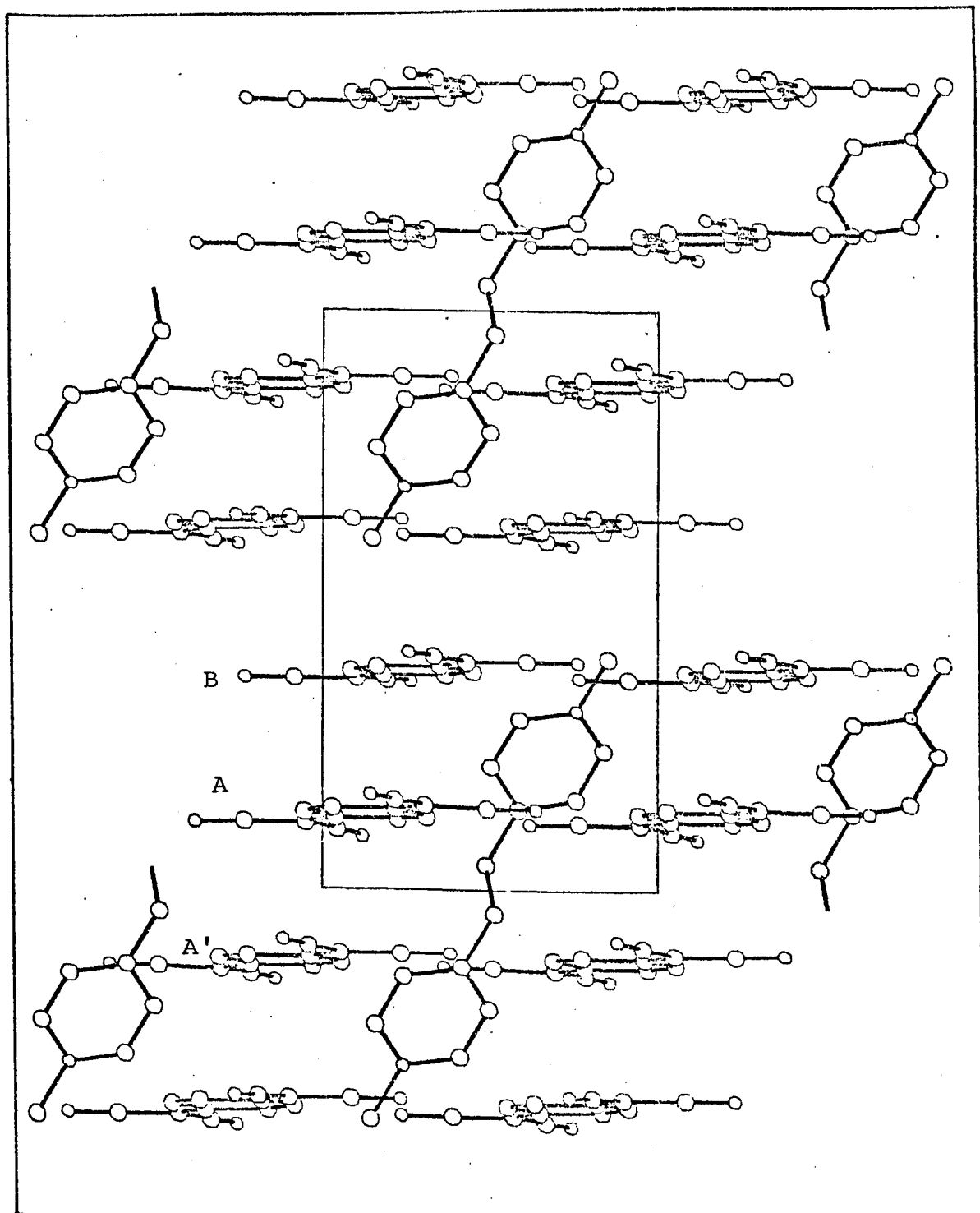


Figure 4.21

DMPA(TCNQ)<sub>4</sub> (I)

Projection of the crystal structure along the c-axis.

plane-to-plane in groups of four with no direct overlap between adjacent tetrads, which are held together by Van der Waals forces. The distance of closest contact between stacks, in the a-direction, is 0.330nm, which is of a similar magnitude to the distance between the TCNQ molecules along the stack. Within the tetrads, two types of overlap are observed. There is a good 'ideal' overlap between the TCNQ molecules labelled A and B in Figure 4.21, with a perpendicular separation of 0.320nm. However, there is a much poorer overlap between A and A', with a perpendicular separation of 0.339nm. Therefore, the crystal structure determination indicates that there is a tendency towards two dimers rather than a tetrad, and the data also suggests the charge is delocalised within each dimer, the TCNQ molecules being indistinguishable with a net charge of  $\frac{1}{2}$ - on each.

The crystals of  $\text{DMPA}(\text{TCNQ})_4$  (I) form in a rectangular platelet shape, and it has been shown that the stacking direction (the crystallographic b-axis) is approximately parallel to the perpendicular to the plate (z-direction). The long dimension of the crystal (x-direction) is approximately parallel to the short dimension of each TCNQ molecule, and corresponds to the crystallographic a-axis. Consequently, the intermediate crystal dimension (y-direction) corresponds to the crystallographic c-axis, perpendicular to the cation planes.

For the crystals studied in this work, the x-, y- and z-axes were those oriented as the rotation axes for crystals 1, 2 and 3 respectively.

At room temperature, a single, symmetrical signal was observed which did not show any evidence of dipolar splitting as the temperature was decreased. Therefore, the angular variation of the g factor was monitored at room temperature, the experimental results being given in Figures 4.22 to 4.24, together with the computer simulations. From these results, the three principal values of the g factor in the x-, y- and z-directions were found to be 2.0039, 2.0032 and 2.0027 respectively, all with an experimental error of  $\pm 0.0003$ . The value associated with the TCNQ stacking direction is once again closest to the free electron value. However, the values of  $g_x$  and  $g_y$  do not agree with the crystal structure and conductivity results. It has been shown that the y-direction has the lowest conductivity, this being expected along the direction through the cation planes and, therefore, would be expected to have the greatest value of the g factor. This discrepancy could possibly have occurred by misorientation of the crystals as, although rectangular platelets, the crystals of the correct size for the e.s.r. experiments were more square-like and, consequently, identification of the x- and y-axes became ambiguous.

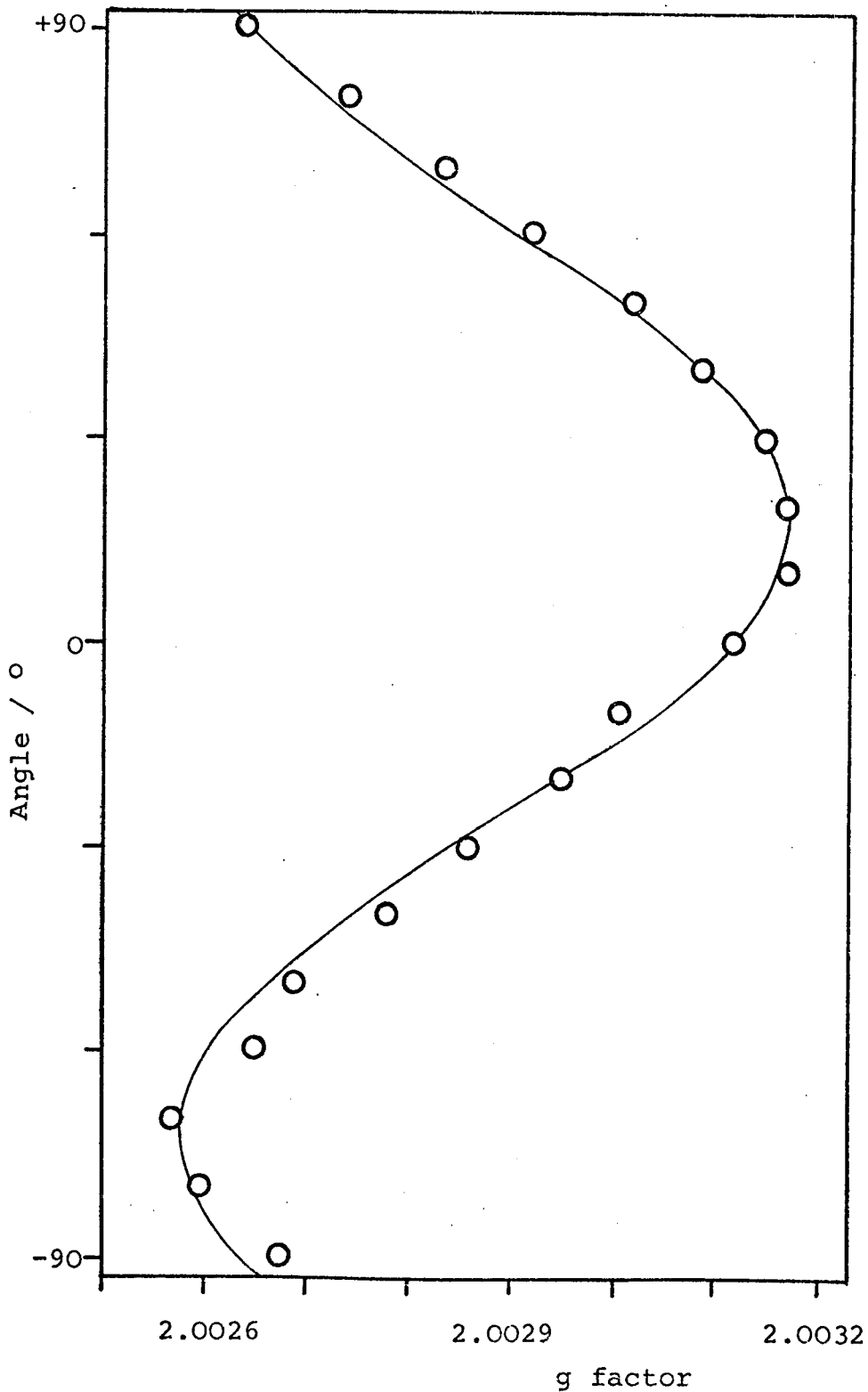


Figure 4.22

DMPA(TCNQ)<sub>4</sub>(I)

Angular variation of g factor at 300K for crystal 1.

Approximate orientations : H//y-axis at +18°.

H//z-axis at -72°.

———— Computer simulation.

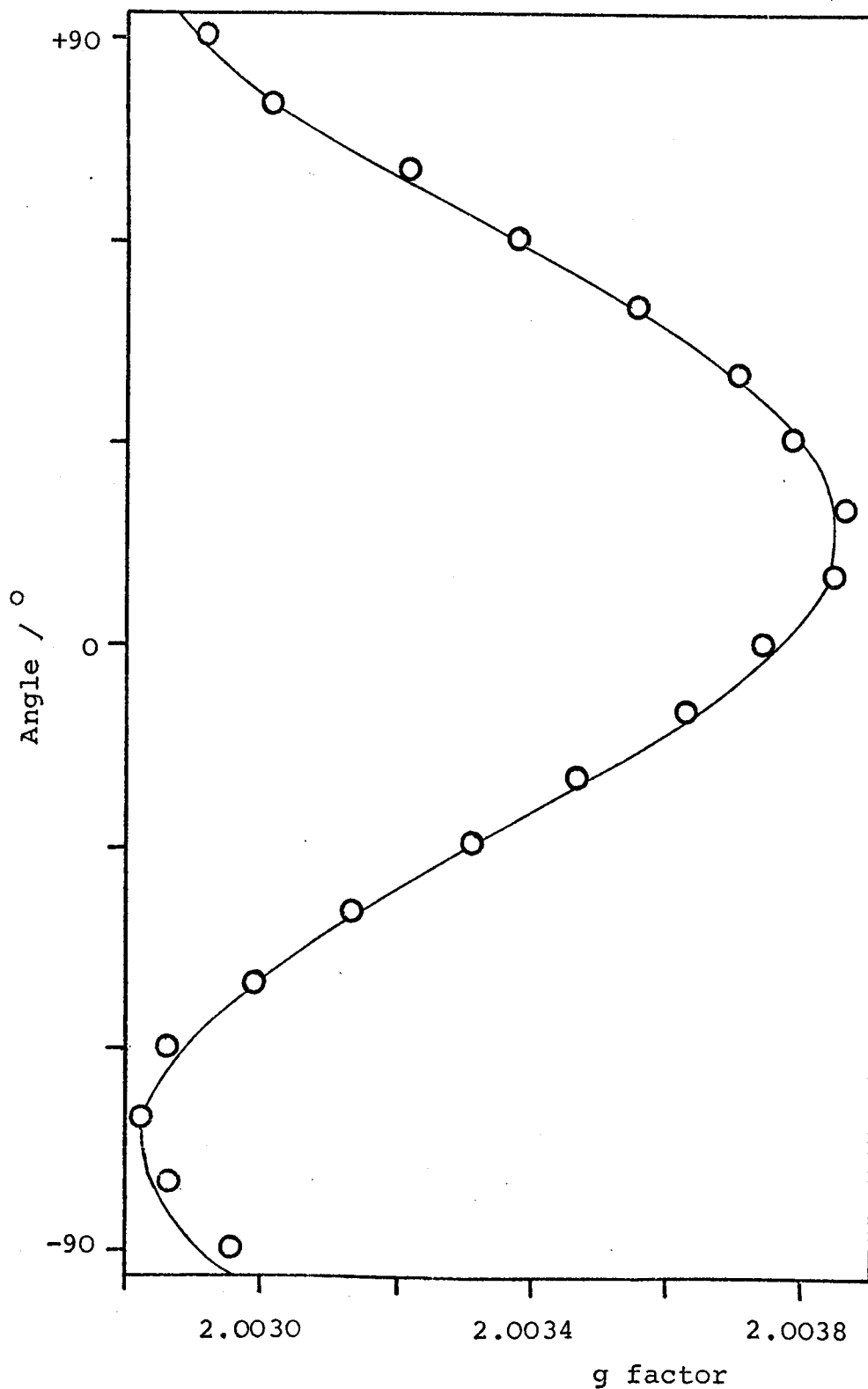


Figure 4.23

DMPA(TCNQ)<sub>4</sub>(I)

Angular variation of g factor at 300K for crystal 2.

Approximate orientations: H//x-axis at +16°

H//z-axis at -74°

———— Computer simulation.

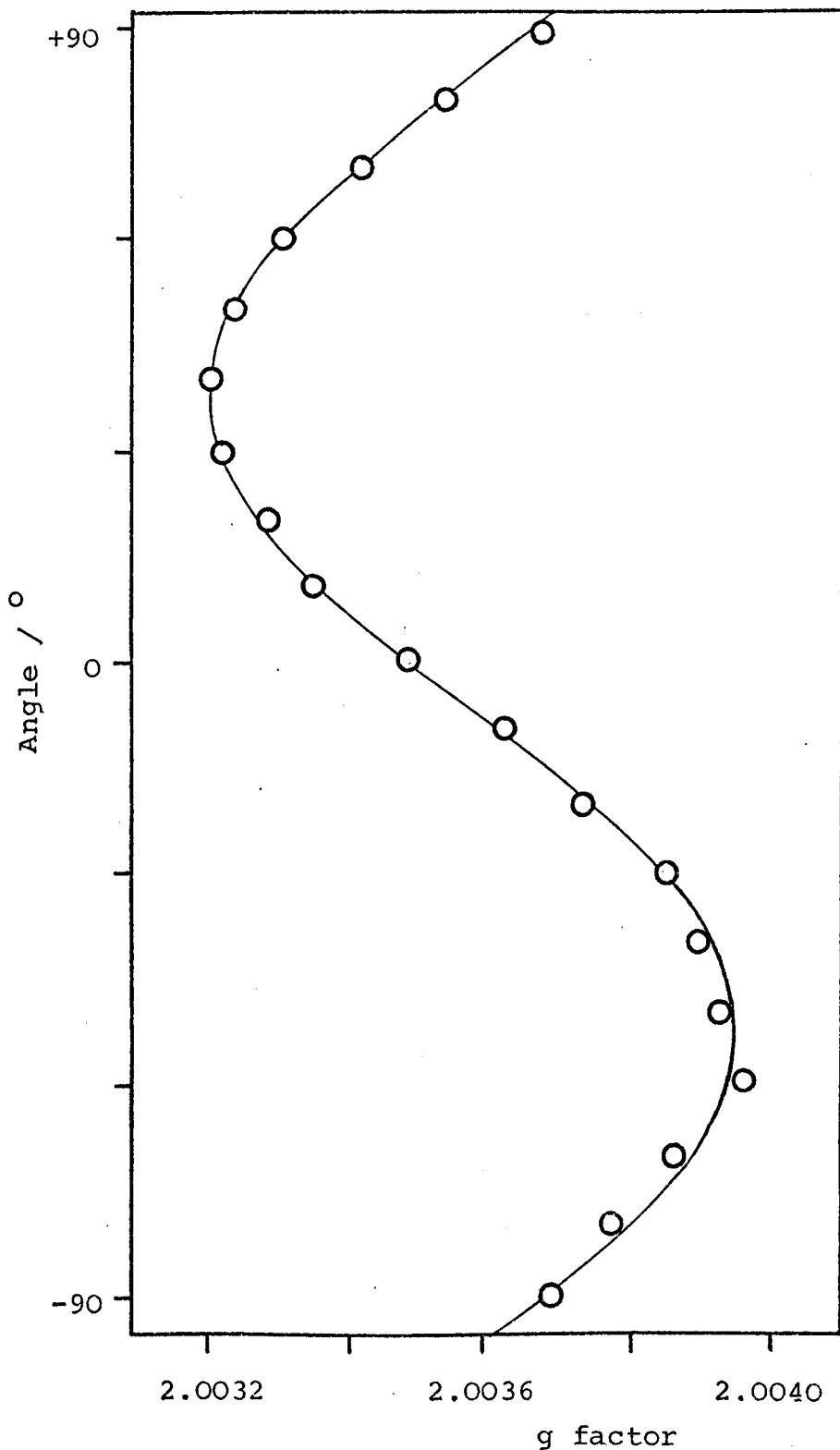


Figure 4.24

DMPA(TCNQ)<sub>4</sub>(I)

Angular variation of g factor at 300K for crystal 3.

Approximate orientations: H//y-axis at +38°  
H//x-axis at -52°

———— Computer simulation.

The angular dependence of the linewidth was also investigated during this study at room temperature and the results are presented in Figures 4.25 to 4.27. The behaviour exhibited in Figures 4.25 and 4.27 are unusual, as the normal behaviour for compounds of this type, having all TCNQ chains equivalent, should match the g factor angular variation<sup>154</sup>. The angular variations of the g factor and the linewidth, shown in Figures 4.23 and 4.26, do in fact match and these results were obtained with  $\gamma$  as the rotation axis. The pattern shown for crystals 1 and 3 has been observed in TCNQ complex salts by other workers<sup>171,172</sup> and has been attributed to specific properties associated with the collapse of fine structure in a nearly two-dimensional conductor. It is interesting to note that the criterion necessary to fulfil in order to observe this unusual pattern is that a highly conducting direction and a poorly conducting direction must be under investigation. This is in fact fulfilled for crystal 1, where the z- and y-axes are under study, and also for crystal 3, where the intermediate-conductivity x-axis and the poorly conducting y-axis are under study. Also, a weak angular dependence of the linewidth is observed for crystal 2, in which the two most highly conducting axes are investigated, this being consistent with the observations made in the previous studies of this behaviour<sup>171,172</sup>. These results are consistent with the crystal structure data, which indicates the stack-to-stack distance is

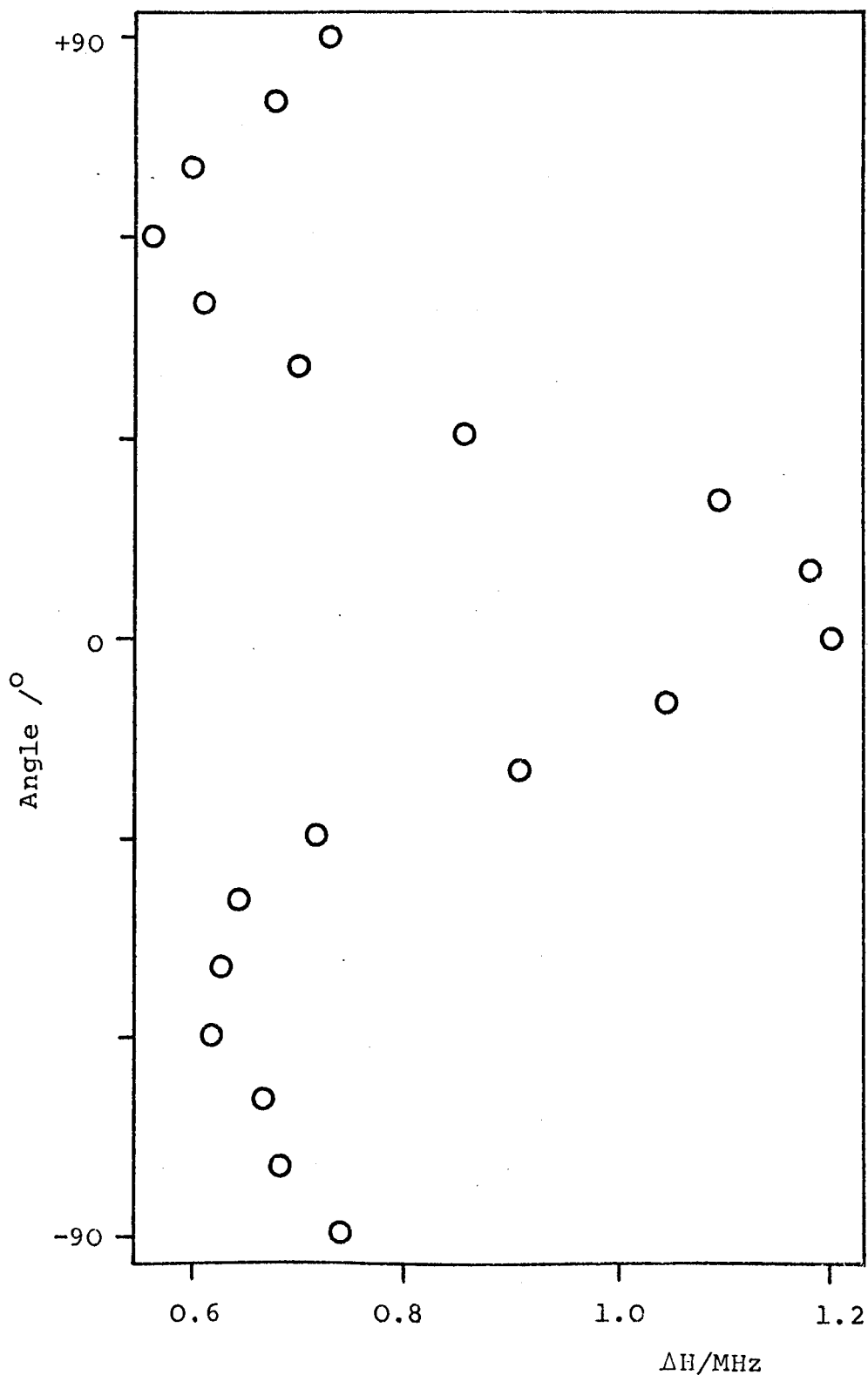


Figure 4.25

DMPA(TCNQ)<sub>4</sub>(I)

Angular variation of linewidth at 300K for crystal 1.

Approximate orientations as for Figure 4.22

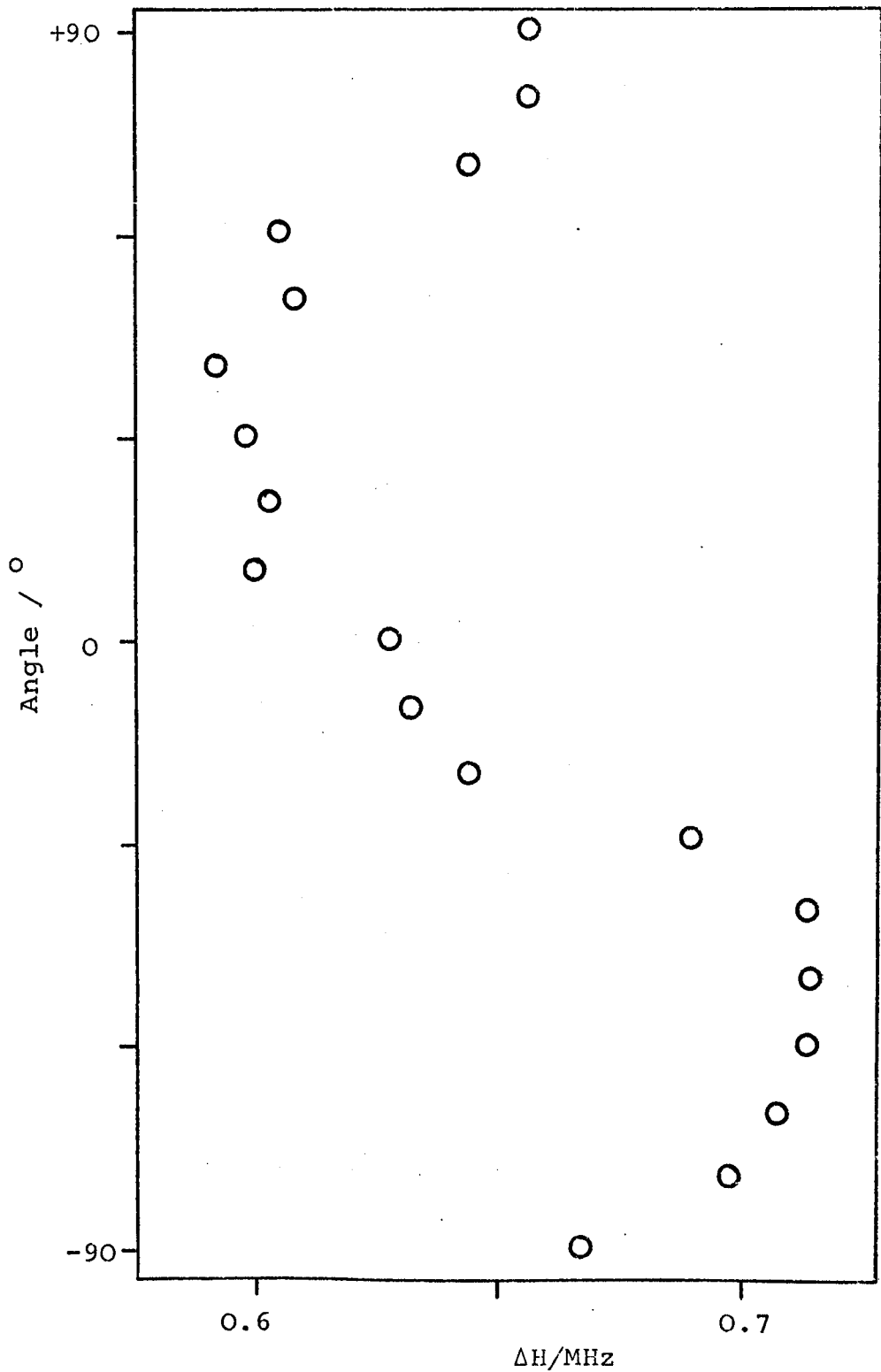


Figure 4.26

DMPA(TCNQ)<sub>4</sub>(I)

Angular variation of linewidth at 300K for crystal 2.

Approximate orientations as for Figure 4.23.

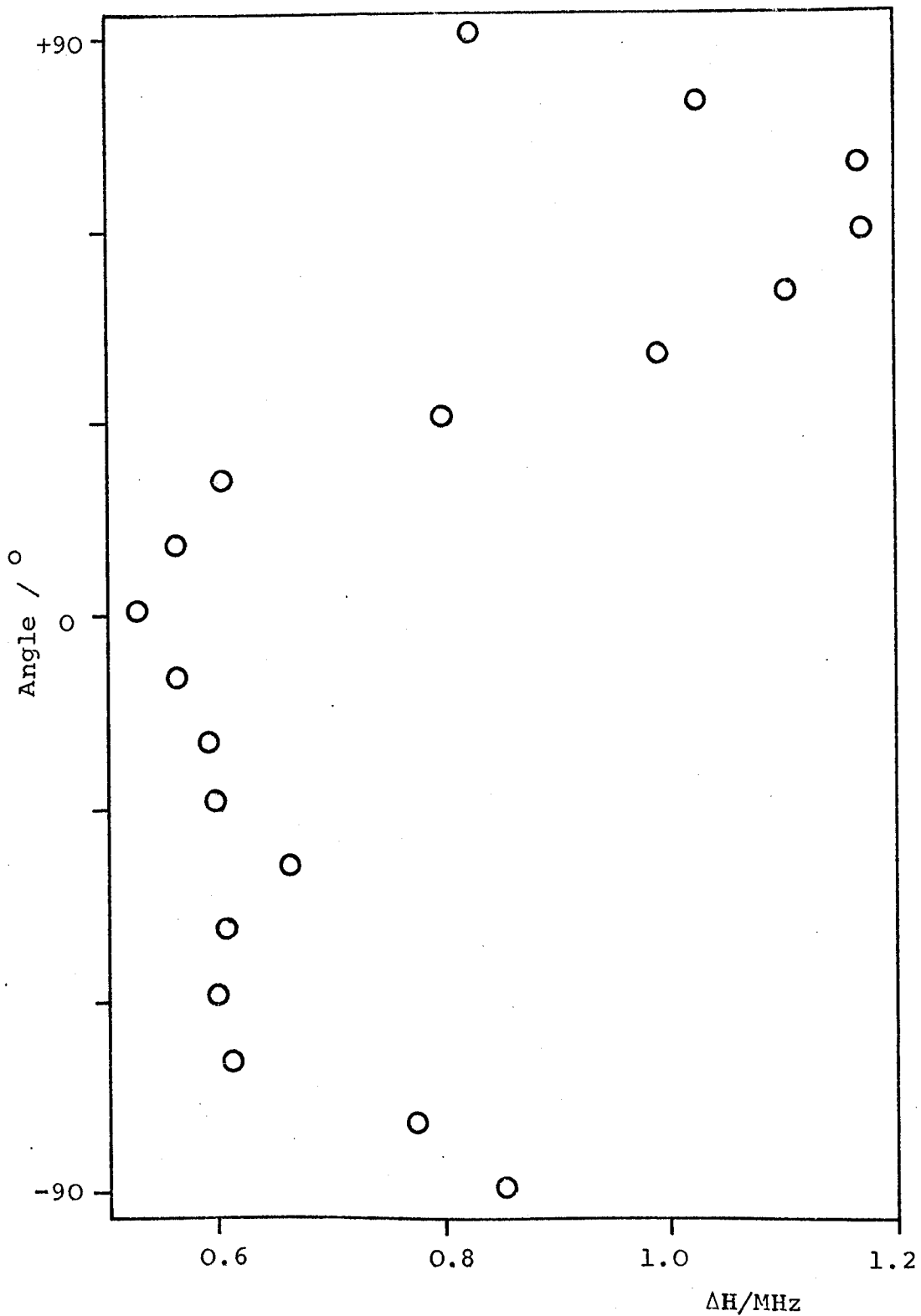


Figure 4.27

DMPA(TCNQ)<sub>4</sub> (I)

Angular variation of linewidth at 300K for crystal 3.

Approximate orientations as for Figure 4.24.

similar to the distance between dimers along the stack and, therefore, suggests some degree of two-dimensionality. However, the d.c. conductivity results do not reflect such behaviour, although the two most highly conducting directions are in the plane of TCNQ molecules, and the poorly conducting axis is along the direction through the cation planes.

An orientation resulting in a maximum or minimum value of the g factor was selected for each of the three crystals, and the variation of the signal intensity was studied as a function of temperature at this orientation. In all cases, the intensity showed a monotonic increase as the temperature was lowered from 300 to 100K. Below this temperature, however, the intensity increased more rapidly, in a Curie law fashion, peaking at 50K and rapidly decreasing in intensity from 50 to 10K, this behaviour being shown in Figure 4.28.

Figure 4.29 shows the  $\log IT$  against  $1/T$  plot obtained from the intensity results and it can be seen that a linear dependence is exhibited in the region where the rapid decrease in intensity is observed. This corresponds to the depopulation of the triplet state in the region where  $J > kT$ , which is the criterion required for calculation of the singlet-triplet energy gap from the relationship given in equation 2.25. The value of the slope

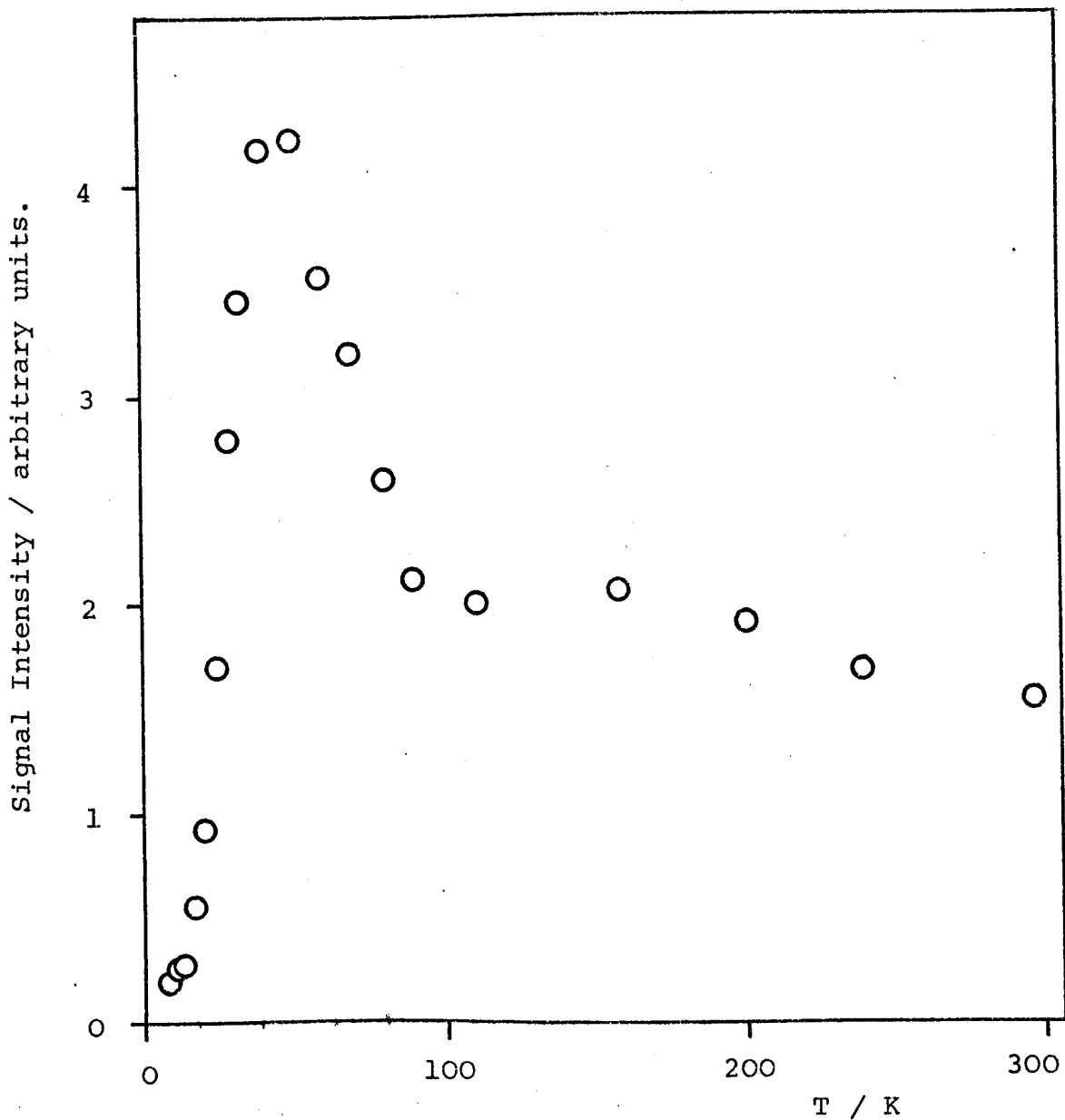


Figure 4.28

DMPA(TCNQ)<sub>4</sub>(I)

Plot of relative intensity against temperature for crystal 3.

H is approximately parallel to the y-axis.

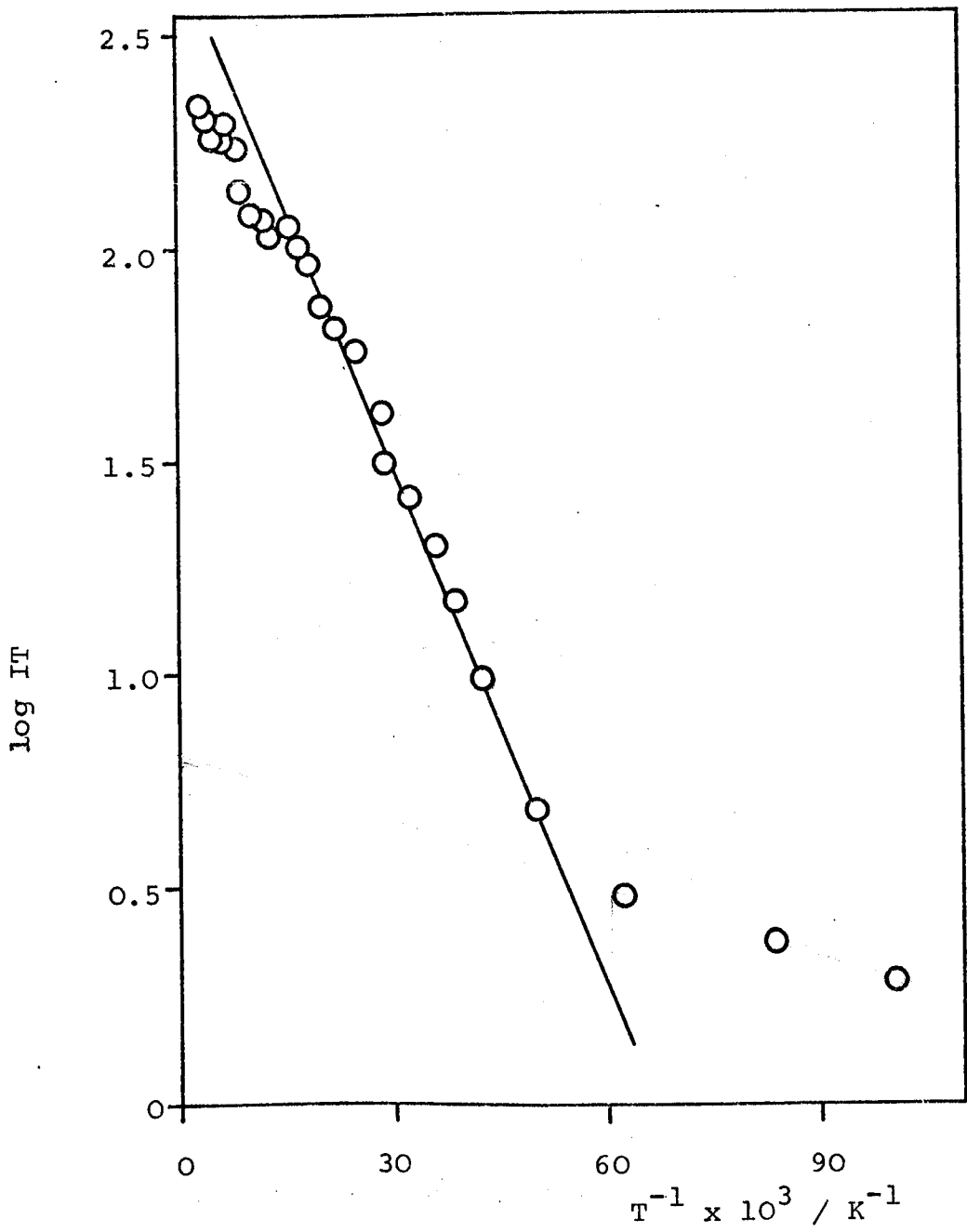


Figure 4.29  
 DMPA(TCNQ)<sub>4</sub>(I)

Semilog plot of the product of the relative intensity and temperature against reciprocal temperature for crystal 2.  
 H is approximately parallel to the x-axis.

for a number of such plots was found to be  $-0.65 \pm 0.12$  kJ mol<sup>-1</sup>. By substituting a value of J of 0.65 kJ mol<sup>-1</sup> into equation 2.26 for localised triplet states, the predicted value of the room temperature molar susceptibility was calculated and found to be  $2.38 \times 10^{-3}$  e.m.u.cm<sup>3</sup> mol<sup>-1</sup>. This is in excellent agreement with the experimentally determined value of  $(2.2 \pm 0.4) \times 10^{-3}$  e.m.u.cm<sup>3</sup> mol<sup>-1</sup> and, therefore, infers the triplet excitons are essentially localised in DMPA(TCNQ)<sub>4</sub> (I).

Calculations using this value of J in equation 2.28, however, yield a value of  $7.83 \times 10^{-3}$  e.m.u. cm<sup>3</sup> mol<sup>-1</sup>, which is substantially larger than the observed value and the value predicted by Kepler's equation. The lack of agreement between the values calculated from equations 2.26 and 2.28 is due to the inequality, given in equation 2.29, being no longer applicable due to the very low value of J, which reflects the large distance separation between the two electrons constituting the triplet state. Etemad's treatment, discussed in section 2.5.1, cannot therefore be used as the situation in this case is outside the range of validity.

Soos and McConnell<sup>108</sup> proposed that, as the temperature is increased, triplet excitons become 'statistically delocalised' even in strongly alternating systems. Thermal energy has the effect of increasing

the separation between the spins forming a triplet excitation for any value of  $\gamma$ . This results in a deviation from triplet behaviour and the excitations resemble pairs of doublets. This is the cause of the deviation from linearity at high temperatures shown in Figure 4.29, and is observed in the region where the experimental term in equation 2.25 becomes smaller than 3, this equation then reducing to that of Curie law behaviour. The observed maximum in intensity resulting from this phenomenon was predicted by Kepler<sup>24</sup>, who proposed the relationship given in 4.3, in which  $T_M$  is the temperature the intensity curve exhibits a maximum.

$$J = 1.61 kT_M \quad \dots(4.3)$$

The value of J calculated from this, using a value of 50K for  $T_M$ , is in excellent agreement with the value obtained from the slopes of the log IT against  $1/T$  plots.

It would appear, therefore, that the triplet excitons in  $\text{DMPA}(\text{TCNQ})_4$  (I) are best described as localised Frenkel spin excitons, but at high temperatures this triplet character is removed by thermal energy and results in magnetic behaviour attributable to non-correlated Curie-type spins.

The curvature at low temperatures shown in Figure 4.29 is, as previously discussed, due to Curie species resulting from isolated monoradical anions

originating from chain-ends and defects in the crystal lattice. Although the intensity with temperature plots only show evidence of a Curie signal below 10K, the effect of the paramagnetism of this signal can be seen in the  $\log IT$  against  $1/T$  plots at much higher temperatures. From the results for all the three crystals studied, an estimate of the number of such species existing per mole of host of  $(5.8 \pm 1.5) \times 10^{21}$  spins  $\text{mol}^{-1}$  was obtained. This value corresponds to a percentage of only 1% and, therefore, is reasonable for such a proposed species.

All the crystals of this complex salt exhibited a very unusual linewidth variation with temperature, this behaviour being illustrated in Figure 4.30. It is interesting to note the close similarity between this plot and that shown in Figure 4.28. It is also interesting that no evidence of dipolar splitting was observed as would be expected from a localised triplet species at temperatures below the region of linewidth broadening. However, although the triplet excitons are considered as localised and, therefore, will have a finite value for the dipolar interaction, this value will only be very small, as indicated by the large distance separation from the crystal structure determination and the very small  $J$  value. Consequently, although dipolar interaction will exist, the very small, but finite, value of the splitting will be undetectable.

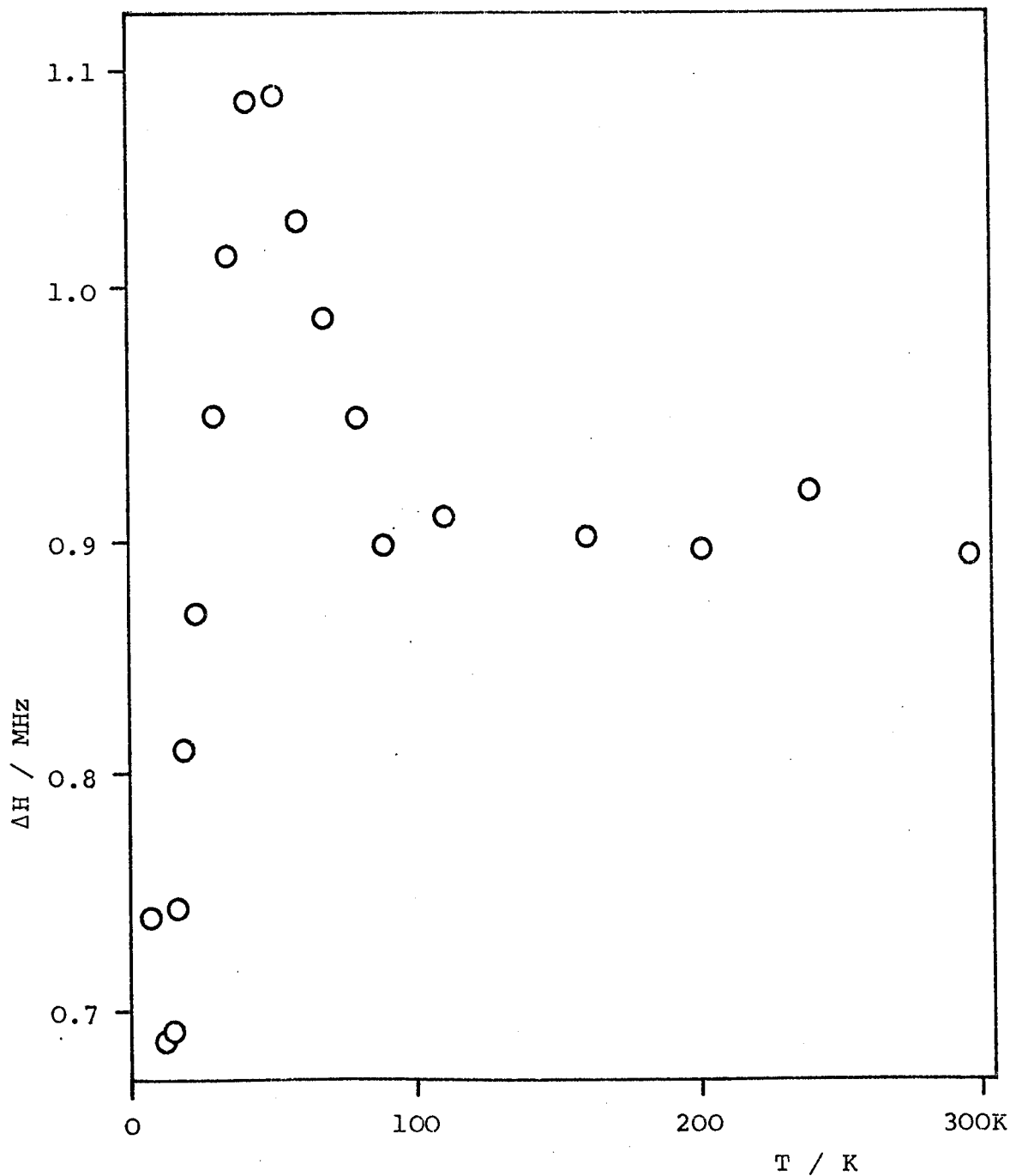


Figure 4.30

DMPA(TCNQ)<sub>4</sub>(I)

Plot of linewidth against temperature for crystal 3.  
H is approximately parallel to the y-axis.

The behaviour shown in Figure 4.30 has been previously reported for t-TTF-TCNQ<sup>58</sup>, TTF-TCNQ<sup>51</sup> and TMTTF-TCNQ<sup>173</sup>. In all these compounds, the maximum in the linewidth occurred at a temperature corresponding to the temperature at which abrupt changes in the susceptibility and conductivity were observed. This was interpreted as a phase transition from an essentially one-dimensional system, having weak interchain couplings, to a three-dimensional system, having strong interchain couplings. For a complete clarification of the situation in DMPA(TCNQ)<sub>4</sub>(I), conductivity and crystal structure data are required in this low temperature region but, unfortunately, these are not available. However, although no definite conclusions can be made at present, such a phase transition in this complex salt is considered unlikely in view of the fact that no sudden change occurs in the intensity plots for all the three crystals studied. The nature of a phase transition in this compound, if indeed present, would most probably be a departure from the dimer structure to a situation where the TCNQ molecules stack in tetrads with a more equal intermolecular spacing. This would be expected, however, to result in greater interaction between the two electrons and a larger J value than is in fact observed. Also, the other phase of this complex salt, DMPA(TCNQ)<sub>4</sub>(II), has magnetic properties more closely assignable to such a mode of packing, these results being discussed in Chapter 5. Therefore, the completely different magnetic properties

exhibited by these two phases would appear inconsistent with such a phase transition.

In order to possibly cast some light on the cause of the unusual linewidth behaviour, relaxation studies were undertaken on a crystal of  $\text{DMPA}(\text{TCNQ})_4(\text{I})$ . Since the lineshapes of the signals were found to be Lorentzian in the entire temperature region above and below the observed maximum in linewidth (figures 4.31 and 4.32), the method described in section 3.2.3(vi) could be used. Figure 4.33 shows typical results obtained for this compound at two of the temperatures studied. The values of  $T_1$  and  $T_2^*$  were obtained from the slope and intercept respectively of such plots, and the resulting temperature variation of these parameters is presented in Figure 4.34.

It can be seen that the spin lattice-relaxation time,  $T_1$ , exhibits a minimum at 50-60K, the exact temperature region at which a maximum in linewidth is observed. Therefore, some phenomenon causing changes in the spin-lattice relaxation time must account for the unusual linewidth behaviour. As discussed in section 4.1, the 'v'-shaped pattern is characteristic of strong exchange interactions in Frenkel exciton systems. Such an explanation in the case of  $\text{DMPA}(\text{TCNQ})_4(\text{I})$  is indeed feasible, as the very small  $J$  values results in a high exciton density

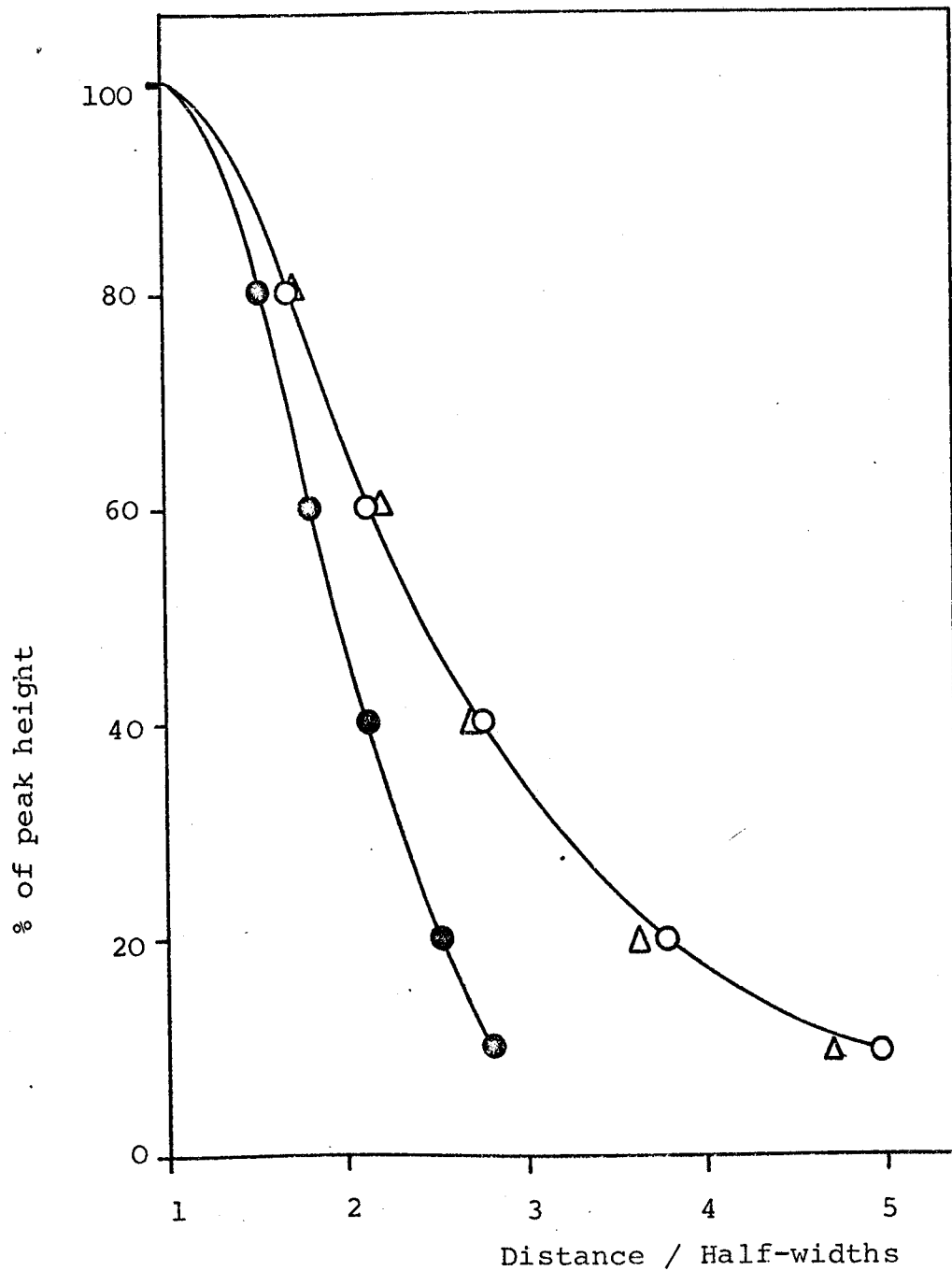


Figure 4.31

DMPA(TCNQ)<sub>4</sub>(I)

Lineshape analysis for crystal 1 at 80K.  
H is approximately parallel to the z-axis.

- Gaussian lineshape.
- Lorentzian lineshape.
- △ Average shape for crystal.

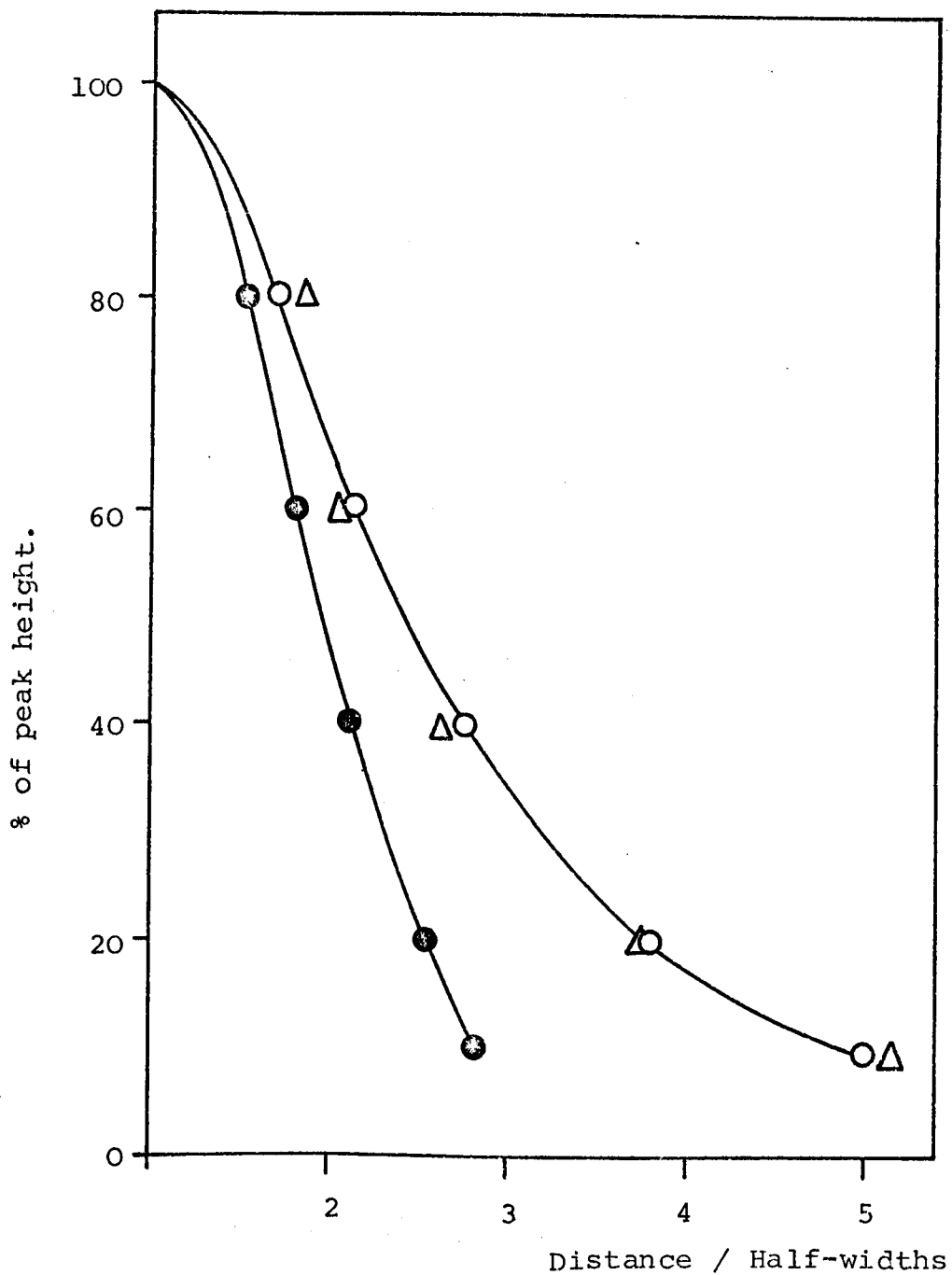


Figure 4.32

DMPA(TCNQ)<sub>4</sub>(I)

Lineshape analysis for crystal 1 at 20K.  
H is approximately parallel to the z-axis.

- Gaussian lineshape.
- Lorentzian lineshape.
- △ Average shape for crystal.

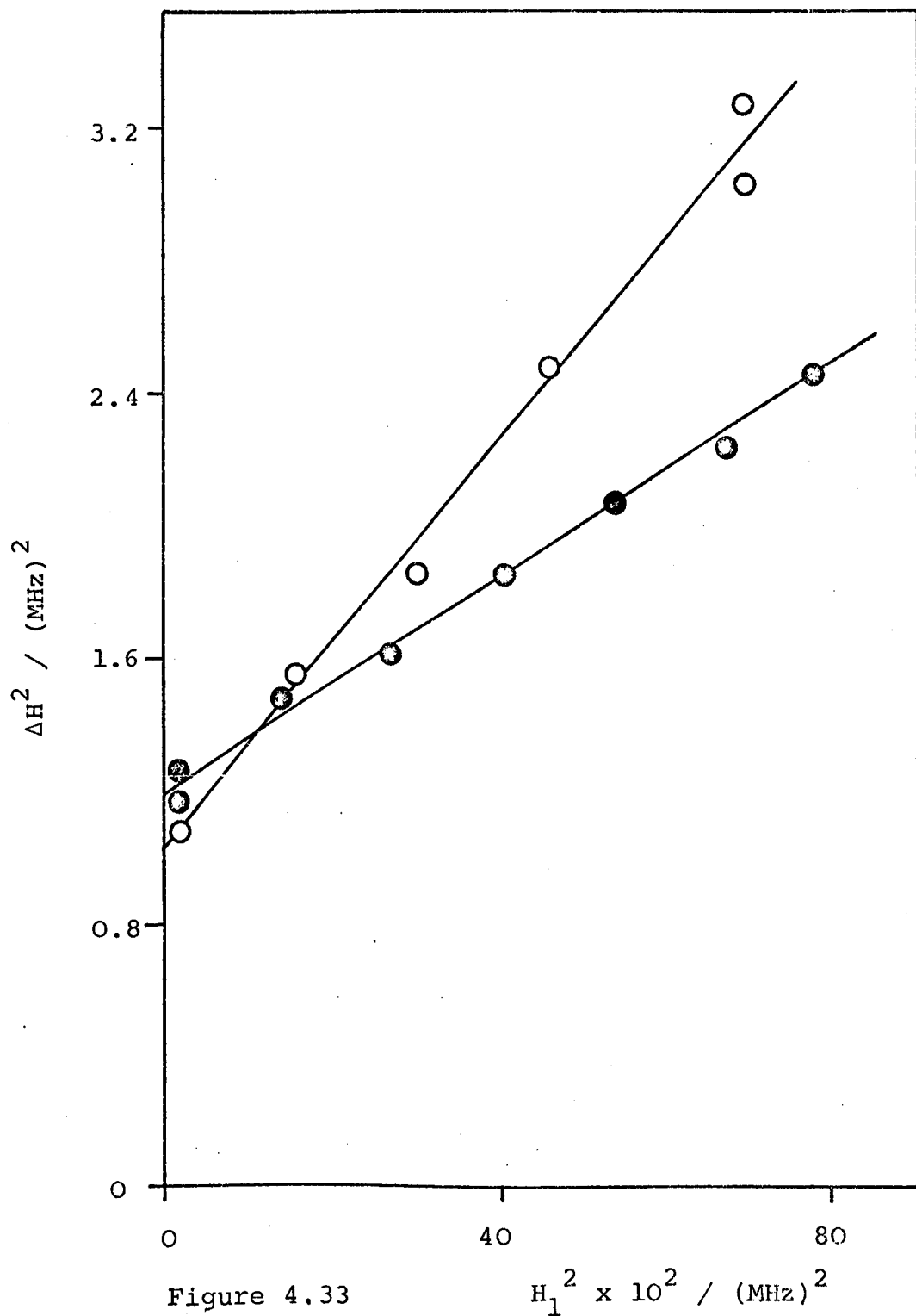


Figure 4.33

DMPA(TCNQ)<sub>4</sub>(I)

Plot of the square of the linewidth against the square of the microwave magnetic field strength for crystal 3 at two temperatures.

H is approximately parallel to the y-axis.

○ 300K , ● 60K.

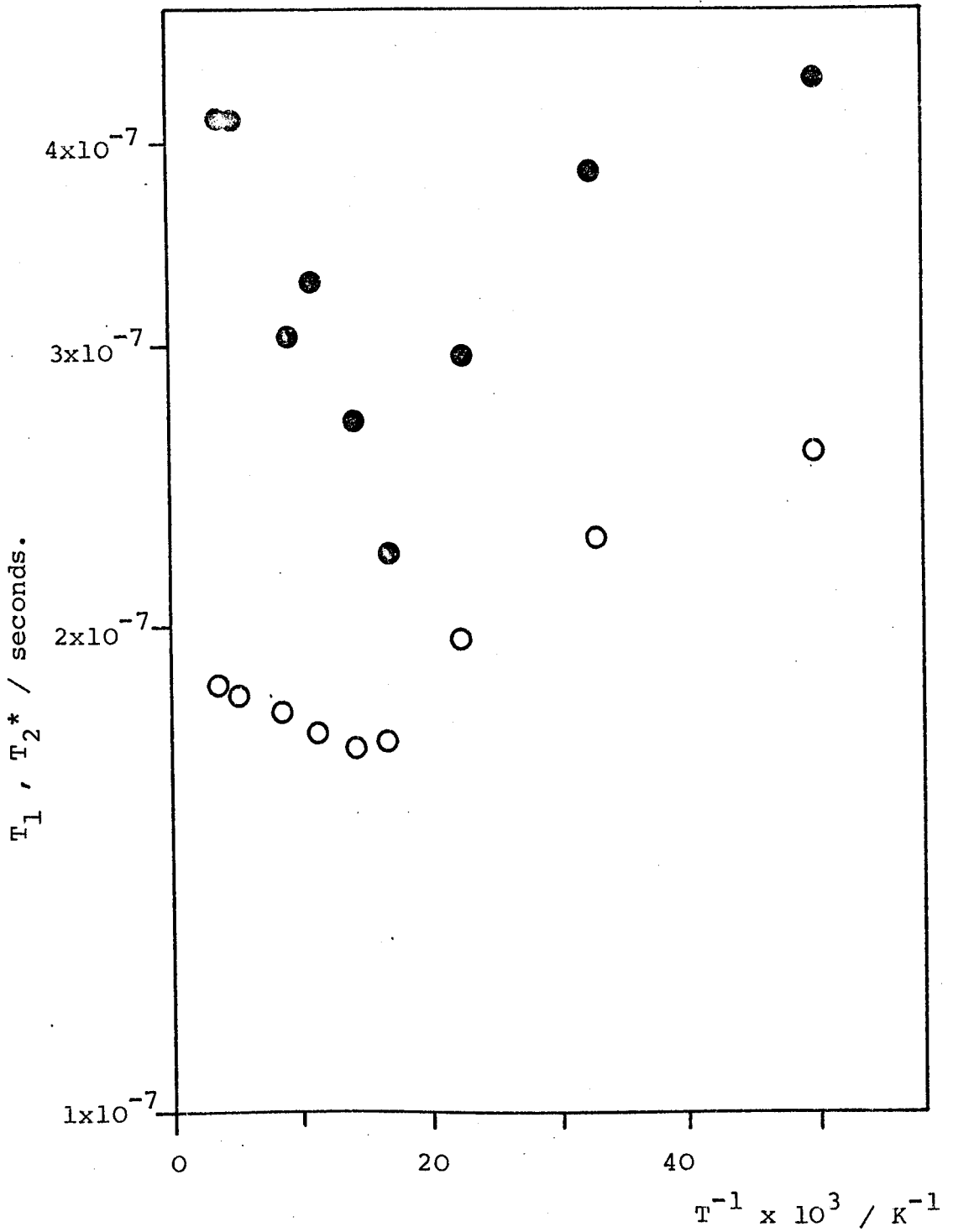


Figure 4.34

DMPA(TCNQ)<sub>4</sub>(I)

Semilog plot of  $T_1$  and  $T_2^*$  against reciprocal temperature for crystal 3.

H is approximately parallel to the y-axis.

●  $T_1$  , ○  $T_2^*$ .

at low temperatures. Exciton-exciton collisions will, therefore, be substantial at low temperatures and any effect on the spin-lattice relaxation time, similar to the mechanism proposed for DCBP(TCNQ)<sub>3</sub>, will have a maximum at the temperature of effective maximum triplet exciton concentration. This is in fact observed, as the position of the maximum in linewidth not only coincides with the minimum in the T<sub>1</sub> plot, but also with the maximum in the intensity variation. The Lorentzian lineshape in the entire temperature region studied supports the proposal of exchange interaction existing even at low temperatures. Such a high exciton density and exchange frequency might also contribute to the cause of the lack of observable dipolar splitting, the exchange interaction possibly modulating the dipolar levels.

Finally, although it has been established that the spin excitations are not the same as the charge excitations<sup>174,175</sup>, support for the proposed localised exciton model is given by the d.c. conductivity of DMPA(TCNQ)<sub>4</sub>(I). The conduction states are higher in energy than the exciton states and so are expected to be more extended in character. Therefore, the low d.c. conductivity observed in these crystals is consistent with a localised model for the interpretation of the magnetic properties.

### 4.3 DPB(TCNQ)<sub>4</sub>

This complex salt readily crystallises from solution with four TCNQ molecules, two formally neutral and two anionic, to each divalent cation 1,4-di(N-pyridinium)butane (DPB). Two types of crystal were obtained, differing in shape and size, and are shown in Figure 4.35. From the crystal structure determination, it appeared that the smaller crystals were crystallographically the same as the larger hexagonal shaped crystals which, if cleaved along one of the diagonals, produced the former type. The diagram illustrates the crystallographic axes a, b and c, these corresponding to the stack-to stack, along the stack and perpendicular to the cation plane directions. The crystals of the type shown in Figure 4.35(a) were those used in the e.s.r. studies, and the axes x, y and z of the laboratory co-ordinate system are therefore, also given in the diagram.

The crystal structure analysis showed the TCNQ molecules to be stacked along the b-axis with groupings of four TCNQ's within the stack. As was the case for DMPA(TCNQ)<sub>4</sub> (I), the perpendicular separation of 0.321nm between molecules labelled A and A' (Figure 4.36) in DPB(TCNQ)<sub>4</sub> is larger than the perpendicular separation of 0.319nm between A and B. Furthermore, there is good 'ideal' overlap between A and B, whereas only poor overlap between A and A'. Therefore, once again the situation is

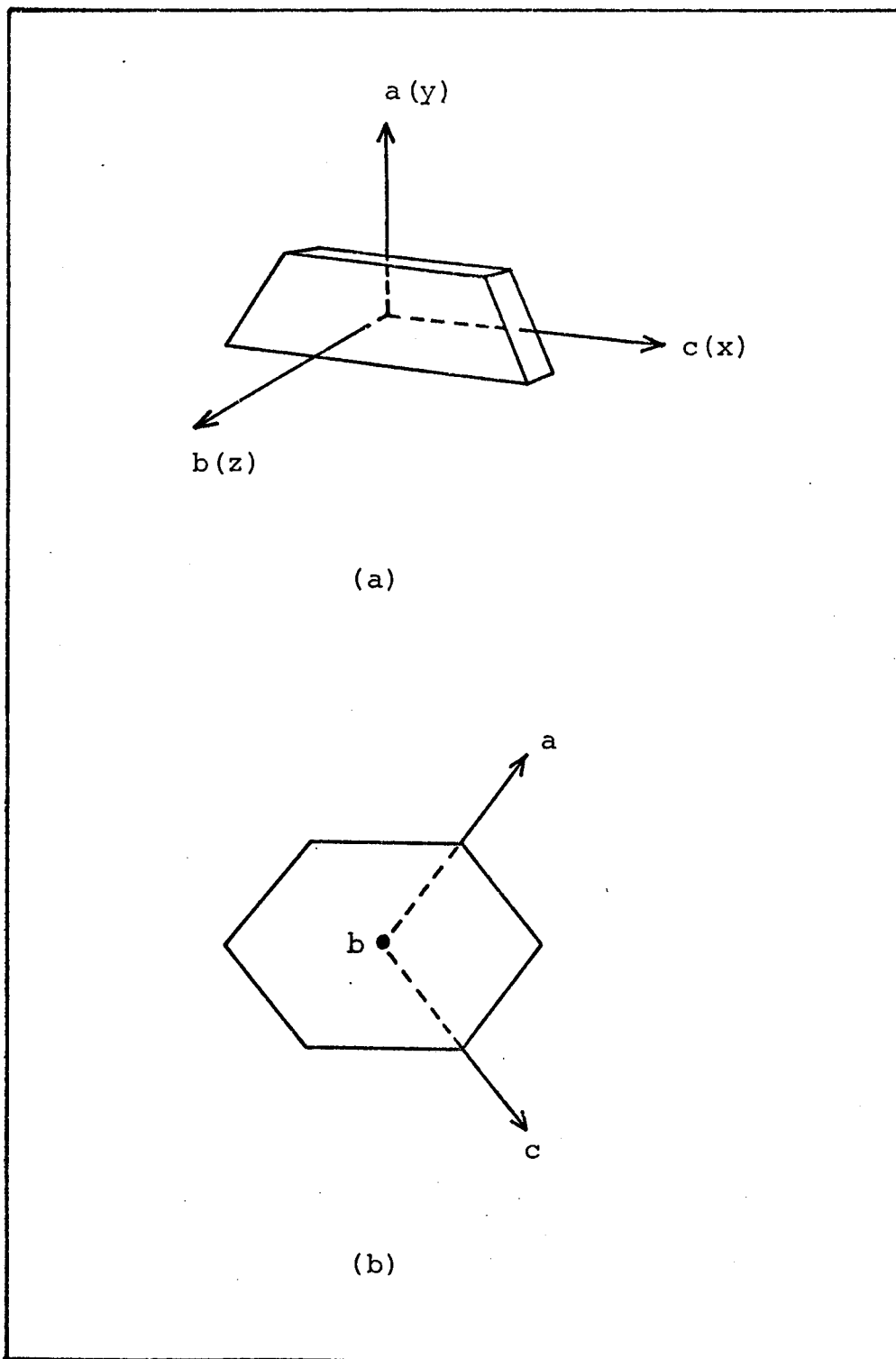
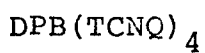


Figure 4.35



The two types of crystal shapes obtained for this complex salt. The crystallographic axes  $a$ ,  $b$  and  $c$  are indicated in both diagrams (For (b) the  $b$ -axis is  $\perp$  to the plane of this figure). The labelling of the external axes is also shown in (a).

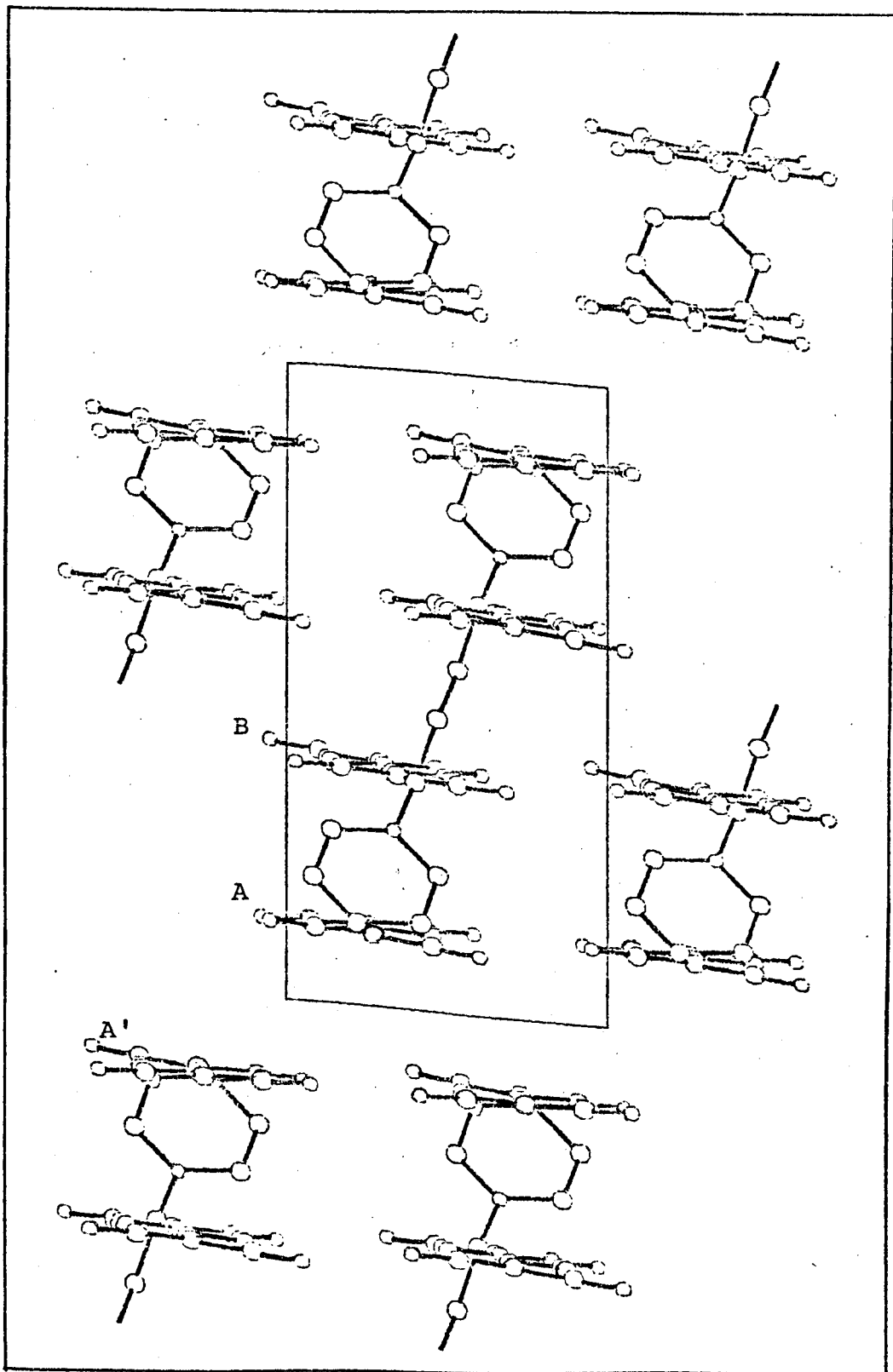


Figure 4.36

DPB(TCNQ)<sub>4</sub>

Projection of the crystal structure along the c-axis.

more closely described by a pair of dimers rather than a tetrad. However, the similarity between the crystal structures of  $\text{DMPA}(\text{TCNQ})_4$  (I) and  $\text{DPB}(\text{TCNQ})_4$  ends at this point. In the latter complex salt, the stack-to-stack distance is greater than the distance between the stacks and the cation molecules. This gives rise to some degree of two-dimensionality in the physical properties of this compound, not of the usual type within the TCNQ sheet, but in the bc plane. The d.c. conductivity results<sup>176</sup> are consistent with the crystal structure, which predicts the conductivity  $\sigma$  should change in such an order  $\sigma_b \approx \sigma_c > \sigma_a$ .

The angular variation of the g factor was investigated at room temperature for crystals 1, 2 and 3, which were oriented with the x-, y- and z-axes respectively as the rotation axis. The results for this study are presented in Figures 4.37 to 4.39, and the average values obtained for  $g_x$ ,  $g_y$  and  $g_z$  were 2.0039, 2.0035 and 2.0030 respectively, all with an error of  $\pm 0.0003$ . It is generally considered that the g values for these compounds reflect the degree to which the unpaired electrons are 'free' and, therefore, the magnitudes would be expected to follow the same order as exhibited by the conductivities along the same axes. However, although this prediction generally holds in these compounds, the g values do not appear to reflect the electron delocalisation indicated by the conductivity results. Therefore, the g factors do not

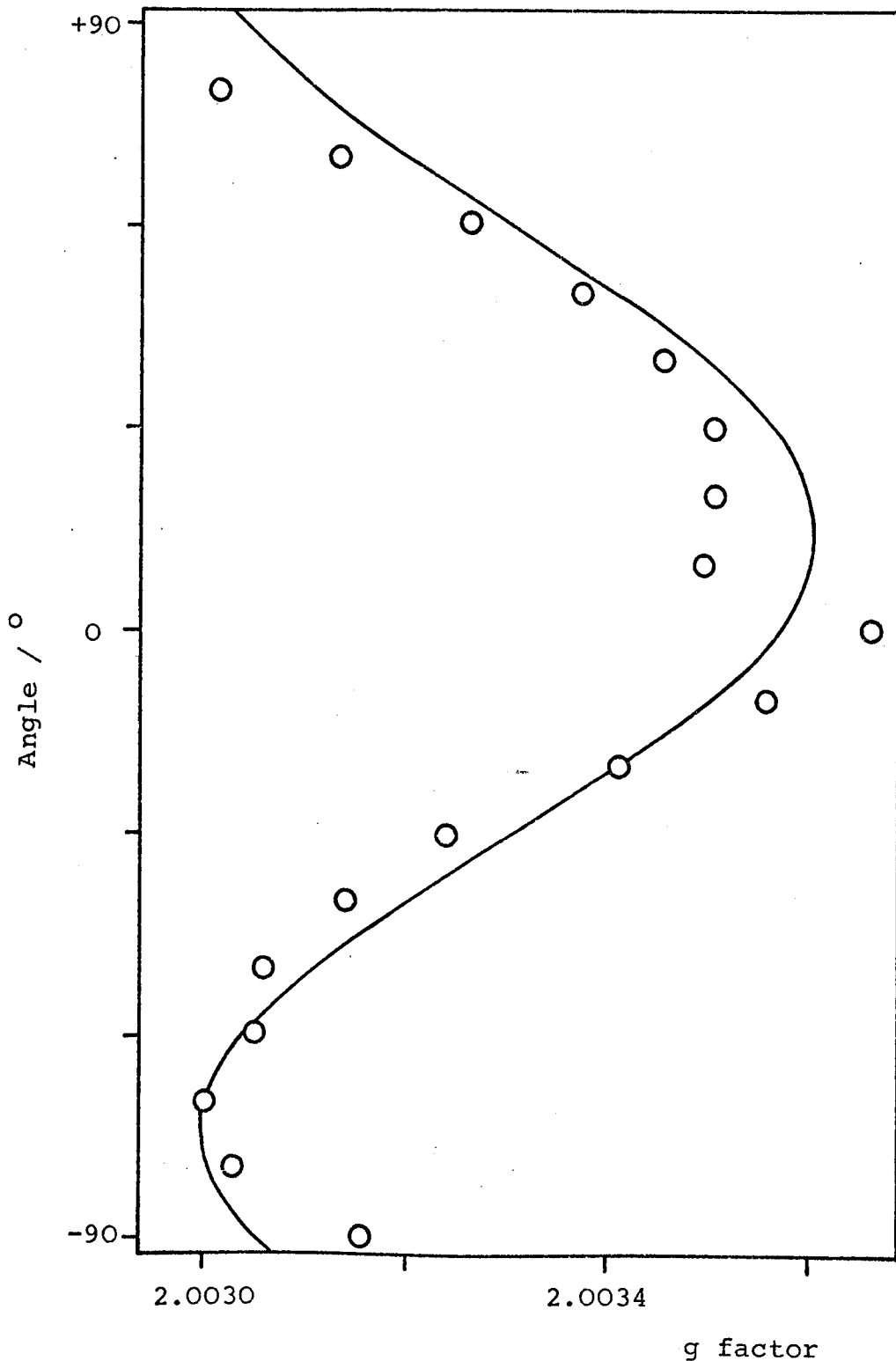


Figure 4.37

DPB(TCNQ)<sub>4</sub>

Angular variation of g factor at 300K for crystal 1.

Approximate orientations: H//y-axis at +15°.

H//z-axis at -75°.

— Computer simulation.

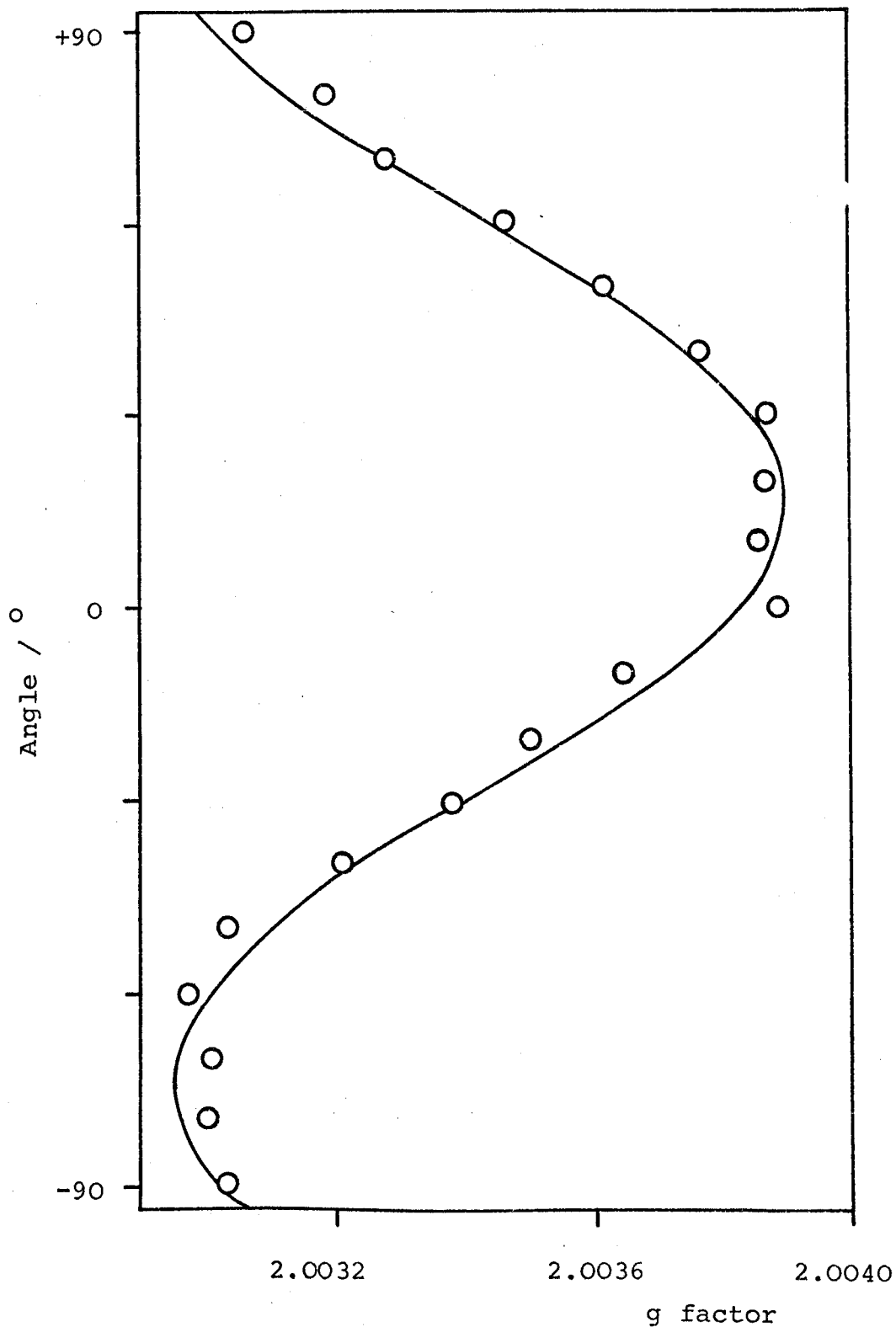


Figure 4.38

DPB(TCNQ)<sub>4</sub>

Angular variation of g factor at 300K for crystal 2.

Approximate orientations: H//x-axis at +16°.

H//z-axis at -74°.

— Computer simulation.

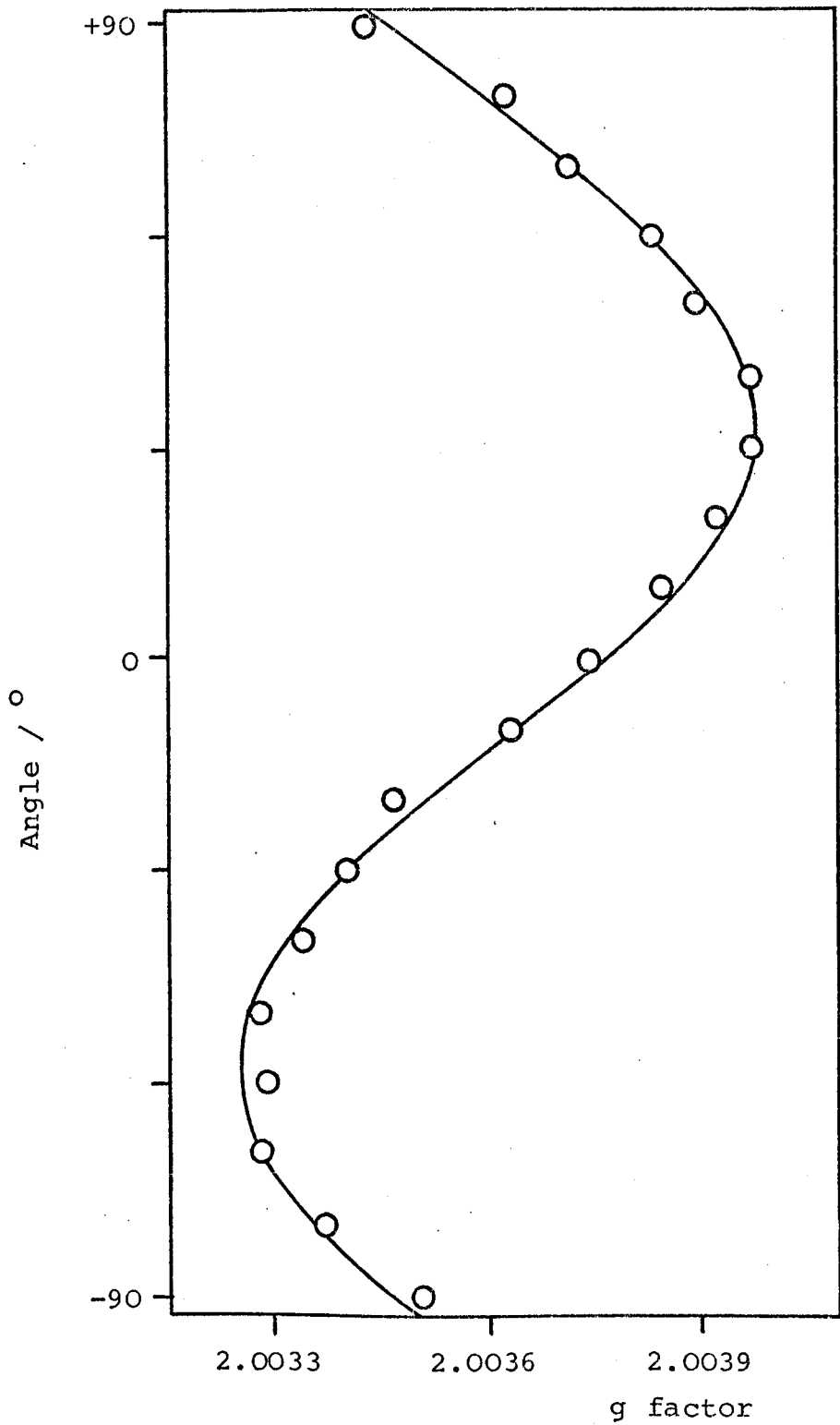


Figure 4.39

DPB(TCNQ)<sub>4</sub>

Angular variation of g factor at 300K  
for crystal 3.

Approximate orientations: H//x-axis at +33°.

H//y-axis at -57°.

———— Computer simulation.

seem to have a great deal of value in the interpretive sense, at least in the case of this complex salt.

The angular variation of the linewidth, also studied at room temperature, is most unusual in that all three crystals exhibited the behaviour previously discussed in section 4.2. This is shown for  $\text{DPB}(\text{TCNQ})_4$  in Figures 4.40 to 4.42. It can be seen that there is a greater degree of linewidth anisotropy when a high conductivity axis and a low conductivity axis are contained in the plane under investigation (Figures 4.40 and 4.42), whereas only a small anisotropy is observed when both high conductivity axes are being studied (Figure 4.41). This is in agreement with the interpretation discussed in section 4.2 for a nearly two-dimensional system, and is also in agreement with the conductivity results and crystal structure data. However, the fact that the linewidth angular variation does not match the g factor angular variation when the two high conductivity axes are under investigation is not readily understood. In the case of  $\text{DMPA}(\text{TCNQ})_4(\text{I})$  the two most highly conducting directions are contained in the TCNQ sheet, whereas in  $\text{DPB}(\text{TCNQ})_4$  this is not the case. Therefore, as linewidths depend on the strength of the interaction between the spin system and its environment, it is possible that this difference might be the cause of the observed behaviour.

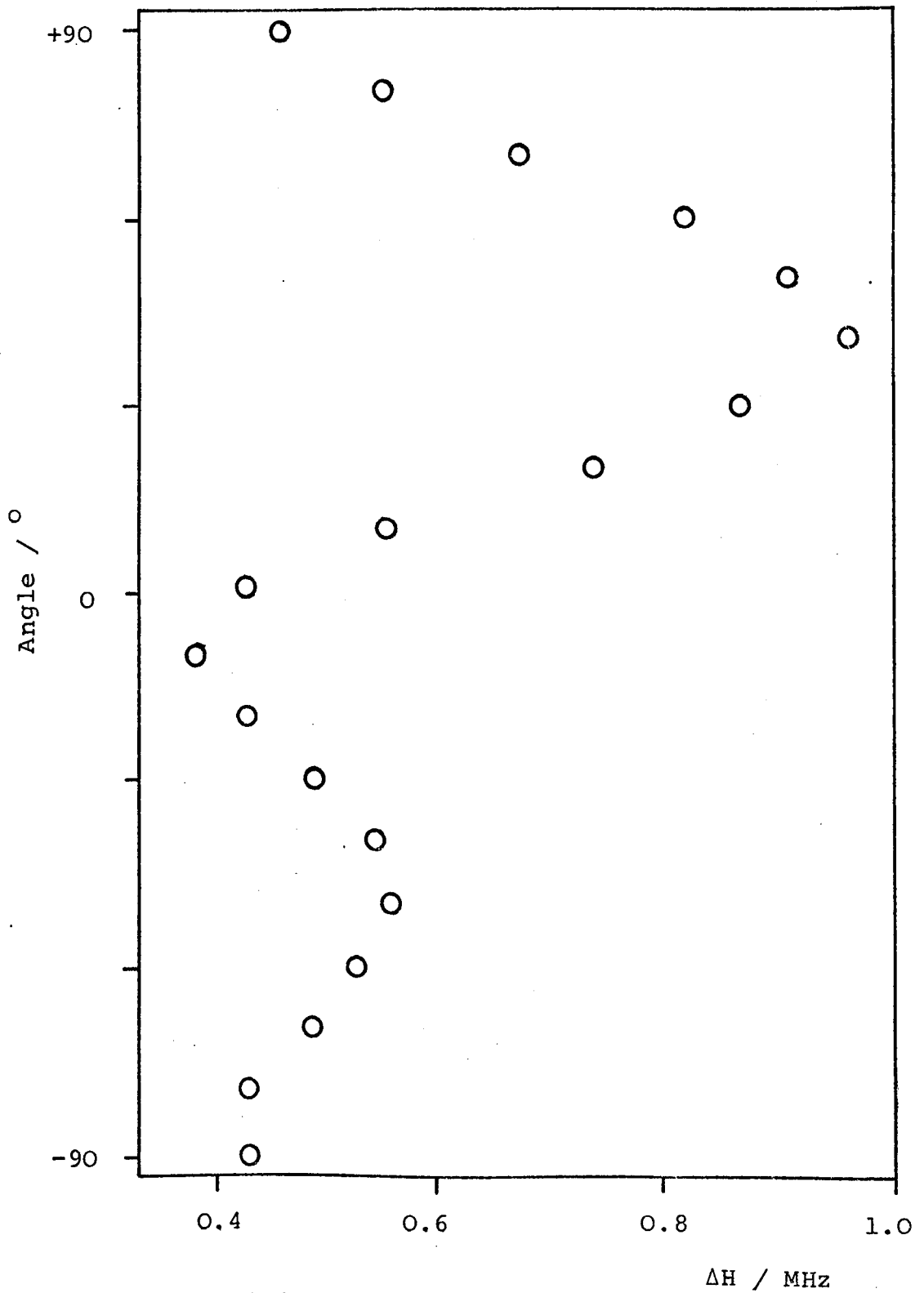


Figure 4.40

DPB(TCNQ)<sub>4</sub>

Angular variation of linewidth at 300K for crystal 1.  
Approximate orientations as for Figure 4.37.

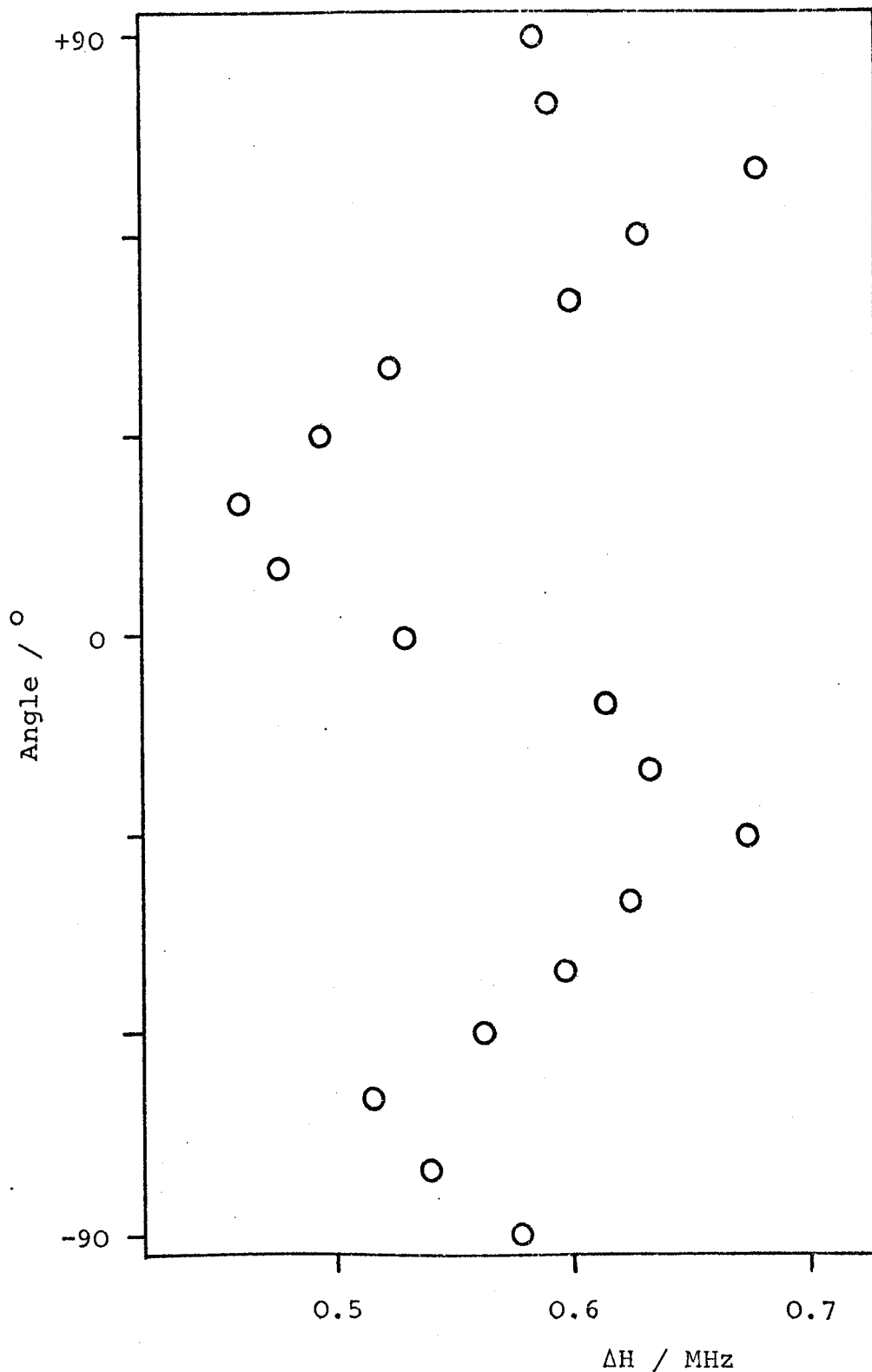


Figure 4.41

DPB(TCNQ)<sub>4</sub>

Angular variation of linewidth at 300K for crystal 2.

Approximate orientations as for Figure 4.38.

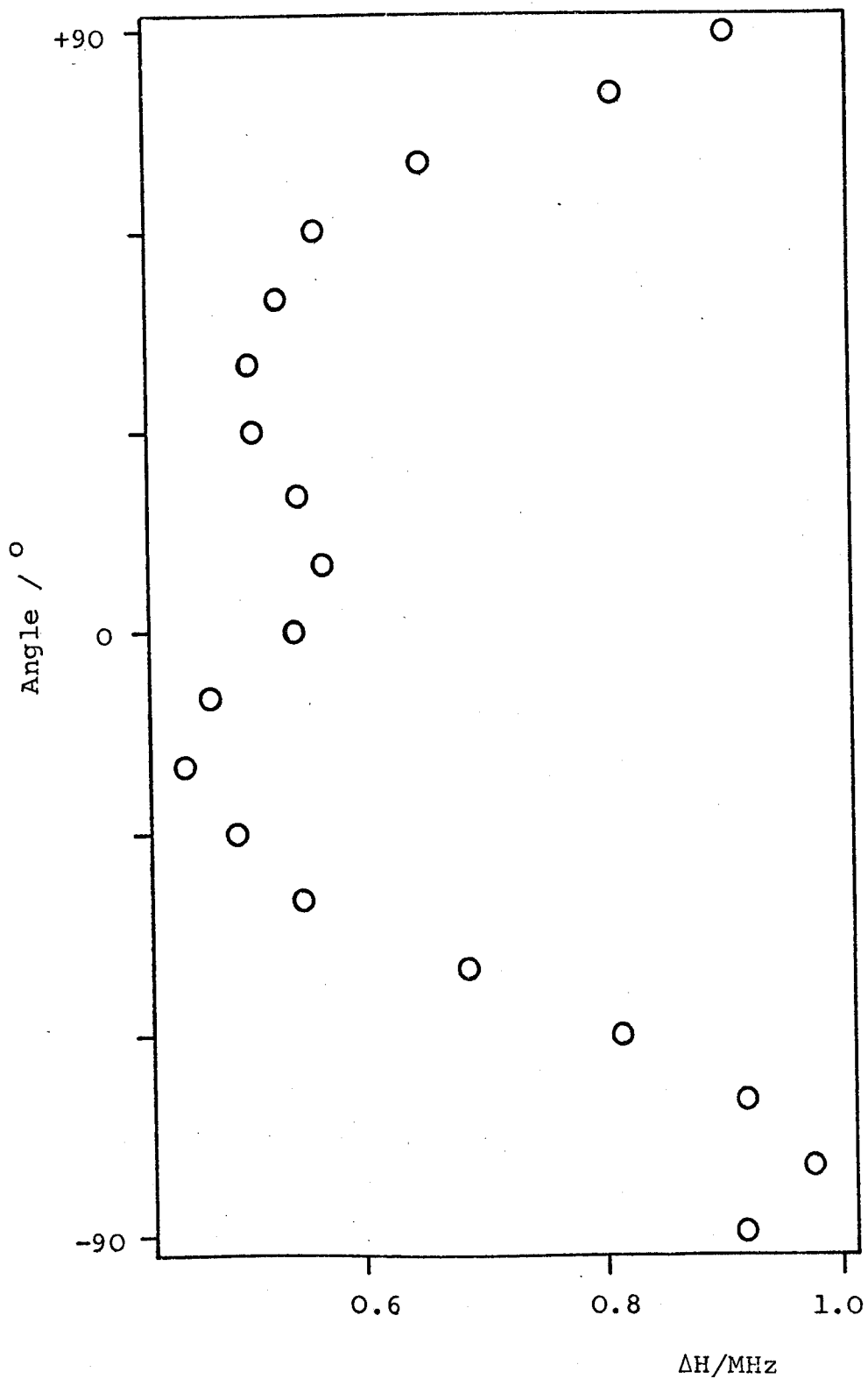


Figure 4.42

DPB(TCNQ)<sub>4</sub>

Angular variation of linewidth at 300K  
for crystal 3.

Approximate orientations as for Figure 4.39.

The temperature dependence of the e.s.r. signal intensity was investigated for all the three crystals, and a typical plot is shown in Figure 4.43. There is a marked similarity between this behaviour and that exhibited by  $\text{DMPA}(\text{TCNQ})_4(\text{I})$ , as is expected from the similarity between the crystal structure data. The intensity plots all show a maximum at approximately 40K and, from the relationship given in equation 4.3, the predicted  $J$  value is  $0.52 \text{ kJ mol}^{-1}$ . This value is very small indeed and reflects the large distance separation, and corresponding small interaction, between the two electrons of the triplet exciton, in agreement with the dimer interpretation of the crystal structure. This small value results in a Curie-like behaviour observed in the temperature region above 40K, as discussed for  $\text{DMPA}(\text{TCNQ})_4(\text{I})$ .

A typical example of the  $\log IT$  against  $1/T$  plots for  $\text{DPB}(\text{TCNQ})_4$  is shown in Figure 4.44 and, again considering only the linear portion where depopulation of the triplet state is occurring in the region  $J > kT$ , the average slope obtained has a value of  $-0.52 \pm 0.05 \text{ kJ mol}^{-1}$ , in excellent agreement with that predicted from equation 4.3. Substituting this value for  $J$  in equation 2.26 yields a room temperature molar susceptibility value of  $2.42 \times 10^{-3} \text{ e.m.u. cm}^3 \text{ mol}^{-1}$ , which is in good agreement with the experimentally observed value of  $(2.9 \pm 0.5) \times 10^{-3} \text{ e.m.u. cm}^3 \text{ mol}^{-1}$ . This indicates that the triplet excitons are localised in this complex salt, which is not surprising in

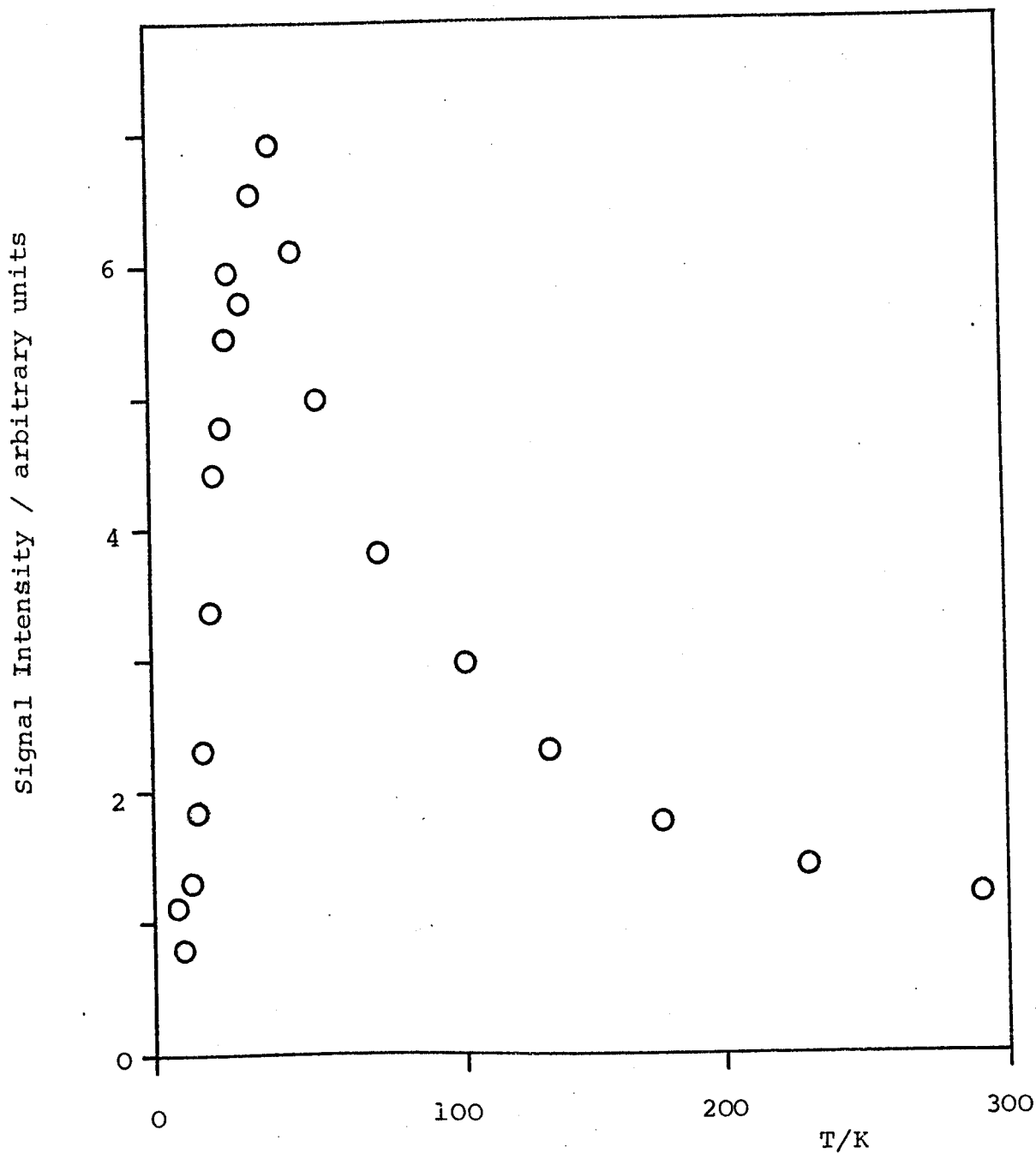


Figure 4.43

DPB(TCNQ)<sub>4</sub>

Plot of relative intensity against temperature  
for crystal 3.

H is approximately parallel to the y-axis.

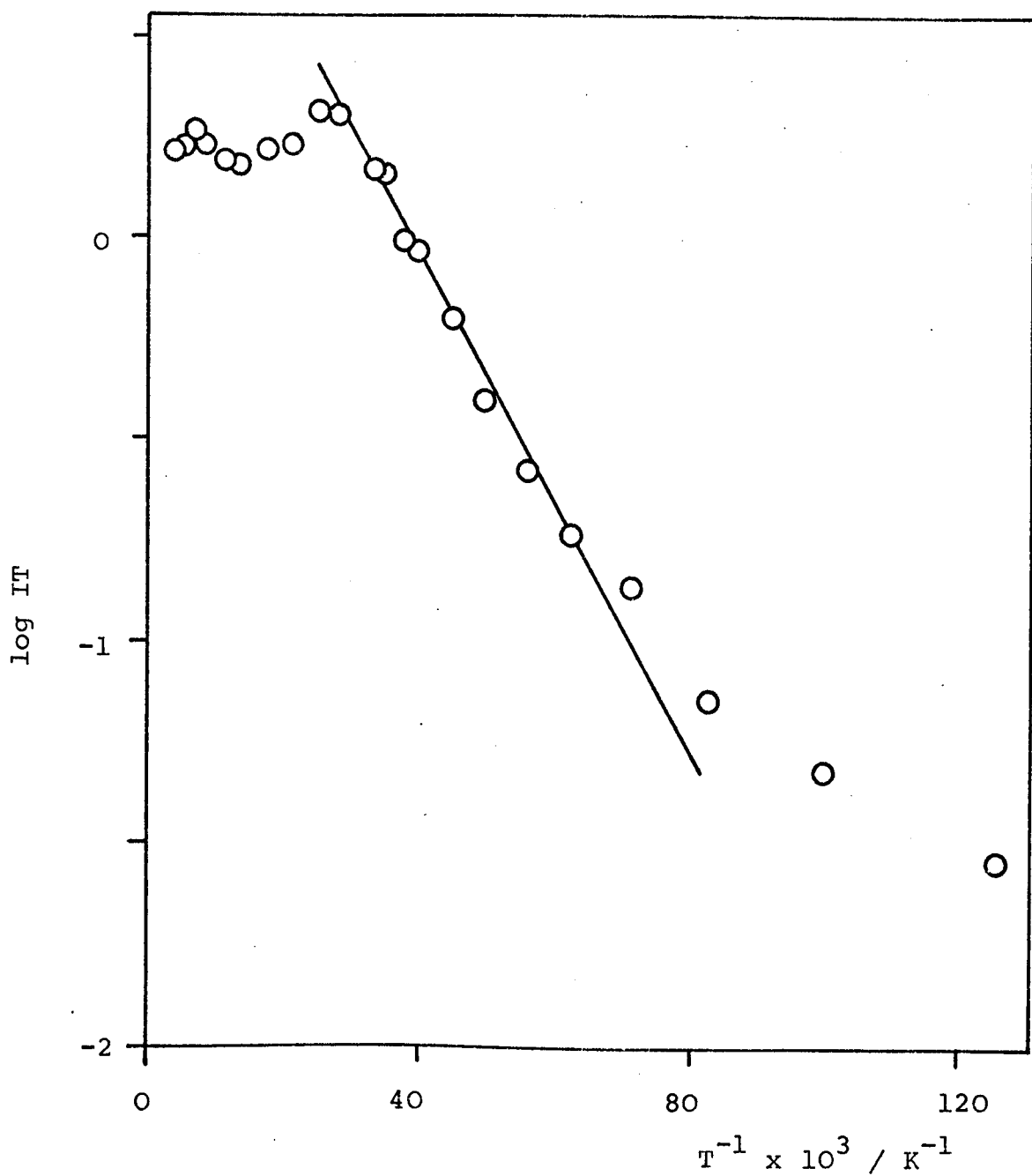


Figure 4.44

DPB(TCNQ)<sub>4</sub>

Semilog plot of the product of the relative intensity and temperature against reciprocal temperature for crystal 1.

H is approximately parallel to the z-axis.

view of the poor overlap along the TCNQ stack. The fact that the experimental value of  $\chi_m$  is rather high most probably arises from the errors involved in assessing the small weight of the single crystal used for this study. Furthermore, for a delocalised exciton, the susceptibility should be less than the value predicted from equation 2.26 and, therefore, the high value would seem to preclude the existence of delocalised excitons in  $\text{DPB}(\text{TCNQ})_4$ . Generally, the observation of a high susceptibility value would suggest a temperature dependent J value. However, in this case, this possibility does not seem likely as there is effectively exciton saturation at temperatures as low as 40K and, as such, quite a remarkable change in J would be required for this to be reflected in the room temperature susceptibility value.

The curvature at low temperatures, shown in Figure 4.44, is due to the effect of the paramagnetism of Curie species. Although the expected increase in intensity was not observed in the intensity against temperature plot even at 6K, therefore indicating the number of species is small, an estimate was obtained from the extrapolation of the curvature. The value obtained for the number of such species in  $\text{DPB}(\text{TCNQ})_4$  is  $(3.7 \pm 0.9) \times 10^{21}$  spins  $\text{mol}^{-1}$ , which corresponds to a percentage of only 0.6%.

At all the temperatures studied, no evidence of

dipolar splitting was observed. Although a localised model is proposed for this complex salt, the very low  $J$  value indicates that the dipolar interaction will also be very small and, consequently, undetectable as was the case for the similar situation for  $\text{DMPA}(\text{TCNQ})_4$  (I). The d.c. conductivity data place this compound in the intermediate-conductivity class and indicate that a hopping mechanism between localised conduction states most closely describes the electrical properties. Therefore, in view of this evidence, localised magnetic exciton states would also be expected. It must be pointed out that, although the observation of dipolar splittings is a firm indication of localised triplet species, the lack of such an observation does not necessarily mean the species are delocalised.

The magnetic properties of  $\text{DPB}(\text{TCNQ})_4$  and  $\text{DMPA}(\text{TCNQ})_4$  (I) are very similar in most respects. However, a striking difference was observed in the temperature dependence of the linewidths. The results for  $\text{DPB}(\text{TCNQ})_4$  are presented in Figure 4.45. It can be seen from this plot that the linewidth remained essentially constant as the temperature was lowered from 300 to 20K, but increased below this temperature. The same behaviour was exhibited for all the crystals studied, and the linewidth maximum observed for  $\text{DMPA}(\text{TCNQ})_4$  (I) was not evident at any orientation.

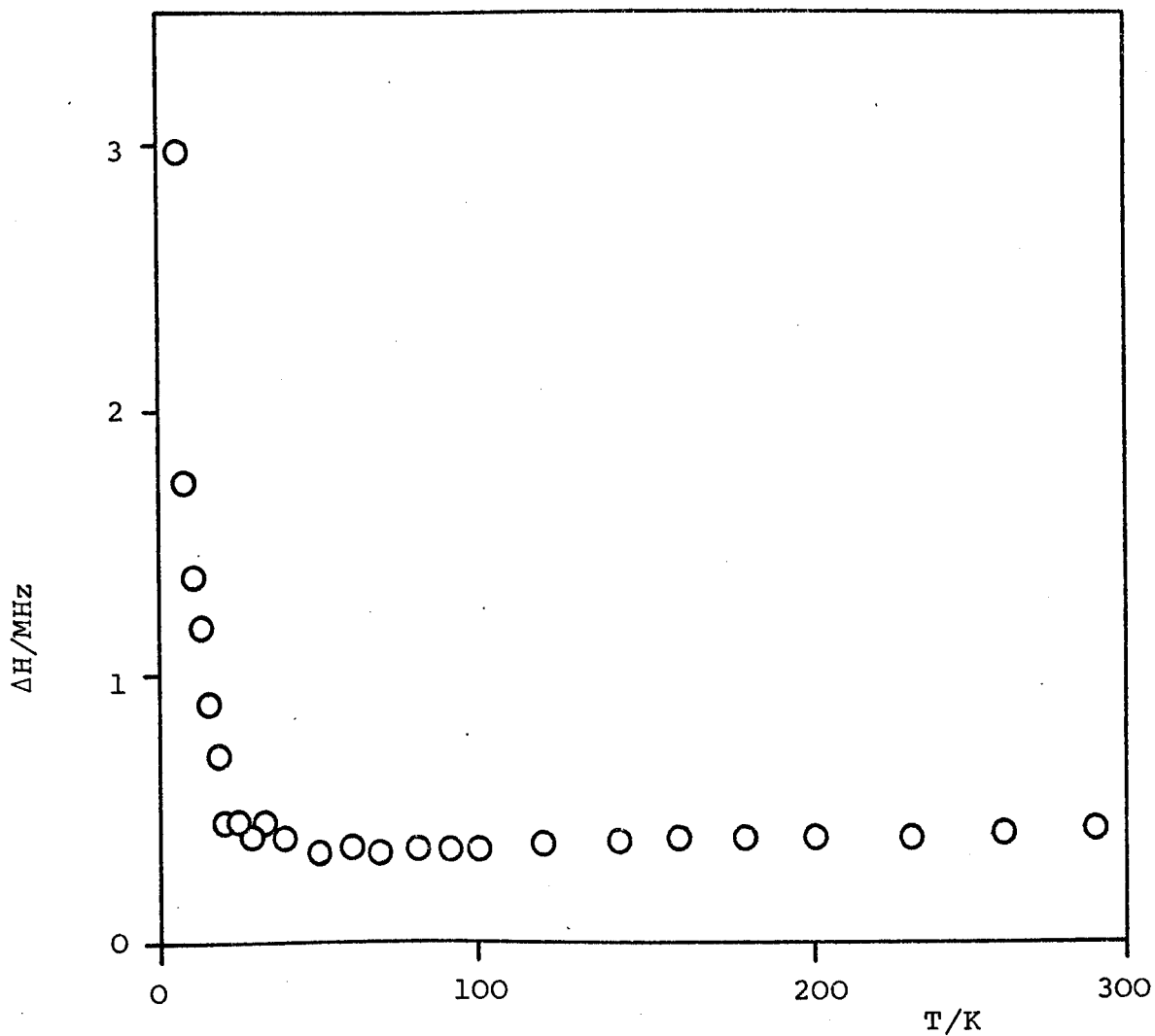


Figure 4.45

DPB(TCNQ)<sub>4</sub>

Plot of linewidth against temperature for crystal 1.

H is approximately parallel to the z-axis.

The linewidth behaviour shown in Figure 4.45 has been previously reported<sup>142</sup> for the Wannier spin exciton systems p-phenylenediamine-chloranil(PDC) and N,N,N',N'-tetramethyl-phenylenediamine(TMPD)-(TCNQ). From theoretical treatments of the linewidth behaviour, exchange narrowing in Wannier systems results in a temperature independent linewidth until low exciton densities, when broadening is observed. This is consistent with the observations for DPB(TCNQ)<sub>4</sub> but is contradictory to the data which indicate a localised Frenkel exciton model. High-pressure studies<sup>142,154,177,178</sup> have been performed on Frenkel and Wannier exciton systems and provide a method for distinguishing between them. For Frenkel systems, the linewidth increases with increasing pressure, whereas the opposite effect is observed for Wannier systems, due to their different dependence on exciton density. Unfortunately, the equipment was not available for such a study on DPB(TCNQ)<sub>4</sub> and, therefore, until measurements of this type are possible an unambiguous assignment of the exciton type cannot be made.

Saturation and modulation broadening were eliminated as being the cause of the increased linewidth at low temperatures. Hyperfine interactions also do not appear to be the dominant broadening process, as this would be expected to result in Gaussian lineshapes, whereas Figure 4.46 shows the lineshape to be Lorentzian. The broadening

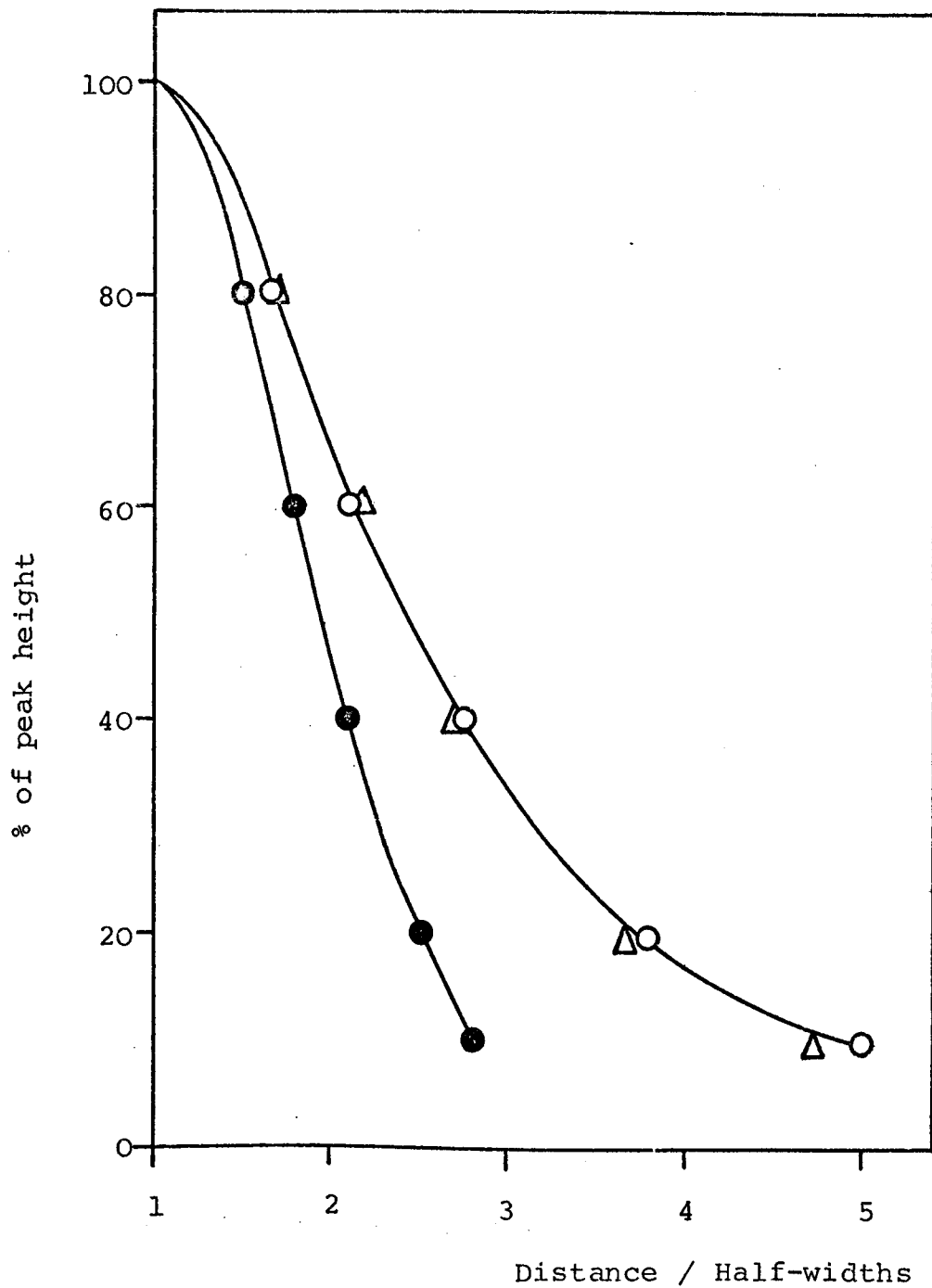


Figure 4.46

DPB(TCNQ)<sub>4</sub>

Lineshape analysis for crystal 1 at 10K.  
H is approximately parallel to the z-axis.

- Gaussian lineshape.
- Lorentzian lineshape.
- △ Average shape for crystal.

could possibly arise from the onset of dipolar splitting in the 'fast' exchange region and an analysis of the low temperature linewidth data, using equation 2.46, yields the points plotted in Figure 4.47. Since the value of  $d_0$  is not available,  $(\Delta H - \Delta H_0)^{-1}$  is plotted in this figure. However, the slopes obtained from such plots gave activation energies for exchange slightly smaller than the singlet-triplet energy gap. Therefore, the broadening seems unlikely to be due entirely to the onset of dipolar splitting.

Relaxation studies were also undertaken and the resulting temperature variation of  $T_1$  and  $T_2^*$  is shown in Figure 4.48. In the temperature region where the broadening occurs, the values of  $T_1$  do decrease slightly, apart from the measurement taken at 10K. This trend would be consistent with that expected for line broadening at the onset of dipolar splitting. However, it is felt that the relaxation results are not in any way conclusive. Consequently, the linewidth broadening below 20K is considered to be due to a number of effects, namely the finite value of the dipolar interaction, hyperfine interaction and the influence of the Curie signal, which begins to have an effect in this temperature region and would be expected to have a broader linewidth.

From the results obtained in this study, it

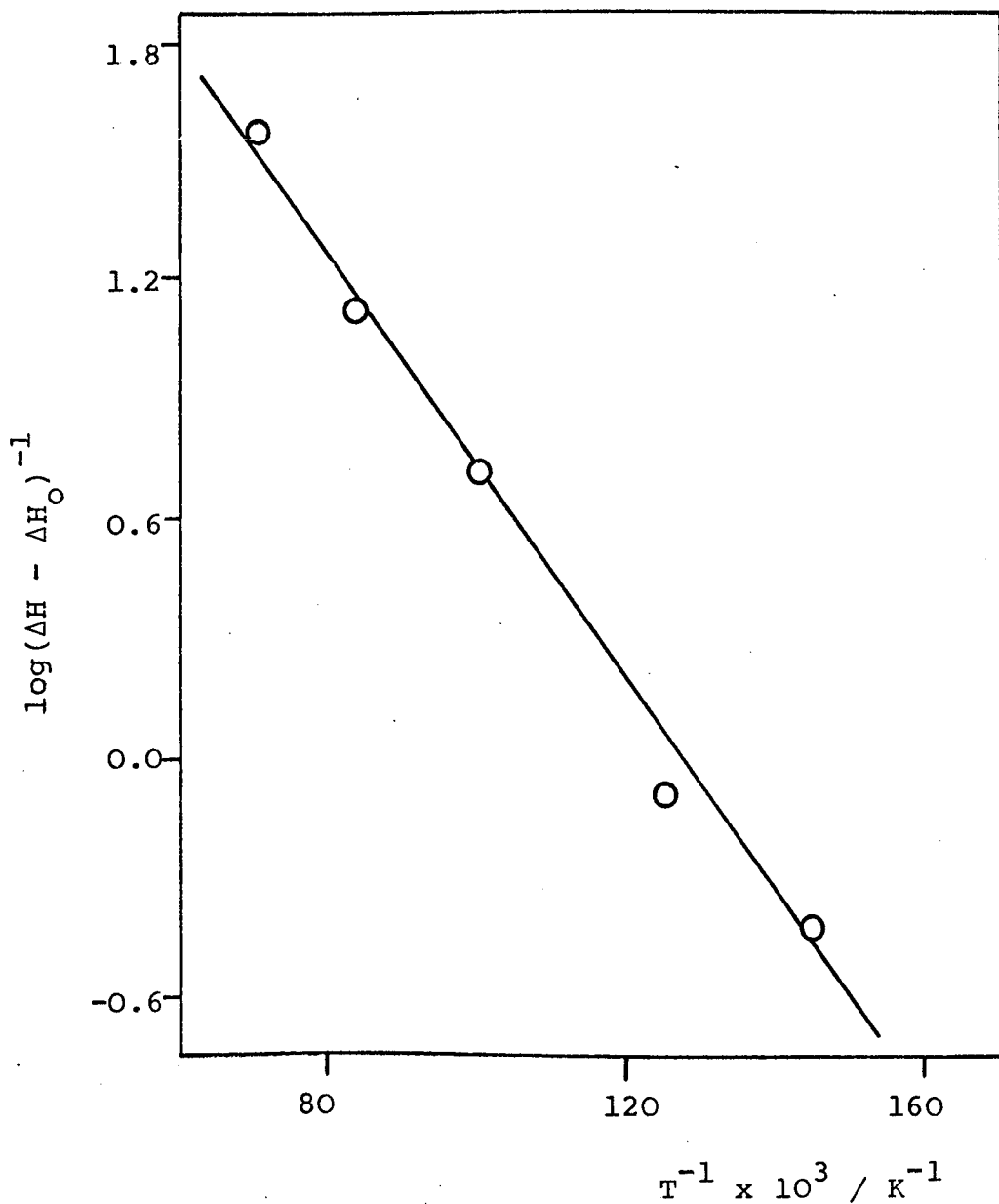


Figure 4.47

DPB(TCNQ)<sub>4</sub>

Semilog plot of  $(\Delta H - \Delta H_0)^{-1}$  against reciprocal temperature for crystal 1.

H is approximately parallel to the z-axis.

$\Delta H$  is the linewidth in MHz.

$\Delta H_0$  is the limiting high temperature linewidth in MHz (=0.4MHz in this case).

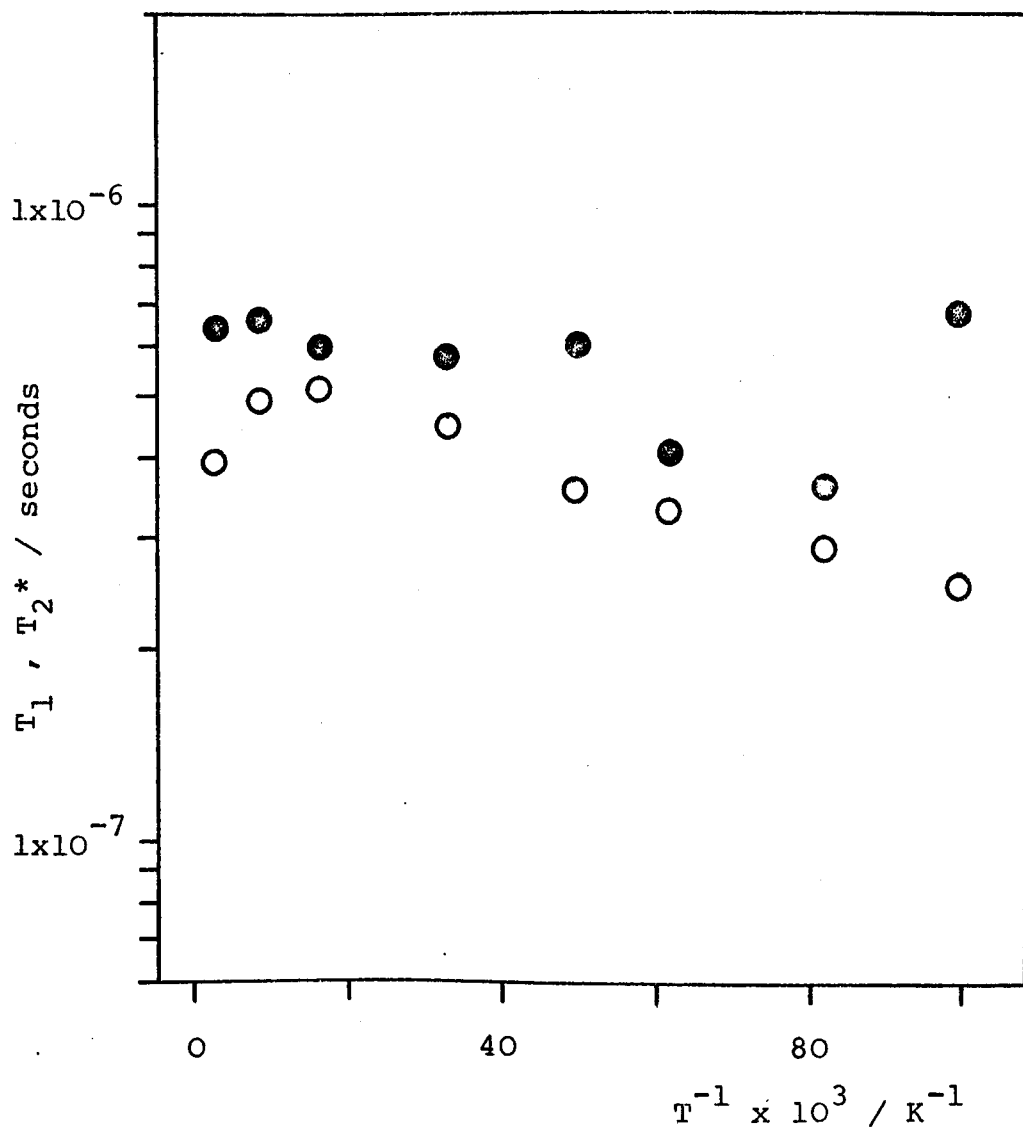


Figure 4.48

DPB(TCNQ)<sub>4</sub>

Semilog plot of  $T_1$  and  $T_2^*$  against reciprocal temperature for crystal 2.

H is approximately parallel to the x-axis.

●  $T_1$  , ○  $T_2^*$

would be reasonable to say that it is not possible to make any definite suggestions concerning the degree of localisation of the low lying electronic states in this complex salt. The crystal structure, conductivity and susceptibility data, plus comparison with the very similar  $\text{DMPA}(\text{TCNQ})_4(\text{I})$ , would seem to suggest localised excitons are more likely in  $\text{DPB}(\text{TCNQ})_4$ . Investigations including high-pressure studies for this and other analogous complex salts in this series would be of interest to determine the parameters influencing the linewidth behaviour.

#### 4.4 TPT(TCNQ)<sub>4</sub>

The cation used in the preparation of this complex salt is 2,4,6-tri-(N-methyl-2-pyridinium)triazine (TPT) and is the only trivalent cation studied in this work. Consequently, there are potentially three unpaired electrons for each tetrad of TCNQ molecules in the complex salt. There have been many complexes prepared having mono- and divalent cations and so it was considered to be of interest to study the effect of cations with higher valencies on the physical properties of TCNQ complex salts.

The crystals were needle-shaped and the external axes were labelled as shown in Figure 3.10(a), with x as the long dimension, y the intermediate and z the short dimension, although the y- and z-axes were almost

indistinguishable due to the pronounced needle shape. The three crystals used in this study were mounted with the x-, y- and z-axes as the rotation axes for crystals 1, 2 and 3 respectively.

This complex salt proved to be most unusual in many respects. The three electrons per tetrad of TCNQ molecules would be expected to be situated quite close together and, therefore, interact more strongly than the usual case of two electrons per tetrad. Preliminary e.s.r. investigations, however, showed no evidence of any splitting, a single symmetrical peak being observed in the entire temperature range studied. Not only were the predictions of the magnetic properties proved to be wrong, but the d.c. conductivity and crystal structure data were also surprising. The crystal structure determination is currently in progress in this department, but the completion of this study has been severely hindered by the apparent high degree of disorder existing within the crystals. At the present time, only a tentative assignment of the crystallographic axes has been made, the external axes x-, y- and z probably corresponding to the TCNQ stacking direction, the direction perpendicular to the cation sheets, and the stack-to-stack direction respectively. Preliminary conductivity measurements<sup>179</sup> showed a temperature dependent conductivity, the activation energy being very small, with similar conductivity values

along the short and intermediate axes, but an almost semi-metallic value along the long axis.

In order to locate the principal magnetic axes, the angular dependence of the  $g$  factor was investigated at room temperature. The results for the three crystals studied are presented in Figures 4.49 to 4.51, and the average values of  $g_x$ ,  $g_y$  and  $g_z$  obtained from the maxima and minima of these plots are 2.0040, 2.0034 and 2.0035 respectively, all with an experimental error of  $\pm 0.0003$ . The values of  $g_y$  and  $g_z$  are very similar, in agreement with the similarity observed between the conductivities along these directions. However, the high conductivity x-axis, which is usually expected to have the  $g$  value closest to the free electron value, has the largest  $g$  factor. This is contradictory to the majority of studies on TCNQ complex salts, which show the stacking direction to have the smallest  $g$  value. The simple explanation of the  $g$  factor anisotropy being governed by electron delocalisation would not seem to hold for  $\text{TPT}(\text{TCNQ})_4$  and is possibly due to the disorder in some way. Therefore, the interpretive value of the  $g$  factors in these compounds appears to once again be suspect.

The angular variation of the linewidth at room temperature for the three crystals is shown in Figures 4.52 to 4.54. The behaviour is very similar to that discussed

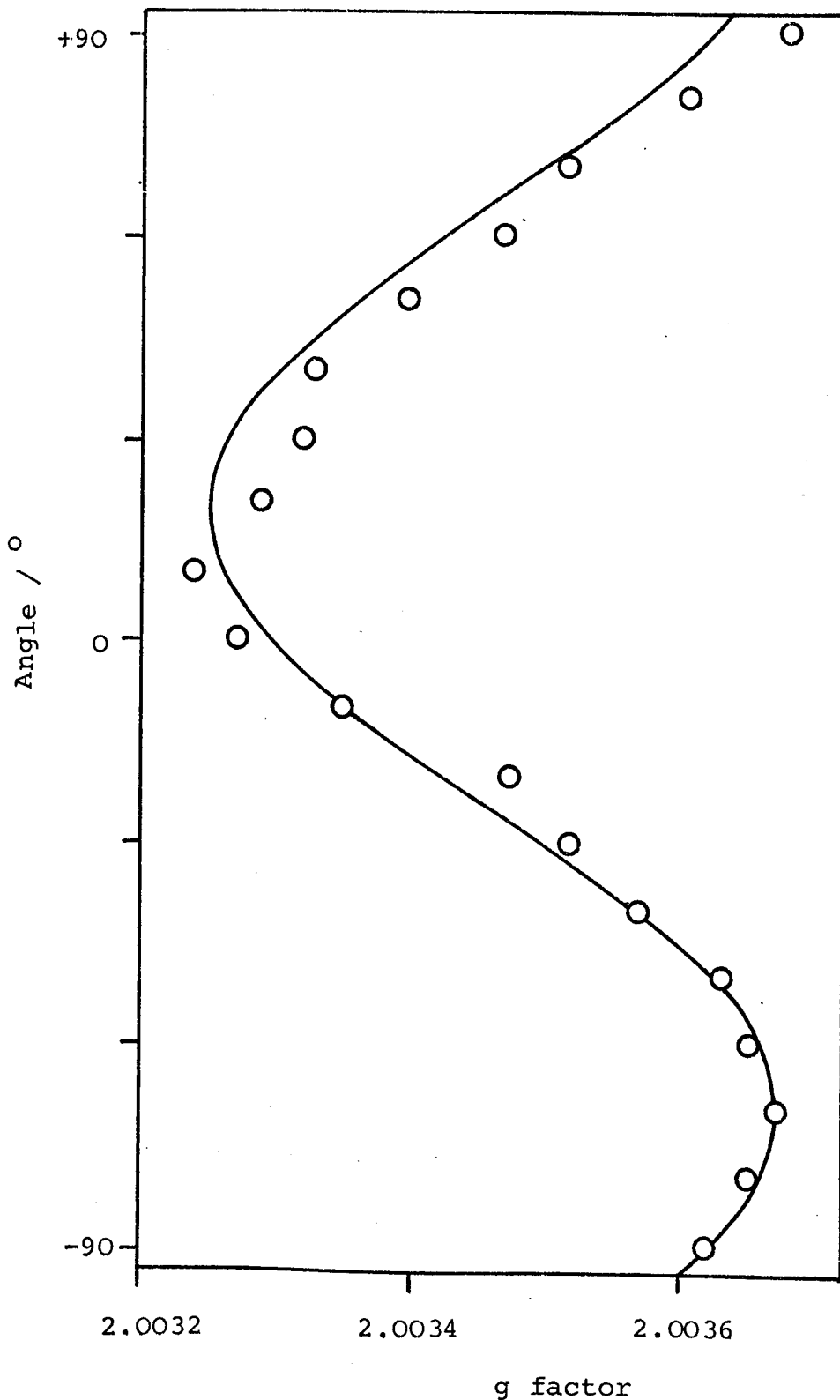


Figure 4.49

TPT(TCNQ)<sub>4</sub>

Angular variation of g factor at 300K  
for crystal 1.

Approximate orientations : H//y-axis at +20°.  
H//z-axis at -70°.

———— Computer simulation

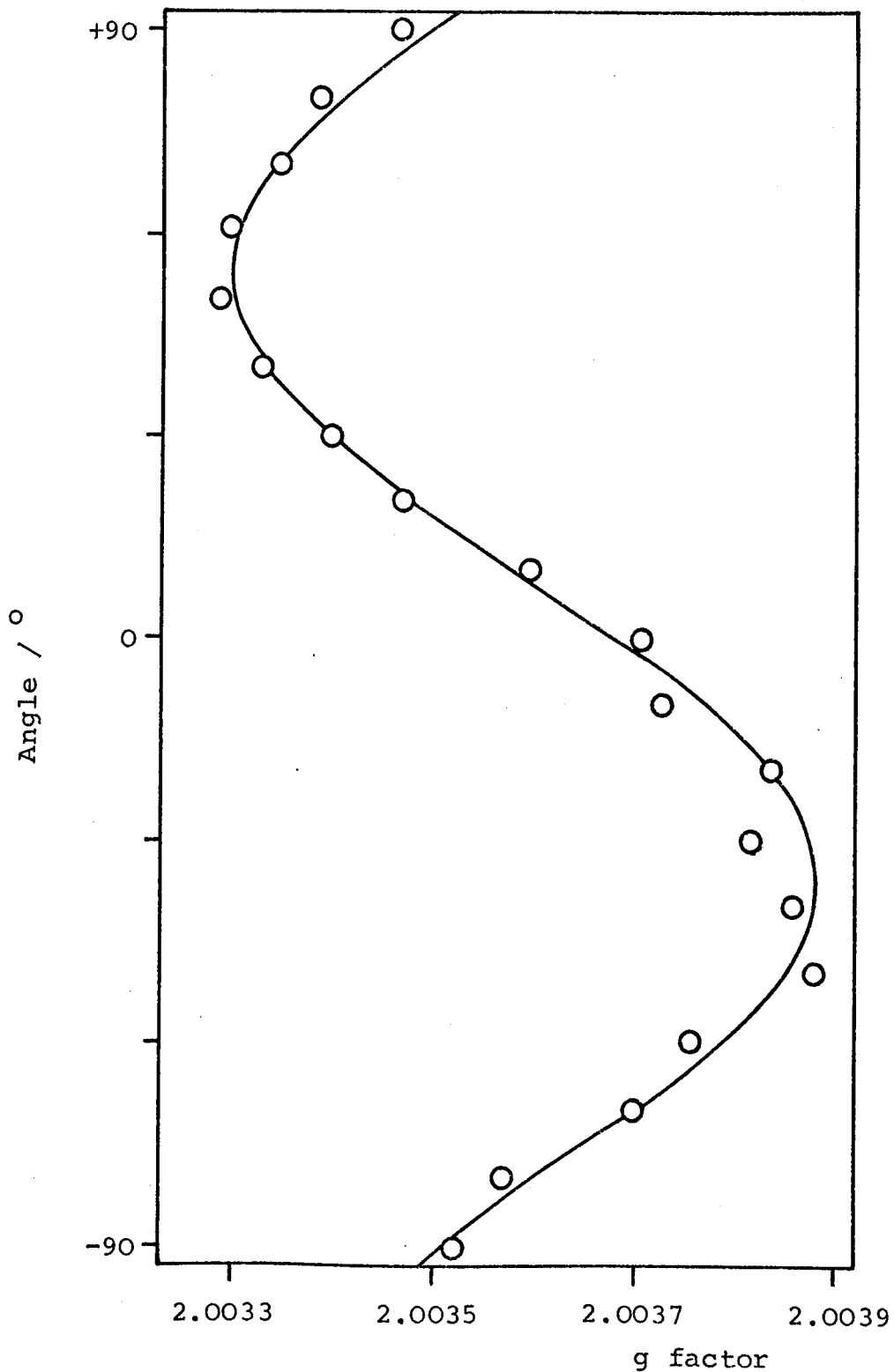


Figure 4.50

TPT(TCNQ)<sub>4</sub>

Angular variation of g factor at 300K  
for crystal 2.

Approximate orientations: H//x-axis at +54°.

H//z; axis at -36°.

———— Computer simulation.

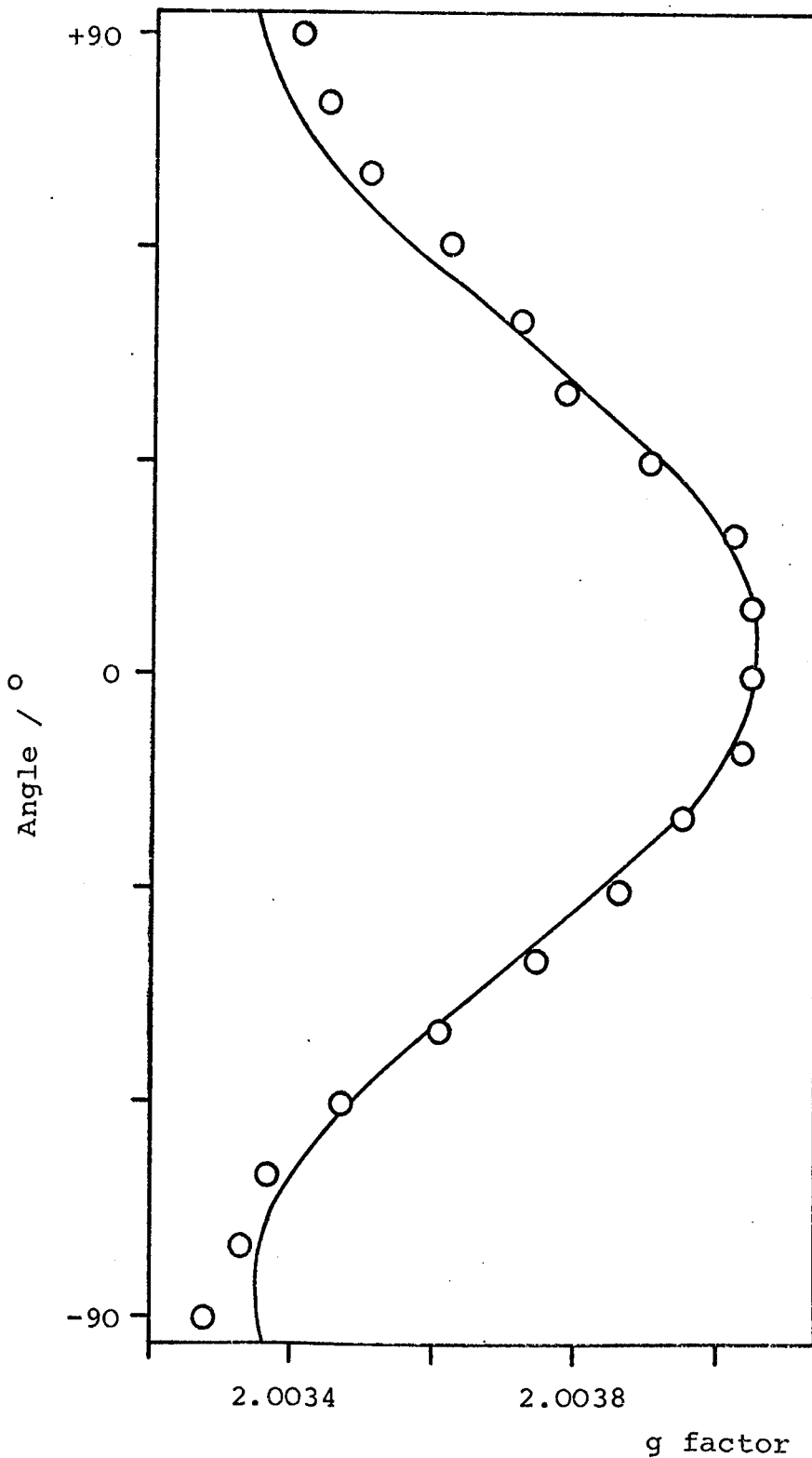


Figure 4.51

TPT(TCNQ)<sub>4</sub>

Angular variation of g factor at 300K  
for crystal 3.

Approximate orientations: H//x-axis at +4°.  
H//y-axis at -86°.

———— Computer simulation.

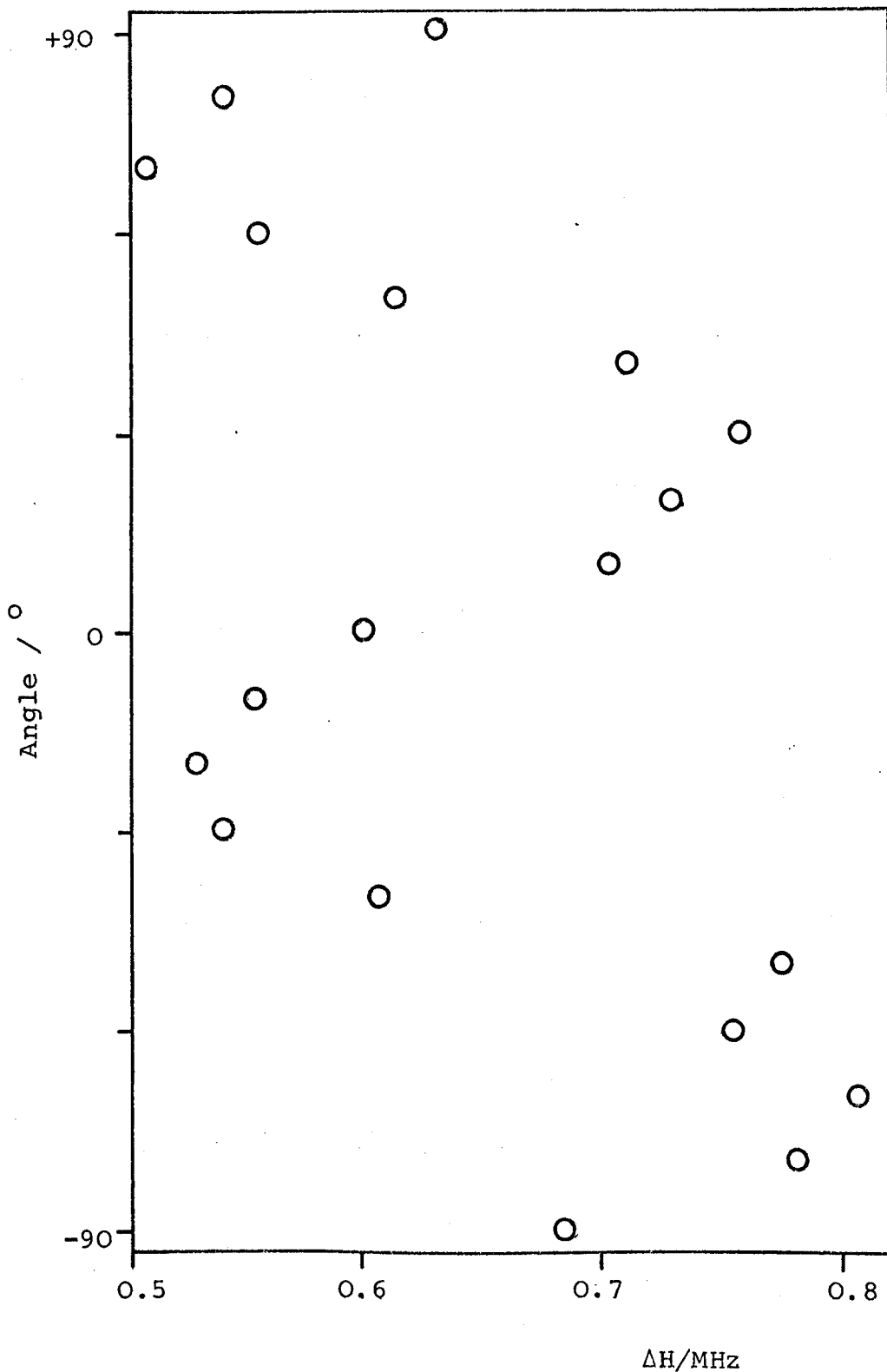


Figure 4.52

TPT(TCNQ)<sub>4</sub>

Angular variation of linewidth at 300K for crystal 1.

Approximate orientations as for Figure 4.49.

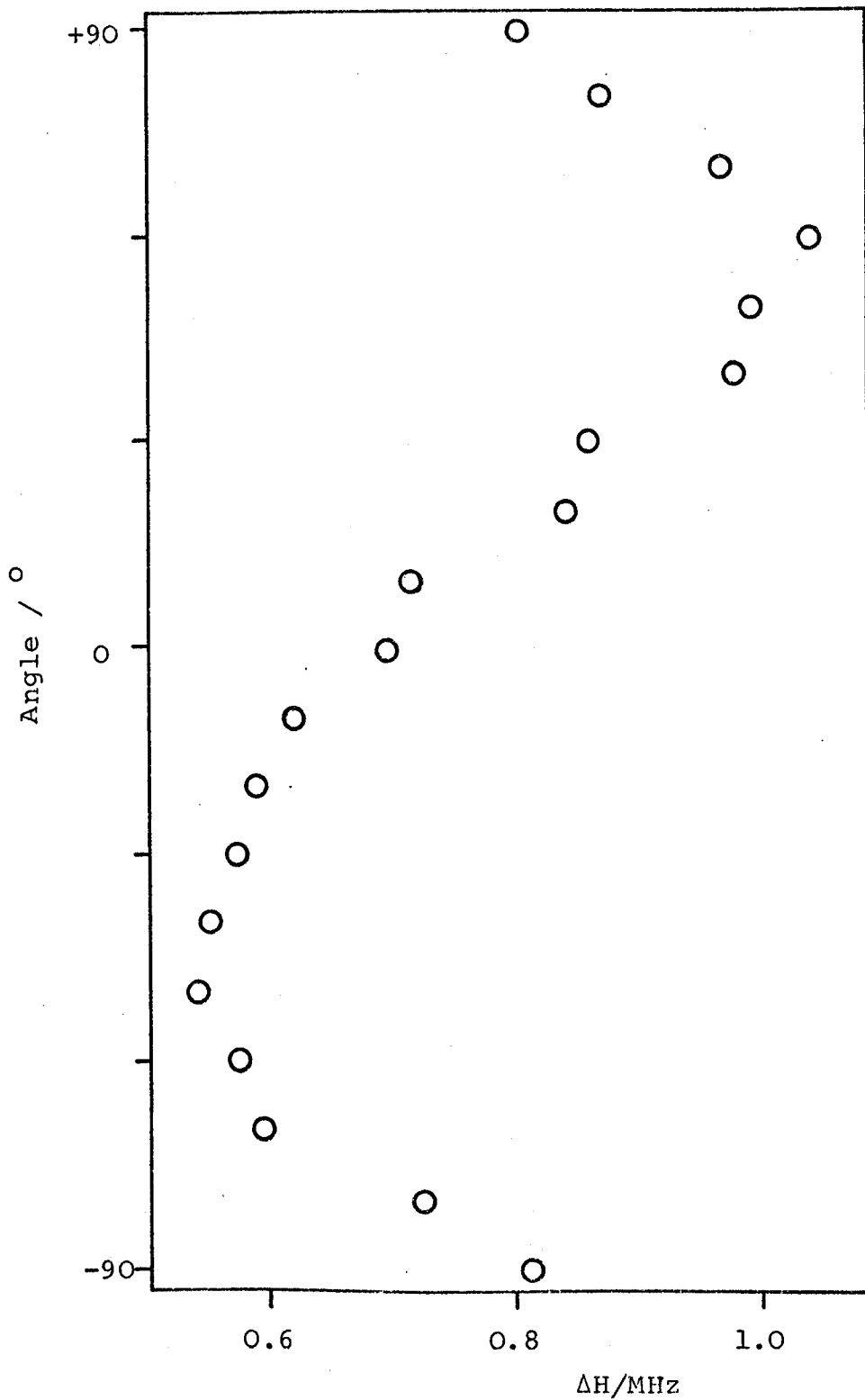


Figure 4.53

TPT(TCNQ)<sub>4</sub>

Angular variation of linewidth at 300K for crystal 2.

Approximate orientations as for Figure 4.50.

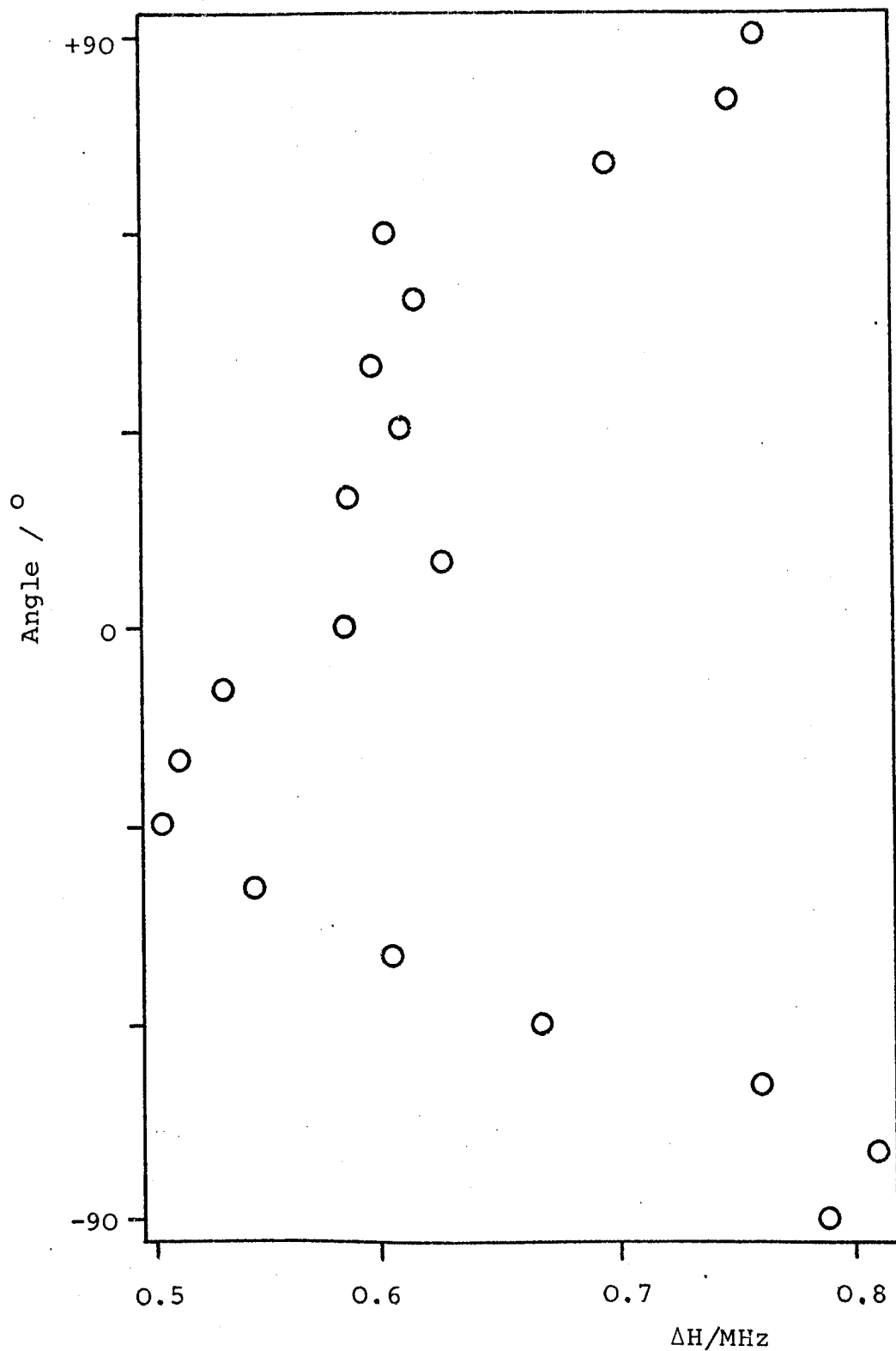


Figure 4.54

TPT(TCNQ)<sub>4</sub>

Angular variation of linewidth at 300K for crystal 3.

Approximate orientations as for Figure 4.51.

for DMPA(TCNQ)<sub>4</sub>(I) and suggests some degree of two-dimensionality in the xz plane for TPT(TCNQ)<sub>4</sub>, which is the plane containing only TCNQ molecules, although this is not reflected in the conductivity results.

The intensity of the e.s.r. signal also exhibited an unusual temperature dependence, shown in Figure 4.55. From the observation of a small activation energy for electrical conduction, the magnetic properties were also expected to show an energy gap in the excitation spectrum and a corresponding activated temperature dependence. However, all the crystals studied had essentially temperature independent intensities from 300K to approximately 100-120K. In all cases, the intensity showed a slight increase in the region 100 to 20K, manifesting itself as a small 'hump' in the intensity plots. Below 20K, the intensity increased rapidly with decreasing temperature indicative of the usual Curie law behaviour. This intensity variation could not be attributed to either singlet-triplet or Curie law behaviour, and log IT against  $1/T$  plots gave no meaningful results, merely reflecting the slope mathematically expected from a plot of log T against  $1/T$ , this being shown in Figure 4.56. The curvature at low temperatures gave an estimate of  $(6.8 \pm 3.0) \times 10^{22}$  spins  $\text{mol}^{-1}$  for the number of Curie species dominating the e.s.r. signal below 20K.

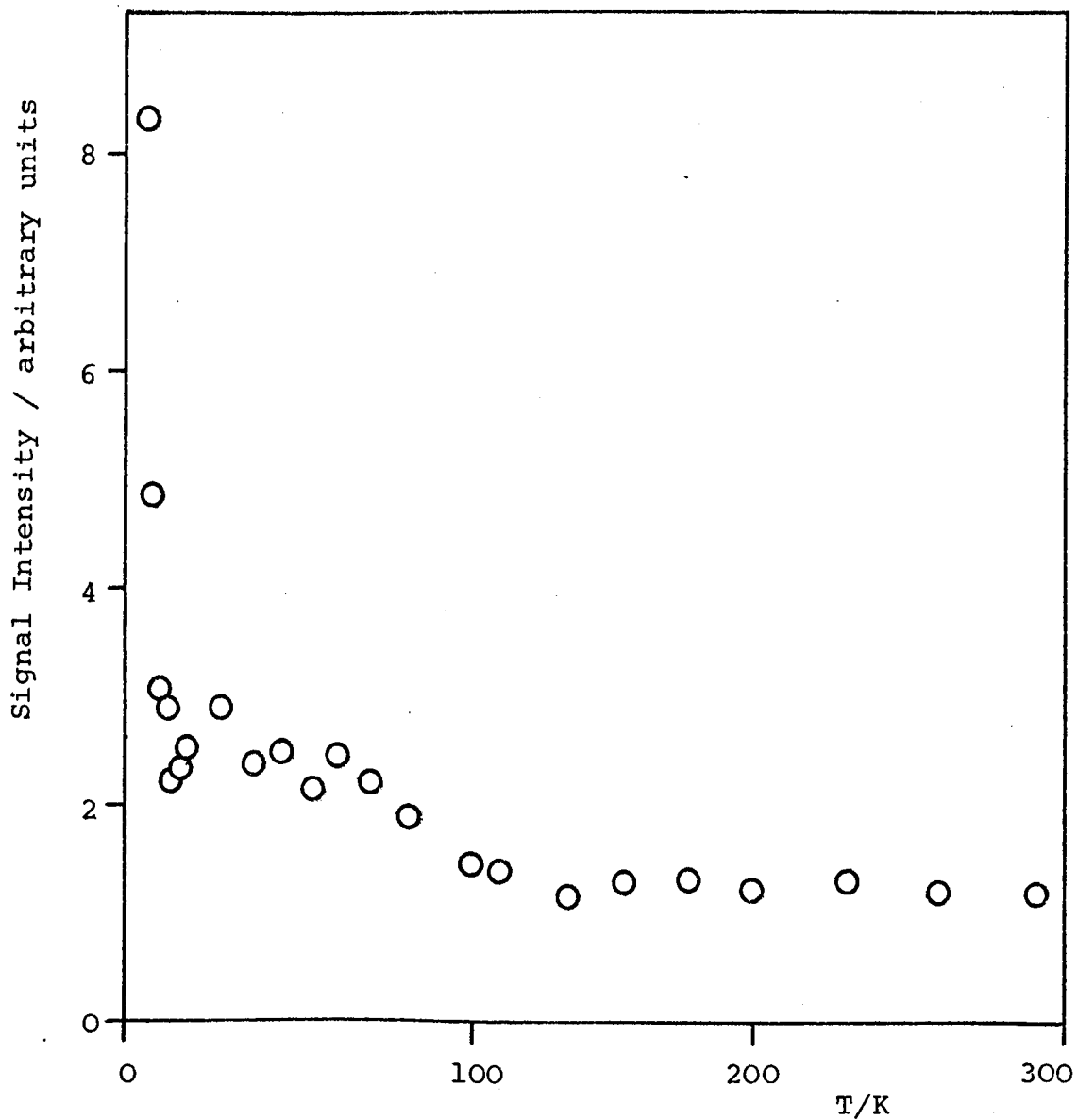


Figure 4.55

$\text{TPT}(\text{TCNQ})_4$

Plot of relative intensity against temperature  
for crystal 1.

H is approximately parallel to the z-axis.

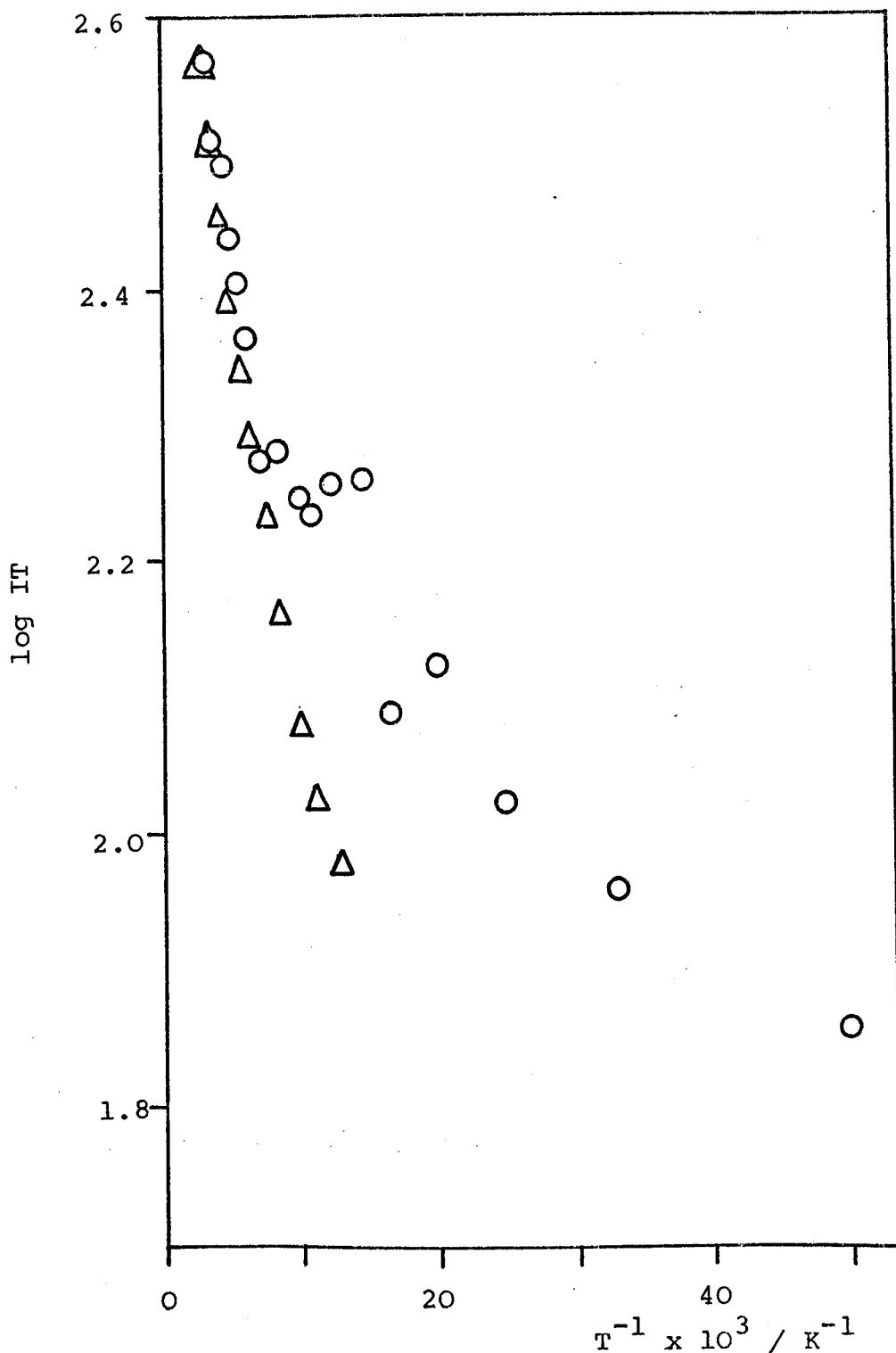


Figure 4.56

TPT(TCNQ)<sub>4</sub>

Semilog plot of the product of the relative intensity and temperature against reciprocal temperature for crystal 1.

H is approximately parallel to the z-axis.

○ Experimental points of  $\log IT$ .

△ Calculated points of  $\log T$  normalised to the room temperature experimental value.

High temperature equipment, described in section 3.2.1(iii), was used to investigate whether the intensity remained constant above 300K. The intensity did, in fact, continue to be temperature independent up to 340K, the maximum temperature available. Therefore, it appeared that  $\text{TPT}(\text{TCNQ})_4$  exhibited the behaviour of Pauli paramagnetism characteristic of metallic systems. This is consistent with the lack of any observable correlation between the electrons and also the observed semi-metallic d.c. conductivity.

Just as the impurities in semiconductors produce energy states in the normally forbidden band gap close to the valence or conduction bands, disorder in TCNQ complex salts also causes this phenomenon, known as band-tailing. This is most commonly found in amorphous solids<sup>180,181</sup>, but a crystal exhibiting a high degree of disorder will produce many states in the band gap and, if sufficient, a merging of the excitation spectrum results with the possibility of metal-like transport properties<sup>180</sup>. This could indeed adequately explain the observed high conductivity, the apparent Pauli paramagnetism and the difficulty encountered in the crystal structure determination. Therefore, the effect of disorder on the energy states forms the basis for a model to explain the physical properties of this complex salt.

Interpretation of the magnetic behaviour of many

other metallic TCNQ complexes has been complicated by the existence of two potentially conducting chains, as for example in TTF-TCNQ. However, a similar shape to that shown in Figure 4.55 for the temperature dependence of the paramagnetism has been observed for the organic metal quinolinium(Qn)-(TCNQ)<sub>2</sub><sup>182</sup>. The interpretation of the behaviour regarded the susceptibility as the sum of two terms. Firstly, there is a contribution from unpaired electrons situated at chain-ends, which gives rise to a Curie temperature dependence, and secondly, an inherent susceptibility arising from singlet-triplet behaviour for which there is a spread of J values. The existence of a band gap was indicated by the small activation energy for conduction observed and, for small band gaps, the effect of disorder is enhanced, therefore producing the spread of J values. However, this treatment predicts a small minimum in intensity in the temperature region where, in fact, a broad maximum was observed for TPT(TCNQ)<sub>4</sub>. The slight increase in intensity between 100 and 20K would be expected from the effect of the Curie signal superimposed on the constant Pauli paramagnetism, rather than on the decreasing paramagnetism exhibited by triplet species.

The interpretation proposed for Qn(TCNQ)<sub>2</sub> also considers disorder as the basis for the model, but does not attribute the magnetic behaviour to Pauli paramagnetism. Therefore, the situation for TPT(TCNQ)<sub>4</sub> is unclear, although

it is considered that Pauli paramagnetism is likely, and the small activation energy for conduction could possibly arise from interruptions in the conduction pathway, which form metallic strands similar to those proposed by Zuse and Keller<sup>183</sup>.

The room temperature susceptibility of  $\text{TPT}(\text{TCNQ})_4$  was found to be  $(1.1 \pm 0.2) \times 10^{-3} \text{ e.m.u. cm}^3 \text{ mol}^{-1}$ . Assuming the intensity behaviour can be attributed to Pauli paramagnetism, equation 2.12 can be used to calculate a value for the density of states at the Fermi level. Such a calculation for this complex salt gave a value of  $17 \pm 3$  per eV per  $\text{TPT}(\text{TCNQ})_4$  unit. This corresponds to  $6 \pm 1$  states per eV per  $(\text{TCNQ})_{1.3}^-$  unit, which is similar to the values obtained for  $\text{Qn}(\text{TCNQ})_2$  which lie in the range 2.3 to 24 states per eV per  $(\text{TCNQ})_2^-$  unit<sup>24,100,184,185</sup>.

The linewidth variation with temperature is shown in Figure 4.57 for two orientations of  $\text{TPT}(\text{TCNQ})_4$ . For all the crystals studied, a decrease in linewidth from room temperature to 100-12K was observed, followed by a continued decrease from 100K to approximately 40K. The linewidth then increased with further decrease in temperature, producing the minimum shown in Figure 4.57. Similar behaviour has been previously reported<sup>64,67</sup> for the metallic  $(\text{TTT})_2\text{I}_3$  and TTF-TNAP. In both cases, a sudden change in linewidth was observed, which was

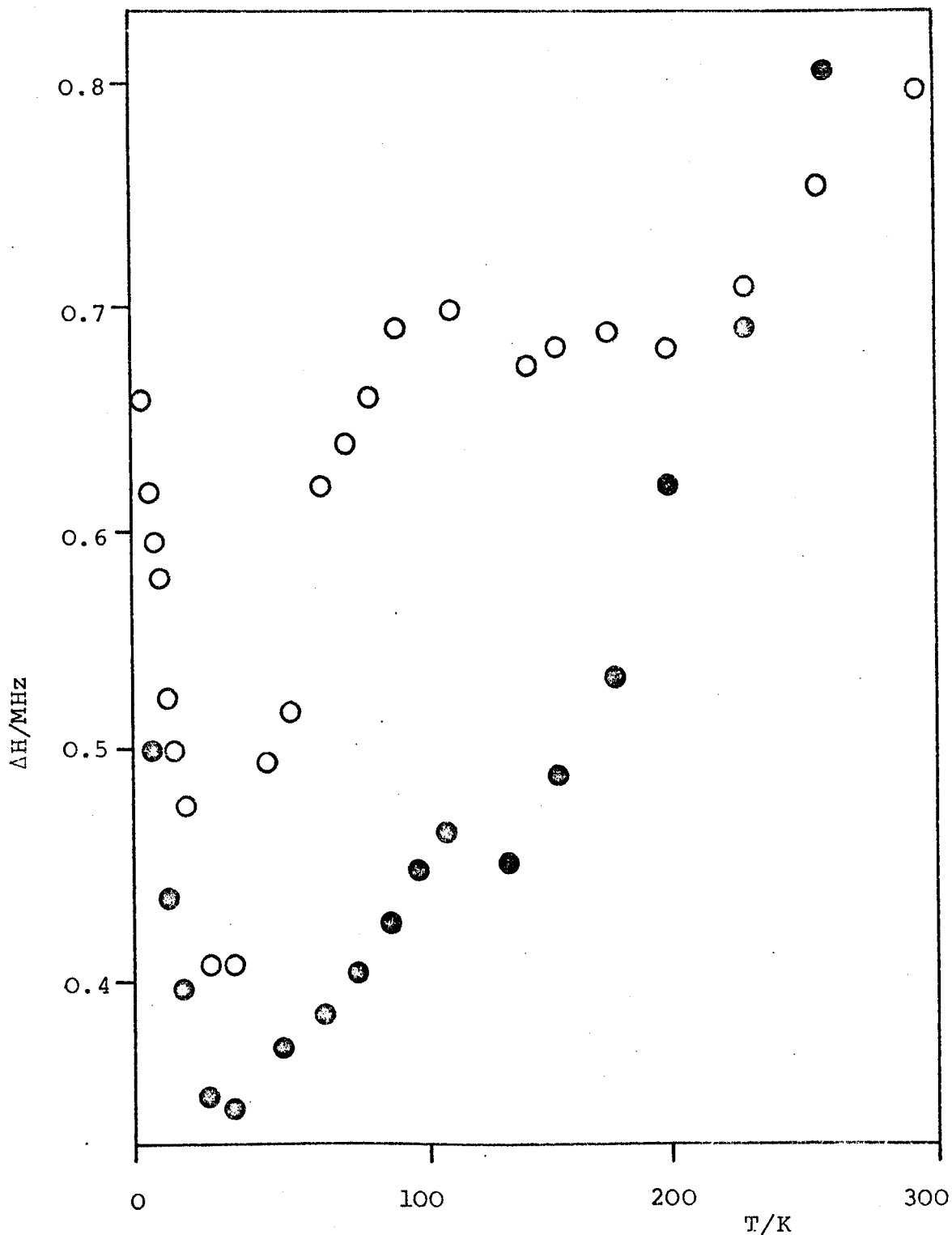


Figure 4.57

TPT(TCNQ)<sub>4</sub>

Plot of linewidth against temperature for two orientations.

- For crystal 1, H approximately parallel to the z-axis.
- For crystal 2, H approximately parallel to the x-axis.

accompanied by a change in conductivity and susceptibility, and interpreted in terms of a phase transition at the temperature involved. Such a phase transition is feasible in  $\text{TPT}(\text{TCNQ})_4$ , although its nature is somewhat obscure, and is consistent with the apparent change in the intensity at approximately 100K observed for all the crystals studied.

The Bloch equations predict Lorentzian lineshapes for a homogeneous spin system in which the relaxation is controlled by spin-lattice interactions, and Figures 4.58 to 4.60 show the lineshape to be Lorentzian throughout the temperature range studied. Indeed, relaxation studies, the results of which are given in Figures 4.61 and 4.62, show the spin-lattice relaxation time to dominate the behaviour of the observed linewidths.

The two most commonly discussed mechanisms for spin-lattice relaxation include a direct process, whereby the spins exchange quanta of energy with lattice modes having the same frequency as the spin resonance frequency, and an indirect process, whereby a spin interacts simultaneously with two lattice modes whose difference frequency is the spin resonance frequency. Although the latter mechanism is a second order and less probable process than the direct process, the number of different combinations of frequency satisfying the necessary resonance condition is very large and, therefore, dominates at

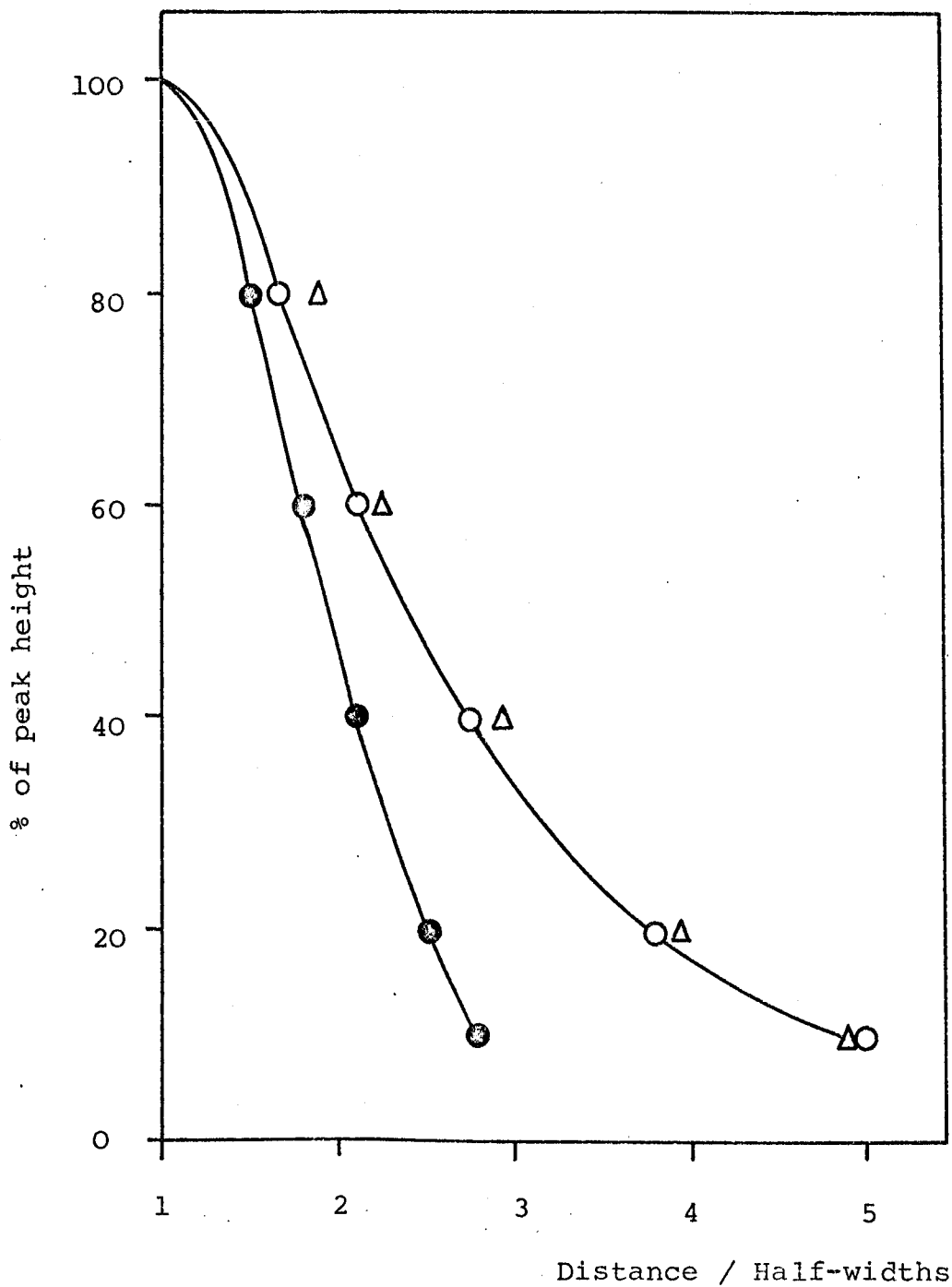


Figure 4.58

TPT(TCNQ)<sub>4</sub>

Lineshape analysis for crystal 3 at 10K.  
H is approximately parallel to the y-axis.

- Gaussian lineshape
- Lorentzian lineshape
- △ Average shape for crystal.

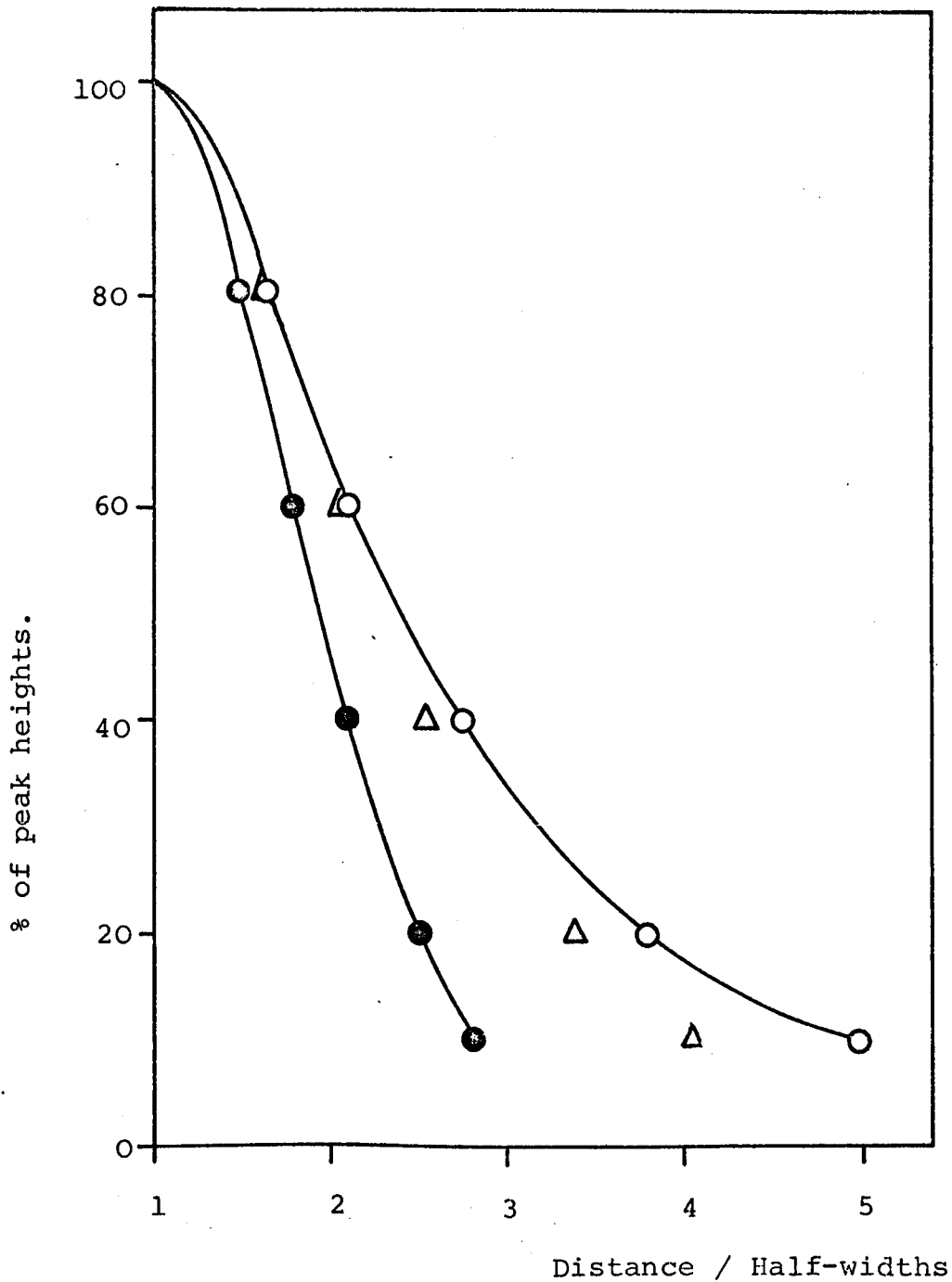


Figure 4.59

TPT(TCNQ)<sub>4</sub>

Lineshape analysis for crystal 3 at 80K.  
H is approximately parallel to the y-axis.

- Gaussian lineshape.
- Lorentzian lineshape.
- △ Average shape for crystal.

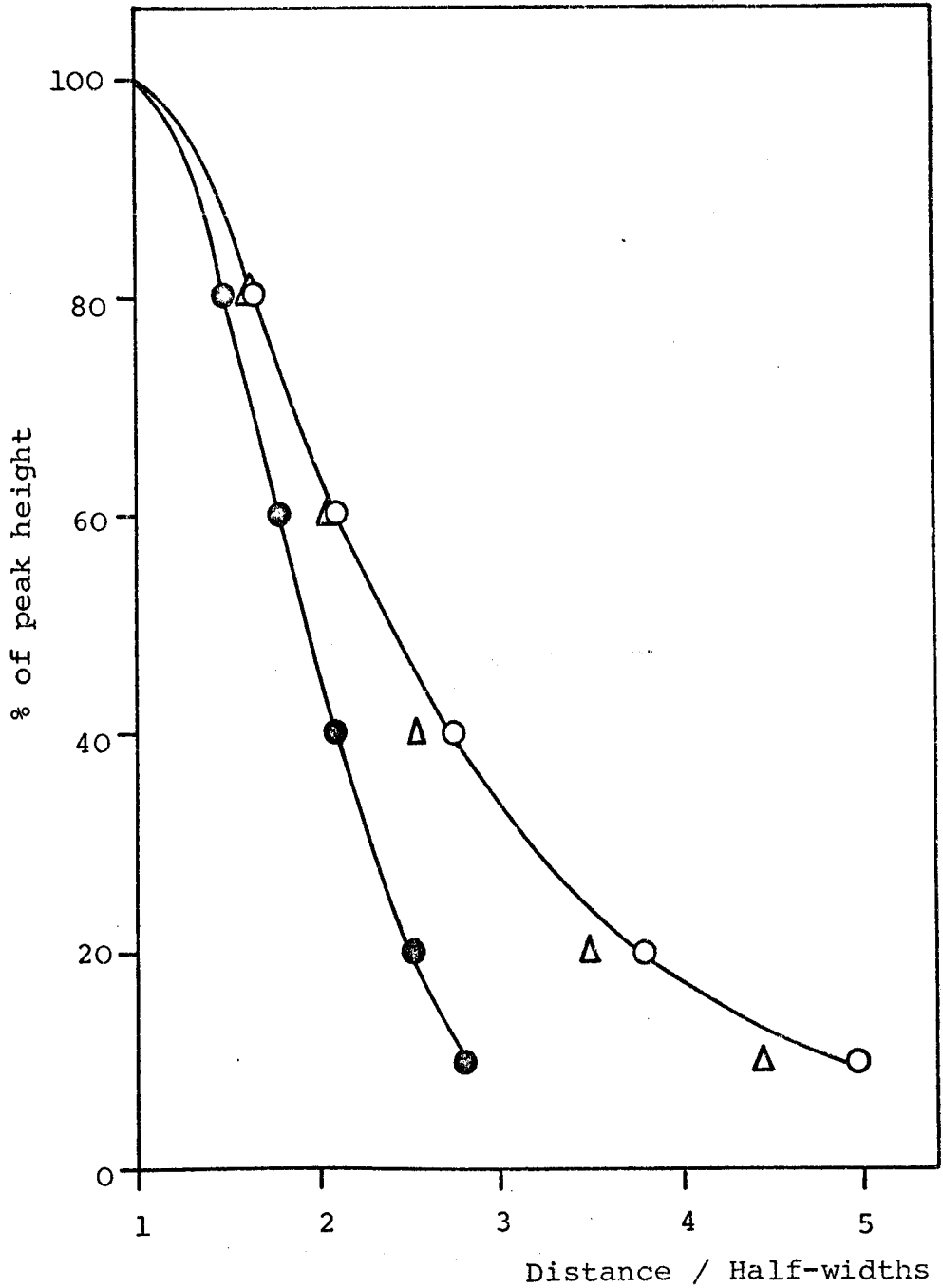


Figure 4.60

TPT(TCNQ)<sub>4</sub>

Lineshape analysis for crystal 3 at 200K.

H is approximately parallel to the y-axis.

●—● Gaussian lineshape.

○—○ Lorentzian lineshape.

△ Average shape for crystal.

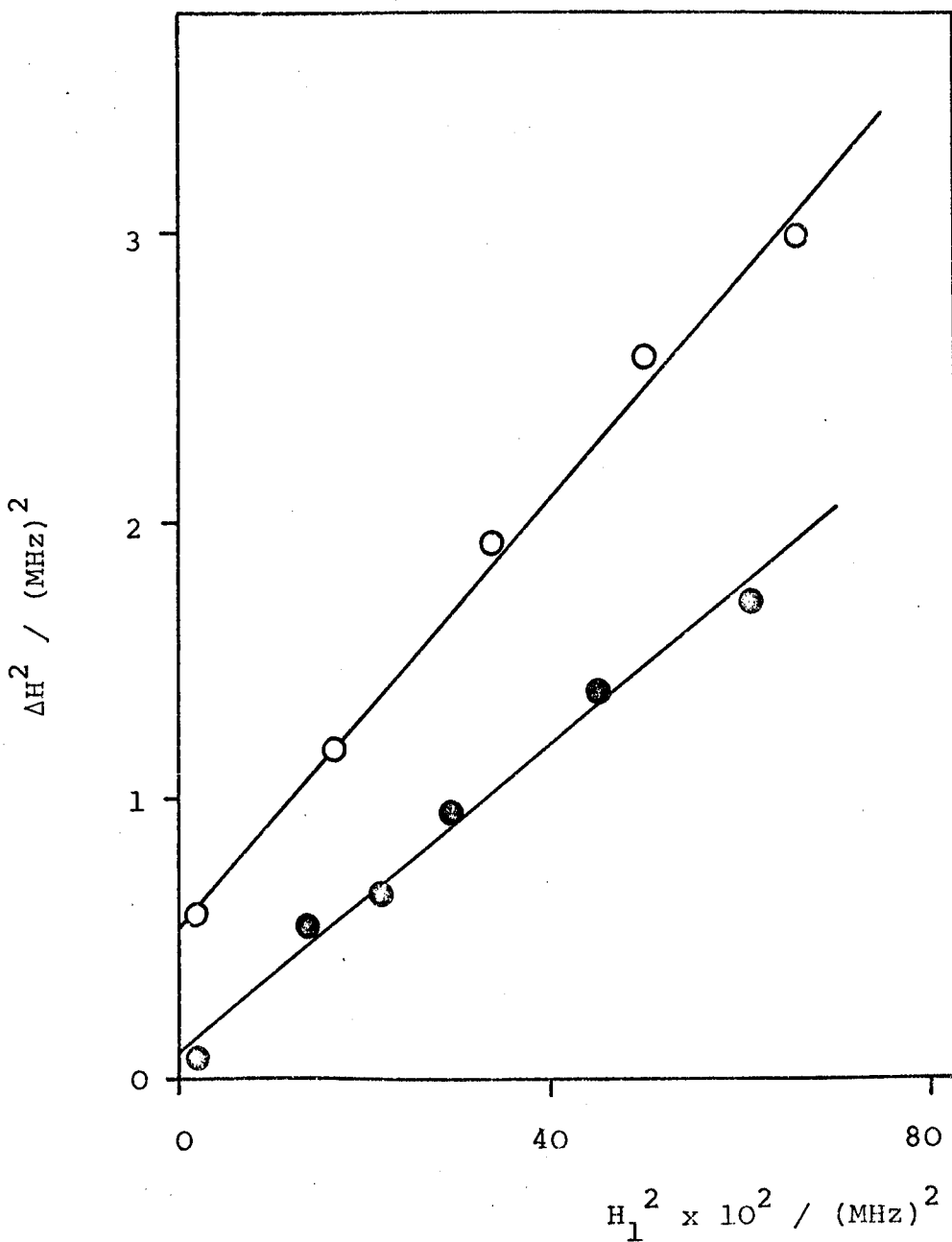


Figure 4.61

TPT (TCNQ)<sub>4</sub>

Plot of the square of the linewidth against the square of the microwave magnetic field strength for crystal 3 at two temperatures.

H is approximately parallel to the y-axis.

○ 300K , ● 40K.

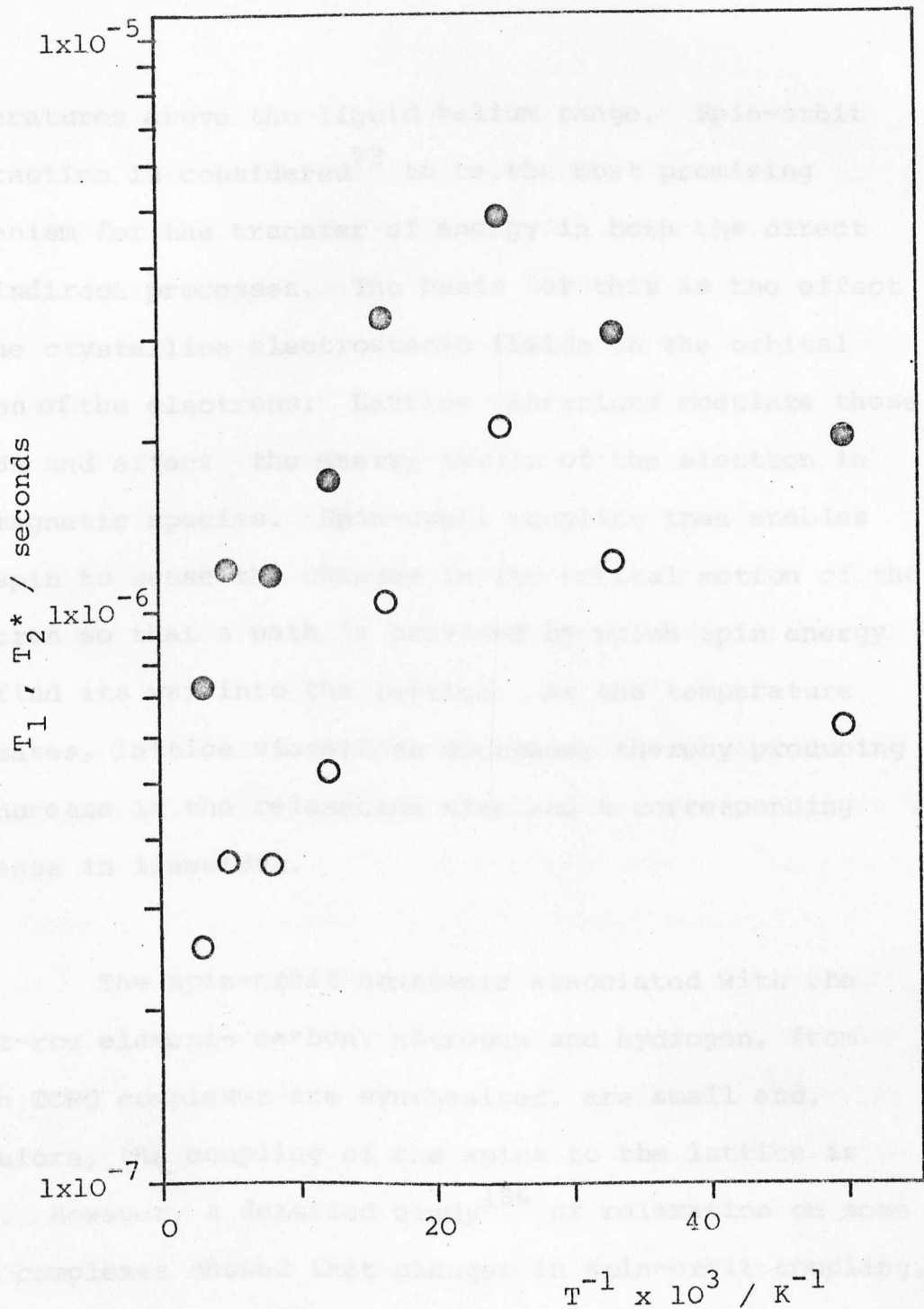


Figure 4.62

TPT(TCNQ)<sub>4</sub>

Semilog plot of  $T_1$  and  $T_2^*$  against reciprocal temperature for crystal 3.

H is approximately parallel to the y-axis.

•  $T_1$  , o  $T_2^*$ .

temperatures above the liquid helium range. Spin-orbit interaction is considered<sup>93</sup> to be the most promising mechanism for the transfer of energy in both the direct and indirect processes. The basis for this is the effect of the crystalline electrostatic fields on the orbital motion of the electrons. Lattice vibrations modulate these fields and affect the energy levels of the electron in paramagnetic species. Spin-orbit coupling then enables the spin to sense the changes in the orbital motion of the electron so that a path is provided by which spin energy can find its way into the lattice. As the temperature decreases, lattice vibrations decrease, thereby producing an increase in the relaxation time and a corresponding decrease in linewidth.

The spin-orbit constants associated with the first-row elements carbon, nitrogen and hydrogen, from which TCNQ complexes are synthesised, are small and, therefore, the coupling of the spins to the lattice is weak. However, a detailed study<sup>186</sup> of relaxation on some TCNQ complexes showed that changes in spin-orbit coupling, produced by changing the cation, resulted in changes in linewidth and linewidth anisotropy. From their results, the authors proposed a mechanism, earlier suggested by Epstein et al<sup>41</sup>, by which spin-orbit interaction can affect the linewidth in these compounds. They suggested a combination of spin-orbit interaction and electron-phonon

interaction, the latter playing a major role in the spin relaxation. The differences in linewidth behaviour exhibited within this family of organic compounds can, therefore, be interpreted in terms of the differences in electron-phonon coupling. The electrons are scattered by lattice phonons, and any scattering mechanism present whereby spins can exchange energy with lattice modes will increase the relaxation process. As temperature is increased, the effects of scattering are increased, which results in a decrease in  $T_1$  and an increase in linewidth.

For the case of  $TPT(TCNQ)_4$ , the high degree of disorder present within the crystal would be expected to result in greater scattering of the electrons. Therefore, the mechanism discussed above could indeed explain the linewidth behaviour in the temperature region 300 to 40K. Below this temperature, the increase in linewidth can be attributed to the effect of the Curie signal which begins to dominate at these low temperatures. It is interesting to note that the  $T_1$  temperature dependence shows a change at 120K also. This is consistent with a possible phase transition in this temperature region, which might be expected to produce such a change.

In conclusion, this complex salt has proved to be most intriguing and outlines the complexity of the interactions and resulting complications to be encountered

in the study of TCNQ complex salts. The mode of packing in these crystals obviously has a large part to play in determining the magnetic properties of these compounds, and it would be of enormous interest to investigate other complex salts having trivalent cations of differing types and sizes, to establish whether the high degree of disorder in  $\text{TPT}(\text{TCNQ})_4$  is a direct result of a particular property associated with this cation. With regard to a possible phase transition, the magnetic results on their own provide no conclusive evidence, and any definite conclusions must await more extensive conductivity investigations at low temperatures and the results of the crystal structure analysis. This study provides a good illustration of the need for more than one type of technique for a complete interpretation of the physical properties of TCNQ complex salts.

CHAPTER 5

RESULTS AND DISCUSSION OF E.S.R. STUDIES  
OF TCNQ COMPLEX SALTS AVAILABLE ONLY IN  
POLYCRYSTALLINE FORM.

"Nothing exists except atoms and empty space;  
everything else is opinion."

Democritos

460-370 BC

### 5.1 DMPA(TCNQ)<sub>4</sub> (II)

The crystal phase of this complex salt has been discussed in section 4.2 and the magnetic properties were interpreted in terms of localised triplet excitons having a small interaction between each pair of unpaired electrons, in agreement with the crystal structure. Polycrystalline samples show distinct differences in the physical properties, exhibiting a higher d.c. conductivity than the crystal phase, although microanalysis and spectroscopic analysis confirmed the two phases were of the same stoichiometry. However, X-ray powder photographs indicated there was a crystallographic difference between the two forms, and this difference accounts for the differences in the electrical and magnetic results.

Two polycrystalline samples of DMPA(TCNQ)<sub>4</sub> (II) were studied, each sample being prepared for investigation as described in section 3.2.1(v). Both samples exhibited spectra of the shape illustrated in Figure 3.9, which is attributed to an axially symmetric g factor. On rotating sample 2 with respect to the static magnetic field, no change in the spectrum was observed. Therefore, the spectrum contained contributions from all possible orientations of the microcrystals, and values of  $g_{\parallel}$  and  $g_{\perp}$  could be obtained, these values being  $2.0042 \pm 0.0003$  and  $2.0031 \pm 0.0003$  respectively. It can be seen that these values are very similar to the g values obtained for the crystal phase of

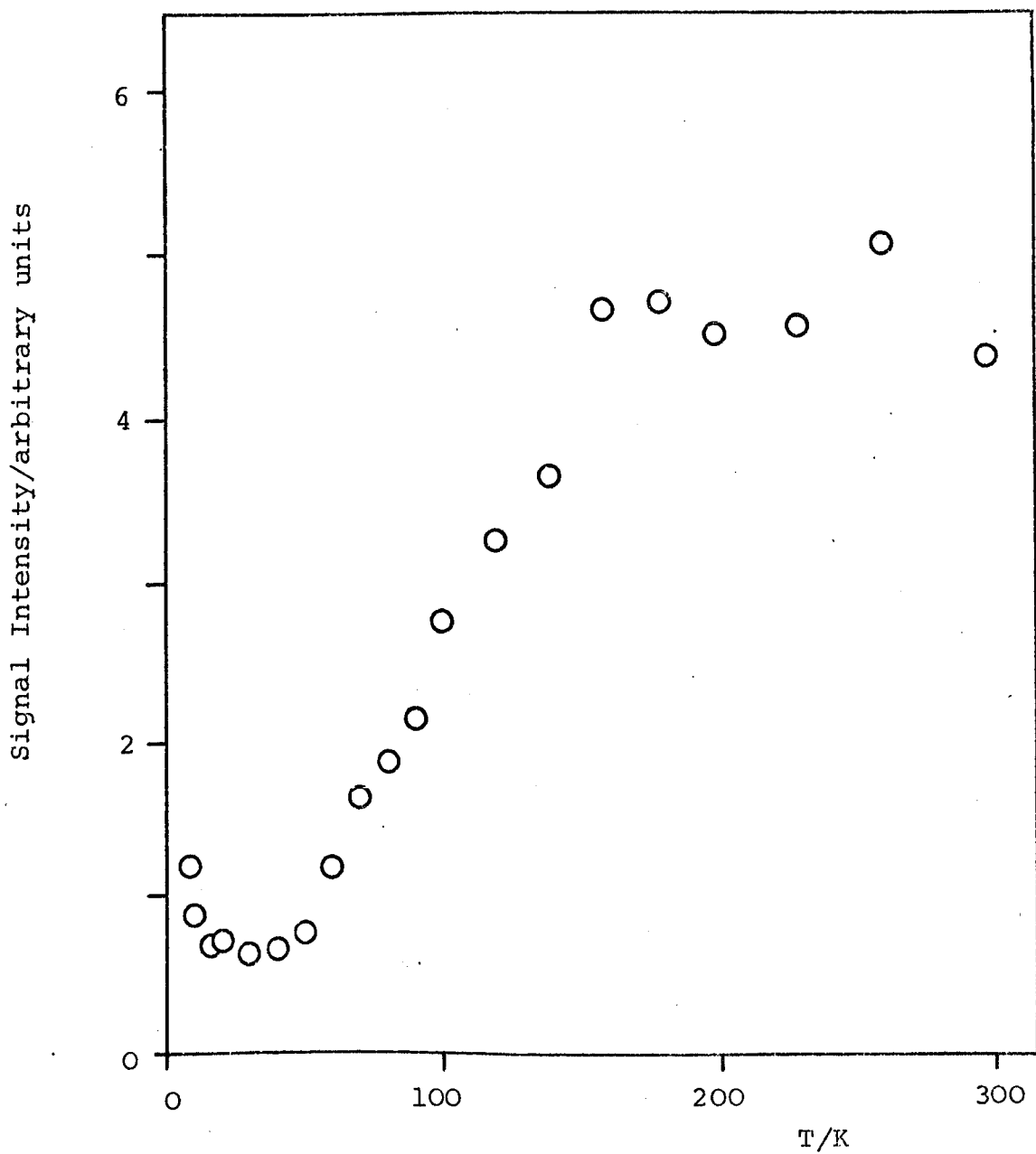


Figure 5.1  
DMPA(TCNQ)<sub>4</sub>(II)

Plot of relative intensity against temperature  
for sample 1.

this complex salt. The fact that  $g_{\perp}$  was found to be closer to the free electron  $g$  value indicates there is some degree of two-dimensionality within this phase of  $\text{DMPA}(\text{TCNQ})_4$ . It would be expected perhaps that the one-dimensionality of the TCNQ stack would result in a spectrum where the unique  $g$  factor would be the high field peak, and the low field peak would correspond to  $g_{\perp}$ , if the  $g$  factors do in fact reflect the electron delocalisation. Indeed, a polycrystalline sample of  $\text{K}(\text{TCNQ})$  was found to have a value of 2.0024 for  $g_{\parallel}$  and 2.0051 for  $g_{\perp}$ <sup>187</sup>. However, many other TCNQ complex salts<sup>127</sup> also exhibit spectra of the type shown in Figure 3.9 and this is usually interpreted as reflecting the delocalisation of the excitons in the two directions of the TCNQ sheet, with the unique  $g$  factor ( $g_{\parallel}$ ) corresponding to the direction perpendicular to the cation sheets.

Figure 5.1 shows the temperature dependence of the integrated e.s.r. intensity for this complex salt. It can be seen that the intensity is essentially constant in the temperature region 300 to 150K and, in fact, the  $Q$  of the cavity was markedly reduced to a value below 3,000, the usual value being between 3,000 and 4,000, and is typical of a highly conducting sample. However, below 150K there is a steady decrease in intensity indicative of singlet-triplet behaviour in a semiconducting complex salt, and the  $Q$  value was observed to increase. The results

obtained from this study were used to obtain the log IT against  $1/T$  plot shown in Figure 5.2. The average slope for both samples studied is equivalent to  $-1.7 \pm 0.1 \text{ kJ mol}^{-1}$ , and the room temperature susceptibility was found to be  $(1.4 \pm 0.3) \times 10^{-3} \text{ e.m.u. cm}^3 \text{ mol}^{-1}$ . Substituting a value of  $1.7 \text{ kJ mol}^{-1}$  for J in equation 2.26 for localised triplet states, yields a value of  $2.0 \times 10^{-3} \text{ e.m.u. cm}^3 \text{ mol}^{-1}$  for the room temperature susceptibility. The experimental value is smaller than predicted for localised triplet excitons and, therefore, suggests some degree of delocalisation of the excitons in  $\text{DMPA}(\text{TCNQ})_4$  (II). Consequently, Etemad's treatment was used to estimate the extent of this delocalisation, which is reflected in the values of  $\gamma$ ,  $a(\gamma)$  and  $\Delta(\gamma)$  calculated from the experimental results.

By extrapolating the linear slope obtained in Figure 5.2, it is possible to obtain an estimate of the intercept on the log IT axis expressed in units of susceptibility. From this estimation a value of  $0.7 \pm 0.1$  is obtained for  $a(\gamma)$  in equation 2.30. In order to use this to obtain a value of  $\gamma$  in Etemad's treatment, it is necessary to know the ratio of the absolute temperature T to the singlet-triplet energy gap J. However, since the slope of Figure 5.2 is equal to  $-J\Delta(\gamma)$ , the value of J is unknown. Therefore, Bulaevskii's treatment<sup>113</sup> must be used at this stage to obtain  $\gamma$ , which is found to be  $0.5 \pm 0.1$ . For the same reason, Bulaevskii's approach must also

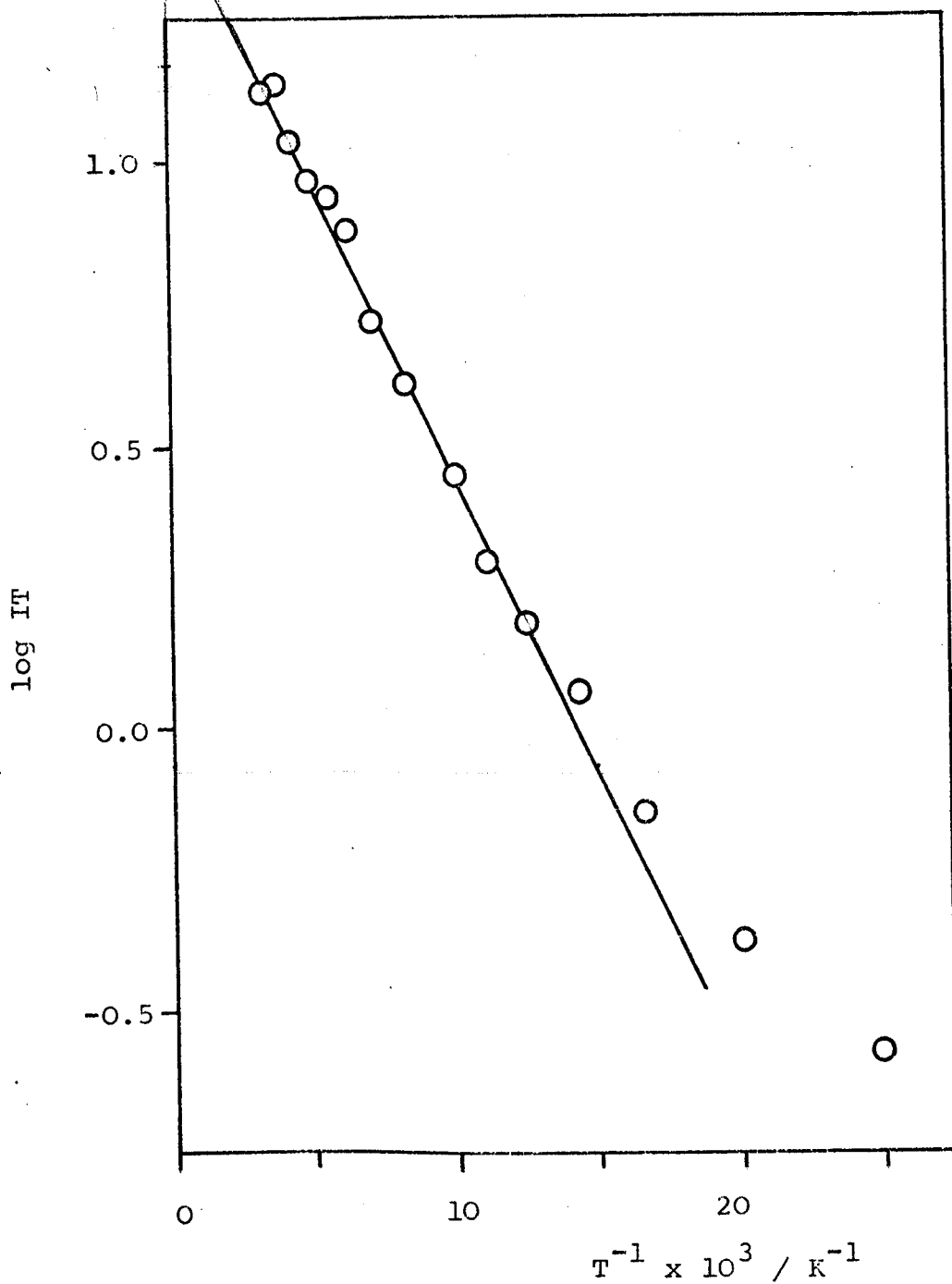


Figure 5.2

DMPA(TCNQ)<sub>4</sub> (II)

Semilog plot of the product of the relative intensity and temperature against reciprocal temperature for sample 1.

be used to obtain a value of  $0.8 \pm 0.1$  for  $\Delta(\gamma)$ . It is now possible to calculate the value for  $J$  and, consequently, the ratio  $T/J$  in the temperature range studied. Using the values of  $T/J$  values in the range of validity given in section 2.5.1, Etemad's treatment can then be used to obtain  $\gamma$  from  $a(\gamma)$ . By an iterative procedure through the calculations of  $\gamma$ ,  $\Delta(\gamma)$  and  $J$ , it is possible to obtain self-consistent estimates of these three parameters. Having found a final value for  $\gamma$ , the exciton bandwidth  $W$  can be obtained. Copies of the relevant graphs from Etemad's work for obtaining all these parameters are presented in Appendix 1.

Using the approach outlined above, values of  $0.5 \pm 0.1$ ,  $0.8 \pm 0.1$ ,  $2.1 \pm 0.3 \text{ kJ mol}^{-1}$  and  $1.3 \pm 0.2 \text{ kJ mol}^{-1}$  are obtained for  $\gamma$ ,  $\Delta(\gamma)$ ,  $J$  and  $W$  respectively. These calculations indicate that there is a triplet exciton band in  $\text{DMPA}(\text{TCNQ})_4$  (II) of width  $1.3 \pm 0.2 \text{ kJ mol}^{-1}$  centred at  $2.1 \pm 0.3 \text{ kJ mol}^{-1}$  above a singlet state. This gives an effective singlet-triplet energy gap of  $1.7 \text{ kJ mol}^{-1}$ , which is in excellent agreement with the value obtained from the slope of the  $\log IT$  against  $1/T$  plots.

Previous applications of this treatment have been supported by X-ray crystal structure determinations, where available, which show equal spacing between molecules in the stacking direction of complexes displaying weak alternation<sup>188</sup>. Although a crystal structure has not been

performed on this phase of DMPA(TCNQ)<sub>4</sub>, because of the lack of single crystals, the interpretation of the magnetic behaviour is consistent with the electrical properties, which are also interpreted in terms of a band model<sup>126</sup>. Also, no dipolar splitting was observed throughout the entire temperature range studied, in agreement with a delocalised model.

As sample 1 was cooled below 40K, the spectral shape shown in Figure 3.9 gradually changed into an almost symmetrical signal. Consequently, the intensity variation of this signal could be investigated using the oscilloscope technique described in section 3.2.2(vi). Figure 5.3 shows a typical example of a series of results obtained using this method in the form of reciprocal relative intensity against temperature. The linear relationship observed shows this signal arises from species obeying the Curie law and, as previously mentioned, these are considered to result from defects in the lattice and chain ends. From the slope of a number of plots, a value of  $(5.2 \pm 1.1) \times 10^{21}$  spins mol<sup>-1</sup> was obtained for the number of Curie species per mole of sample. The deviation of the high temperature points from a linear relationship (Figure 5.3) is the result of a gradual population of the triplet state, just as the curvature at low temperatures in Figure 5.2 results from a significant contribution to the signal intensity from the Curie species. From the extrapolated limit of this

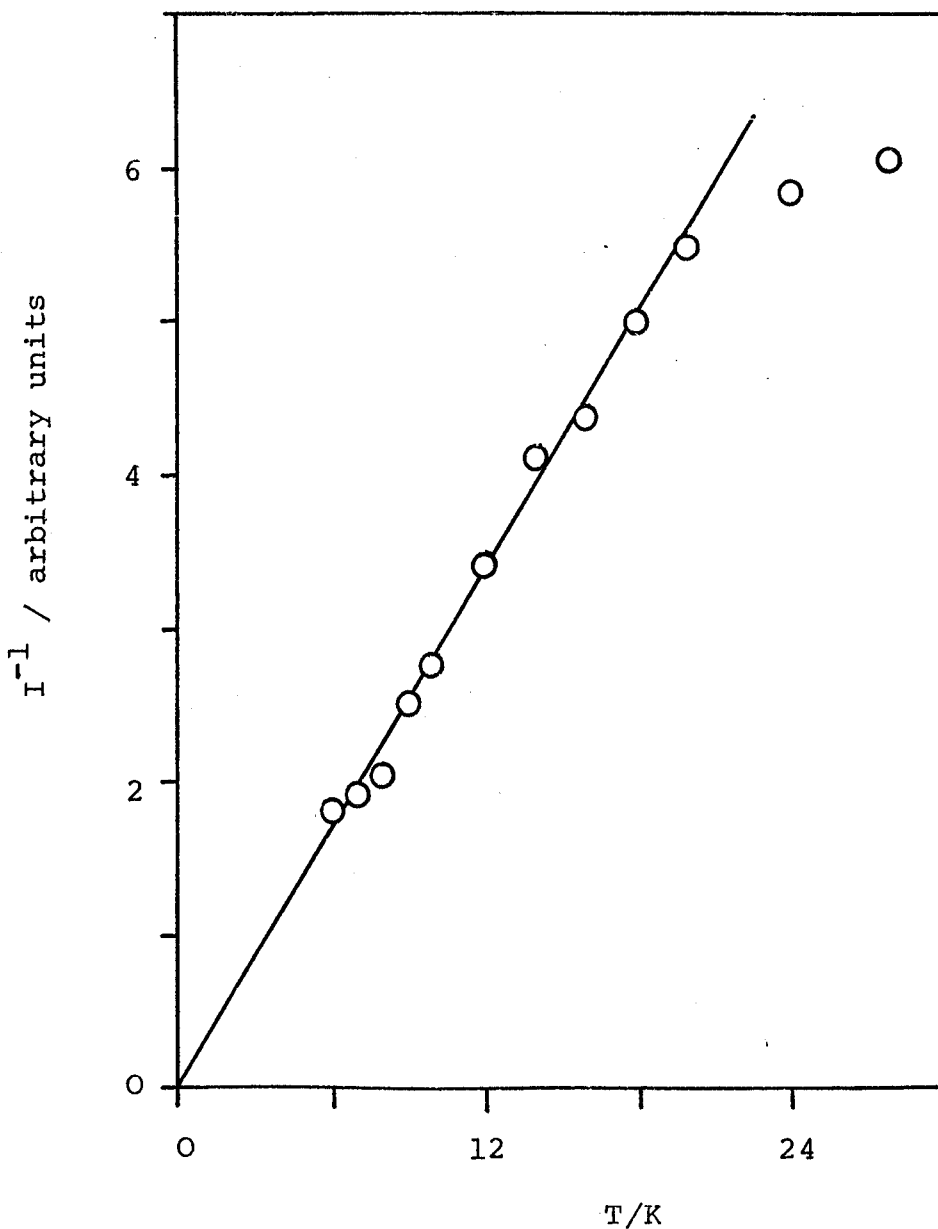


Figure 5.3

$\text{DMPA}(\text{TCNQ})_4$  (II)

Plot of the reciprocal relative intensity (obtained from oscilloscope measurements) against temperature for sample 1.

low temperature curvature, and using the room temperature molar susceptibility value, a value of  $(5.3 \pm 1.9) \times 10^{21}$  spins  $\text{mol}^{-1}$  is calculated for the number of such species, which is in excellent agreement with the value obtained using the oscilloscope technique.

From 300 to 150K the separation of the peaks coincident with  $g_{\parallel}$  and  $g_{\perp}$  for sample 2 remained constant. However, below 150K this separation increased with decreasing temperature. A g factor study was performed at 80K but was not accurate enough to distinguish any change in the g factors. This peak separation behaviour is shown in Figure 5.4, error bars also being shown at each end of the temperature scale, although the error in all the points is  $\pm 2\%$ . It is interesting to note that the temperature at which this increase in peak separation begins is the same temperature at which a maximum in intensity is observed (Figure 5.1).

Similar observations to this have been reported<sup>142,189</sup> and two explanations emerged. Firstly, hopping of an exciton between crystallographically inequivalent chains in the lattice was proposed and, secondly, the effect was explained in terms of motional averaging of the g factors as a result of exciton migration from one crystallite to another. The latter explanation would seem more reasonable in the case of  $\text{DMPA}(\text{TCNQ})_4$  (II) because the TCNQ chains are generally

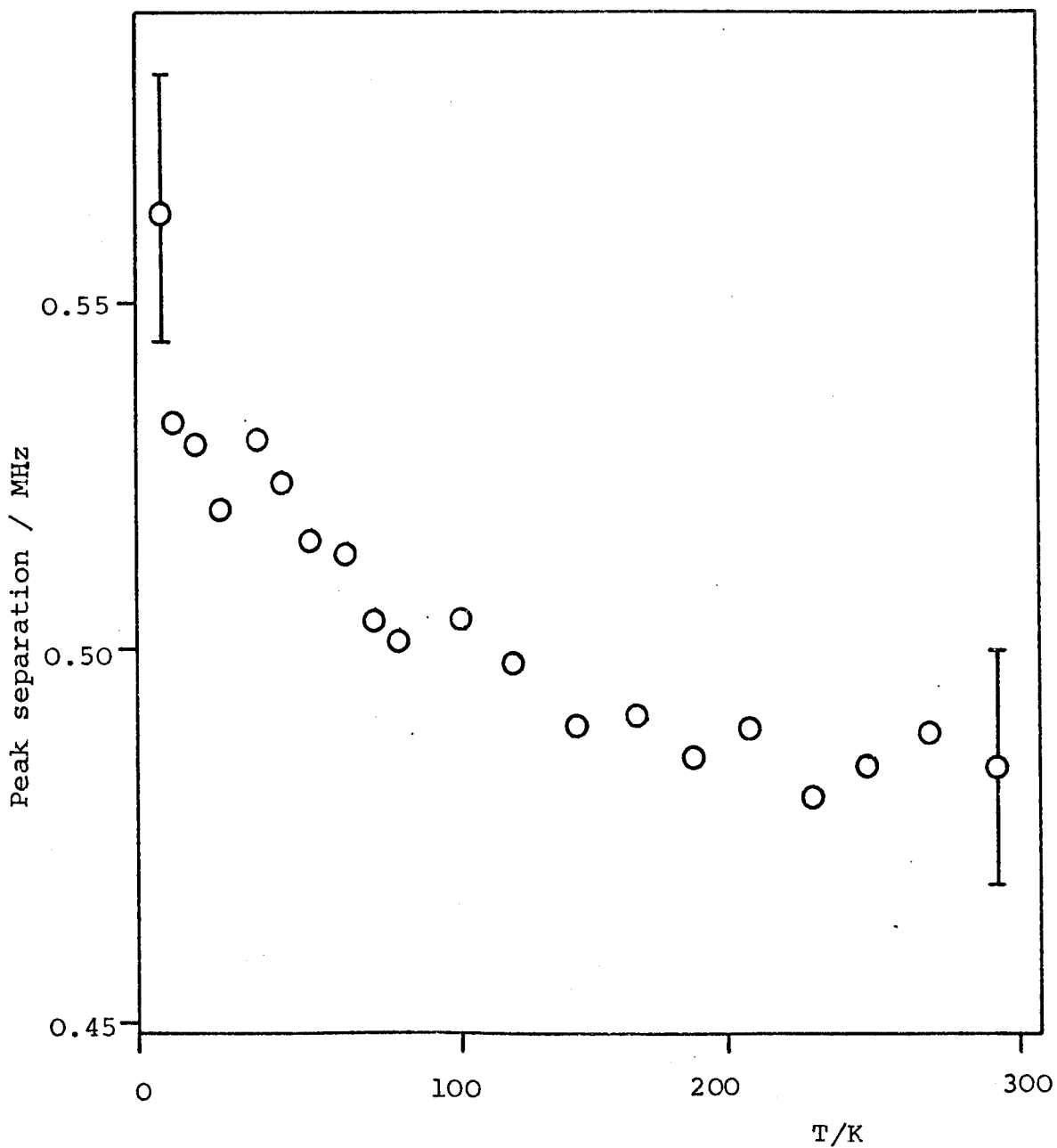


Figure 5.4

DMPA(TCNQ)<sub>4</sub>(II)

Plot of the peak separation against temperature  
for sample 2.

known to be equivalent in these complex salts, as shown by the reported crystal structures for these compounds<sup>150,170,190</sup>. Although separation of the crystallites has been found<sup>127</sup> not to remove this behaviour, this explanation is nevertheless still considered possible. Many of the crystallites exist in 'clumps' consisting of several microcrystals attached to each other, and the observation of an activation energy could certainly result from migration of excitons from one portion of the crystallite to another across the interface. This proposal for intracrystallite migration has been considered<sup>127</sup> as inconsistent with the existence of an exciton band, since such migration should be non-activated. However, the interface between adjoining crystallites represents an interruption in the band and an activation energy is, therefore, not surprising.

The appropriate equation to describe such behaviour would be equation 2.44, in which  $d_0$  would represent the limiting peak separation at low temperature,  $d$  would represent the peak separation at a given temperature, and  $v$  would represent the rate of exciton migration at that particular temperature. The results of this analysis for  $\text{DMPA}(\text{TCNQ})_4$  (II) are presented in Figure 5.5, and the observed linear relationship indicates the migration process is activated, the slope of this plot giving an activation energy for migration of  $0.3 \text{ kJ mol}^{-1}$ . This value is of the correct order of magnitude expected

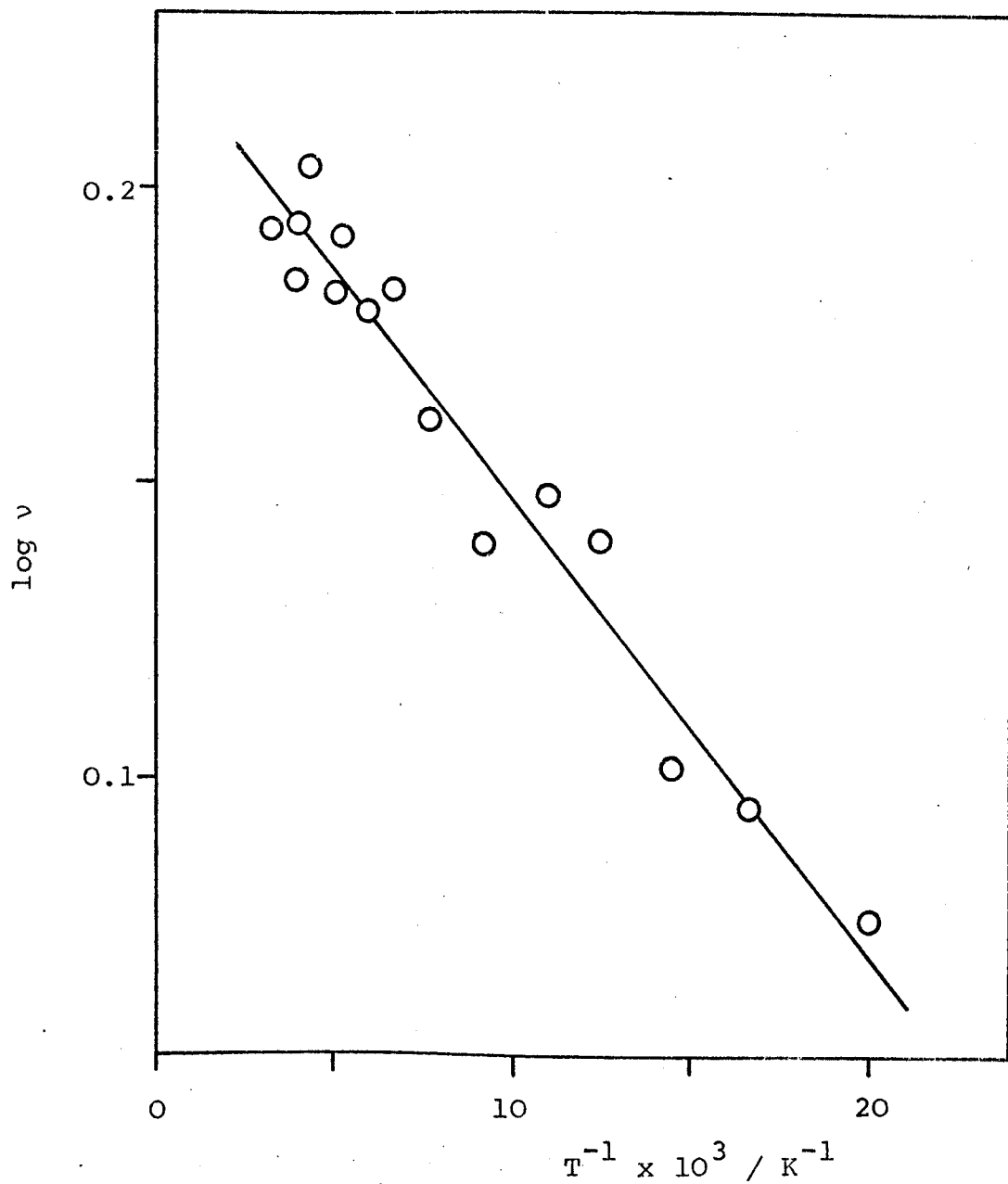


Figure 5.5

DMPA(TCNQ)<sub>4</sub> (II)

Semilog plot of the rate (in MHz) of exciton migration (calculated from equation 2.46) against reciprocal temperature for sample 2.

from exciton migration and, therefore, the decrease of the peak separation as the temperature increases to 150K, can be reasonably attributed to averaging of the g factor resulting from exciton motion.

It must be mentioned that the observed magnetic behaviour can also be interpreted in terms of a metallic phase above 150K and a semiconducting phase below this temperature. A phase transition of this kind incorporates change of lattice dimensions and would be expected to produce changes in the g factor and Q values. However, this possibility can only be verified by additional conductivity results in this temperature region and by investigation of single crystals.

In conclusion, the differences in the magnetic properties of the two phases of  $\text{DMPA}(\text{TCNQ})_4$  appear to be due to the mode of packing within the solid. The very low J value observed for  $\text{DMPA}(\text{TCNQ})_4$  (I) shows the interaction between the two electrons constituting the triplet state to be weak, in agreement with the large separation indicated by the crystal structure. The much higher J value, however, for the polycrystalline phase reflects the greater interaction between the electrons. In the absence of structural data, the magnetic results can be interpreted as indicating the existence of tetrads of TCNQ molecules in  $\text{DMPA}(\text{TCNQ})_4$  (II), as opposed to the dimer structure of the

crystal phase. Also, the magnetic susceptibility results for both phases indicate the crystal form contains localised triplet excitons, whereas delocalised excitons are proposed for the polycrystalline samples. This interpretation is consistent with the electrical data, which shows the polycrystalline samples to be more highly conducting by a factor of  $10^3$  and requires a band model for the interpretation of the conductivity behaviour.

## 5.2 DPPE(TCNQ)<sub>5</sub>

Since the discovery of the organic metal 1,2-di(N-ethyl-4-pyridinium)ethylene (DEPE)-(TCNQ)<sub>4</sub> in this department, interest has obviously been aroused in other TCNQ complex salts containing cations in the same series as DEPE. The next one along the series is 1,2-di(N<sup>n</sup>propyl-4-pyridinium)ethylene (DPPE) and microanalysis and spectroscopic results indicated the complex salt has a stoichiometry of five TCNQ molecules per cation. Unfortunately, although many preparations were undertaken, only polycrystalline samples could be obtained, this series of compounds apparently being very difficult to obtain in crystal form.

The d.c. conductivity was measured as part of this work, the results being given in Appendix 2. The conductivity was found to be in the semi-metallic region, having a room temperature average value of  $0.3 \text{ ohm}^{-1} \text{ cm}^{-1}$  with a small

activation energy of  $10.6 \text{ kJ mol}^{-1}$ .

Two weighed samples were prepared for the e.s.r. measurements and both displayed the spectrum type shown in Figure 3.9. A g factor study could not be performed, however, as the spectra obtained were not representative of all possible orientations of the crystallites. The intensity of the e.s.r. signals was studied as a function of temperature and exhibited the previously discussed intensity behaviour for triplet excitons having a low value of the singlet-triplet energy gap. The broad intensity maximum was observed at approximately 80K, with a slight decrease in intensity above this temperature due to thermal energy partially removing the triplet character of the electrons. Below 80K the intensity decreased rapidly, and the slope obtained from the  $\log IT$  against  $1/T$  plots, a typical example being shown in Figure 5.6, was calculated as  $-0.9 \pm 0.1 \text{ kJ mol}^{-1}$ . Using this value for  $J$  in equation 2.26 yields a value of  $2.3 \times 10^{-3} \text{ e.m.u. cm}^3 \text{ mol}^{-1}$ , which is considerably larger than the experimental value of  $(1.3 \pm 0.4) \times 10^{-3} \text{ e.m.u. cm}^3 \text{ mol}^{-1}$ . This suggests that delocalised triplet excitons exist in  $\text{DPPE}(\text{TCNQ})_5$  and the slope of the  $\log IT$  against  $1/T$  plots is representative of an effective energy gap of  $J\Delta(\gamma)$ . This is also supported by the lack of any observed dipolar splitting throughout the temperature range investigated.

log IT

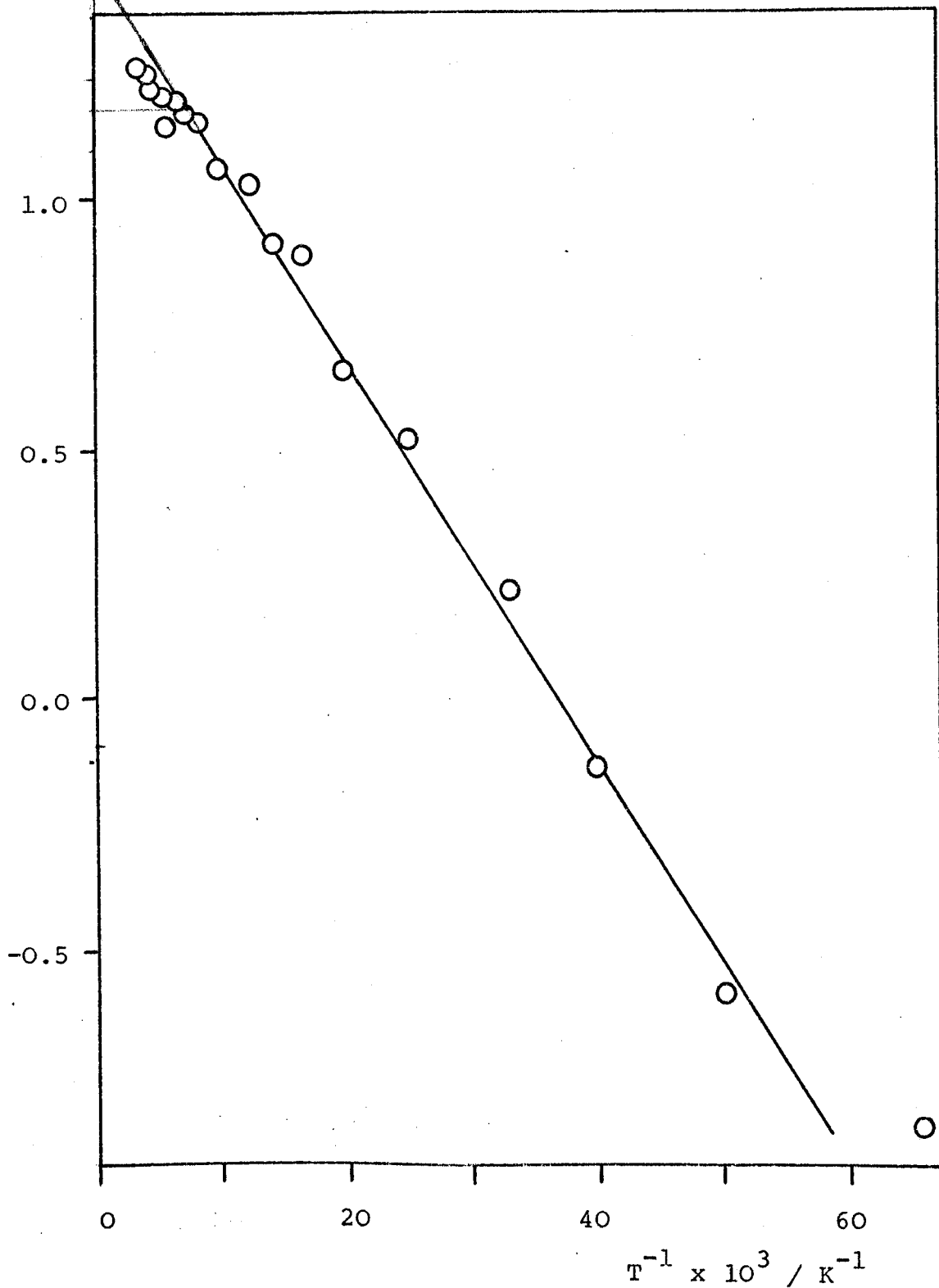


Figure 5.6

DPPE(TCNQ)<sub>5</sub>

Semilog plot of the product of the relative intensity and temperature against reciprocal temperature for sample 1.

Using the approach outlined in the previous sections, estimations of  $a(\gamma)$ ,  $\gamma$ ,  $\Delta(\gamma)$ ,  $J$  and  $W$  can be calculated and are found to be  $0.5 \pm 0.1$ ,  $0.6 \pm 0.1$ ,  $0.7 \pm 0.1$ ,  $1.3 \pm 0.2 \text{ kJ mol}^{-1}$  and  $1.1 \pm 0.2 \text{ kJ mol}^{-1}$  respectively. It can be seen from these values that the degree of delocalisation is similar to that found for  $\text{DMPA}(\text{TCNQ})_4$  (II) which has similar magnetic properties and high value for the conductivity. However, the values for  $J$  are slightly different and this reflects the interaction between the electrons in the solid. In  $\text{DMPA}(\text{TCNQ})_4$  (II), the two unpaired electrons are distributed over four TCNQ molecules and, therefore, a greater interaction is expected than for  $\text{DPPE}(\text{TCNQ})_5$  in which the electrons are distributed over five molecules, assuming the extent of molecular overlap is the same.

The value of  $\gamma$  obtained for  $\text{DPPE}(\text{TCNQ})_5$  indicates the exchange coupling is not strongly alternating and the exciton is delocalised, but the value is bordering on the region where Etemad's treatment is specified as being no longer valid. However, this treatment has been used by other workers<sup>191</sup> outside the limits in which the theory can be applied and, since this treatment is only approximate, it is considered to give a reasonable description of the energy states in this complex salt. Also, the continued linearity of the  $\log IT$  against  $1/T$  plot supports the view taken as to the wider application of the theory.

Below 14K, the signal intensity was observed to increase due to the usual onset of Curie law behaviour. As the spectra from both samples collapsed at low temperatures to give a single symmetrical peak, an estimate of the number of these doublet species could be obtained using the oscilloscope technique. A typical plot of the results is presented in Figure 5.7 and shows the intensity does in fact obey the Curie law. The average value of this estimate, calculated from a number of such plots is  $(3.1 \pm 1.5) \times 10^{21}$  spins  $\text{mol}^{-1}$  and compares very well with the average value of  $(2.8 \pm 0.8) \times 10^{21}$  spins  $\text{mol}^{-1}$  obtained from the low temperature curvature of the  $\log IT$  against  $1/T$  plots. The signal was found to be symmetrical enough for a lineshape analysis to be performed in this temperature region, and Figure 5.8 shows the lineshape to deviate from the Lorentzian shape associated with migrating species. This supports the suggestion that the signal is caused by isolated monanion radicals rather than by triplet excitons.

The magnetic behaviour of  $\text{DPPE}(\text{TCNQ})_5$  is well described by the model of delocalised triplet excitons and is consistent with the high d.c. electrical conductivity observed. Whether the properties of the cation or the extra TCNQ molecule per cation are responsible for the differences in magnetic properties between this complex salt and the metallic phase of  $\text{DEPE}(\text{TCNQ})_4$  is not clear and

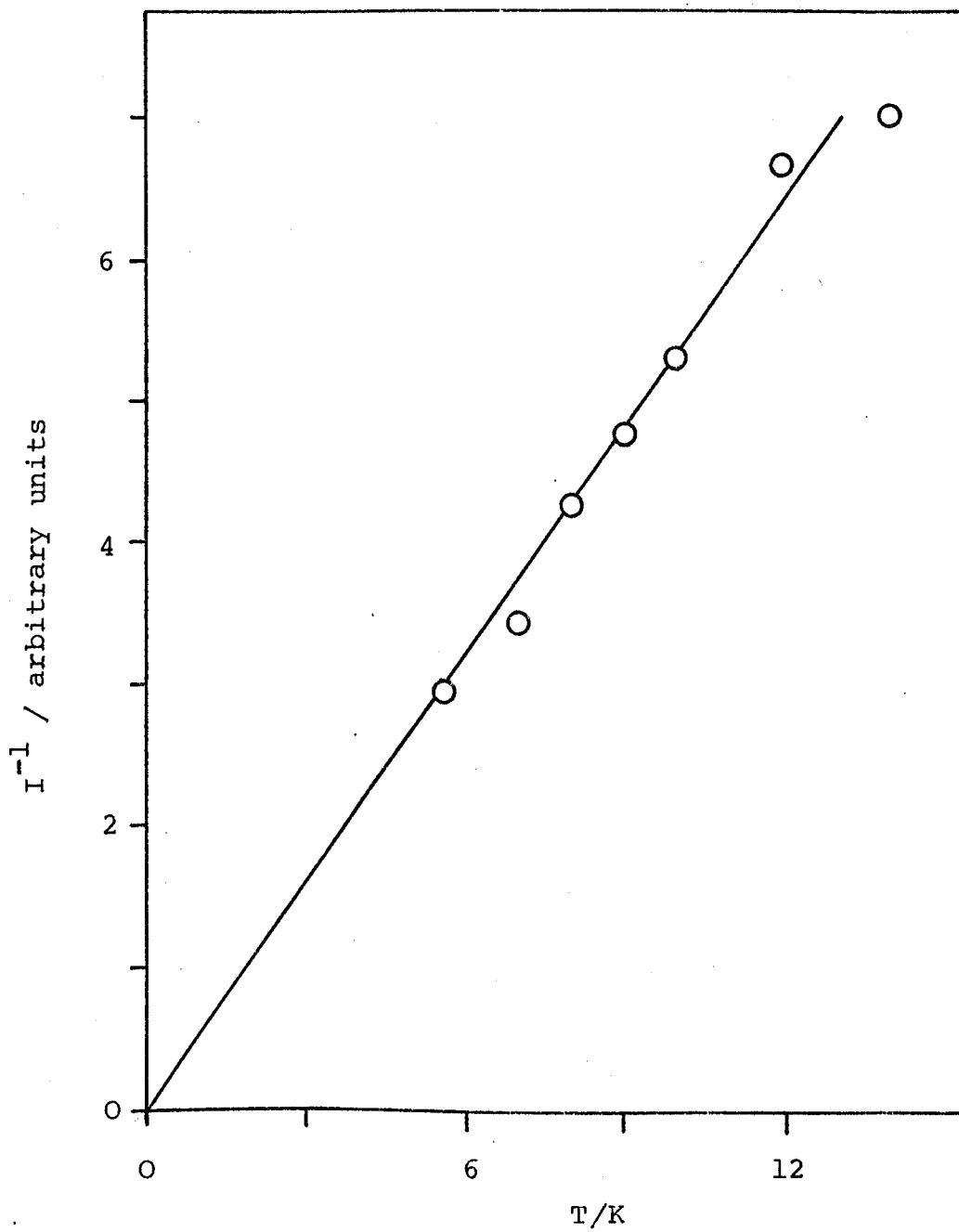


Figure 5.7

DPPE(TCNQ)<sub>5</sub>

Plot of the reciprocal relative intensity (obtained from oscilloscope measurements) against temperature for sample 2.

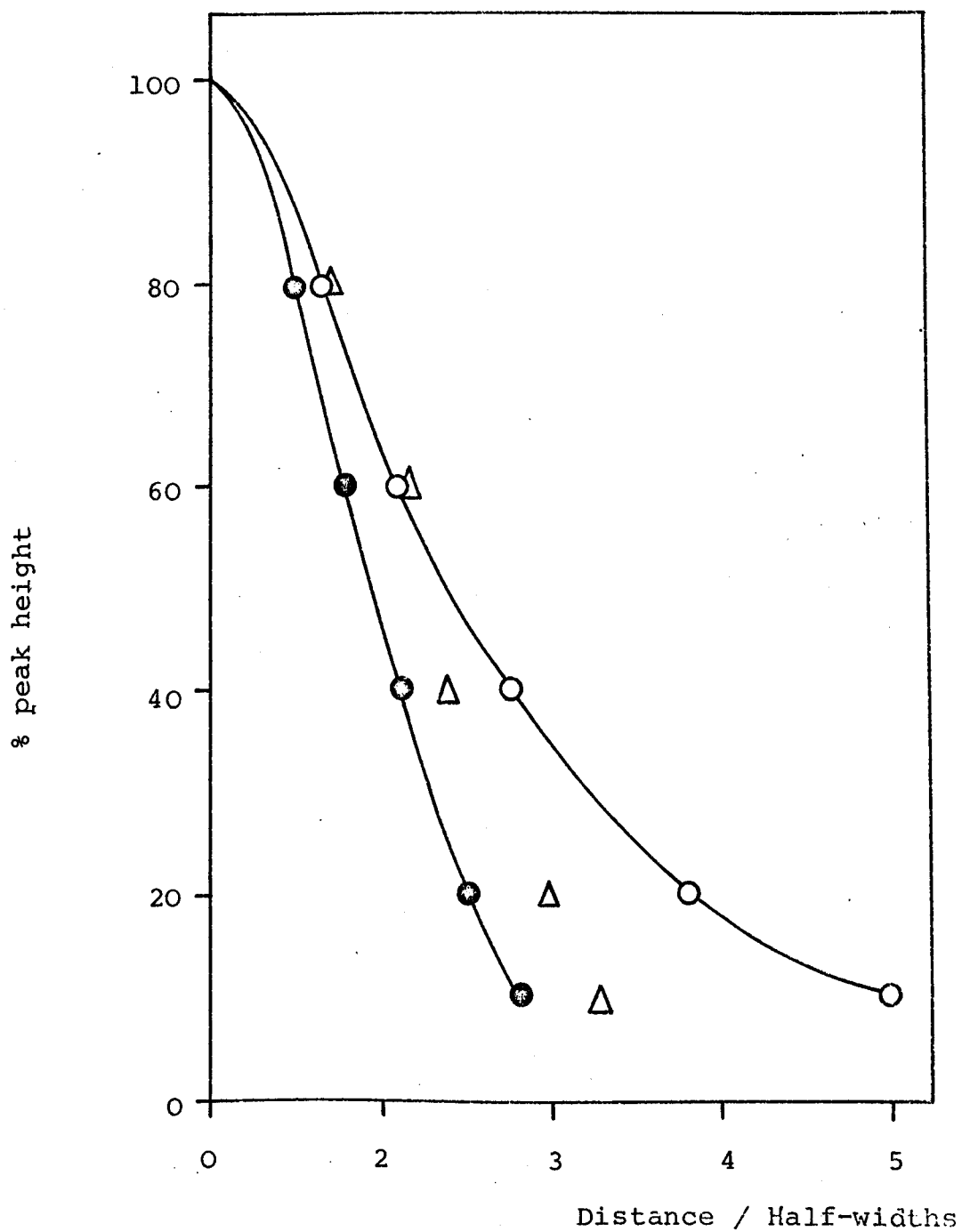


Figure 5.8

DPPE(TCNQ)<sub>5</sub>

Lineshape analysis for sample 2 at 8K.

●—● Gaussian lineshape.

○—○ Lorentzian lineshape.

△ Average lineshape for sample.

studies of single crystals of these compounds might prove useful, as the information derived from polycrystalline samples is somewhat limited.

### 5.3 DBPE(TCNQ)<sub>5</sub>

The cation used in the preparation of this complex salt is also from the same series as DEPE, and is 1,2-di(N<sup>n</sup>-butyl-4-pyridinium)ethylene (DBPE). Again, only polycrystalline samples were available, and the d.c. conductivity results for this complex salt are presented in Appendix 2. The room temperature value of the conductivity was observed to be much lower than for DPPE(TCNQ)<sub>5</sub>, being  $3.6 \times 10^{-2} \text{ ohm}^{-1} \text{ cm}^{-1}$  with an activation energy for conduction of  $15.4 \text{ kJ mol}^{-1}$ .

The magnetic properties of two samples were studied and both exhibited the spectrum typical of an axially symmetric g factor with the high field and low field peaks corresponding to  $g_{\perp}$  and  $g_{\parallel}$  respectively. As with DPPE(TCNQ)<sub>5</sub>, the spectrum was observed not to contain contributions from all possible orientations of the microcrystals. Consequently, a g factor study was not possible. This is due to the large size of the microcrystals in these particular samples, which were obtained during attempts to achieve the correct experimental conditions for preparation of single crystals. Therefore, in the small weight of sample required for the e.s.r. experiments,

a sufficient number of microcrystals was not present for a g factor study to be possible.

The signal intensity of both samples increased slightly from 300K to approximately 80K, below which the intensity rapidly decreased. A typical log IT against  $1/T$  plot is shown in Figure 5.9 and the average slope obtained from these plots is  $-1.3 \pm 0.1$  kJ mol<sup>-1</sup>. The value of the room temperature susceptibility was found to be  $(1.8 \pm 0.2) \times 10^{-3}$  e.m.u. cm<sup>3</sup> mol<sup>-1</sup> and, using a value of 1.3 kJ mol<sup>-1</sup> for J in equation 2.26 for localised triplet states, the predicted susceptibility is  $2.2 \times 10^{-3}$  e.m.u. cm<sup>3</sup> mol<sup>-1</sup>. The experimental value is slightly lower than this, although the agreement is very close. Therefore, any degree of delocalisation in this complex salt is small. An attempt was made to assess any such degree of delocalisation using Etemad's treatment, but the value of  $\gamma$  calculated from the experimental results was found to be zero, the value expected for strongly alternating localised triplet excitons. Consequently, it might be expected that the evidence for dipolar splitting would be observed at low temperatures if indeed a localised model is applicable for DBPE(TCNQ)<sub>5</sub>. No such evidence was observed in the entire temperature range investigated. However, the value for the singlet-triplet energy gap indicates the overlap of the wave functions is small. Therefore, any dipolar interaction between them may also be small and result in fine structure smaller in

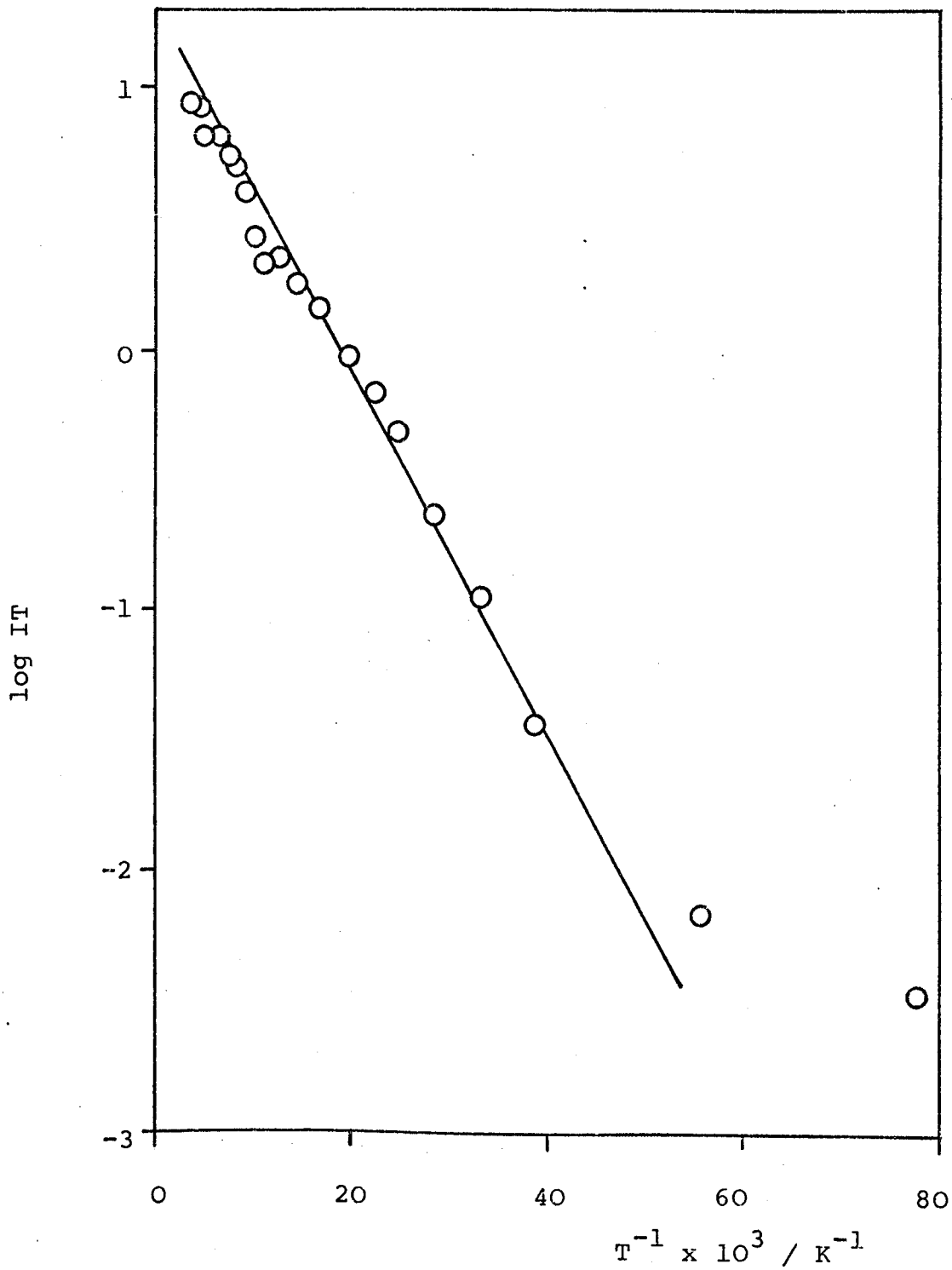


Figure 5.9

DBPE(TCNQ)<sub>5</sub>

Semilog plot of the product of the relative intensity and temperature against reciprocal temperature for sample 1.

magnitude than the g factor anisotropy. Furthermore, at low temperatures, where only a single almost symmetrical signal was observed, the linewidth for  $\text{DBPE}(\text{TCNQ})_5$  was considerably larger than observed for the other polycrystalline complex salts studied. This would be expected from localised species experiencing hyperfine and dipolar broadening at low temperatures.

Below 10K, the intensity increased as the signal from the Curie species began to dominate. The spectrum displayed on the oscilloscope was approximately symmetrical and, consequently, the number of such species could be evaluated using measurements taken from the screen. A typical set of results is presented in Figure 5.10 and this study gave an estimate of  $(1.2 \pm 0.6) \times 10^{21}$  spins per mole of sample, which compares well with the value of  $(0.8 \pm 0.3) \times 10^{21}$  spins  $\text{mol}^{-1}$  obtained from the log IT against  $1/T$  plots.

The magnetic properties of  $\text{DBPE}(\text{TCNQ})_5$  appear, from the results obtained in this work, to be best described by a localised triplet exciton model, and this is consistent with the semiconducting electrical properties observed and the high activation energy for conduction. These results differ from those obtained for the closely related  $\text{DPPE}(\text{TCNQ})_5$ , which has a higher semi-metallic conductivity, small activation energy, and magnetic

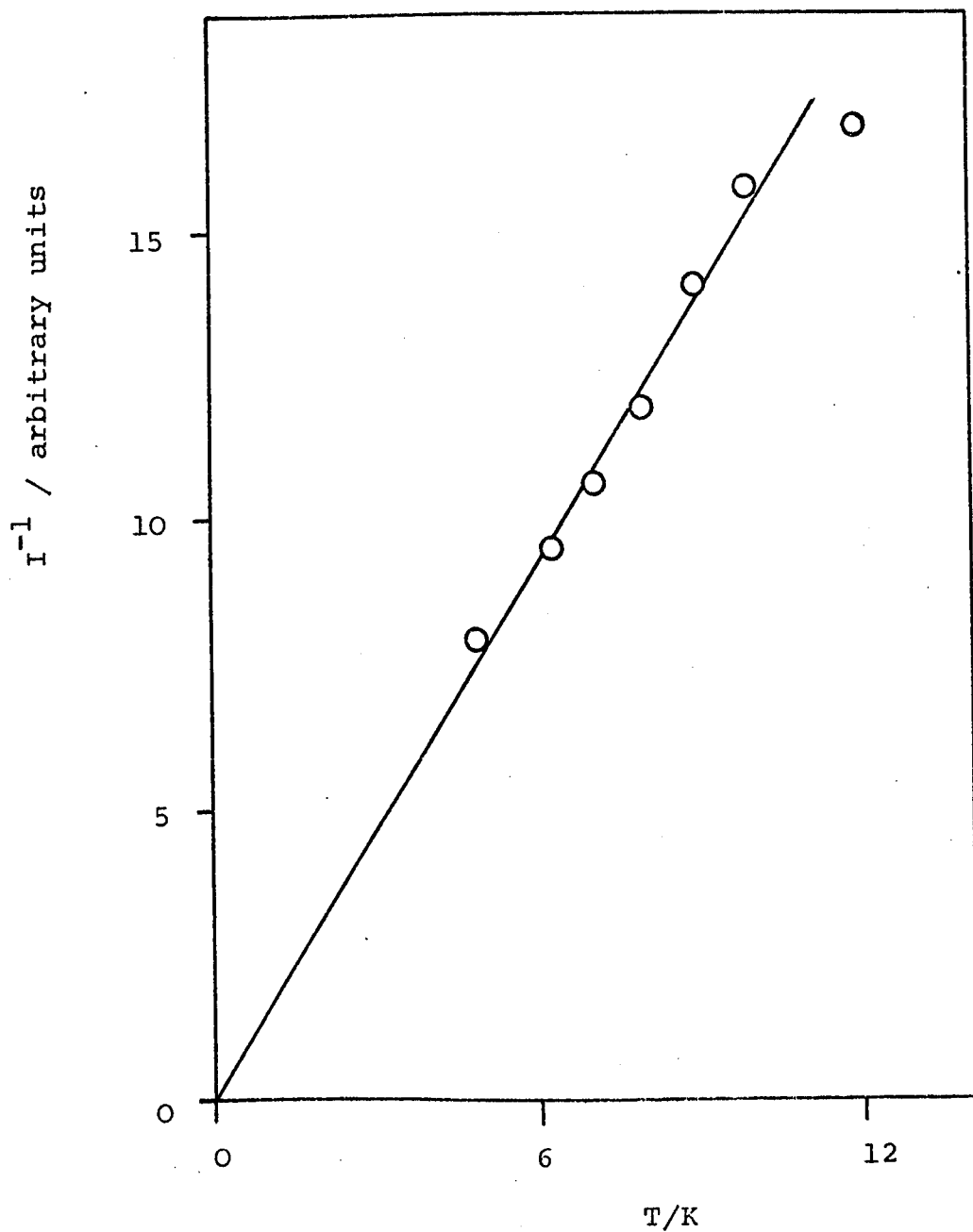


Figure 5.10

DBPE(TCNQ)<sub>5</sub>

Plot of the reciprocal relative intensity (obtained from oscilloscope measurements) against temperature for sample 2.

properties associated with delocalised triplet excitons. The only structural difference between  $\text{DBPE}(\text{TCNQ})_5$  and  $\text{DPPE}(\text{TCNQ})_5$  is the presence of an extra methylene group at each end of the cation DBPE. It would appear, therefore, that the differences in the physical properties are due to the change in cation and degree of polarisability. The number of defect sites in both compounds is similar and would not be expected to cause such differences in the physical properties. Indeed, the activation energy for conduction would be expected to be greater, not smaller, in  $\text{DPPE}(\text{TCNQ})_5$  merely from considering the effect of defects on the transport properties. Therefore, the effect of the cation would seem to play a major role in determining the extent of overlap of the molecular wave functions and, subsequently, the energy states in these compounds. However, once again, single crystals are required for definite statements to be made concerning the structural differences between these two complex salts.

#### 5.4 DHPE(TCNQ)<sub>5</sub>

The cation 1,2-di(N-cyclohexyl-4-pyridinium)-ethylene (DHPE) is also from the same series as DEPE, DPPE and DBPE. As was the case for the latter two cations, preparations of the TCNQ complex salt of DHPE yielded only polycrystalline samples.

The two samples used for the e.s.r. investigations

gave spectra of the type shown in Figure 3.9, and were observed to contain contributions from all possible orientations of the microcrystals. Therefore, a g factor study could be performed and the values for  $g_{\parallel}$  and  $g_{\perp}$  were found to be  $2.0043 \pm 0.0003$  and  $2.0034 \pm 0.0003$  respectively. These values can be interpreted as reflecting the two-dimensionality within the cation sheet, with the unique g factor corresponding to the direction through the cation planes.

The temperature dependence of the signal intensity was very similar to the behaviour observed for  $\text{DPPE}(\text{TCNQ})_5$  and  $\text{DBPE}(\text{TCNQ})_5$ . A typical example of the  $\log IT$  against  $1/T$  plots for this complex is shown in Figure 5.11, and the average value of the slope was found to be  $-1.4 \pm 0.1 \text{ kJ mol}^{-1}$ . If this were a true representation of  $J$ , a room temperature susceptibility of  $2.2 \times 10^{-3} \text{ e.m.u. cm}^3 \text{ mol}^{-1}$  would be expected. However, the experimental value was only  $(0.9 \pm 0.2) \times 10^{-3} \text{ e.m.u. cm}^3 \text{ mol}^{-1}$ , which is considerably lower than the predicted value. Therefore, the slope of the  $\log IT$  against  $1/T$  plots is only representative of the effective singlet-triplet energy gap  $J\Delta(\gamma)$  produced by delocalisation of the excitons to give an exciton band. Application of Etemad's treatment for  $\text{DHPE}(\text{TCNQ})_5$  gives rise to values of  $0.3 \pm 0.1$ ,  $0.8 \pm 0.1$ ,  $0.4 \pm 0.1$ ,  $3.5 \pm 0.8 \text{ kJ mol}^{-1}$ , and  $4.1 \pm 0.8 \text{ kJ mol}^{-1}$  for  $a(\gamma)$ ,  $\gamma$ ,  $\Delta(\gamma)$ ,  $J$  and  $W$  respectively. These results show that there

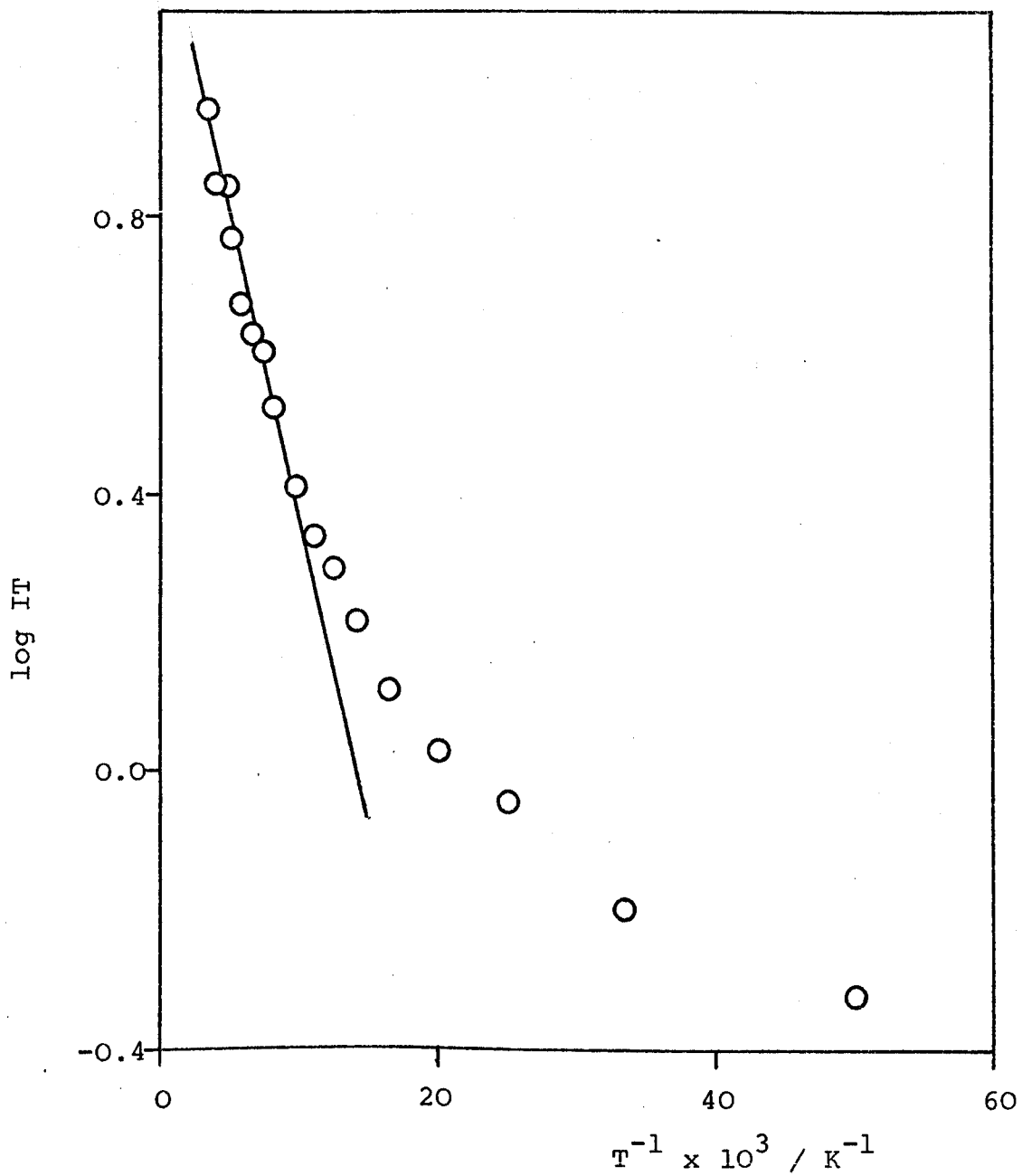


Figure 5.11

DHPE(TCNQ)<sub>5</sub>

Semilog plot of the product of the relative intensity and temperature against reciprocal temperature for sample 1.

is a very broad exciton band of width  $4.1 \pm 0.8 \text{ kJ mol}^{-1}$  centred at  $3.5 \pm 0.8 \text{ kJ mol}^{-1}$  above a ground singlet state. This gives an effective singlet-triplet energy gap of  $1.5 \text{ kJ mol}^{-1}$  which is in very good agreement with the value obtained from the log IT against  $1/T$  plots. The interactions which produce this broad exciton band would be expected to also produce a broad conduction band, and this is borne out by the high conductivity of  $0.2 \text{ ohm}^{-1} \text{ cm}^{-1}$  for  $\text{DHPE}(\text{TCNQ})_5$ . Also, if it is assumed that the very small activation energy for conduction ( $5.8 \text{ kJ mol}^{-1}$ ) mostly arises from crystallite boundary effects, the results obtained from polycrystalline samples indicate that single crystals of this complex salt may possibly be metallic.

The value for  $\gamma$  of 0.8 is greater than 0.5 and, therefore, is outside the range of validity specified in Etemad's work. However, the continued linearity of Figure 5.11 gives confidence that this treatment provides a reasonable description of the exciton states in this complex salt. Further support is given by the d.c. conductivity data, measured as part of this work, the results of which are presented in Appendix 2. Lack of any dipolar splitting is also consistent with the interpretation of delocalised excitons.

Below 50K, the spectra began to collapse and produced a single symmetrical peak at low temperatures.

Consequently, an estimate of the number of Curie species present in  $\text{DHPE}(\text{TCNQ})_5$  could be obtained using the oscilloscope technique. An example of the results is presented in Figure 5.12, and from a number of such plots an average value of  $(8.7 \pm 3.1) \times 10^{21}$  spins  $\text{mol}^{-1}$  was calculated. This is in reasonable agreement with the value obtained by extrapolation of the curvature shown in Figure 5.11, which gives an estimate of  $(2.0 \pm 1.9) \times 10^{21}$  spins  $\text{mol}^{-1}$ . Both values are somewhat greater than the values obtained for  $\text{DPPE}(\text{TCNQ})_5$  and  $\text{DBPE}(\text{TCNQ})_5$  and may be interpreted as reflecting the differences in the efficiency of quaternisation of the cations in the three compounds under investigation. The signal obtained at low temperatures was sufficiently symmetric for a lineshape analysis to be performed in the region where the Curie signal dominates. Figure 5.13 shows the lineshape to be between Gaussian and Lorentzian, this being expected for isolated doublet species having a small degree of motion, which is fast enough for hyperfine structure to be unresolved but slow enough for hyperfine interactions to affect the lineshape.

The increase in peak separation with decreasing temperature previously discussed for  $\text{DMPA}(\text{TCNQ})_4$  (II) was also observed with  $\text{DHPA}(\text{TCNQ})_5$ . This behaviour is shown in Figure 5.14 and the results of the analysis, also described in section 5.1, are given in Figure 5.15. Once again, a linear relationship is observed, and the value of the

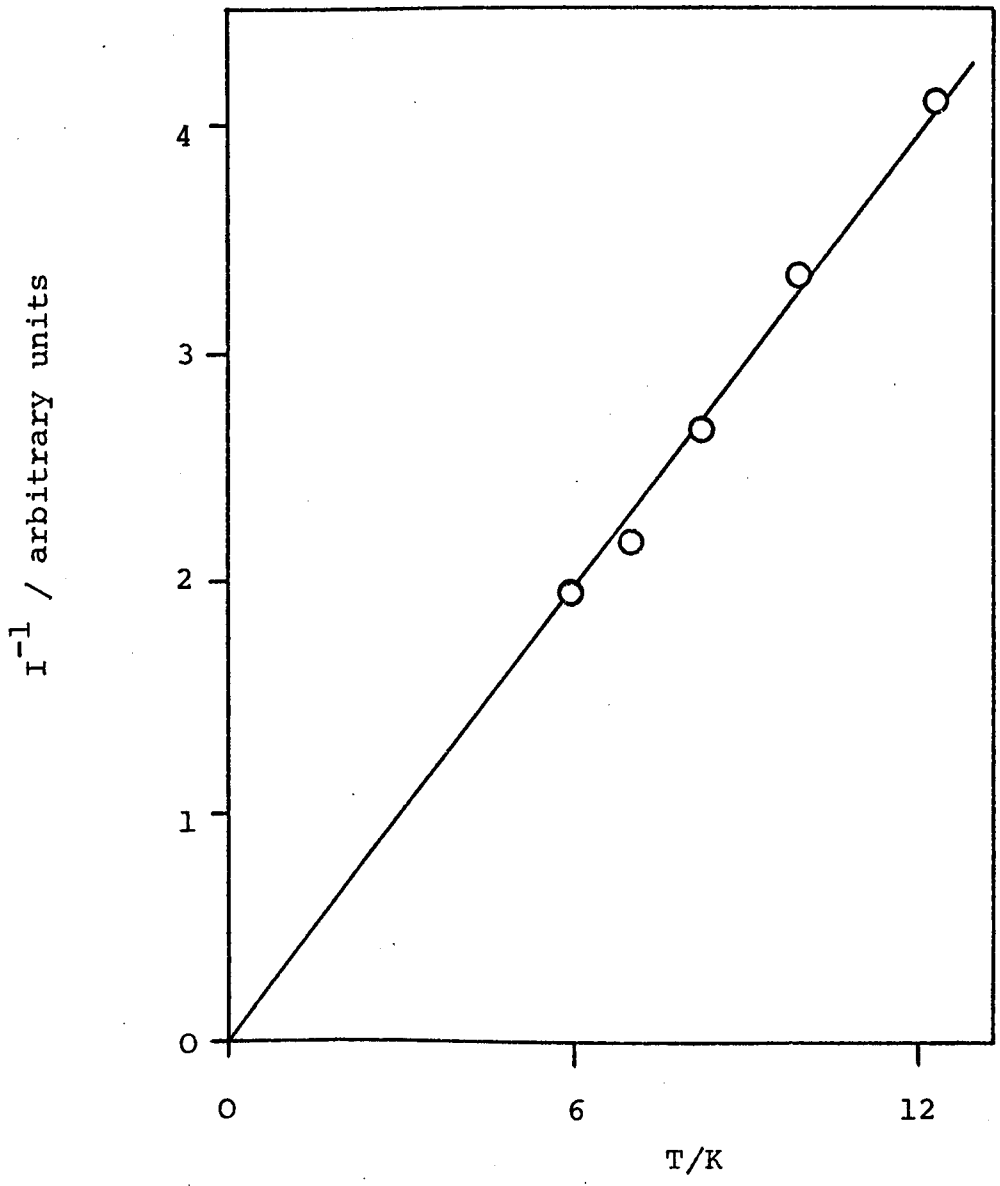


Figure 5.12

DHPE(TCNQ)<sub>5</sub>

Plot of the reciprocal relative intensity (obtained from oscilloscope measurements) against temperature for sample 2.

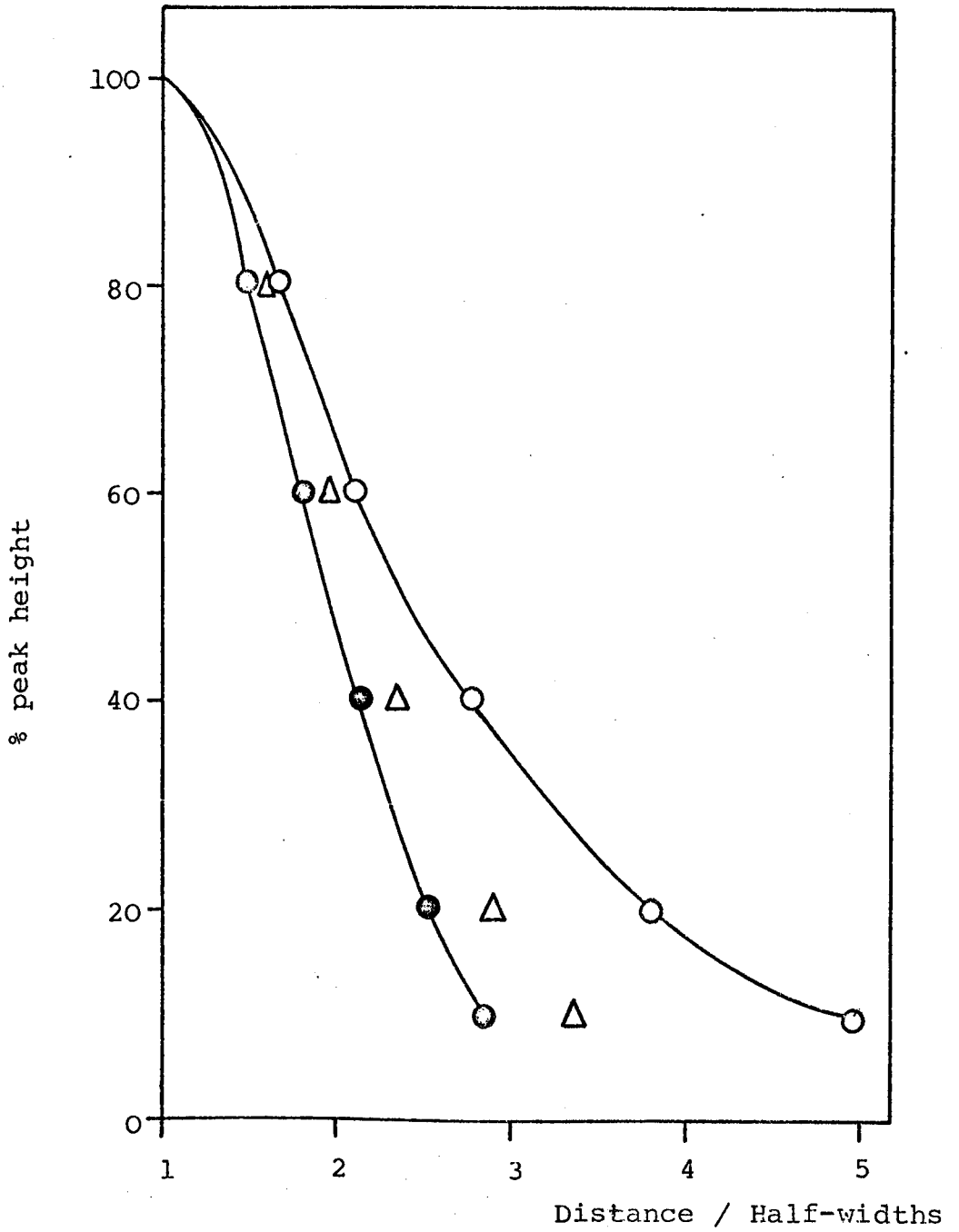


Figure 5.13

DHPE(TCNQ)<sub>5</sub>

Lineshape analysis for sample 2 at 6K.

●—● Gaussian lineshape.

○—○ Lorentzian lineshape.

△ Average shape for sample.

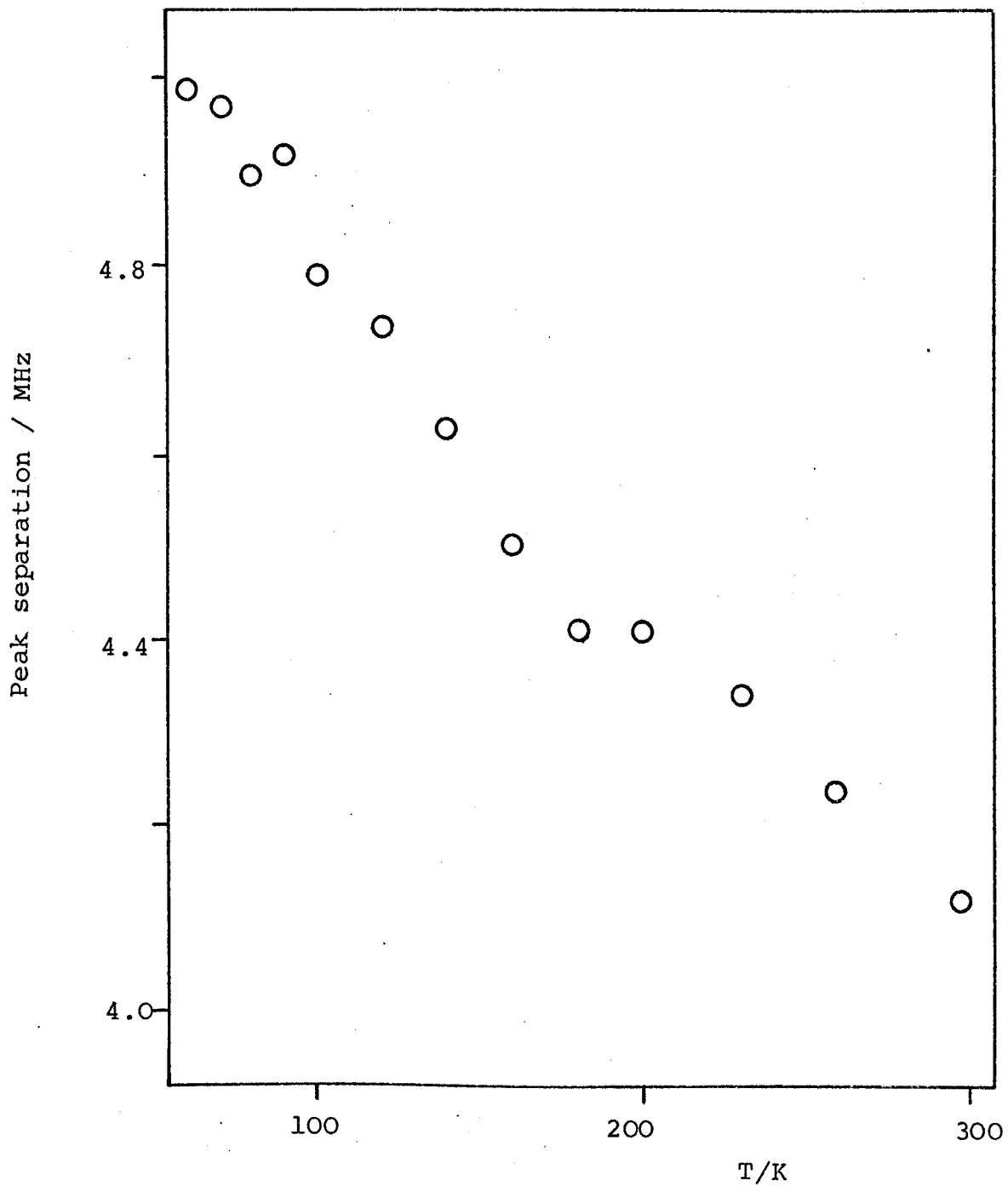


Figure 5.14

DHPE(TCNQ)<sub>5</sub>

Plot of the peak separation against temperature  
for sample 2.

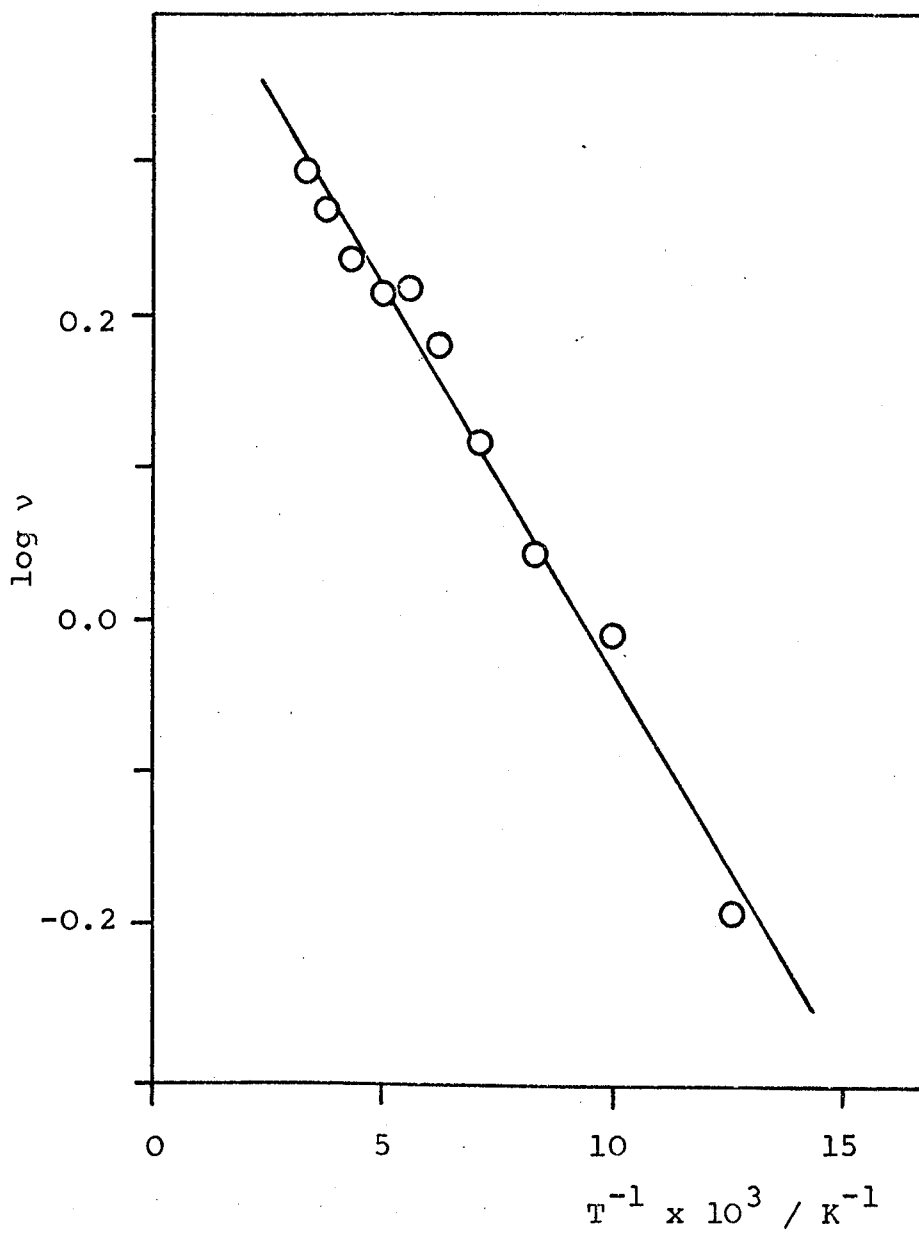


Figure 5.15

DHPE(TCNQ)<sub>5</sub>

Semilog plot of the rate (in MHz) of exciton migration (calculated from equation 2.46) against reciprocal temperature for sample 2.

activation energy for exciton migration obtained from the slope is  $1.0 \text{ kJ mol}^{-1}$ . This value is larger than that observed for  $\text{DMPA}(\text{TCNQ})_4$  (II) and this is most probably due to differences in the interfaces of the microcrystals. Nevertheless, this value is reasonable for the peak separation behaviour to be attributed to exciton migration.

The three compounds discussed in sections 5.2 to 5.4 have cations belonging to the same series and, therefore, their TCNQ complex salts might be expected to exhibit similar properties. Indeed,  $\text{DPPE}(\text{TCNQ})_5$  and  $\text{DHPE}(\text{TCNQ})_5$  do have similar physical properties, both having semi-metallic d.c. conductivities and magnetic properties associated with delocalised triplet excitons. However,  $\text{DBPE}(\text{TCNQ})_5$  has a lower conductivity, and a localised triplet exciton model most closely describes the observed magnetic properties. As all three complex salts have five TCNQ molecules per cation, it appears that the cation governs the properties of these compounds. Consequently, further investigations on other cations in this series and the preparation of single crystals of these compounds could prove most interesting.

CHAPTER 6

CONCLUDING REMARKS

"Science has the first word on everything,  
and the last word on nothing."

Victor Hugo

1802 - 1885

The results presented in this thesis are consistent with the majority of literature in this field with respect to the observation of singlet-triplet magnetic behaviour in TCNQ complex salts. The triplet state is relatively uncommon in e.s.r. studies and these compounds provide a unique opportunity for theoreticians and experimentalists to investigate such species and the associated phenomena. Indeed, explanations of the observed behaviour of triplet excitons have been difficult in the past because of the lack of theoretical models, but the intensive attention focused on TCNQ complex salts has led to a partial understanding of these systems.

The common factor in all the compounds studied, with the exception of  $\text{TPT}(\text{TCNQ})_4$ , is the presence of triplet excitons, whether these be localised or delocalised. However, the various manifestations of this behaviour vary from compound to compound depending on the interactions occurring within the solid. Although the common structural features are the stacking behaviour of the TCNQ molecules, some degree of two-dimensionality in the TCNQ sheets, and segregation of these sheets by cation planes, the very small variations in distance separation and overlap of these molecules give rise to different magnetic properties. This confirms the suggestion that these properties are a sensitive function of the mode of packing in the solid, in which the cation plays an important role, as indicated by the results

for DPPE(TCNQ)<sub>5</sub>, DBPE(TCNQ)<sub>5</sub> and DHPE(TCNQ)<sub>5</sub>. Furthermore, this sensitivity to slight structural differences illustrates the complexity of the interactions within these systems and why a fully comprehensive understanding of the properties governing the electrical and magnetic behaviour has not yet been achieved.

The majority of past studies has been concentrated on TCNQ complex salts of monovalent and divalent cations, whose structures fall into the categories of one-dimensional TCNQ stacks and two-dimensional TCNQ sheets. The trivalent cation, TPT, studied in this work is a good example of how drastically the change of cation type can alter the structure of the solid and, consequently, the physical properties. Therefore, it is felt that the next phase in the study of TCNQ complex salts should be directed towards compounds of differing structural types.

The technique of low temperature e.s.r. has proved to be a valuable tool in the investigation of TCNQ complex salts, providing a great deal of information regarding the existing magnetic states, particularly in the single crystal studies. However, although these results provide a basis for proposed interpretations, they do not on their own provide conclusive evidence for definite statements to be made, as exemplified by all the cases discussed in this work. Certain correlations exist between the magnetic

and electrical properties, both of which bear a relationship to the crystal structure. Unfortunately, only preliminary investigations of the electrical properties of DCBP(TCNQ)<sub>3</sub> and TPT(TCNQ)<sub>4</sub> have been performed and, therefore, the interpretation of the magnetic behaviour must at present remain speculative. Similarly, the possibility of phase transitions in some of these compounds can only be verified with electrical and structural data in the low temperature region of interest, which currently remains an obstacle to be overcome in this department. This illustrates the interdependence of the various techniques required to adequately explain the properties of these compounds. However, it is felt that, even with these limitations, the low lying electronic states can be reasonably described from their magnetic behaviour, and provide valuable evidence in the quest to elucidate the theoretical models applicable.

The role of defect sites in the lattice has proved most interesting. The existence of these sites would appear to have several different effects on the magnetic properties, as shown by the central signal in DCBP(TCNQ)<sub>3</sub>, the unusual temperature independence of the signal intensity in TPT(TCNQ)<sub>4</sub>, and the usual Curie signal observed at low temperatures in the vast majority of TCNQ complexes. Consequently, further work may be of value in investigating these species, combined with different

preparative techniques to study how these species might be either eliminated or their number controlled. This is particularly important with respect to the transport properties in these compounds, as the presence of defects has quite a significant effect on the conductivity.

It has been mentioned that the g factors do not seem to have much value in the interpretive sense although, on the whole, the g values are in agreement with the degree of delocalisation of the electrons, as indicated by the conductivity results. However, it is considered that the interpretation of the g factor anisotropy is valid but possibly over-simplified, the interactions which govern these values being of a more complex nature in TCNQ complex salts.

The unusual angular variation of the linewidth observed at room temperature with  $\text{DMPA}(\text{TCNQ})_4$  (I),  $\text{DPB}(\text{TCNQ})_4$  and  $\text{TPT}(\text{TCNQ})_4$  has been interpreted in previous reports for other compounds in terms of incomplete averaging of dipolar splitting in nearly two-dimensional magnetic systems. However, in all the three complex salts mentioned above no evidence of dipolar splitting was observed even at low temperatures and, therefore, any effect from such a small interaction would be expected to be completely removed at room temperature. Consequently, this explanation would not seem valid for these particular

compounds. Although this phenomenon has been reported by other workers, no detailed theoretical investigation has been undertaken. However, the compounds do appear to have some degree of two-dimensionality, as indicated by the crystal structure and electrical results and, therefore, are in partial agreement with the interpretation.

The temperature dependence of the linewidths in these compounds also proved most interesting. The complex salts  $\text{DMPA}(\text{TCNQ})_4$  (I) and  $\text{DPB}(\text{TCNQ})_4$  have very similar crystal structures, d.c. conductivities, and magnetic properties, with the exception of the linewidth behaviour. Once again, although such variations of behaviour have been experimentally reported, few theoretical investigations have been performed. The explanation in terms of Wannier excitons in  $\text{DBP}(\text{TCNQ})_4$  would not be consistent with the susceptibility and electrical data, although this possibility cannot be entirely ruled out until high-pressure studies are available.

There have been many suggestions concerning the mechanism of spin-lattice relaxation and all consider selective transfer of electron spin energy to lattice modes resonant with the spins. However, although the phenomenon of e.s.r. is quite well understood, the position of relaxation effects is not nearly as

satisfactory. Experimental observations have been numerous, but theoretical accounts have had varying degrees of success. It is clear from the wide range of linewidth behaviour exhibited by the TCNQ complex salts discussed in this thesis, particularly in the single crystal studies, that more intensive investigations including other relaxation techniques are required for a complete understanding of the parameters governing the linewidth.

The intention of this work was to investigate the magnetic properties of TCNQ complex salts and use these results, together with crystal structure and electrical data to propose consistent theoretical models to account for the observations. Although all aspects of the magnetic behaviour cannot be readily explained, correlations with the crystal structure determinations and conductivity results were obtained, and the models proposed in this work are indeed consistent with these properties. Therefore, it would seem reasonable to conclude that the aim of this work has been successfully fulfilled.

## REFERENCES

1. A.Pochettino, *Acad.Lincei Rendiconti*, 15(1), 355(1906).
2. A.Szent-Györgyi, *Nature*, 148, 157(1941).
3. S.Baxter and A.B.D.Cassie, *Nature*, 148, 408(1941).
4. S.Baxter, *Trans.Faraday Soc.*, 34, 207(1943).
5. A.Szent-Györgyi, *Nature*, 157, 875(1946).
6. D.D.Eley, *Nature*, 162, 819(1948).
7. A.T.Vartanyan, *Zhur.Fiz.Khim.*, 22, 769 (1948).
8. H.Akamatu and H.Inokuchi, *J.Chem.Phys.*, 18, 810(1950).
9. H.Akamatu, H.Inokuchi, and Y.Matsunaga, *Nature*, 173, 168(1954).
10. D.Bijl, H.Kainer, and A.C.Rose-Innes, *J.Chem.Phys.*, 30, 765(1959).
11. J.Bardeen, L.N.Cooper, and J.R.Schrieffer, *Phys.Rev.*, 108, 1175(1957).
12. W.A.Little, *Phys.Rev.*, 134A, 1416(1964).
13. R.A.Ferrell, *Phys.Rev.Lett.*, 13, 330(1966).
14. C.G.Kuper, *Phys.Rev.*, 150, 189(1966).
15. K.F.G.Paulus, *Mol.Phys.*, 10, 381(1966).
16. D.S.Acker, R.J.Harder, W.R.Hertler, W.Mahler, L.R.Melby, R.E.Benson, and W.E.Mochel, *J.Am. Chem.Soc.*, 82, 6408(1960).
17. P.H.Rieger and G.K.Frenkel, *J.Chem.Phys.*, 37, 2795(1962).
18. R.E.Long, R.A.Sparks, and K.N.Træblood, *Acta Cryst.*, 18, 932(1965).
19. C.J.Fritch, Jr., *Acta Cryst.*, 20, 892(1966).
20. D.A.Lowitz, *J.Chem.Phys.*, 46, 4698(1967).
21. L.R.Melby, R.J.Harder, W.R.Hertler, W.Mahler, R.E.Benson, and W.E.Mochel, *J.Am.Chem.Soc.*, 84, 3374(1962).
22. W.J.Siemons, P.E.Bierstedt, and R.G.Kepler, *J.Chem.Phys.*, 39, 3523(1963).

23. D.B.Chestnut and W.D.Phillips, *J.Chem.Phys.*, 35, 1002(1961).
24. R.G.Kepler, *J.Chem.Phys.*, 39, 3528(1963).
25. O.H.LeBlanc, Jr., *J.Chem.Phys.*, 42, 4307(1965).
26. J.H.Lupinski and K.D.Kopple, *Science*, 146, 1038(1964).
27. A.Rembaum, A.M.Hermann, F.E.Stewart, and F.Gutmann, *J.Phys.Chem.*, 73, 513(1969).
28. D.W.Bonniface, M.J.Braithwaite, D.D.Eley, R.G.Evans, R.Pethig, and M.R.Willis, *Disc.Faraday Soc.*, 51, 131 (1971).
29. H.Hatano, S.Kambara, and S.Okamoto, *J.Polymer Sci.*, 51, 526(1961).
30. W.Slough, *Trans.Faraday Soc.*, 58, 2360(1962).
31. I.F.Shchegolev, *Phys.Stat.Sol.*, 12(a), 9(1972).
32. P.A.Fedders and J.Kommandeur, *J.Chem.Phys.*, 52, 2014 (1970).
33. D.B.Chestnut and P.Arthur, *J.Chem.Phys.*, 36, 2969(1962).
34. R.G.Kepler, P.E.Bierstedt, and P.E.Merrifield, *Phys. Rev.Lett.*, 5, 503(1960).
35. D.J.Dahm, P.Horn, G.R.Johnson, M.G.Miles, and J.D.Wilson, *J.Cryst.Mol.Structure*, 5, 27(1975).
36. D.B.Chestnut and R.W.Mosely, *Theor.Chim.Acta*, 13, 230(1969).
37. J.B.Torrance, *Conf. on Synth. and Prop. of Low-Dimensional Materials*, ed. J.S.Miller, 1977.
38. A.N.Bloch, R.B.Weisman, and C.M.Varma, *Phys.Rev.Lett.*, 28, 753(1972).
39. G.Milhaly, K.Holczer, A.Janossy, G.Grüner, and M. Miljak, *Proc. Conf. on Organic Conduct. and Semi-Conduct.*, Siófok, Hungary, 553(1976).
40. A.F.Garito and A.J.Heeger, *Accts. of Chem.Res.*, 7, 232(1974).
41. A.J.Epstein, S.Etemad, A.F.Garito, and A.J.Heeger, *Phys.Rev.*, 5B, 952(1972).
42. W.L.McCubbin, *Phys.Lett.*, 19, 461(1965).

43. J.M.Thomas, *Nature*, 244, 56(1973).
44. A.J.Epstein, S.Etemad, A.F.Garito, and A.J.Heeger, *Solid State Comm.*, 9, 1803(1971).
45. V.Walatka and J.H.Pperlstein, *Mol.Cryst. and Org.Cryst.*, 15, 269 (1971).
46. J.H.Pperlstein, M.J.Minot, and V.Walatka, *Materials Research Bull.*, 7, 44(1972).
47. J.Ferraris, D.O.Cowan, V.Walatka, and J.H.Pperlstein, *J.Am.Chem.Soc.*, 95, 943(1973).
48. T.J.Kistenmacher, T.E.Phillips, and D.O.Cowan, *Acta Cryst.*, B30, 763(1974).
49. D.L.Coffen, J.Q.Chambers, D.R.Williams, P.E.Garrett, and N.D.Canfield, *J.Am.Chem.Soc.*, 93, 2258(1971).
50. L.B.Coleman, M.J.Cohen, D.J.Sandman, F.G.Yamagishi, A.F.Garito, and A.J.Heeger, *Solid State Comm.*, 12, 1125(1973).
51. Y.Tomkiewicz, B.A.Scott, L.J.Tao, and R.S.Title, *Phys.Rev.Lett.*, 32, 1363(1974).
52. A.N.Bloch, J.P.Ferraris, D.O.Cowan, and T.O.Poehler, *Solid State Comm.*, 13, 753(1973).
53. D.E.Shafer, G.A.Thomas, F.Wudl, J.P.Ferraris, and D.O.Cowan, *Solid State Comm.*, 14, 347(1974).
54. R.E.Peierls, "Quantum Theory of Solids", Oxford University Press, London, 1955.
55. A.N.Bloch, D.O.Cowan, K.Bechgaard, R.E.Pyle, R.H.Banks, and T.O.Poehler, *Phys.Rev.Lett.*, 34, 1561(1975).
56. G.J.Ashwell, D.D.Eley, and M.R.Willis, *Nature*, 259, 201(1976).
57. S.Etemad, T.Penney, E.M.Engler, B.A.Scott, and P.E.Seiden, *Phys.Rev.Lett.*, 34, 741(1975).
58. G.Keryer, J.Amiell, S.Flandrois, P.Delhaes, E.Toreilles, J.M.Fabre, and L.Giral, *Solid State Comm.*, 26, 541 (1978).
59. R.E.Pyle, A.N.Bloch, D.O.Cowan, K.Bechgaard, T.O.Poehler, T.J.Kistenmacher, V.Walatka, R.Banks, W.Krug, and T.E.Phillips, *Bull.Am.Phys.Soc.*, 20, 415(1975).

60. L.I.Buravov, O.N.Eremenko, R.B.Lyubovskii, L.P. Rozenberg, M.L.Khidekel, R.P.Shibaeva, I.F.Shchegolev, and E.B.Yagubskii, *J.E.T.P. Letters*, 20, 208(1974).
61. L.C.Isett and E.A.Perez-Albuerne, *Solid State Comm.*, 21, 433(1977).
62. V.F.Kaminskii, M.L.Khidskel, R.B.Ljubovskii, I.F.Shchegolev, R.P.Shibaeva, E.B.Yagubskii, A.V. Zvarykina, and G.L.Zvereva, *Phys.Stat.Sol.A*, 44(1), 77(1977).
63. G.Milhaly, A.Janossy, and G.Gruner, *Solid State Comm.*, 22, 771(1977).
64. R.B.Somoano, S.P.S.Yen, V.Hadek, S.K.Khanna, M.Novotny, T.Datta, A.M.Hermann, and J.A.Woollam, *Phys.Rev.*, 17B, 2853(1978).
65. L.V.Interrante, K.W.Browall, H.R.Hart, Jr., I.S.Jacobs, G.D.Watkins, and S.H.We, *J.Am.Chem.Soc.*, 97, 889 (1975).
66. K.W.Browall and L.V.Interrante, *J.Coord.Chem.*, 3, 27 (1973).
67. P.A.Berger, D.J.Dahm, G.R.Johnson, M.G.Miles, and J.D.Wilson, *Phys.Rev.*, 12B, 4085(1975).
68. I.Maki, Y.Matsunaga, M.Nakakura, and A.Nonaka, *Bull. Chem.Soc.Japan*, 48, 1368(1975).
69. Y.Matsunaga and Y.Narita, *Bull.Chem.Soc.Japan.*, 45, 408(1972).
70. D.Gordon and M.J.Hove, *J.Chem.Phys.*, 59, 3419(1973).
71. H.R.Zeller, "Low Dimensional Cooperative Phenomena", ed.H.J.Keller, New York:Plenum, 215(1975).
72. F.B.Burt, *J.Chem.Soc.*, 1171(1910).
73. R.L.Greene, G.B.Street, and L.J.Suter, *Phys.Rev. Lett.*, 34, 577(1975).
74. E.Zavoisky, *J.Phys.*, U.S.S.R., 9, 211(1945).
75. B.M.Kozyrev and S.G.Salikhov, *Doklady Akad.Nauk S.S.S.R.*, 58, 1023(1947).
76. L.S.Singer and J.Kommandeur, *Bull.Am.Phys.Soc.*, 4, 421(1959).

77. P.L.Nordio, Z.G.Soos, and H.M.McConnell, *Ann.Rev. Phys.Chem.*, 17, 237(1966).
78. H.Goldstein, "Classical Mechanics", Addison-Wesley, Reading, Mass., 1957.
79. P.Pascal, *Compt.Rend.*, 147, 56, 242, 742(1908); 148, 143(1909); 150, 1167(1910); 152, 862, 1010(1911); *Ann.de.Chim.et.Phys.*, 19, 5(1910); 25, 289(1912); 28, 218(1913).
80. S.S.Bhatnagar and K.N.Mathur, "Physical Principle and Applications of Magnetochemistry", Macmillan and Co., London, 1935.
81. C.Kittel, "Introduction to Solid State Physics", John Wiley and Sons, New York, 4th ed., 1971.
82. W.Pauli, *Z.Physik.*, 41, 81(1927).
83. L.Landau, *Z.Physik*, 64, 629(1930).
84. A.H.Wilson, "The Theory of Metals", Cambridge University Press, New York, 2nd ed., 1953.
85. P.Weiss, *J.Phys.*, 6, 667(1907).
86. N.Bohr, *Phil.Mag.*, 26, 1, 476, 857(1913).
87. G.E.Uhlenbeck and S.Goudsmit, *Nature*, 117, 264(1926).
88. W.Pauli, *Z.Physik*, 43, 601(1927).
89. C.G.Darwin, *Proc.Roy.Soc.A*, 116, 227(1927).
90. P.A.M.Dirac, *Proc.Roy.Soc.A*, 117, 610(1928).
91. O.Stern, *Z.Physik*, 7, 249(1921).
92. W.Gerlach and O.Stern, *Ann.Phys.Leipzig*, 74, 673(1924).
93. P.B.Ayscough, "Electron Spin Resonance in Chemistry", Methuen and Co.Ltd., London, 1967.
94. N.Atherton, "Electron Spin Resonance", John Wiley and Sons, New York, 1973.
95. F.Bloch, *Phys.Rev.*, 70, 460(1946).
96. A.M.Portis, *Phys.Rev.*, 91, 1071(1953).
97. G.E.Pake, "Paramagnetic Resonance", W.A.Benjamin, Inc., New York, 1963.

98. A.Abragam and M.H.L.Pryce, Proc.Roy.Soc.A., 205, 135 (1951).
99. W.Slough, Trans.Farad.Soc., 61, 408 (1965).
100. P.Delhaes, F.Aly, and P.Dupuis, Sol.Stat.Comm., 12, 1099 (1973).
101. R.S.Mulliken, J.Am.Chem.Soc., 74, 811 (1952).
102. D.B.Chestnut, H.Foster, and W.D.Phillips, J.Chem.Phys., 34, 684 (1961).
103. H.M.McConnell and R.M.Lynden-Bell, J.Chem.Phys., 36, 2393 (1962).
104. R.M.Lynden-Bell and H.M.McConnell, J.Chem.Phys., 37, 794 (1962).
105. R.M.Lynden-Bell, Mol.Phys., 8, 71 (1964).
106. D.B.Chestnut, J.Chem.Phys., 40, 405 (1964).
107. Z.G.Soos, J.Chem.Phys., 43, 1121 (1965); 44, 1729 (1966); 46, 4284 (1967); Ann.Rev.Phys.Chem., 25, 121 (1974).
108. Z.G.Soos and H.M.McConnell, J.Chem.Phys., 43, 3780 (1965).
109. Z.G.Soos and R.C.Hughes, J.Chem.Phys., 46, 253 (1967).
110. Z.G.Soos and D.J.Klein, J.Chem.Phys., 55, 3284 (1971).
111. J.Des Cloizeaux and J.J.Pearson, Phys.Rev., 128, 2131 (1962).
112. J.C.Bonner and M.E.Fisher, Phys.Rev., 135A, 640 (1964).
113. L.N.Bulaevskii, J.E.T.P., 16, 685 (1963); 17, 684 (1963); Sov.Phys.Sol.Stat., 11, 921 (1969).
114. W.Duffy and K.P.Barr, Phys.Rev., 165, 647 (1968).
115. J.G.Vegter, Ph.D. Thesis, University of Groningen, 1972.
116. T.Hibma, Ph.D. Thesis, University of Groningen, 1974.
117. R.S.Knox, "Theory of Excitons", Solid State Physics, Supplement 5, Academic Press, New York, 1963.
118. S.Etemad, Ph.D. Thesis, University of Pennsylvania, 1972.

119. J.H.Van der Waals and M.S.de Groot, Mol.Phys., 2, 333(1959).
120. J.C.Bailey and D.B.Chestnut, J.Chem.Phys., 51, 5118 (1969).
121. T.Hibma, P.Dupuis, and J.Kommandeur, Chem.Phys.Lett., 15, 17(1972).
122. M.T.Jones and D.B.Chestnut, J.Chem.Phys., 38, 1311 (1963).
123. D.D.Thomas, H.Keller, and H.M.McConnell, J.Chem.Phys., 39, 2321(1963).
124. G.J.Ashwell, Ph.D.Thesis, University of Nottingham, 1973.
125. G.D.Welch, Ph.D. Thesis, University of Nottingham, 1976.
126. N.J.Drew, Ph.D.Thesis, University of Nottingham, 1978.
127. J.Woodward, Ph.D.Thesis, University of Nottingham, 1976.
128. P.L.Hall, J.Phys., 5D, 673(1972).
129. M.L.Randolph, Rev.Sci.Instr., 31, 949(1960).
130. B.Venkataraman, B.G.Segal, and G.K.Frenkel, J.Chem. Phys., 30, 1006(1959).
131. W.Duffy and D.L.Strandburg, J.Chem.Phys., 46, 456 (1967).
132. J.A.Lyons and W.E.Watson, J.Poly.Sci., 18, 141(1955).
133. S.A.Al'tschuler and B.M.Kozyrev, "Electron Paramagnetic Resonance", Academic Press, New York, 1964.
134. J.R.Singer, "Paramagnetic Resonance", Vol.2, Proc.of the 1st Int.Conf., Academic Press, New York, 1963.
135. A.Van Itterbeek and M.Labro, Physica, 30, 157(1964).
136. R.H.Poirer, E.J.Kahler, and F.Benington, J.Org.Chem., 17, 1437(1952).
137. R.S.Alger, "Electron Paramagnetic Resonance", John Wiley and Sons, New York, 1968.

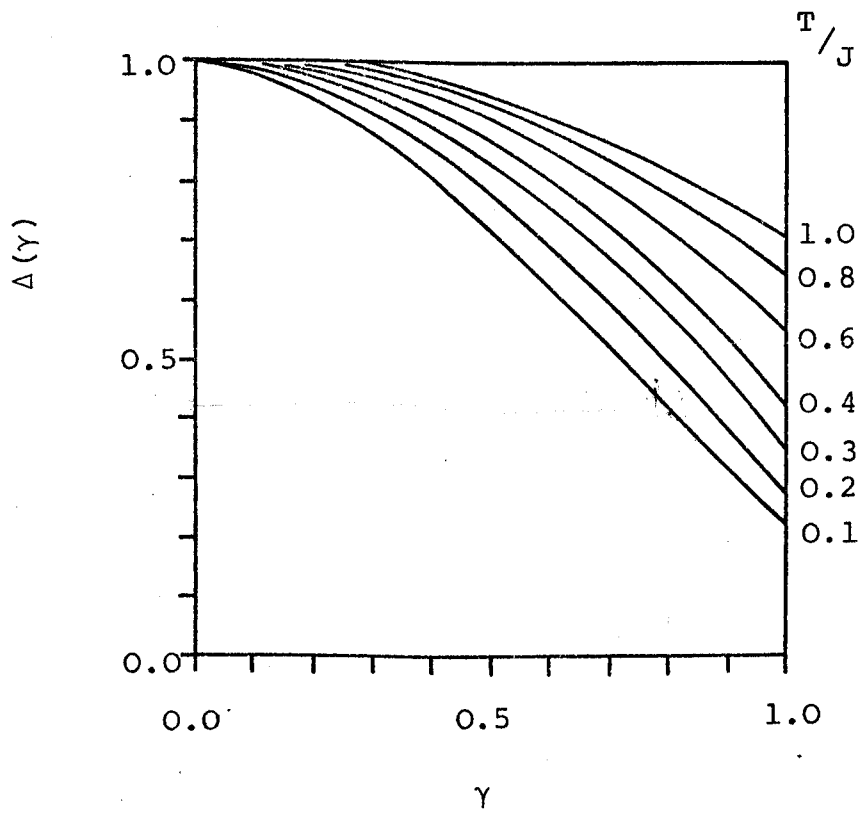
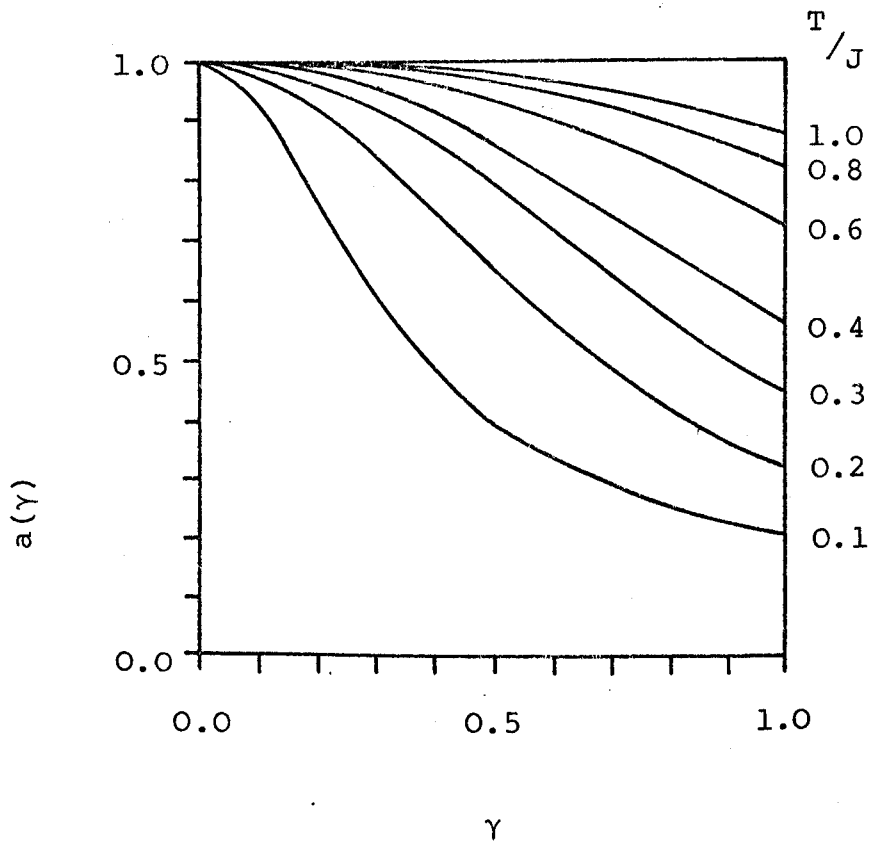
138. J.E.Wertz, Chem.Rev., 55, 829 (1955).
139. P.C.Taylor, J.F.Baughner, and H.M.Kriz, Chem.Rev., 75, 203 (1975).
140. J.H.Van der Waals and M.S.de Groot, Mol.Phys., 3, 190 (1960).
141. W.A.Yager, E.Wasserman, and R.M.R.Cramer, J.Chem.Phys., 37, 1148 (1962).
142. R.C.Hughes and Z.G.Soos, J.Chem.Phys., 48, 1066 (1968).
143. H.Inokuchi, K.Ikeda, and H.Akamatu, Bull.Chem.Soc. Jap., 33, 1622 (1960).
144. M.E.Browne, A.Ottenberg, and R.L.Brandon, J.Chem. Phys., 41, 3265 (1965).
145. G.J.Ashwell, D.D.Eley, S.C.Wallwork, and M.R.Willis, Proc.Roy.Soc.Lond.A., 343, 461 (1975).
146. F.K.Kneubühl, J.Chem.Phys., 33, 1074 (1960).
147. J.W.Searl, R.C.Smith, and S.J.Wyard, Proc.Phys.Soc.A, 74, 491 (1959).
148. J.W.H.Schreurs, G.E.Blomgren, and G.K.Frenkel, J.Chem.Phys., 32, 1861 (1960).
149. D.Bell, private communication.
150. T.Sundareson and S.C.Wallwork, Acta Cryst., B28, 2474 (1972).
151. Y.Suzuki and Y.Iida, Bull.Chem.Soc.Jap., 46, 2056 (1973).
152. L.Shields, J.Chem.Soc., Farad.Trans.II, 70, 1372 (1974).
153. A.W.Hornig and J.S.Hyde, Mol.Phys., 6, 33 (1963).
154. B.M.Hoffman and R.C.Hughes, J.Chem.Phys., 52, 4011 (1970).
155. S.Flandrois and D.Chasseau, Acta Cryst., B33, 2744 (1977).
156. A.J.Silverstein and Z.G.Soos, Chem.Phys.Lett., 39, 525 (1976).
157. S.Flandrois, J.Amiell, F.Carmona, and P.Delhaes, Solid State Comm., 17, 287 (1975).

158. T.Hibma and J.Kommandeur, *Phys.Rev.B*, 12, 2608(1975).
159. M.T.Jones, *J.Chem.Phys.*, 40, 1837(1964).
160. P.W.Anderson, *J.Phys.Soc.Jap.*, 9, 316(1954).
161. D.D.Thomas, A.W.Merkl, A.F.Hildebrandt, and H.M.McConnell, *J.Chem.Phys.*, 40, 2588(1964).
162. T.D.Buckman, O.H.Griffith, and H.M.McConnell, *J.Chem.Phys.*, 43, 2907(1965).
163. I.M.Brown and M.T.Jones, *J.Chem.Phys.*, 51, 4687(1969).
164. G.J.Gorter and J.H.Van Vleck, *Phys.Rev.*, 72, 1128(1947).
165. J.H.Van Vleck, *Phys.Rev.*, 74, 1168(1948).
166. N.Bloembergen and S.Wang, *Phys.Rev.*, 93, 72(1954).
167. R.B.Griffiths, *Phys.Rev.*, 124, 1023(1961).
168. J.P.Goldsborough, M.Mandel, and G.E.Pake, *Phys.Rev.Lett.*, 4, 13(1960).
169. G.J.Ashwell, D.D.Eley, M.R.Willis, and J.Woodward, *Phys.Stat.Solidi (b)*, 79, 629(1977).
170. G.J.Ashwell, D.D.Eley, N.J.Drew, S.C.Wallwork, and M.R.Willis, *Acta Cryst.*, B33, 2598(1977).
171. S.Takagi and K.Kawabe, *Solid State Comm.*, 18, 1467(1976).
172. S.Takagi, S.Izumida, and K.Kawabe, *Phys.Lett.*, 57A, 189(1976).
173. E.Ehrenfreund, S.K.Khanna, A.F.Garito, and A.J.Heeger, *Solid State Comm.*, 22, 139(1977).
174. Y.Tomkiewicz, A.R.Taranko, and J.B.Torrance, *Phys.Rev.*, 15B, 1017(1977).
175. S.Takagi, S.Izumida, and K.Kawabe, *Phys.Lett.*, 63A, 161(1977).
176. D.D.Eley, G.A.Owens, W.Waclawek, S.C.Wallwork, and M.R.Willis, *Proc.Roy.Soc.Lond.* (to be published).
177. A.W.Merkl, R.C.Hughes, L.J.Berliner, and H.M.McConnell, *J.Chem.Phys.*, 43, 953(1965).
178. R.C.Hughes, A.W.Merkl, and H.M.McConnell, *J.Chem.Phys.*, 44, 1720(1966).

179. D.Bates, private communication.
180. N.F.Mott and E.A.Davis, "Electronic Processes in Non-Crystalline Materials", Clarendon Press, Oxford, 1971.
181. E.A.Davis, Endeavour, 30, 55 (1971).
182. K.Holczer, G.Milhaly, A.Janossy, and G.Grüner, Mol. Cryst.Liq.Cryst., 32, 199 (1976).
183. D.Kuse and H.R.Keller, Phys.Rev.Lett., 27, 1060 (1971).
184. E.Ehrenfreund, S.Etemad, L.B.Coleman, E.F.Rybaczewski, A.F.Garito, and A.J.Heeger, Phys.Rev.Lett., 29, 269 (1972).
185. S.Etemad, A.F.Garito, and A.J.Heeger, Phys.Lett., 40A, 45 (1972).
186. Y.Tomkiewicz, E.M.Engler, and T.D.Schultz, Phys.Rev. Lett., 35, 456 (1975).
187. J.P.Faucher and H.Robert, C.R.Acad.Sci.Paris, Ser.B, 270, 174 (1970).
188. A.W.Hanson, Acta Cryst.B, 19, 610 (1965); 24, 768 (1968).
189. A.Kriesler and G.Alquie, J.Mag.Res., 16, 377 (1974).
190. G.J.Ashwell, D.D.Eley, S.C.Wallwork, and M.R.Willis, Proc.Roy.Soc.Lond.A, 343, 461 (1975).
191. R.Somoano, V.Hadek, S.P.S.Yen, A.Rembaum, and R.Deck, J.Chem.Phys., 62, 1061 (1975).

## APPENDIX 1

Graphs showing the triplet exciton band parameters as a function of the alternation parameter.



Figures A.1.1 and A.1.2

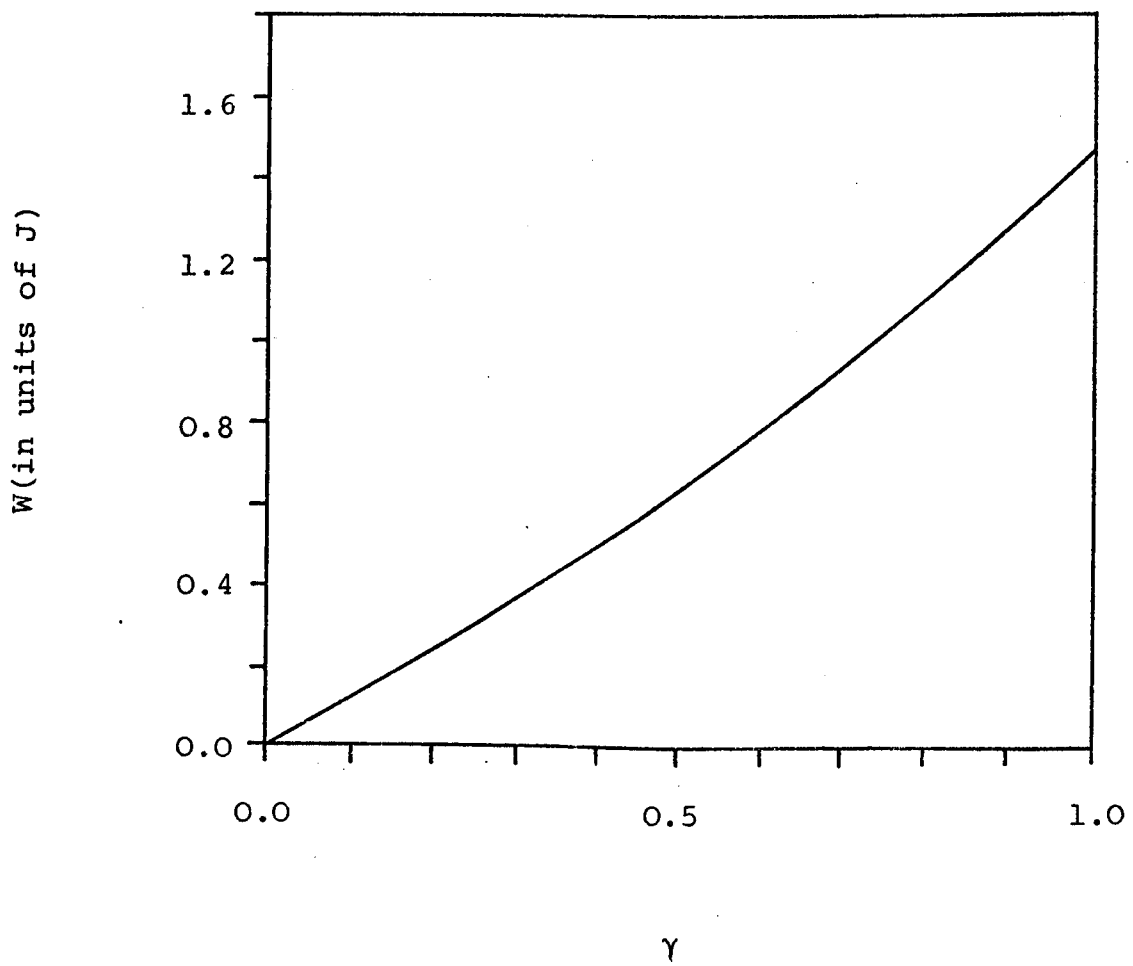


Figure A.1.3

## APPENDIX 2

Conductivity results for the polycrystalline TCNQ complex salts DPPE(TCNQ)<sub>5</sub>, DBPE(TCNQ)<sub>5</sub>, and DHPE(TCNQ)<sub>5</sub>.

The d.c. conductivities of most of the TCNQ complex salts, the magnetic properties of which are presented in this thesis, were measured by various members of the semiconductor group in this department. However, the electrical properties of DPPE(TCNQ)<sub>5</sub>, DBPE(TCNQ)<sub>5</sub> and DHPE(TCNQ)<sub>5</sub> have not been previously investigated. Therefore, as such information is of value in the interpretation of the magnetic properties, the conductivities of these compounds were measured as part of this work.

Polycrystalline samples were compressed for two minutes at 75 MPa in an evacuated die. The resulting disc was prepared for the experiment by attaching copper wires to either side of the disc using Acheson high-conductivity silver paint as electrodes. The compactions were then placed in a conductivity cell and degassed at 330K for sixteen hours under vacuum. Conductivity measurements were then made using standard potentiometer circuits, and helium as a heat transfer gas, for temperatures ranging from 330K to 150K.

Typical results obtained are presented in Figures A.2.1 to A.2.3 and, from the average slopes of a number of such graphs, the activation energies for conduction were found to be 10.6, 15.4, and 5.8 kJ mol<sup>-1</sup> for DPPE(TCNQ)<sub>5</sub>, DBPE(TCNQ)<sub>5</sub>, and DHPE(TCNQ)<sub>5</sub> respectively. The conductivity values at 300K were also obtained and

found to be 0.3,  $3.6 \times 10^{-2}$ , and  $0.2 \text{ ohm}^{-1} \text{ cm}^{-1}$  for DPPE  
(TCNQ)<sub>5</sub>, DBPE(TCNQ)<sub>5</sub>, and DHPE(TCNQ)<sub>5</sub>.

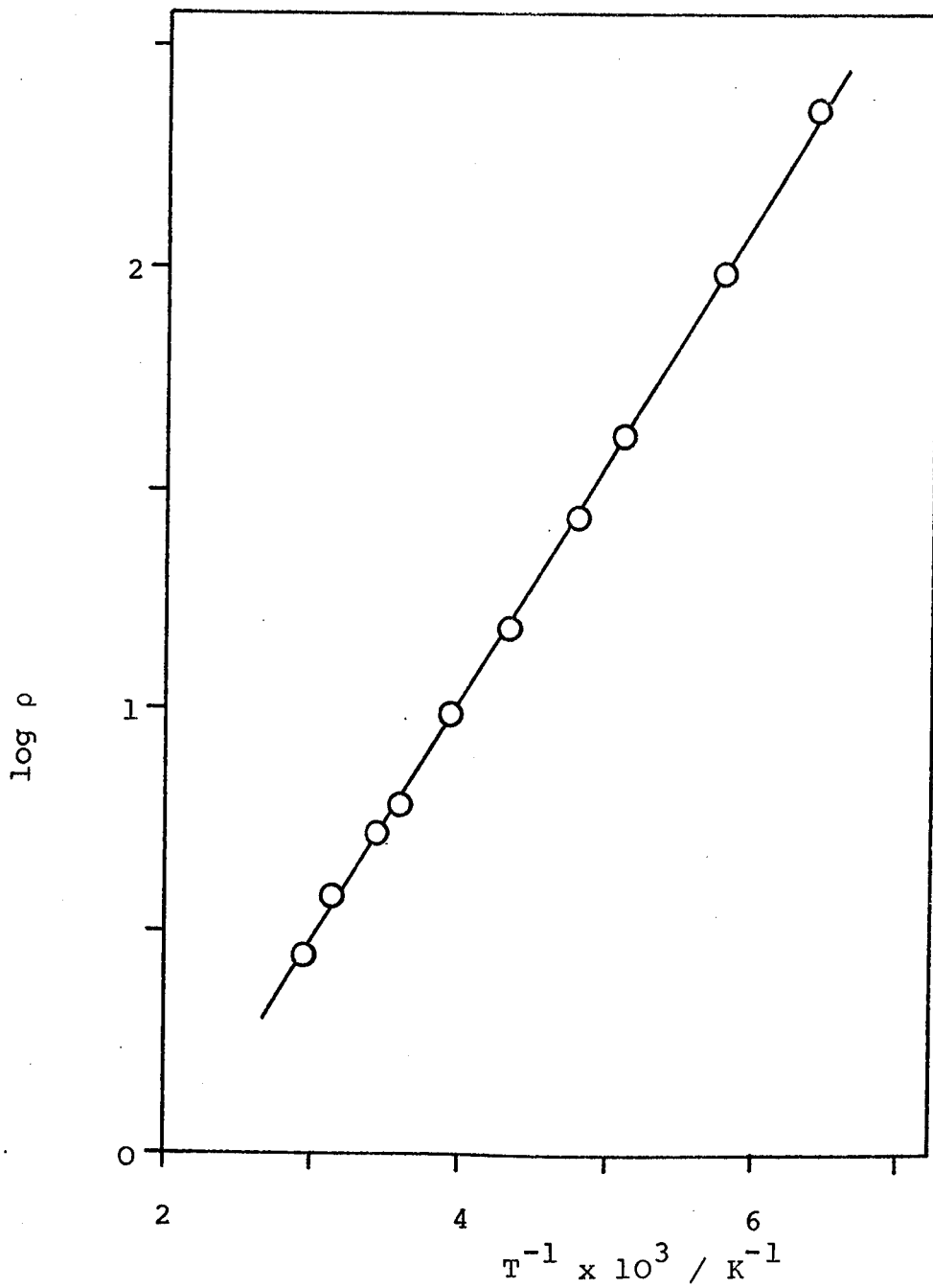


Figure A.2.1

DPPE(TCNQ)<sub>5</sub>

Semilog plot of the resistivity,  $\rho$  (in ohm cm),  
against reciprocal temperature.

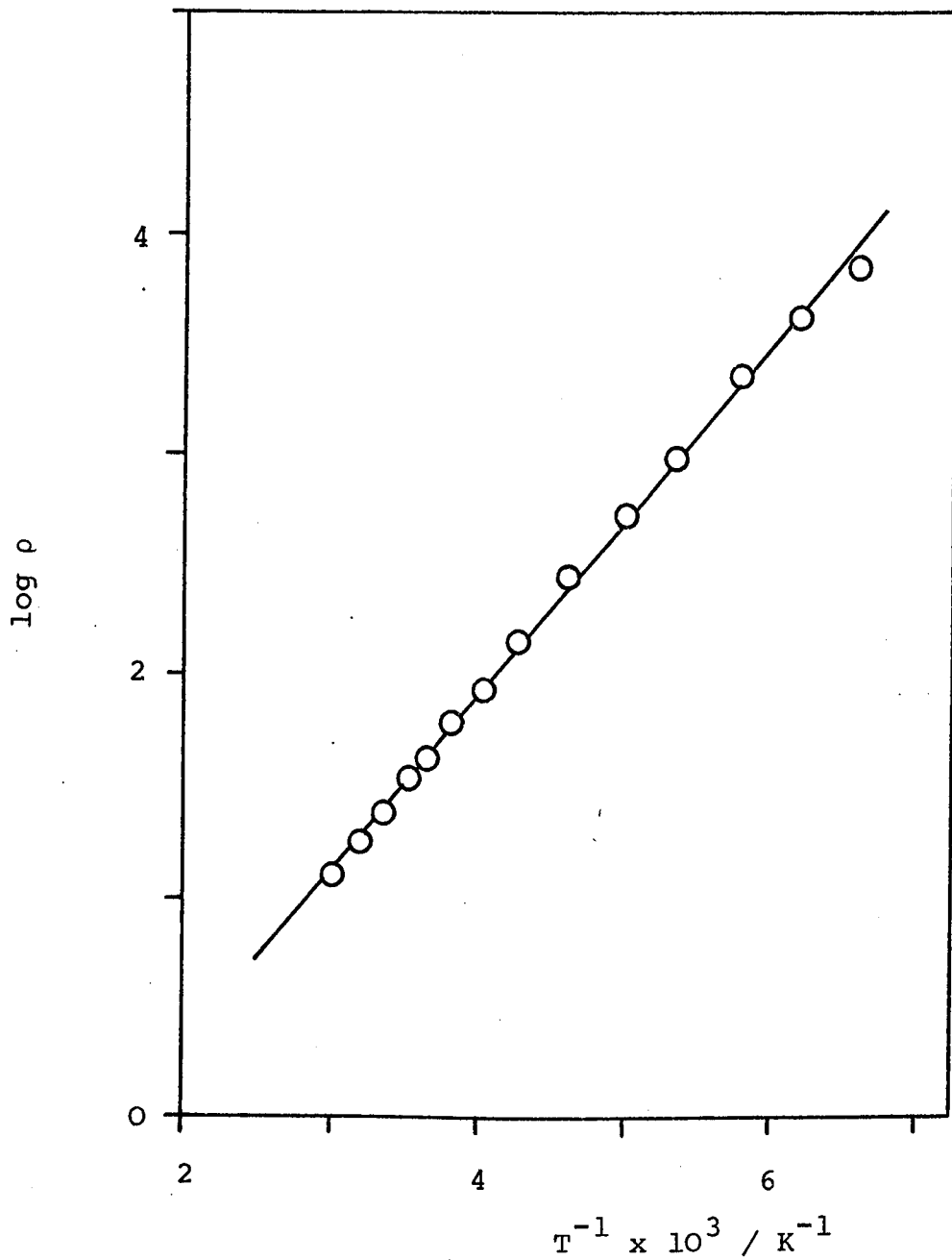


Figure A.2.2

DBPE(TCNQ)<sub>5</sub>

Semilog plot of the resistivity,  $\rho$  (in ohm cm),  
against reciprocal temperature.

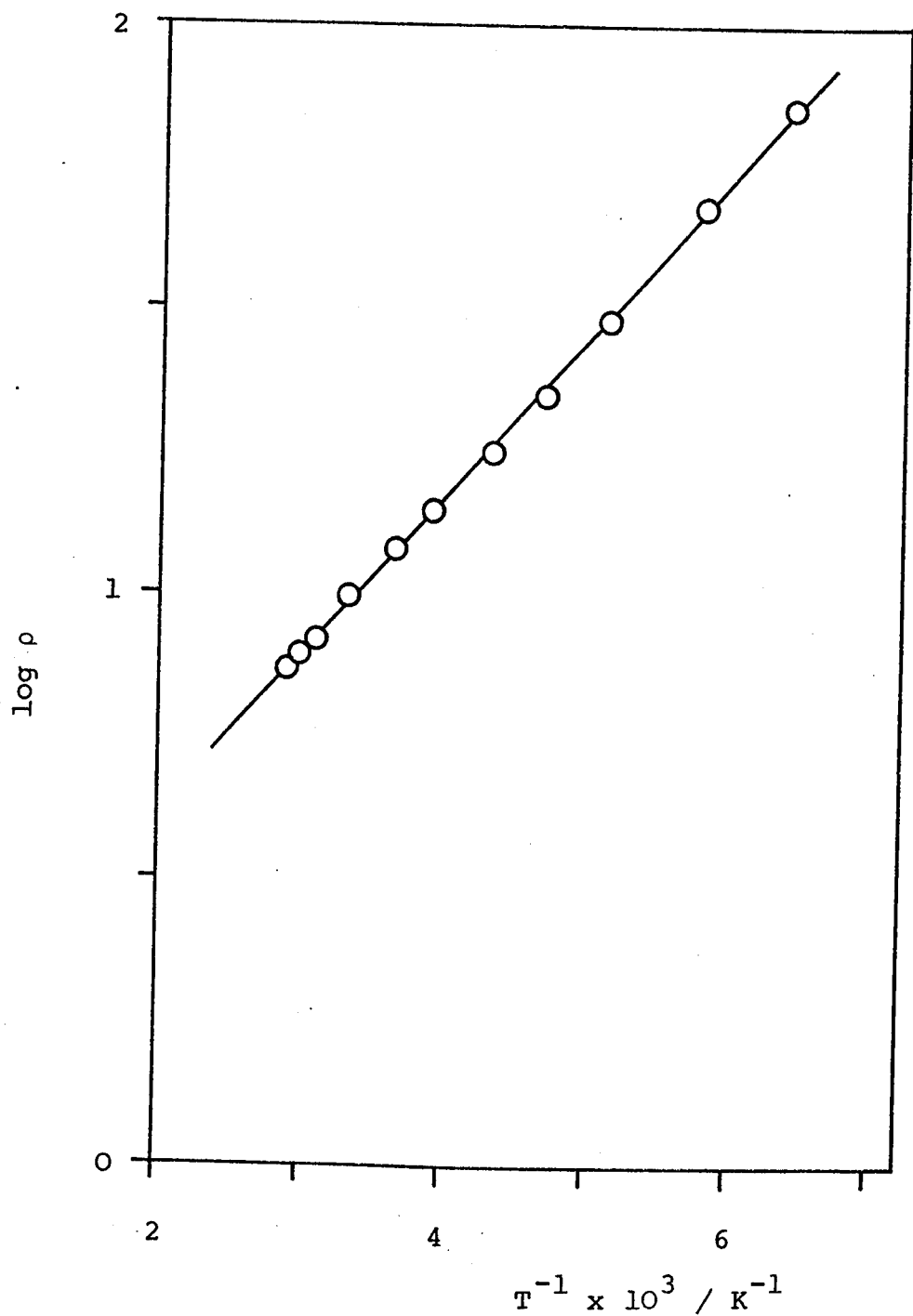


Figure A.2.3

DHPE(TCNQ)<sub>5</sub>

Semilog plot of the resistivity,  $\rho$  (in ohm cm), against reciprocal temperature.